DOCTOR OF PHILOSOPHY

Percolation properties of ferromagnetic and frustrated replicated Ising models

Akritidis, Michail

Award date:
2023

Awarding institution:
Coventry University

COVENTRY UNIVERSITY

Doctoral Thesis

Percolation properties of ferromagnetic and frustrated replicated Ising models

Author:
Michail Akritidis

Supervisory team:
Ass. Prof. Nikolaos G. Fytas
Prof. Martin Weigel
Ass. Prof. Thierry Platini

A thesis submitted in fulfilment of the requirements for the degree of Doctoral of Philosophy

in the

Faculty of Engineering, Environment and Computing
Coventry University

April 20, 2023

Certificate of Ethical Approval

Applicant:	Michail Akritidis
Project Title:	Simulations on spin glasses

This is to certify that the above named applicant has completed the Coventry University Ethical Approval process and their project has been confirmed and approved as Low Risk

Date of approval:	10 Jun 2022
Project Reference Number:	P138150

Abstract

In this thesis, the percolation properties of the ferromagnetic as well as a disordered and frustrated multi-replica Ising model in two dimensions are considered. The investigated systems can be understood as a collection of non-interacting copies (replicas) at the same temperature. In this setup we define a correlated percolation problem, where we introduce and study two types of clusters, namely the soft and hard constraint clusters. For the ferromagnetic case the 1-, 2-, and 3-replica Ising models have been considered, with some preliminary results concerning the 4-replica case. By means of Monte Carlo simulations on relatively large system sizes and a finite-size scaling analysis we investigate the critical behaviour of the system and provide estimates of the critical exponents. Specifically, for the 1-replica Ising model the critical exponents concerning the percolation strength and average cluster size are determined, by considering the influence on the estimates of the exponents when particular cluster sets are included or excluded in the definition of the observables. Subsequently, for the 2- and 3-replica case the critical behaviour of the system have been discussed in terms of the percolation point, and the critical exponents concerning the correlation length, percolation strength, and average cluster size for the soft and hard constraint clusters have been computed, respectively. The inclusion or exclusion of different cluster sets in the definitions of percolation strength and average cluster size have been also considered. Some preliminary results for the 4-replica Ising model are also given. For the frustrated Ising model, i.e., the Edwards-Anderson spin-glass, the percolation properties of Houdayer's clusters have been investigated. Such clusters define a percolation process similar to the 2-replica Ising ferromagnet, with the obvious distinction that interactions are now random.

Summary of PhD work

This thesis is an account of research undertaken by the author between September 2018 and September 2022 at the Centre for Fluid and Complex Systems (FCS) of Coventry University, United Kingdom.

The material presented here is based mostly on numerical simulations which were designed and carried out by the author himself. In particular, all the necessary codes for generating the actual numerical data but also those relevant to the statistical analysis part were developed by the author. Note that only for the fitting analysis the standard `gnuplot`'s in-built routine was used. Scripts were written using the `FORTRAN 90` programming language and a part of the data analysis using `Python`. All figures presented in this thesis (configurational snapshots, scaling plots and fittings on various observables) were extracted from the performed simulations by the author.

The vast majority of simulations were caried out on the High Performance Computing clusters of Coventry University *Zeus* and *EPYC* using a trivially multi-node parallelisation scheme, also mastered by the author. The total simulation of the work presented in this thesis is the equivalent to ≈ 20 years of a single-core CPU time.

This work has already yielded one peer-reviewed publication, and another one is expected soon. In particular:

1. M. Akritidis, N. G. Fytas, and M. Weigel, "Corrections to scaling in geometrical clusters of the 2D Ising model", J. Phys.: Conf. Ser. **2207**, 012004 (2022).

2. M. Akritidis, N. G. Fytas, and M. Weigel, "Geometrical clusters in the overlap of the Ising model" (to be submitted).

Complementary to the core project, over the years of his PhD studies the author has been involved into three additional side projects, for which several peer-reviewed publications are expected in the coming months:

1. N.G. Fytas, M. Akritidis, and M. Weigel, "Scaling of the random-field Ising model at the upper critical dimension".

2. M. Akritidis, A. Vasilopoulos, N.G. Fytas, G. Barkema, and M. Weigel, "Universality in the critical dynamics of the two-dimensional Ising model under the presence of quenched randomness".

3. M. Akritidis, A. Vasilopoulos, N.G. Fytas, and M. Weigel, "Critical dynamics of cluster algorithms in the two-dimensional Baxter-Wu model".

Στον παππού μου Μιχάλη,

που δεν πρόλαβε να δει

την εργασία αυτή να ολοκληρώνεται …

Acknowledgments

First and foremost I would like to thank my supervisors Ass. Prof. Nikolaos G. Fytas and Prof. Martin Weigel for their support and guidance throughout these years. From the numerous discussions we had, I came to realize that not only are they great scientists and supervisors but more importantly great people too.

Furthermore, I would like to thank the Centre for Fluid and Complex Systems and specifically Prof. Alban Potherat, Dr. Lorna Everall and Prof. Eun-jin Kim for the financial support during a critical stage of my studies. Additionally, I would like to acknowledge the allocation of significant CPU time on the supercomputers Zeus and EPYC HPC of Coventry University, as well as the valuable help of our administrator Ass. Prof. Alex Pedcenko. I am also particularly thankful to Maddy Janickyj for proofreading this thesis. My gratitude also goes to Ass. Prof. Abhishek Kumar for consistently supporting me emotionally and motivating me to continue during all stages of my PhD.

My special thanks also goes to my colleagues Alex, Jerry, Anthony, Gene, Adrian, Sanjay for the countless hours that we spent in and out of the office, discussing, working and of course drinking. Finally, I am deeply indebted to my family for being on my side and supporting me in all possible ways since the beginning.

Contents

List of Figures

List of Tables

Chapter 1

Introduction

The theory of critical phenomena is one of the most intriguing and challenging areas in the field of statistical and condensed matter physics [1–10]. It concerns changes of matter from one thermodynamic state to another when an external parameter of the system, e.g., temperature, is varied. Such changes are characterized by discontinuities or divergences of the associated physical observables, resulting from the complicated interactions among the large (eventually infinite) number of degrees of freedom. Additionally, the study of the behaviour of such systems, theoretically as well as experimentally, has revealed the fundamental concepts of *scaling* and *universality*, which can be understood in the framework of the *renormalization group* [11–14]. From the theoretical point of view, the Ising model which serves as a simplified prototype for studying magnetism, is considered one of the pillars of statistical physics.

In the study of the Ising model, and spin systems in general, graphical representations have played a crucial role in deepening our understanding and gaining geometric insights for the nature of the phase transition. One natural framework of such an approach[1] is *percolation theory* [18–20], which can be regarded as the simplest model that exhibits a phase transition. In its simplest formulation percolation concerns the study of clusters formed by neighbouring occupied sites which are *randomly* and *independently* distributed on a lattice. Depending on the probability p for a site to be occupied, clusters of different sizes can occur. For small values of p only clusters of small size appear, while as p increases the average size of clusters increases. If p exceeds a certain value p_c, then a cluster that spans the whole system emerges, which will be of infinite size as the size of the system becomes infinite. Such a cluster is called a *percolating* cluster and the value of the probability where this occurs is p_c, the *percolation threshold*. Despite its simple formulation percolation theory is still an active topic in mathematics, in particular in probability theory, and physics. This is for example illustrated by the award of the Fields Medal to Prof. Hugo Duminil-Copin for his contribution in the probabilistic theory of phase transitions; see Ref. [21] for a short exposition of his work.

For spin models, however, finding a suitable percolation process that properly describes the critical behaviour of the system is not an easy task. The difficulty lies in the existence of correlations among sites (spins), which are expressed via the Hamiltonian of the system. Nonetheless, Fortuin and Kasteleyn (FK) [22–25] showed that the q-state Potts model can be mapped onto a site-bond correlated percolation problem (the random cluster model), in which with a certain temperature-dependent probability bonds are placed among neighbouring like

[1] Another approach is to generate graphs using high-temperature expansions; see, e.g., Ref. [15–17].

spins and sites that are connected via a path of consecutive bonds are considered to be in the same cluster. It turns out, that these FK clusters percolate at the thermal transition point with critical exponents identical to the thermal ones. The success of such a description is that FK clusters propagate the spin correlations of the system, as the probability of two spins belonging to the same cluster is equal to the spin correlation function [26]. Additionally, the FK representation of the q-state Potts model is also the core idea behind the powerful algorithms of Swendsen and Wang [27] and Wolff [28], which significantly reduce critical slowing down in the vicinity of the critical point.

Despite the success of the FK representation to properly describe the q-state Potts model, initially, however, it was believed that clusters constructed by neighbouring spins with the same orientation (*geometrical clusters*) are capable to propagate the spin correlations of the system. Nonetheless, these geometrical clusters are not capable of describing the phase transition of the system as their associated exponents do not coincide with the thermal ones, and generally they do not percolate at the thermal transition point. On the other hand, the geometrical clusters of the q-state Potts model are still of some importance as in two dimensions they percolate at the thermal transition point [29–31], and they are found to encode the tricritical behaviour of the site-diluted Potts model for $0 \leq q \leq 4$, see Refs. [32, 33] and references therein. Additionally, the fractal boundaries of such clusters have been studied in the framework of *stochastic Loewner evolution* (SLE), where various critical exponents, previously conjectured on the basis of Coulomb gas map [34–38] and conformal invariance [39], have been obtained analytically.

So far we have seen how the FK graphical representation can be a powerful tool in the study of ferromagnetic systems, for the case of spin glasses, however, such a description is no longer valid. The reason is that the FK clusters cannot properly propagate the spin fluctuations of the system, as the spin correlation function is not equal to the probability of finding two spins in the same cluster [40], resulting in a percolation transition at higher temperatures compared to that of the thermal one [40, 41]. Of course spin glasses possess their own challenges, where most interesting questions remain still unclear (see Refs. [42–47] for a review). However, the study of their critical behaviour in terms of a graphical representation has received, thus far, little attention in comparison with ferromagnets. Two existing methods, though, are Houdayer's clusters [48], and the spin-glass versions of the FK clusters [49] and Chayes, Machta, and Redner (CMR) clusters [50, 51] proposed in Ref. [40]. Such methods utilise a number of non-interacting copies (replicas) which are at the same temperature, and study the percolation properties of clusters defined in the overlap of such copies. From the computational point of view, these clusters can be seen as the dynamics of a Monte Carlo process for sampling configurations, giving access to system sizes that are unreachable by local-dynamic algorithms, e.g., Metropolis [52]. Although Houdayer's clusters, supported by local update moves to ensure ergodicity, define an acceptable Monte Carlo process, the properties of such clusters have received less attention. Complementary to that, the study of percolation defined from the overlap of such replicas for the ferromagnetic case, remains elusive. On the other hand, for the percolation properties of clusters defined in Ref. [40], some studies can be found in Refs. [40, 53].

Consequently, the motivation of this work is to achieve a better understanding of the percolation properties for clusters defined from the overlap of such replicas, for the ferromagnetic and for Houdayer's clusters, respectively. By means of extensive Monte Carlo simulations on relative large system sizes, we study the cases of 1-(standard Ising), 2-, and 3-replica Ising

models in two dimensions, for the case of the ferromagnet; some preliminary results for the 4-replica Ising model will also be discussed. To determine the critical behaviour we use the theory of finite size scaling, from which the exponents concerning the correlation length, average cluster size, and percolation strength may be obtained. Comparisons between estimates of the exponents resulting from the different definitions of the involved observables will be discussed. Finally, for the case of Houdayer's clusters a more qualitative analysis will be given. The outline of this thesis' contents is presented below.

Chapter 2 is devoted to an introduction to the basic theory of statistical physics, which is necessary for the discussion of results that will follow in the later chapters. Specifically, the theory of phase transitions and critical phenomena is discussed, where some characteristic properties, scaling relations, and definition of critical exponents is given, in connection with the ideas from renormalization group (RG) and finite size scaling (FSS). Afterwards, the theory of percolation is described, followed by a discussion regarding its connection with phase transitions of spin systems, i.e., the q-state Potts model. The basic properties of spin glasses will be addressed in the last section of this chapter, with particular emphasis on the two, quite distinct, pictures of replica symmetry breaking and droplet theory.

The numerical methods utilised in this thesis will be discussed in Chapter 3. After a short introduction to the general theory of Monte Carlo simulations - where we recall the Metropolis algorithm - we will review the cluster algorithms of Swendsen-Wang and Wolff as methods for efficiently simulating the Ising and the q-state Potts model in the vicinity of the critical point. Subsequently, the method of parallel tempering as a procedure which substantially reduces the equilibration time for the spin-glass problem, will be discussed and various temperature schedules which aim on improving the performance of the algorithm will be covered. The cluster algorithm of Houdayer, which leads to simulation efficiency for the spin-glass problem only for two-dimensional systems, is presented in the last section of this chapter. Lastly, some aspects regarding autocorrelation times, histogram reweighting technique, and error estimations are discussed in Appendix A.

In Chapter 4 we discuss the percolation properties of geometrical clusters for the two-dimensional Ising model. We start by defining various wrapping probabilities and verifying their interrelations. Then, we proceed with the estimation of the critical exponents concerning the average cluster size and percolation strength, where we extend their "conventional" definitions (coming from ordinary percolation) with the inclusion of various sets of clusters. Additionally, as the values of such exponents are known analytically, we speculate the existence of scaling corrections for the different cluster sets used.

In Chapter 5, which forms the core part of this thesis, we study the percolation properties of geometrical clusters of the multi-replica Ising ferromagnet in two dimensions, which can be understood as a stack of statistically independent copies (replicas) of the initial system at the same temperature. The inclusion of multiple replicas introduces a new percolation problem which allows to define various cluster types. In the present study we discuss the so-called soft and hard constraint types of clusters, where the soft constraint clusters are the same as the ones of Houdayer's cluster algorithm. Based on extensive Monte Carlo simulations for large system sizes, the percolation properties for the cases of 2- and 3-replicas are discussed. Specifically, by employing FSS the critical behaviour in terms of transition temperature and critical exponents for both cluster types are obtained, by utilising the various sets of clusters as introduced in Chapter 4. Lastly, some preliminary results for the 4-replica case are given.

Chapter 6 concerns the study of the percolation properties of Houdayer's clusters for the

two-dimensional Edwards-Anderson spin-glass problem. Since equilibration at low temperatures is quite hard to achieve for such systems, we begin with an exposition of various criteria that ensures it. Additionally, a comparison between some temperature schedules, that aim to increase the performance of the parallel tempering algorithm is given. The chapter closes with a qualitative description of the percolation properties of Houdayer's clusters.

Finally, Chapter 7 contains our conclusions and some outlook for future work.

Chapter 2

Theoretical Background

In the field of statistical physics and critical phenomena one of the most intensively studied models is undoubtedly the Ising model. Its simple formulation and being one of the few models in statistical physics that a rigorous solution is available at least in one and two dimensions, established the Ising model as one of the reference-point models in the field. Additionally, its connection with percolation theory, has greatly enhanced our understanding of phase transitions based on a geometrical interpretation. The core idea for such a description is the introduction of clusters capable of propagating the spin fluctuations of the system. Although, such clusters are well defined for the case of the Ising ferromagnet, for systems with randomness, such as spin glasses, an appropriate cluster definition remains elusive.

2.1 Phase Transitions and Critical Phenomena

Statistical mechanics is a field of physics which focuses on the thermodynamic behaviour of systems constituted of an enormous number of particles, typically of the order of Avogadro's number $N_A \sim 10^{23}$. Although the equations of motion of each particle can be mathematically well defined from classical or quantum mechanics, it is impossible to solve this gigantic number of equations. Additionally, these equations are of little use for deriving the thermodynamic properties of the system, which arise from the collective behaviour of all particles in the system. Instead, statistical mechanics provides a probabilistic description which allows us to compute average values and fluctuations of thermodynamic observables. Such systems could have different phases, and changes from one phase to another are known as *phase transitions*. These are remarkable collective phenomena, resulting in abrupt changes on the physical properties of the system, when an external parameter such as temperature, pressure, magnetic field, etc., is varying. The points where these changes take place are called *transition points* and signify the transition from one state of matter to another. The spectrum of such transitions is quite vast, ranging from the "ordinary" solid-liquid-gas transitions of water to liquid-crystals up to the transition of the more "exotic" phases of superconductivity and superfluidity. For a pedagogical introduction to phase transitions see, e.g., Refs. [1–10].

Depending on the nature of the phase transition, they are classified in two main categories: *first-order* and *continuous* (second order). At first-order transitions two phases are separated by a transition point and each phase has its own distinct macroscopic properties. Exactly at the transition point, phases coexist which implies a mixed-phase regime where different

spatial parts of the system are at different phases. For example, when water is exactly at its freezing temperature it coexists with ice domains. Even slightly away from the critical point the system will be in one of its unique phases. In such cases we expect to find discontinuities in various thermodynamic observables as we pass through the transition point or equivalently from one stable state to another. Finally, one important characteristic of such transitions is that the correlation length (to be described shortly) is finite.

The situation is quite different for continuous phase transitions. In that case there exists a point where the correlation length is infinite, thus fluctuations become important at all length scales, which forces the system to be in a unique critical phase; such a point is called a *critical point*. This means that as we approach the critical point the two phases will gradually start to resemble each other and exactly at the critical point they will become identical, and thus one unique phase will characterize the system. The first experimental realisation of a continuous phase transitions was the phenomenon of *critical opalescence*, which concerns the liquid-gas transition. In the vicinity of the transition point the liquid has a milky appearance caused by the density fluctuations at all possible wavelengths and due to the anomalous diffusion of light. What makes continuous phase transitions such interesting and challenging phenomena is the fact that the correlation length is extended to the size of the system leading to strong correlations among all degrees of freedom[1], hence making standard perturbative techniques inadequate for the description of the phenomena. An appropriate description for such phenomena is feasible under the framework of *renormalization group*, which will be discussed in Sec. 2.2.

In order to continue our discussion about phase transitions, let us now introduce the Ising model, which has a central role in the study of critical phenomena (as well as in this thesis), serving as a prototype for the study of magnetic systems. To this end we define a *finite* lattice in d dimensions, at the sites i of which we place Boolean variables σ_i (spins) taking the values ± 1. The Hamiltonian of the Ising model is given by

$$\mathcal{H} = -J \sum_{\langle i,\, j \rangle} \sigma_i \sigma_j - H \sum_i \sigma_i, \tag{2.1}$$

where J is the interaction among spins ($J > 0$), H the external magnetic field, and $\langle\, ,\, \rangle$ indicates that the sum is restricted to nearest neighbours. Denoting a possible spin configuration as μ and assuming that the system is in thermal equilibrium, and that we are in the *canonical ensemble*[2], the probability for the spin configuration μ to occur is given by the Boltzmann weight

$$p\,(\mu) = \frac{e^{-\mathcal{H}(\mu)/k_{\mathrm{B}}T}}{Z}, \tag{2.2}$$

where $\mathcal{H}(\mu)$ is the energy of the configuration μ given in Eq. (2.1), T is the temperature,

[1] In the context of statistical physics, degrees of freedom is the number of independent parameters (variables) required to describe the state of a physical system. For example, in three dimensions the state of an atom at any moment is defined by six independent variables, i.e., three components of its position and three components of its momentum; here we consider the atom as a point-like particle with no internal structure. Thus, for a system consisting of N atoms the number of degrees of freedom is $6N$. For the Ising model, see Eq. (2.1), the number of degrees of freedom is equal to the total number of spins.

[2] In the canonical ensemble the system is placed in a heat bath of fixed temperature and we allow to exchange energy with its environment; for that and also as a survey in statistical mechanics see, e.g., Refs. [54–56].

k_{B} is the Boltzmann's constant, and Z is the *partition function*. Adopting now the common notation $\beta \equiv 1/k_{\mathrm{B}}T$, the partition function is defined as

$$Z\left(\beta, H\right) = \sum_{\mu} \exp\left[-\beta \mathcal{H}(\mu)\right], \tag{2.3}$$

where the summation is over all the possible spin configurations μ of the system. Equation (2.3) ensures that the probabilities defined in Eq. (2.2) are properly normalized, i.e., $\sum_{\mu} p\left(\mu\right) = 1$. Besides a normalisation constant, the partition function is of great importance as it encodes the statistical properties of the system; this can be realised from the connection with basic thermodynamic quantities. For any observable O its expectation value $\langle O \rangle$ is given by averaging over all configurations with the appropriate Boltzmann weight

$$\langle O \rangle = \frac{1}{Z} \sum_{\mu} O(\mu)\, e^{-\beta \mathcal{H}(\mu)}. \tag{2.4}$$

In this framework the *free energy* of the system is defined as [56]

$$F = -\frac{1}{\beta} \ln Z. \tag{2.5}$$

From thermodynamics, the free energy is related to the *internal energy* $U \equiv \langle H \rangle$ and *entropy* S as [56]

$$F = U - TS. \tag{2.6}$$

The internal energy U using Eqs. (2.3) and (2.4), can be written in terms of the partition function Z as

$$U = \langle \mathcal{H} \rangle = \frac{1}{Z} \sum_{\mu} \mathcal{H}(\mu)\, e^{-\beta \mathcal{H}(\mu)} = -\frac{\partial \ln Z}{\partial \beta}. \tag{2.7}$$

Since the free energy F is the Legendre transform of U with respect to entropy S we can write [56]

$$S = -\left(\frac{\partial F}{\partial T}\right)_{H} = \beta^2 \frac{\partial F}{\partial \beta} = -k_{\mathrm{B}}\, \beta\, \frac{\partial \ln Z}{\partial \beta} + k_{\mathrm{B}} \ln Z. \tag{2.8}$$

Accordingly, the specific heat C is given as

$$C = \left(\frac{\partial U}{\partial T}\right)_{H} = k_{\mathrm{B}}\, \beta^2\, \frac{\partial^2\, \ln Z}{\partial \beta^2} = k_{\mathrm{B}}\, \beta^2 \left[\, \langle E^2 \rangle - \langle E \rangle^2 \,\right], \tag{2.9}$$

where we adapt the more common notation for the internal energy, i.e., $\langle \mathcal{H} \rangle \equiv \langle E \rangle$. From Eqs. (2.5), (2.7), (2.8), and (2.9) we see that the knowledge of the partition function allows the calculation of the various thermodynamic observables. Note that Eq. (2.9) allows also the calculation of the specific heat from the variance of the internal energy, which is frequently used in Monte Carlo studies [57–60].

Another important observable for magnetic systems is the *magnetisation* M which gives the sum of all spins in the system, i.e., $\langle M \rangle \equiv \langle \sum_i \sigma_i \rangle$, and it can be expressed in terms of the free energy as [56]

$$\langle M \rangle = -\left(\frac{\partial F}{\partial H}\right)_T . \tag{2.10}$$

Additionally, the *magnetic susceptibility* X, using Eq. (2.5), can be expressed as [56]

$$X = \left(\frac{\partial \langle M \rangle}{\partial H}\right)_T = \frac{1}{\beta}\frac{\partial^2 \ln Z}{\partial H^2} = \beta \left[\langle M^2 \rangle - \langle M \rangle^2 \right]. \tag{2.11}$$

We note again the connection of Eqs. (2.10) and (2.11) with the partition function, and that similarly to Eq. (2.9), the magnetic susceptibility can be calculated from the variance of the magnetisation.

An observable of particular interest is the *two-point connected correlation function*, which is a measure of the relative alignment between two spins at sites i and j

$$G(i,j) = \langle \sigma_i \sigma_j \rangle - \langle \sigma_i \rangle \langle \sigma_j \rangle. \tag{2.12}$$

If we assume that the system is *translational invariant*, then Eq. (2.12) depends only on the distance difference, i.e., $\vec{i} - \vec{j} \equiv \vec{r}$, and $\langle \sigma_i \rangle = \langle \sigma_j \rangle \equiv \langle \sigma \rangle$. Note here that translational symmetry requires a system of infinite size, defining the so-called *thermodynamic limit*. Hence, we can rewrite Eq. (2.12) as

$$G(\vec{r}) = \langle \sigma_i \sigma_j \rangle - \langle \sigma \rangle^2. \tag{2.13}$$

Away from the critical point and for large distances the correlation function decays exponentially with distance $|\vec{r}|$ [1], i.e.,

$$G(\vec{r}) \sim e^{-|\vec{r}|/\xi}, \quad |\vec{r}| \gg \xi, \tag{2.14}$$

where ξ is the *correlation length* which provides a measure of the extent of correlations among spins, thus spins are uncorrelated with each other as long as $|\vec{r}| \gg \xi$. Exactly at the critical point the correlation length becomes infinite and Eq. (2.14) is no longer valid. Though, based on experimental facts and studies on simplified lattices it has been realised that at the critical point the correlation length follows a power law behaviour [3, 8, 9], i.e.,

$$G(\vec{r}) \sim \frac{1}{|\vec{r}|^{d-2+\eta}}, \tag{2.15}$$

where η is called *anomalous dimension*, and it is a first example of a *critical exponent*. At Sec. 2.2 we will discuss the set of critical exponents and the relations among them.

In order to characterize the transition and the separation between two (or more) phases, it is useful to define a parameter, which will signify the onset of order at the phase transition. This parameter is called *order parameter* and its definition depends each time on the particular system of study. For the Ising model, this parameter is the magnetisation [Eq. (2.10)]. Above the critical temperature $T > T_c$ it is zero and the system is in the *paramagnetic phase* and for $T < T_c$ it takes non-zero values and the system is in the *ferromagnetic phase*.

There is also a close connection between the order parameter of the system and the symmetries of the Hamiltonian. Setting $H = 0$ in Eq. (2.1), we see that the Hamiltonian is invariant under a global flip of all spins (Z_2-symmetry). At $T > T_c$ the magnetisation is zero and spins do not have a preferred orientation, thus the symmetries of the Hamiltonian are

preserved. For $T < T_c$ the majority of spins are aligned to a specific direction (either up or down), hence the system in that phase has less symmetries than the Hamiltonian. This is known as *spontaneous symmetry breaking*, see, e.g., Refs. [8, 55]. For finite systems though, such a break of symmetry will *never* occur, as for $T < T_c$ the two ground states are equivalent and the system spends equal time in both states (for a sufficiently long time), resulting in a zero average magnetisation and hence the absence of a phase transition, see e.g., Refs. [57, 59]. This is also true though for the case where the number of spins is infinite, i.e., thermodynamic limit, and in the absence of a magnetic field. In order to break the symmetry then one has to introduce a magnetic field, which after the thermodynamic limit is taken, we set H to zero. The magnetic field aligns all spins to the direction of the field, meaning that one out of the two ground states is selected. After the thermodynamic limit is taken, setting $H = 0$ would result the spins to maintain their position, since flipping each one separately would require an infinite amount of energy. Lastly, note that the symmetry can be also broken if we *"force"* the spins on the boundaries to point in the same directions and then take the thermodynamic limit [56].

One of the striking features of phase transitions is the concept of *universality*, see, e.g., Refs. [61, 62]. It was experimentally realised that systems of different nature could have the same critical behaviour, as long as they have the same dimensionality, symmetry of the order parameter, and range of interactions. This means that the critical behaviour is independent of the microscopic details, and different systems could be grouped into broad classes characterised by the same critical properties, which are called *universality classes*. This provides a major aid, as one can characterise the critical behaviour of a certain class of systems, by studying the simplest possible model of that class. Although initially experimentally realised, universality is well-justified in the context of the *renormalization group*, which will be presented in the next section (Sec. 2.2).

2.2 Renormalization Group

In the development of the theory of phase transitions many characteristic features were extracted mainly from experimental data or theoretical assumptions, e.g., relations between scaling exponents, Widom's scaling hypothesis [63], universality. Renormalization group (RG) theory provides the appropriate description of phase transitions where the above facts arise naturally from the underlying theory. The theory was initiated by Kadanoff [11] and it was further developed by Wilson [12–14]. In principle, RG performs a coarse-graining transformation to the degrees of freedom of the system, which results in decreasing their number and changing the length scales of the system. At the critical temperature though, the correlation length is infinite and the system is *scale invariant*, thus a change of scales under this coarse-grained procedure will not change the properties of the system. The points where the system is invariant under the RG transformation are called *fixed points*. Besides the original papers of Kadanoff and Wilson, a discussion regarding the RG theory can be found in Refs. [3, 5–9, 64].

Let us consider an arbitrary system which is described by a Hamiltonian $\mathcal{H}$. In what follows we will absorb the factor $\beta = 1/k_{\mathrm{B}}T$ into the various parameters in $\mathcal{H}$, i.e., $\mathcal{H} \to \mathcal{H}/k_{\mathrm{B}}T$. This is known as the *reduced* hamiltonian. We introduce the renormalization group operator $\mathbf{R}$ which transforms $\mathcal{H}$ to a new Hamiltonian $\mathcal{H}'$, by reducing the number of degrees

of freedom from N to N'. The latter defines the *scale factor* b, as $b^d \equiv N/N'$, where d is the dimension of the system. The two Hamiltonians are related as follows:

$$\mathcal{H}' = \mathbf{R}\mathcal{H}. \tag{2.16}$$

For example in a magnetic system spins can be reduced by some coarse-graining procedure, where we replace a block of spins by a single spin according to some rule. This is known as *block-spin transformation*. Specifically, consider that we partition the lattice of $\mathcal{H}$ in Eq. (2.1) into blocks of length b, then each block will contain b^d spins. At each block i we now define a new spin variable σ_i' according to the following rule:

$$\sigma_i' = \begin{cases} +1, & \sum_{j\in\text{block}} \sigma_j > 0 \\ -1, & \sum_{j\in\text{block}} \sigma_j < 0 \end{cases}. \tag{2.17}$$

This is called the *majority rule*, as the sign of each spin σ_i' is determined by the majority of spins in the block [8, 65]. Note that in the case where the number of $+1$ spins is equal to the number of -1 spins in the block, one can proceed by choosing the value of σ_i' at random, giving equal probability to plus or minus sign. Thus, the renormalized Hamiltonian $\mathcal{H}'$ will have N' spins, which will take ± 1 values according to the rule of Eq. (2.17). Another rule that works quite well for one dimensional systems is the *decimation rule*, see, e.g., [8].

As the RG transformation only involves the reduction of the number of spins, the Hamiltonians $\mathcal{H}, \mathcal{H}'$ should still describe the same system, which means that the partition functions are invariant under this transformation:

$$Z_{N'}(\mathcal{H}') = Z_N(\mathcal{H}). \tag{2.18}$$

Rewriting now the free energy F to the reduced free energy, i.e., $F \to F/k_\text{B}T$, we have

$$\begin{aligned} f(\mathcal{H}) = \frac{F(\mathcal{H})}{N} =& \frac{1}{N} \ln Z_N(\mathcal{H}) = \\ & b^{-d} \frac{1}{N'} \ln Z_N(\mathcal{H}) = \\ & b^{-d} \frac{1}{N'} \ln Z_{N'}(\mathcal{H}') = b^{-d} f(\mathcal{H}'), \end{aligned} \tag{2.19}$$

where f is the reduced free energy per spin. Thus, the free energy of the two Hamiltonians are related by the scale factor b. This is the starting point for the extraction of the critical exponents, as we will see later on in this section.

Now the next step is to study the behaviour of $\mathcal{H}$ near the fixed point. For that let us express the Hamiltonian as

$$\mathcal{H} = \sum_i K_i A_i, \tag{2.20}$$

where A_i are local operators which are functionals of the degrees of freedom of the system, and K_i is its conjugate field, i.e., coupling constants. Let us denote as $K \equiv \{K_1, K_2, \ldots, K_n\}$ the vector which describes the position of the system in the multi-dimensional parameter space. The RG transformation corresponds then to a change (move) in this parameter space

$$K' = \mathbf{R}K. \tag{2.21}$$

If the system is at a *fixed point* of $\mathbf{R}$ it remains at that point,

$$K = \mathbf{R}K. \tag{2.22}$$

Now under the RG transformation the length scales are reduced by a factor b. Hence, we can write for the correlation length

$$\xi(K') = \xi(K)/b. \tag{2.23}$$

Since the correlation length decreases after an RG transformation, this means that the system moves away from the critical point. Though, if we are at the fixed point

$$\xi(K) = \xi(K)/b, \tag{2.24}$$

which indicates that ξ is either infinite of zero. The $\xi = \infty$ fixed points are called *critical fixed points* and the $\xi = 0$ *trivial fixed points*.

If our system is close to a fixed point, K^*, then $K_n = K_n^* + \delta K_n$. Performing an RG transformation $K' = \mathbf{R}K$, we can write K_n' as

$$\begin{aligned} K_n' = K_n^* + \sum_m \left.\frac{\partial K_n'}{\partial K_m}\right|_{K_m = K_m^*} \delta K_m + \mathcal{O}\left((\delta K)^2\right) = \\ K_n^* + \sum_m M_{nm}\delta K_m + \mathcal{O}\left((\delta K)^2\right), \end{aligned} \tag{2.25}$$

where

$$M_{nm} = \left.\frac{\partial K_n'}{\partial K_m}\right|_{K_m = K_m^*} \tag{2.26}$$

is the linearised RG transformation close to the fixed point K^*.

We denote the corresponding eigenvalues of the M matrix as λ_i, and we note that these should depend on the values of the scaling factor b, $\lambda_i(b)$. If we perform two successive RG transformations of scales b_1, b_2, then the total scale will change as $b_1 b_2$. For the eigenvalues that means [5, 6]

$$\lambda_i(b_1)\lambda_i(b_2) = \lambda_i(b_1 b_2). \tag{2.27}$$

Additionally, if the scale factor is $b = 1$, meaning that the RG transformation leaves the system unchanged, then $\lambda_i(1) = 1$. Consequently, this property in connection with Eq. (2.27) implies that the eigenvalues $\lambda_i(b)$ are of the form:

$$\lambda_i(b) = b^{y_i}, \tag{2.28}$$

where y_i is a number independent of b.

Neglecting now non-linear terms, Eq. (2.25) can be rewritten as

$$\delta K' = \mathbf{M}\delta K. \tag{2.29}$$

Expressing now δK in the base of the eigenvectors μ_i of the matrix $\mathbf{M}$, Eq. (2.29) becomes:

$$\delta K' = \mathbf{M}\sum_i c_i\mu_i = \sum_i c_i\, b^{y_i}\,\mu_i = \sum_i c_i'\,\mu_i, \tag{2.30}$$

where c_i, c_i' are coefficients satisfying the relation $c_i' = b^{y_i}c_i$. We see then that close to the fixed point the flow of the Hamiltonian in the parameter space depends strongly on the initial state c_i and on the sign of y_i. If $y_i > 0$ then c_i' increases under successive RG transformations and the system flows away from the fixed point. In that case the μ_i eigenvector is said to be *relevant*. If $y_i < 0$ then c_i' decreases under successive RG transformations and the system is moving closer to the fixed point. In that case the μ_i eigenvector is said to be *irrelevant*. If now $y_i = 0$, c_i' is not changing, and we cannot conclude from these linearised equations whether the system moves to or away from the fixed point. In that case the μ_i eigenvector is said to be *marginal*.

Under the RG transformation the free energy of Eq. (2.19) has contributions from an analytic and a non analytic part, which both are functions of K. The analytic part of the free energy can be understood as a *background* term, which does not exhibit any singular behaviour, even at the critical point [7, 8, 64]. Since we are interested in the critical behaviour of the system we can neglect the analytic part, and thus Eq. (2.19) can be written as

$$f_{\rm s}(K) = b^{-d} f_{\rm s}(K'), \tag{2.31}$$

where the subscript s stands for the singular (non analytic) part of the free energy. Near the fixed point K, K' can be written in terms of $\{c_i, c_i'\}$ respectively and recalling that $c_i' = b^{y_i}c_i$ we can write

$$f_{\rm s}(c_1, c_2, c_3, \dots) = b^{-d} f_{\rm s}(b^{y_1}c_1, b^{y_2}c_2, b^{y_3}c_3, \dots). \tag{2.32}$$

For a magnetic system, such as the Ising model, the two relevant variables are $c_1 = t, c_2 = h$, where $t \equiv (T - T_{\rm c})/T_{\rm c}$ and $h \equiv H/k_{\rm B}T$, and we will rename y_1, y_2 to y_t, y_h, which is considered as the standard notation. Thus, Eq. (2.32) can be written as

$$f_{\rm s}(t, h, c_3, \dots) = b^{-d} f_{\rm s}(b^{y_t}t, b^{y_h}h, b^{y_3}c_3, \dots). \tag{2.33}$$

Note that c_3 is an irrelevant variable ($y_3 < 0$), which should vanish in the limit of infinite RG transformations; the same applies to the rest of the irrelevant variables (if present). With appropriate derivations of Eq. (2.33) we can extract the relation between y_t, y_h and the critical exponents. For example, we consider here the specific heat at zero field which scales as $C|_{H=0} \sim t^{-\alpha}$. Hence[3],

$$C|_{h=0} \sim \left.\frac{\partial^2 f_{\rm s}}{\partial t^2}\right|_{h=0} = b^{-d+2y_t}\widetilde{f}(b^{y_t}t, 0) = t^{d/y_t-2}\widetilde{f}(\pm 1, 0), \tag{2.34}$$

from which we can read off that $\alpha = 2 - d/y_t$. Note that for the last step in Eq. (2.34) we proceed by setting $b^{y_t}|t| = 1$, which moves the temperature dependence to the prefactor while

[3] Note that we have set the irrelevant variables to zero here.

leaving the function with a constant argument. Following the same procedure for the rest of the observables, the critical exponents can be expressed as follows [5, 6, 8]:

$$\alpha = 2 - \frac{d}{y_t}, \tag{2.35a}$$

$$\beta = \frac{d - y_h}{y_t}, \tag{2.35b}$$

$$\gamma = \frac{2y_h - d}{y_t}, \tag{2.35c}$$

$$\delta = \frac{y_h}{d - y_h}, \tag{2.35d}$$

where we can immediately deduce the following scaling relations

$$a + 2\beta + \gamma = 2, \tag{2.36}$$

$$\gamma = \beta\left(\delta - 1\right). \tag{2.37}$$

Additional exponents could be derived from the scaling form of the correlation function, which under an RG transformation can be written as [8]

$$G\left(\vec{r}, t, h, c_3, \dots\right) = b^{-2(d-y_h)} G\left(b^{-1}\vec{r}, b^{y_t} t, b^{y_h} h, c_3, \dots\right). \tag{2.38}$$

Setting $b^{y_t}\left|t\right| = 1$ and $h = 0$ to Eq. (2.38) and omitting the irrelevant variables we obtain

$$G\left(\vec{r}, t\right) = t^{2(d-y_h)/y_t} G\left(\vec{r}t^{1/y_t}, 1\right). \tag{2.39}$$

From Eq. (2.14) we see that for large distances $\vec{r}$, G behaves as $e^{-|\vec{r}|/\xi}$, thus we can identify the correlation length as $\xi \sim |t|^{-1/y_t}$. Additionally, as the critical temperature is approached ξ diverges with an exponent ν as $\xi \sim |t|^{-\nu}$, and consequently we have [7, 8]

$$\nu = \frac{1}{y_t}. \tag{2.40}$$

At the critical point $t = 0$, according to Eq. (2.38) G takes the form

$$G\left(\vec{r}\right) \sim \left|\vec{r}\right|^{-2(d-y_h)}, \tag{2.41}$$

where we have set $h = 0$, and $b = |\vec{r}|$; the irrelevant variables are ignored. Thus, comparing Eq. (2.41) with Eq. (2.15) we have for the critical exponent η:

$$\eta = d + 2 - 2y_h. \tag{2.42}$$

From ν and η we can write two more relations among the critical exponents [6–8]

$$a + d\nu = 2, \tag{2.43}$$

$$\gamma = \nu\left(2 - \eta\right), \tag{2.44}$$

where Eq. (2.43) is called *hyperscaling* relation. This is valid below and at the *upper critical dimension* d_u; d_u is the dimension above which the critical exponents are assigned their mean field values [7, 8]. For $d > d_u$ not only Eq. (2.43) fails but the whole RG description, as presented above, needs to be reformulated in order to predict the correct exponents [8, 66]. For a discussion regarding hyperscaling see Ref. [67].

2.3 Finite-size Scaling

Phase transitions occur in the limit where the size of the system goes to infinity, where thermodynamic quantities approach zero or they diverge as the critical point is approached. On the other hand, in experiments on real systems or numerical methods, such as Monte Carlo simulations, the size of the system is finite. Hence, a question arises: Is there a way from which we can probe the asymptotic behaviour of the infinite system by studying systems of finite size? The answer is affirmative, and it can be accomplished under the framework of *finite-size scaling* (FSS); see Refs. [68–71] for some standard bibliography.

Using the renormalization group language of Sec. 2.2, the free energy density for a finite system of linear size L can be expressed under a renormalization group transformation of a scaling factor b as [70, 72, 73]

$$f\left(t, h, L^{-1}\right) = b^{-d} f_{\mathrm{s}}\left(b^{y_t} t, b^{y_h} h, b^{y_1} u, b L^{-1}\right) + f_{\mathrm{a}}\left(t, h\right), \tag{2.45}$$

where the relevant field variables $t \equiv (T - T_{\mathrm{c}})/T_{\mathrm{c}}$ and $h \equiv H/k_{\mathrm{B}}T$ are the reduced temperature and magnetic field, respectively. The exponents y_t and y_h are the relevant (positive) eigenvalues of t and h. For simplicity we consider only one irrelevant scaling field u which corresponds to the *largest* irrelevant (negative) eigenvalue y_1. Using the standard notation [74, 75] we define $y_1 \equiv -\omega$, where ω is the *leading correction-to-scaling exponent*. The function f_{s} is the singular part of the free energy density, and f_{a} is the analytic part resulting from the RG transformation [75]. By setting now $L = b$, Eq. (2.45) gives

$$f\left(t, h, L^{-1}\right) = L^{-d} f_{\mathrm{s}}\left(L^{y_t} t, L^{y_h} h, L^{-\omega} u\right) + f_{\mathrm{a}}\left(t, h\right). \tag{2.46}$$

Taking appropriate derivates of Eq. (2.46) with respect to t and h, various thermodynamic quantities can be extracted. For example, the derivative of f with respect to h gives the magnetisation per spin,

$$m = -\frac{\partial f}{\partial h} = L^{-d+y_h}\, \widetilde{m}\left(L^{y_t} t, L^{y_h} h, L^{-\omega} u\right) = L^{-\beta/\nu}\, \widetilde{m}\left(L^{y_t} t, L^{y_h} h, L^{-\omega} u\right), \tag{2.47}$$

where the β/ν exponent results from the scaling relations of Eqs. (2.35c) and (2.40). Additionally, the analytical part of the free energy f_{a} does not scale with L, thus as far as the scaling behaviour of m is concerned, it can be neglected [8]. Considering similar derivatives of the free-energy density, the specific heat, and magnetic susceptibility scaling forms can be obtained. Additionally, if we are interested in the case of zero magnetic field ($h = 0$) and we neglect corrections to scaling the above quantities (all considered per spin here) take the form

$$c = L^{\alpha/\nu}\widetilde{c}\left(tL^{1/\nu}\right), \tag{2.48a}$$

$$m = L^{-\beta/\nu}\widetilde{m}\left(tL^{1/\nu}\right), \tag{2.48b}$$

$$\chi = L^{\gamma/\nu}\widetilde{\chi}\left(tL^{1/\nu}\right), \tag{2.48c}$$

where $\widetilde{c}$, $\widetilde{m}$, and $\widetilde{\chi}$ are called *scaling functions*, and they are independent of L, up to the point where corrections to scaling are not important. Note that corrections to scaling can be neglected if we are close to the critical point and for relatively large system sizes [74].

Thus, one can utilise Eq. (2.48), to extract the critical exponents. Additionally, the critical exponent ν and critical temperature T_c need also to be obtained. For the exponent ν, Binder showed [76] that the probability distribution of the magnetisation can be expressed as

$$P(m) = L^{\beta/\nu}\widetilde{P}\left(\xi/L, mL^{\beta/\nu}\right), \tag{2.49}$$

where $\widetilde{P}$ is a scaling function. The n-th order cumulant of the magnetisation can then be expressed as [75, 76]

$$\begin{aligned}\langle m^n\rangle &\equiv L^{\beta/\nu}\int dm\, m^n \widetilde{P}\left(\xi/L, mL^{\beta/\nu}\right)\\ &\sim L^{-n\beta/\nu}\int dz\, z^n \widetilde{P}\left(\xi/L, z\right) = L^{-n\beta/\nu}\widetilde{P}_k(\xi/L),\end{aligned} \tag{2.50}$$

where $z = mL^{\beta/\nu}$ and $\widetilde{P}_k$ as a new scaling function. The fourth-order Binder cumulant of the magnetisation [76], is defined as[4]

$$Q = 1 - \frac{\langle m^4\rangle}{3\langle m^2\rangle^2}, \tag{2.51}$$

which is a dimensionless quantity, that does not scale with the size of the system. It is easy to check from Eqs. (2.50) and (2.51), that the maximum of the derivative of the Binder cumulant with respect to temperature scales as

$$\left.\frac{dQ}{dT}\right|_{\max} \sim L^{1/\nu}. \tag{2.52}$$

Thus, one can use Eq. (2.52) to obtain the exponent ν. An alternative method for the estimation of the ν exponent is proposed in Ref. [74]. In that, ν is estimated by considering logarithmic derivatives of powers of the magnetisation with respect to temperature, i.e.,

$$\frac{\partial}{\partial T}\ln\langle m^n\rangle = \frac{1}{\langle m^n\rangle}\frac{\partial}{\partial T}\langle m^n\rangle = \frac{1}{T^2}\left(\frac{\langle m^n E\rangle}{\langle m^n\rangle} - \langle E\rangle\right), \tag{2.53}$$

where the maximum of the slope should scale similar to Eq. (2.52) [74], i.e.,

[4]Similar cumulants can be defined for the internal energy, i.e., $Q_E = 1 - \frac{\langle E^4\rangle}{3\langle E^2\rangle^2}$.

$$\left.\frac{\partial \ln \langle m^n \rangle}{\partial T}\right|_{\max} \sim L^{1/\nu}. \tag{2.54}$$

After ν has been estimated, one can proceed with the estimation of the critical temperature. For that, one well established technique is known as the *crossing method* [76], where one considers pairs of system sizes (L_1, L_2) , with $L_1 < L_2$, and the critical temperature is determined from the crossings of these curves. Specifically, it can be shown [76, 77] that the temperatures where such pairs of system sizes cross $T_{\rm cross}(L)$ scales with the system size as

$$T_{\rm cross}\,(L, r) = T_{\rm c} + a_3 L^{-1/\nu-\omega}\left(\frac{r^{-\omega}-1}{r^{1/\nu}-1}\right), \tag{2.55}$$

where a_3 is a non-universal scaling parameter, $r \equiv L_2/L_1$ is the ratio of the two system sizes, ω is the leading correction-to-scaling exponent, and L can be either the smaller (L_1) or the larger (L_2) system size of each considered pair.

A more commonly used approach for the estimation of the critical point, is from the location of the peaks of various thermodynamic quantities, such as the specific heat or the magnetic susceptibility [74]. For finite systems the location of the peaks correspond to the position where the scaling function becomes maximum, cf. Eqs. (2.48a) and (2.48c). Thus, if the maximum, say of the specific heat, is at $L^{1/\nu}t^* \equiv x^*$ then one can write

$$\frac{T^*(L) - T_{\rm c}}{T_{\rm c}}\, L^{1/\nu} = x^*, \tag{2.56}$$

or equivalently

$$T^*(L) = T_{\rm c} + T_{\rm c}\, x^* L^{1/\nu}. \tag{2.57}$$

Thus the location of the peaks as a function of L creates a sequence of pseudo-critical points $T^*(L)$, which approach the asymptotic temperature of the infinite system $T_{\rm c}$ as the size of the system increases. Note, that Eq. (2.57) is valid as long as the sizes of the systems are relatively large and for temperatures close to $T_{\rm c}$, otherwise one has to consider scaling correction terms [74].

If we now want to calculate α/ν, β/ν or γ/ν, an a priori knowledge of the infinite-volume critical temperature results in constant expressions for the scaling functions of Eqs. (2.48). Thus, exponent ratios could be determined by plotting the involved observable as a function of L on a log-log plot and calculating the slope (using a fitting routine) of this straight line. This can also be accomplished by considering the pseudo-critical points $T^*(L)$, as described above, which results again in constant scaling functions. In any case, however, if corrections to scaling are strong then the above procedure is no longer valid and one has to take them into account [74], i.e.,

$$A = b_1 L^x \left(1 + b_2 L^{-\omega}\right), \tag{2.58}$$

where A is one of the c, m, χ of Eqs. (2.48) with x the appropriate exponent, ω is the leading correction-to-scaling exponent and b_1, b_2 are non-universal scaling parameters.

Practical implementations of all the above, as well other, FSS schemes have been developed over the years to the analysis of critical phenomena, see Refs. [64, 74, 78–82] for some

examples. From the above discussion it is clear that FSS is an important tool for the identification of critical exponents. Although, the discussion here was limited to the case where the external parameters were the temperature and the magnetic field, same considerations are applicable to other systems which exhibit critical behaviour, provided that a suitable control parameter(s) exist. In the following section percolation is discussed, which is one of simplest models that exhibits a phase transition, and has a close connection with the study of phase transitions in spin systems. In this framework, FSS is an important tool in the investigation of the critical properties of percolation models and it has been extensively used in this thesis too.

2.4 Percolation

2.4.1 Ordinary percolation

Percolation is one of the simplest models that exhibits a phase transition [18–20]. In order to define the model let us consider a d-dimensional lattice where each site is occupied *independently* with a probability $p \in [0, 1]$. A *cluster* is defined as an object, constituted of neighbouring occupied sites. For small values of p we have few clusters of small size but for p values close to one there exists a cluster that spans the whole lattice with size proportional to the system. The size of this spanning cluster becomes infinite as the size of the system goes to infinity. The existence of an infinite spanning cluster is related to a value p_c called the *percolation threshold*, below which only clusters of finite size emerge while above it an infinite cluster appears in the infinite system. Percolation focuses on the study of the properties of such clusters.

The above system defines the site percolation problem. Another variant is the bond percolation, where all sites are occupied and bonds are placed randomly between neighbouring sites in the lattice. A cluster is then defined by groups of sites connected by bonds. Further modifications of percolation exist ranging from the site-bond percolation to more exotic variants such as explosive and bootstrap percolation, which are beyond the scope of the present thesis; for different variants of percolation see e.g., Ref. [83] and references therein. Now we turn our attention to the basic observables which are necessary for the description of the percolation transition.

From the above discussion it is clear that the percolation transition is evidenced by the appearance of a spanning cluster for $p > p_c$, while only finite-size clusters occur for $p < p_c$ [19]. Exactly at p_c there is no spanning cluster with probability one, but rather very large clusters [84]. From that we define the *spanning probability* $R(p)$, which for a fixed value of p gives the probability that a spanning cluster occurs. For finite systems, R is a smooth increasing function of p, which varies from 0 at $p = 0$ to 1 at $p = 1$. As the size of the system increases, $R(p)$ becomes sharper near p_c and transforms into a step-function when the size of the system is infinite, where $R(p) = 0$ for $p < p_c$ and $R(p) = 1$ for $p > p_c$. Another quantity of interest is the *percolation strength*, $P_\infty(p)$, which denotes the probability that a site belongs to the infinite cluster. For $p < p_c$, $P_\infty(p)$ is zero as there is no spanning cluster while it takes non-zero values for $p > p_c$ and $P_\infty = 1$ at $p = 1$ meaning that all spins belong to the cluster. Similar to magnetisation of the Ising model, P_∞ serves as an order parameter for the percolation problem. Additionally, a useful quantity is the *cluster size distribution* $n_s(p)$, which denotes the number of finite size clusters containing s sites, per lattice site. Since

$s\,n_s(p)$ gives the probability that a site belongs to a finite size cluster of size s, we can write the following relation [19]

$$\sum_s s n_s(p) + P_\infty(p) = p, \tag{2.59}$$

where the sum is restricted to finite size clusters.

Now, the *average cluster size* S of the finite size clusters can be computed as follows

$$S(p) = \frac{\sum_s s^2 n_s(p)}{\sum_s s n_s(p)}. \tag{2.60}$$

Note that the sums in Eq. (2.60) are restricted to finite size clusters only. The above definition is consistent with what the average cluster size would be if we randomly pick a site that belongs to a finite cluster, whereas $\sum_s s n_s(p)/\sum_s n_s(p)$ is consistent with what the average cluster size would be if every cluster was chosen with equal probability [19].

We can now define the correlation function $G_{\rm C}(r)$, which gives the probability that two sites at distance $|\vec{r}|$ belong to the same cluster[5]. Away from the critical point and for large distances $G_{\rm C}(|\vec{r}|)$ decays exponentially,

$$G_{\rm C}(\vec{r}) \sim e^{-|\vec{r}|/\xi}, \quad |\vec{r}| \gg \xi, \tag{2.61}$$

where the correlation length ξ is related to the average distance between two sites that belong to the same cluster and it can be defined from the second moment of the correlation function as [19]

$$\xi^2 = \frac{\sum_r r^2 G_{\rm C}(\vec{r})}{\sum_r G_{\rm C}(\vec{r})}. \tag{2.62}$$

This is known as the *second moment correlation length*[6].

The m-th moment of the cluster size distribution is given as $M_m(p) = \sum s^m n_s(p)$. Several observables, as the ones introduced above, can be written in terms of specific moments of the cluster size distribution as [18, 19, 83]

$$\text{Average number of clusters, } A(p): \qquad A(p) \sim \sum n_s(p), \tag{2.63a}$$

$$\text{Percolation strength, } P_\infty(p): \qquad P_\infty(p) \sim 1 - \sum s\, n_s(p), \tag{2.63b}$$

$$\text{Average cluster size, } S(p): \qquad S(p) \sim \sum s^2\, n_s(p). \tag{2.63c}$$

Exactly at p_c, the correlation length diverges, $\xi \to \infty$, such that the system is scale invariant and the percolating cluster behaves as a self-similar (fractal) object. This is valid also for $p \neq p_c$ as long as the length-scale L on which the system is investigated is much smaller than the correlation length; here L can be regarded as the scaling window on which we observe the infinite system or the linear size of a finite system. For $L \ll \xi$ the mass of the cluster M will scale as $M \sim L^D$, where D is the fractal dimension of the cluster. Above p_c

[5] The subscript C declares that, such observables are defined in the context of percolation.

[6] Note that the ξ's as defined in Eqs. (2.61) and (2.62) are not equivalent, though their difference is quite small; see the discussion in Ref. [85].

we have $L \gg \xi$, and the infinite cluster is a homogeneous object of mass $M \sim \xi^D (L/\xi)^d$ [19], where d is the dimensionality of the system. Thus, the scaling behaviour of the percolating cluster can be summarized as follows,

$$M \sim \begin{cases} L^D, & L \ll \xi \\ \xi^D (L/\xi)^d, & L \gg \xi. \end{cases} \tag{2.64}$$

In the vicinity of p_c the cluster size distribution takes the form [19]

$$n_s \sim s^{-\tau} f\left(c\left(p\right) s\right), \tag{2.65}$$

where τ is a critical exponent, and $c\left(p\right)$ vanishes at p_c as $c\left(p\right) \sim |p - p_c|^{1/\sigma}$, which defines the σ exponent. As a consequence, near p_c observables exhibit a power-law behaviour of the form [18, 19]

$$\text{Average number of clusters, } A(p): \qquad A(p) \sim |p - p_c|^{2-\alpha}, \tag{2.66a}$$

$$\text{Percolation strength, } P_\infty(p)\,(p > p_c): \qquad P_\infty(p) \sim (p - p_c)^{\beta}, \tag{2.66b}$$

$$\text{Average cluster size, } S(p): \qquad S(p) \sim |p - p_c|^{-\gamma}, \tag{2.66c}$$

$$\text{Correlation length, } \xi(p): \qquad \xi(p) \sim |p - p_c|^{-\nu}, \tag{2.66d}$$

where α, β, γ, ν are the critical exponents. These exponents, including D, are not independent and can be expressed in terms of τ, σ as [18, 19]

$$2 - \alpha = \frac{\tau - 1}{2}, \qquad \beta = \frac{\tau - 2}{\sigma}, \qquad \gamma = \frac{3 - \tau}{\sigma}, \qquad D = \frac{d}{\tau - 1}, \qquad \nu = \frac{\tau - 1}{d\,\sigma}, \tag{2.67}$$

from which we can obtain the following relations

$$\alpha + 2\beta + \gamma = 2, \qquad D = \frac{1}{\nu}\left(\beta + \gamma\right). \tag{2.68}$$

Assuming now that *hyperscaling* holds we have

$$d\,\nu = 2 - \alpha, \qquad D = d - \frac{\beta}{\nu}. \tag{2.69}$$

The last equation of Eq. (2.69) can be obtained from the fact that the mass M is proportional to $L^d P_\infty$ and equating this with Eq. (2.64) and expressing everything in terms of $(p - p_c)$ with the use of Eqs. (2.66b) and (2.66d).

In two dimensions exact results give $\tau = 187/96$ and $\sigma = 36/91$, and in three dimensions best estimates are $\tau \approx 2.18$ and $\sigma \approx 0.45$ [19]. The upper critical dimension is $d_u = 6$ and the obtained exponents for $d \geq 6$ are $\alpha = -1$, $\beta = \gamma = 1$, $\nu = \sigma = 1/2$ and $\tau = 5/2$. Thus, while Eqs. (2.68) holds for any dimension, Eqs. (2.69) becomes invalid for $d > 6$.

2.4.2 Correlated percolation

In Sec. 2.4.1 we introduced the theory of percolation, as one of the simplest models that possesses a phase transition. The crucial feature of this model was that sites on the lattice were occupied independent of each other. However, percolation can also be extended to the case where correlations among sites exist. One example, which is closely related to critical phenomena, is the use of clusters in the study of liquid-gas or ferromagnetic-paramagnetic transitions. In such cases one attempts to transform the problem of interacting particles or spins (for the case of magnets) to a problem of non-interacting clusters [18]. If such clusters are properly defined then one can utilise them to study the critical behaviour of the system. The properties of such clusters were described by Fisher [86] in his *droplet model*, where the constructed clusters should percolate at the transition point, the correlation length of the clusters should be the same with that of the actual model, and that the mean cluster size should diverge as the susceptibility.

Specifically, for the Ising model, these clusters were initially constructed by neighbouring spins in the same state (geometrical clusters), and it was believed that such clusters should describe the critical behaviour of the system. It was shown numerically [87] and then rigorously proven [29–31], that in two dimensions such clusters percolate at the Ising critical point, however the average cluster size diverge with an exponent different from the one of the magnetic susceptibility - this was shown by using series expansions at [88] and later it has been shown exactly at [89]. Additionally, in three dimensions it was shown numerically [90] that the "minority" spins percolate at a temperature lower than the critical one. As it turned out geometrical clusters are too big to properly describe the critical behaviour of the system. One reason is because of correlations and the other is purely geometrical [26, 91]. At infinite temperature and zero magnetic field there are no correlations among spins resulting in a concentration $p = 0.5$ of up and down spins. If spins are placed in a lattice with $p_c < 0.5$, e.g., simple cubic lattice with $p_c \approx 0.3$, percolating clusters of up and down spins will occur. Thus, even in the absence of correlations among spins percolating clusters will emerge, making geometrical clusters inadequate for the description of the critical behaviour of the system.

The appropriate geometrical description was given by Fortuin and Kasteleyn [22–25], where they showed that the q-state Potts model is equivalent to a site-bond percolation problem (random cluster model) [92]. Given the connection between these models, clusters are defined as neighbouring spins with same orientation which are also connected by an additional bond of certain probability. These Fortuin and Kasteleyn clusters (FK) percolate at the critical temperature of the system, and more importantly they encode the critical behaviour of the system, resulting in critical exponents identical to the thermal ones.

2.4.3 Random cluster model

In this section we present the random cluster model and its connection with the q-state Potts model. Here we will follow a more mathematical representation compared to Sec. 2.4.1, as we believe that it will address in a more concrete way the key features of the model.

We consider a graph (lattice) with V vertices and E edges, i.e., $G = (V, E)$. On each edge $e \in E$ we assign a vector $\omega = (\omega(e) : e \in E)$, where we consider the edge e to be *open* if $\omega(e) = 1$ and *closed* if $\omega(e) = 0$. The set of possible bond configurations is denoted as

$\Omega = \{0,1\}^E$, members of which are the vectors $\omega(e)$. We denote by $C(\omega)$ the number of connected components (clusters).

Let now $p \in [0,1]$ be the probability that a bond is open, respectively $(1-p)$ for a bond to be closed, and each cluster is weighted by a factor of $q \in (0,\infty)$. The measure $\phi_{p,q}$ on a configuration $\omega \in \Omega$ is given as [92]

$$\phi_{p,q}(\omega) = \frac{1}{Z_{\mathrm{RC}}} q^{C(\omega)} \prod_{e \in E} p^{\omega(e)} (1-p)^{1-\omega(e)}, \tag{2.70}$$

where Z_{RC} is the partition function of the random cluster model given by

$$Z_{\mathrm{RC}}(p,q) = \sum_{\omega \in \Omega} \left\{ q^{C(\omega)} \prod_{e \in E} p^{\omega(e)} (1-p)^{1-\omega(e)} \right\}. \tag{2.71}$$

Note that setting $q = 1$ to Eq. (2.71) we obtain the ordinary bond percolation, i.e., each edge is open or closed independently with probability p and $(1-p)$ respectively.

Let us now define the q-state Potts model, where on each vertex i of G we assign a variable σ_i which can take one of the $1, 2, \ldots, q$ possible values. We can then define as sample space the set $\Sigma = \{1, 2, \ldots, q\}^V$ and a configuration $\sigma = (\sigma_i : i \in V) \in \Sigma$. Thus, the Hamiltonian of the model can be written as

$$H = -J \sum_{e \in E} \delta_{\sigma_i \sigma_j}, \tag{2.72}$$

where δ_{ij} is the Kronecker delta, and J is the edge-strength. For $q = 2$ we can rewrite $\delta_{\sigma_i \sigma_j}$ as $\frac{1}{2}(\sigma_x \sigma_y + 1)$, which apart from an unimportant constant is the Ising model for coupling-strength $J' = 2J$. A probability measure is given then as

$$\pi_{\beta,q}(\sigma) = \frac{e^{-\beta H(\sigma)}}{Z_{\mathrm{P}}}, \tag{2.73}$$

where β is the inverse temperature $\beta = 1/T$ (where the Boltzmann's constant is $k_{\mathrm{B}} = 1$) and Z_{P} is the partition function of the Potts model. Fortuin and Kasteleyn showed that the Potts models can be recast as random cluster models, and thermal quantities of the Potts model can be understood via the cluster properties of the random cluster models [22–25]. The connection between the two models can also be seen under the representation of Edwards and Sokal [92, 93], where they defined a site-bond-correlated percolation problem of interacting Potts spins along with bond variables which are activated by a certain choice of the bond probability $p = 1 - e^{-\beta J}$. Starting from the product sample space $\Sigma \times \Omega$, where $\Sigma = \{1, 2, \ldots, q\}^V$ and $\Omega = \{0,1\}^E$, we can define a measure $\mu(\sigma, \omega)$ as

$$\mu(\sigma,\omega) = Z^{-1} \prod_{e \in E} \left\{ (1-p)\, \delta_{\omega(e),0} + p\, \delta_{\omega(e),1}\, \delta_e(\sigma) \right\}, \tag{2.74}$$

where $\delta_e(\sigma)$ is $\delta_{\sigma_i \sigma_j}$, and Z is the partition function of this product space which is defined as

$$Z = \sum_{(\sigma,\omega) \in \Sigma \times \Omega} \prod_{e \in E} \left\{ (1-p)\, \delta_{\omega(e),0} + p\, \delta_{\omega(e),1}\, \delta_e(\sigma) \right\}. \tag{2.75}$$

Consequently the measure of the Potts Eq. (2.73) and the measure of the random cluster model Eq. (2.70) are coupled via the measure of Eq. (2.74), which is called the *Edwards-Sokal coupling*.

Under this representation we can derive the following [92, 93]:

1. The *marginal* measure on Σ, $\mu_1(\sigma) = \sum_{\omega\in\Omega}\mu(\sigma,\omega)$, is the Boltzmann measure of the q-state Potts model at temperature β:

$$\mu_1(\sigma) = \frac{1}{Z_{\mathrm{P}}}\exp\left\{-\beta\sum_{e\in E}\delta_e(\sigma)\right\}.$$

2. The *marginal* measure on Ω, $\mu_2(\omega) = \sum_{\sigma\in\Sigma}\mu(\sigma,\omega)$, is the random cluster model with p, q parameters:

$$\mu_2(\omega) = \frac{1}{Z_{\mathrm{RC}}}\, q^{\,C(\omega)} \prod_{e\in E} p^{\omega(e)}\,(1-p)^{1-\omega(e)}\,.$$

3. The partition functions $Z_{\mathrm{P}}, Z_{\mathrm{RC}}$ satisfy the following equation

$$Z_{\mathrm{RC}} = e^{-\beta|E|}Z_{\mathrm{P}},$$

   where $|E|$ is the number of edges.

4. The *conditional* measure $\mu(\sigma\,|\,\omega)$ on Σ is obtained by assigning on each connected component (cluster) a value chosen equiprobably from the set $\{1, 2, \ldots, q\}$, thus all spins that belongs in the same cluster have the same value.

5. The *conditional* measure $\mu(\omega\,|\,\sigma)$ on Ω is obtained by setting $\omega(e) = 0$ if for the edge e, which connects the i, j vertices, $\sigma_i \neq \sigma_j$ and if $\sigma_i = \sigma_j$ then $\omega(e) = 1$ with probability p or $\omega(e) = 0$ with probability $1 - p$.

6. The probability that two vertices i, j belong to the same cluster is proportional to the two-point correlation function of spins σ_i, σ_j.

Therefore, we see that the Edwards-Sokal coupling provides a clear connection between the Potts and the random cluster model. As a final remark to this section we note that the above conclusions resulting from the Edward-Sokal representation can be extended to the case where the interactions among spins are generally different, as long as they are positive. Unfortunately, in the presence of frustration (see Sec. 2.5) this is no longer valid.

2.4.4 Geometrical clusters

Although intuitively plausible, geometrical clusters fail to properly describe the phase transition of the q-state Potts model, whereas the FK formulation turns out to be the *"success story"* behind such a description. Nonetheless, geometrical clusters still possess features which make them interesting to study on an individual basis. Geometrical clusters of the q-state Potts model define a site correlated percolation process which still undergoes a (percolation)

transition. In the limiting case of infinite temperature, $T \to \infty$, one recovers ordinary (site) percolation and for $T = 0$ one arrives at the FK definition of clusters ($p = 1$). Additionally, it has been argued that geometrical clusters provide a description of the tricritical Potts model for $q \leq 4$ in two dimensions, which also reflects a connections between geometrical and FK clusters [32, 33].

Moreover, cluster boundaries of two-dimensional critical systems have been studied analytically in the framework of *stochastic Loewner evolution* (SLE). SLE was introduced by Schramm [94] based on the work of Loewner, and is a subject of probability theory where families of random planar curves with conformally invariant probability measures are generated. Several results of critical exponents that were conjectured before under the Coulomb gas mapping [34–38] or conformal invariance [39] have been rigorously obtained from this method (for an overview see Refs. [95–98]).

In two dimensions the q-state Potts model undergoes a continuous phase transition for $q \leq 4$ and turns to first-order for $q > 4$. This has been initially stated by Baxter [99], in connection with other statistical models, but renormalization group approaches could not reveal the first-order character for $q > 4$. By extending the pure model to include vacant sites Nienhuis et al. [100] managed to show the first-order nature of the transition and provide indications of a relation between critical and tricritical behaviour. Specifically, the geometrical clusters of the pure Potts model encode the tricritical behaviour of the site-diluted Potts model. Stella and Vanderzande showed [89, 101] this connection for the $q = 2$ Potts model, i.e., Ising model, and the $q = 1$ tricritical Potts model. In line with arguments from renormalization, conformal invariance, and numerical simulations they found that the critical exponents of the geometrical clusters of the two-dimensional Ising model are given by the critical exponents of the $q = 1$ tricritical Potts model. These results were then generalized for $q \leq 4$ [102, 103]. The connection between critical and tricritical branches also dictates a connection between geometrical and FK clusters, i.e., the two cluster types are mapped with the same transformation that maps the critical and tricritical regimes.

Following the notation of [32], the q-state Potts model can be parametrized as follows [35]

$$\sqrt{q} = -2\cos(\pi/\kappa), \quad 1 \leq \kappa \leq 2, \quad \text{and} \quad \kappa = \frac{1+m}{m}, \quad m = 1, 2, 3, \ldots \tag{2.76}$$

where κ is connected to the central charge c via [39]

$$c = 1 - \frac{6\,(1-\kappa)^2}{\kappa}. \tag{2.77}$$

From Eqs. (2.76) and (2.77) we see that $\kappa = 2,\ 3/2,\ 4/3,\ 6/5$ correspond to $q = 0,\ 1,\ 2,\ 3,\ 4$ Potts models with $c = -2,\ 0,\ 1/2,\ 4/5,\ 1$, respectively.

With the above formulation various fractal dimensions of the FK clusters can be expressed

in terms of κ [37, 104, 105]

$$y_t = 1 - \frac{3}{2}\kappa, \tag{2.78a}$$

$$D = 1 + \frac{1}{2\kappa} + \frac{3}{8}\kappa, \tag{2.78b}$$

$$D_{\mathrm{h}} = 1 + \frac{\kappa}{2}, \tag{2.78c}$$

$$D_{\mathrm{ep}} = 1 + \frac{1}{2\kappa}, \tag{2.78d}$$

$$D_{\mathrm{rb}} = 1 - \frac{3}{2\kappa} + \frac{\kappa}{2}, \tag{2.78e}$$

where $y_t = 1/\nu$ is the thermal eigenvalue, D the fractal dimension, D_{h} the fractal dimension of the hulls, D_{ep} the fractal dimension of the external perimeter, and D_{rb} the fractal dimension of the red bonds. In ordinary percolation sites are considered in the *hull*, if they belong to the cluster and are neighbours with vacant sites which are connected to the outside. *External perimeter* sites are vacant sites connected to the outside of the cluster, which neighbour sites that belong to the hull of the cluster. For both cluster boundaries see Refs. [106, 107], also see Ref. [33] for a nice illustration of the difference between hull and external perimeter sites. The *red bonds* [26, 108] correspond to bonds that upon deleting one of them the cluster splits. Additionally, the are certain relations among the various fractal dimensions introduced above, see Ref. [32] and references therein.

The mapping of the two cluster types is reflected in the fact that both have the same central charge [103]. From Eq. (2.77) it is easy to see that for given c the two values of κ (κ_+, κ_-) satisfy the relations $\kappa_+\kappa_- = 1$, with $\kappa_+ \geq 1$ and $\kappa_- \leq 1$. Thus, the central charge is invariant under the transformation $\kappa \to 1/\kappa$, i.e., $c(\kappa) = c(1/\kappa)$, where $\kappa \equiv \kappa_+$. Applying this transformation to the set of Eqs. (2.78) we obtain [32]

$$y_t^{\mathrm{g}} = 1 - \frac{3}{2\kappa}, \tag{2.79a}$$

$$D^{\mathrm{g}} = 1 + \frac{1}{2}\kappa + \frac{3}{8\kappa}, \tag{2.79b}$$

$$D_{\mathrm{h}}^{\mathrm{g}} = 1 + \frac{1}{2\kappa}, \tag{2.79c}$$

$$D_{\mathrm{rb}}^{\mathrm{g}} = 1 - \frac{3\kappa}{2} + \frac{1}{2\kappa}. \tag{2.79d}$$

These exponents are in agreement with the ones of the geometrical clusters for $1 \leq \kappa \leq 2$ [89, 102, 103], hence the superscript g. Thus we can conclude that the geometrical clusters are images of the FK clusters under the transformation $\kappa \to 1/\kappa$. Finally, the external perimeter of the FK clusters has no image under the transformation because geometrical clusters are characterized by only one fractal dimension, i.e., $D_{\mathrm{ep}}^{\mathrm{g}} = D_{\mathrm{h}}^{\mathrm{g}}$ [32, 33] .

The tricritical Potts branch can be parametrized as [39]

$$\sqrt{q} = 2\cos\left(\frac{\pi}{m}\right) = -2\cos\left(\frac{1+m}{m}\pi\right) = -2\cos\left(\frac{\pi}{\kappa_-}\right), \tag{2.80}$$

where the last equation comes from the relation of κ with m at Eq. (2.76) and the fact that $\kappa_- = 1/\kappa_+ = 1/\kappa$. Equation (2.80) states that the critical and tricritical regimes are mapped

onto each other via the transformation $\kappa \to 1/\kappa$. At the same time, as we saw before, this transformation maps the geometrical and FK clusters. Thus, we can conclude that for a given central charge the FK clusters of the tricritical q-state Potts model are the geometrical clusters of the pure q'-sate Potts model [32, 109]. Exact values of the several fractal dimensions and their numerical verification are given in Refs. [32, 33, 109, 110].

In conclusion, geometrical clusters might not be the appropriate geometrical representation that describes the critical fluctuations of the Potts model, nonetheless its connection with its diluted version is still of some significance. Additionally, the more sophisticated FK clusters properly describe the phase transition, however they cannot be applied to systems which are characterised by disorder. For example, in spin glass systems the presence of frustration results in failure of the above description. Although spin glasses are a challenging problem on its own terms, an appropriate cluster description would be beneficial for the understanding of the model. We will come back to this point in Chap. 6, for now we continue our discussion by describing some of the essential features of spin glasses.

2.5 Spin Glasses

Spin glasses are magnetic materials in which competition between ferromagnetic and antiferromagnetic interactions among magnetic moments (spins) leads to a magnetically disordered phase at low temperatures. At this phase spins are "frozen" in random orientations and there is no long-range order, leading presumably to a new kind of magnetic ordering. The inherent complexity and rich properties of those systems, accompanied by a vast number of experimental realisations, have been stimulating the interest of many scientists (not strictly physicists) over the last decades; thus exploring this novel and unconventional state of matter. In the literature there is a plethora of scientific papers, review articles, books, etc., concerning the study of spin glasses. Some of the standard references can be found in Refs. [42–47] and for application of spin glasses to areas outside physics see Refs. [111, 112] and references therein.

Initially, spin glasses were introduced to describe the properties of magnetic alloys. These are materials in which a small amount of magnetic impurity, typically Mn or Fe, is randomly diluted inside a non-metallic magnetic host, e.g., CuMn or AuFe. Experiments on AuFe [113] revealed a cusp in the magnetic susceptibility at low magnetic fields, signalling a new ordered phase at low temperatures. On the other hand, the specific heat did not show any singularity, but rather a broad maximum at higher temperatures than the peak of the magnetic susceptibility. Additionally, neutron scattering and other experimental techniques which concern the magnetic structure indicated that at low temperatures no long-range order appears, with spins remaining frozen in random orientations. Finally, not only magnetic alloys exhibit a spin-glass behaviour but a relatively broad class of materials ranging from certain insulators, such as $Eu_xSr_{1-x}S$, up to crystalline and amorphous materials. For an extended review on the experimental results of spin glasses see Ref. [42].

Although the spin-glass behaviour arises from the competing ferromagnetic and antiferromagnetic interactions, the mechanisms on an atomic scale responsible for such interactions differs substantially from one class of materials to the other. For the magnetic alloys it arises from the Ruderman-Kittel-Kasuya-Yosida (RKKY) interactions between the localized impurity spins, mediated by the conduction electrons. Mathematically the interaction between two spins separated by distance r can be expressed as

$$J(r) = J_0 \frac{\cos\left(k_{\mathrm{F}}\, r + \phi_0\right)}{\left(k_{\mathrm{F}}\, r\right)^3}, \tag{2.81}$$

where k_{F} is the Fermi wavevector, and ϕ_0, J_0 are constants which depend on the material. From Eq. (2.81) we see that as r changes, interactions change from ferromagnetic $[J(r) > 0]$ to antiferromagnetic $[J(r) < 0]$, and the interaction strength decreases as r increases. The timescale of spin diffusion is considerably larger than the experimental timescales, thus for all purposes interactions among spins are considered to be *quenched*. Additionally, as impurities are *randomly* distributed inside the material, interactions among spins have equal probability of being ferromagnetic or antiferromagnetic. These two features of spin glasses are often called *quenched disorder*.

In 1975 Edwards and Anderson [114] proposed a simplified model that should capture the main features of spin glasses, the so called Edwards-Anderson (EA) model. For that, let us consider a d-dimensional lattice, where at each of its vertices, i, we place localized magnetic moments (spins) and allow them to interact via a Hamiltonian

$$\mathcal{H} = -\sum_{\langle i,j \rangle} J_{ij}\sigma_i\sigma_j - H\sum_i \sigma_i, \tag{2.82}$$

where, as in Eq. (2.1), σ_i takes the values ± 1, H is the external field, $\langle\ ,\ \rangle$ indicates that the sum is restricted to nearest neighbours, and J_{ij} is a fixed random variable which can take positive and negative values, and indicates the interactions between spins. Interactions among spins can be chosen in several ways, though for simplicity we consider them as independent random variables following the same distribution. Two common choices of distributions are the *Gaussian* distribution, with mean zero and variance one

$$P\left(J_{ij}\right) = \frac{1}{\sqrt{2\pi}} \exp\left(-\frac{J_{ij}^2}{2}\right), \tag{2.83}$$

and the *bimodal* distribution[7]

$$P\left(J_{ij}\right) = p\,\delta\left(J_{ij} - 1\right) + (1-p)\,\delta\left(J_{ij} + 1\right), \tag{2.84}$$

where $J_{ij} = 1$ with probability p and $J_{ij} = -1$ with probability $(1-p)$.

In the spin glass phase spins are frozen, which means that the average local magnetisation is non-zero, $m_i = \langle\sigma_i\rangle \neq 0$ and the average is over all possible states for a given realisation of disorder. On the other hand, the total magnetisation, $M = \sum_i m_i$, is zero as on average half of the spins are constantly pointing up and the other half down. Thus, magnetisation is not a good order parameter. A more natural order parameter that captures the spin-glass transition was introduced by Edwards and Anderson:

$$q_{\mathrm{EA}} = \frac{1}{N}\sum_i \langle\sigma_i\rangle^2, \tag{2.85}$$

where N is the total number of spins.

[7] We note here that since the distribution takes only two values, i.e., ± 1, the term *binary* might be more relevant. However, we employ the term bimodal as it is widely used among the spin glass community.

One important feature of the EA model is the presence of *frustration* [115]. In order to describe it let us consider Eq. (2.82), where we set the external field H to zero for simplicity. To minimize the energy of the system each term in the sum of Eq. (2.82) has to be minimized. This is of course dictated by the sign of the interaction J_{ij} among spins i and j, as for $J_{ij} > 0$ spins should point in the same direction, whereas for $J_{ij} < 0$ spins should point in the opposite direction. Frustration now arises from the fact that, given a bond configuration, there is no spin configuration that satisfies all interactions simultaneously. More generally, for dimensions greater or equal than two all spins along a closed loop $\mathcal{C}$ cannot satisfy simultaneously all interactions if

$$\prod_{\langle i,j\rangle \in \mathcal{C}} J_{ij} < 0. \tag{2.86}$$

Note that frustration could also be present because of geometrical reasons. For example a system with antiferromagnetic interactions on a triangular lattice has all plaquettes frustrated. Finally, the presence of frustration accompanied with quenched disorder, as described above, are the two essential features of the spin glass theory.

2.5.1 Mean field picture

In order to gain insight into the nature of the transition, a conventional approach in statistical physics is to construct and solve a mean-field theory of the model at hand. Mean-field theory suppress fluctuations, leading to a simplified version of the model whose solution is usually a straightforward procedure. For the spin-glass problem, however, the solution turned out to be exceptionally difficult, and revealed several new and intriguing phenomena.

An infinite-range interaction version of the EA model was introduced by Sherrington and Kirkpatrick [116], its Hamiltonian is

$$H = -\frac{1}{\sqrt{N}} \sum_{1\le i<j\le N} J_{ij}\sigma_i\sigma_j, \tag{2.87}$$

where N is the total number of spins and J_{ij} is again a random variable drawn from a Gaussian distribution with zero mean and variance one. The $1/\sqrt{N}$ factor ensures a finite limit of the free energy per spin as the thermodynamic limit is approached ($N \to \infty$). The disorder averaged free energy is $-\beta F = \overline{\ln Z}$, where the over-bar denotes an average over the disorder distribution. As $\overline{\ln Z}$ is hard to calculate, one makes use of the identity $\ln(x) = \lim_{n\to 0} (x^n - 1)/n$ and the free energy becomes

$$-\beta F = \lim_{n\to 0} \frac{\overline{Z^n} - 1}{n}, \tag{2.88}$$

Thus, one proceeds by considering $n \in \mathbb{N}$ independent replicas of the system with the same disorder realisation, then averaging over all disorder realisations, and at the end taking the limit $n \to 0$. This is known as the *replica method*[8]. We can then define an *overlap* between two replicas α and β, which serves as an order parameter [112]

[8] An alternative approach is the cavity method [117].

$$q_{\alpha\beta} = \frac{1}{N}\sum_{i=1}^{N} \langle\sigma_i\rangle_\alpha \langle\sigma_i\rangle_\beta \,. \tag{2.89}$$

Initially, the *replica-symmetric* (RS) solution was proposed, meaning that replicas are indistinguishable

$$q_{\alpha\beta} = \frac{1}{N}\sum_{i=1}^{N} \langle\sigma_i\rangle^2 = q_{\mathrm{EA}}. \tag{2.90}$$

Thus, the RS solution coincides with the Edward-Anderson order parameter. The RS solution predicts a phase transition at $T_c = 1$, with a cusp of the magnetic susceptibility and specific heat at this temperature. However, it does not describe the low temperature phase correctly as the entropy becomes negative. The failure of such description was first attributed to the inappropriate exchange of limits $n \to \infty$ and $N \to \infty$. However, it was realised later that the problem pertained to something deeper, namely the assumption of replica-symmetry was incorrect.

In the following years other solutions to the mean field problem were proposed. Thouless, Anderson and Palmer (TAP) [118] proposed an alternative mean field description by the inclusion of the Onsager reaction field term. Additionally, the RS solution of the SK model was studied by de Almeida and Thouless (AT) [119] on the $T - h$ plane. It was found that the RS solution is stable only in the paramagnetic phase and becomes unstable under a phase boundary, known as the AT line.

With the above observations in mind, it became apparent that for a correct description of the spin-glass phase, the symmetry of replicas must be broken [119, 120]. However, there is not a unique way to break the symmetry of the replicas. Thus, the only way to find an appropriate physical solution was by trial and error [112]. In a series of papers Parisi [121–124] proposed a solution for the SK model by constructing an appropriate ansatz of the replica symmetry matrix. Parisi's solution for the SK model is known as the replica symmetry breaking (RSB) solution.

One of the striking features of RSB is that for a given disorder realisation in the spin glass phase there exist many pure states, which are not connected by any symmetry transformation[9]. The connection between the different phases can be expressed via Eq. (2.89), where now α, β indicate the pure phases and not the replicas as before, and $q_{\alpha\beta}$ satisfies the relation $-q_{\mathrm{EA}} \leq q_{\alpha\beta} \leq q_{\mathrm{EA}}$; note that this corresponds again to a specific choice of the couplings. Consequently, one can define the *overlap distribution* $P_J(q)$ as [46, 47]

$$P_J(q) = \sum_{\alpha,\beta} P_\alpha \, P_\beta \, \delta\left(q - q_{\alpha\beta}\right). \tag{2.91}$$

where the indices α, β indicate pure states of the system, P_α is the probability for the system to be in the pure state α, $q_{\alpha\beta}$ is the overlap between the pure states α and β, and the subscript J indicates the specific disorder realisation. Another interesting feature of spin glasses is that the overlap distribution $P_J(q)$ is not *self-averaging* [125–128]. This means that two different disorder realisations will have, in general, non-vanishing weights at different

[9] A counterexample is the Ising ferromagnet, where in the low-temperature phase and in the absence of a magnetic field two pure states exist, which are related by a global spin-flip transformation.

values of q. Thus, it is expected that averaging over all disorder realisations will result in non-vanishing weights for all values of q. Of course, each realisation always has a non-zero contribution from $q = \pm\, q_{\mathrm{EA}}$.

RSB also shows some form of hierarchical structure known as *ultrametricity* [125, 129, 130]. This means that given three states α, β, and γ, the following inequality is always satisfied:

$$q_{\alpha\gamma} \geq \min\left(q_{\alpha\beta},\, q_{\beta\gamma}\right). \tag{2.92}$$

This property defines a measure over the space of states, namely for each pair of states α and γ, the overlap $q_{\alpha\gamma}$ is obtained by going back in the tree until reaching the first common level.

The RSB scenario also supports the idea of *rugged free-energy landscapes*, i.e., the free energy is characterized by many local minima separated by large energy barriers the size of which increases with the size of the system. That leads to many *metastable* states, where the system is trapped and thus cannot explore the full phase space. This is a typical problem in Monte Carlo simulations of spin glasses as we will see in Chap. 3. Consequently, the dynamics in the spin glass phase is very slow, and as the system size goes to infinity this could lead to *ergodicity-breaking* [131, 132].

2.5.2 Droplet theory

An alternative theory of spin glass systems is *droplet* theory [133–140], which provides markedly different physical insights and conclusions in comparison with the RSB. The droplet is a compact area of coherently flipped spins with respect to the ground state, which is assumed to govern the thermodynamic behaviour of the system. The surface of a droplet with typical size l is assumed to have a fractal dimension $D_{\mathrm{drop}} < d$, where d is the dimensionality of the system. The free-energy cost of generating a droplet of linear size l is

$$F_l \sim Y l^{\theta}, \tag{2.93}$$

where θ is the so-called *stiffness exponent*, Y the *stiffness modulus* and $\theta < (d-1)/2$ (for an explanation see Appendix A of Ref. [140]). One particularly important result is that the scaling form of the correlation function for models with continuous distribution of the interactions and in the absence of magnetic field at temperatures close to zero scale as [47, 134]

$$\overline{G^2(i,j)} = \overline{\langle \sigma_i\, \sigma_j \rangle^2} - \overline{\langle \sigma_i \rangle^2}\; \overline{\langle \sigma_j \rangle^2} \sim \frac{T}{Y\, |\vec{r}|^{\theta}}, \tag{2.94}$$

where $\vec{i} - \vec{j} \equiv \vec{r}$, i.e., the distance between site i and site j, and T is the temperature. We define now the overlap between two configurations $\sigma^{\alpha}, \sigma^{\beta}$ which are statistically independent, and have the same equilibrium distribution and bond realisation as

$$q = \frac{1}{N} \sum_{i=1}^{N} \sigma_i^{\alpha} \sigma_i^{\beta}. \tag{2.95}$$

where N is the total number of spins in each configuration. Then it can be shown [47, 134] that Eq. (2.94) implies that the variance of the distribution of q is approaching zero as $L^{-\theta}$.

Thus, in the thermodynamic limit the distribution consists of two delta functions at $\pm q_{\mathrm{EA}}$. Consequently, the droplet picture supports a single pair of pure states, contrary to the RSB picture. Lastly note, that for models with discrete bond distribution Eq. (2.94) has to be modified, though it is believed that the type of interactions will not modify the single pair of pure states [47].

In the presence of a magnetic field H, the energy cost for flipping a droplet scales as $l^{\theta} - Hl^{d/2}$, and since $\theta < (d-1)/2$ the spin-glass phase remains unstable for all values of H. This is in contrast with RSB, which predicts a spin glass phase for all $H > 0$ below the AT line.

Whether RSB or the droplet theory is appropriate for the description of the low temperature phase of spin glasses in finite dimensions is still hotly debated. The main source of information regarding the nature of the transition in two- and three-dimensional systems comes from numerical simulations (some of the basic techniques will be discussed in Chap. 3), which in turn gives controversial results. For completeness we note that although the RSB and droplet theory are the most fully developed theories for the spin glasses, there exist two additional theories, namely the TNT picture [141, 142] and the chaotic pairs picture [143]. For a short review of the different pictures see Ref. [144]. Finally, we should point out that spin glasses show also remarkable off-equilibrium behaviour, such as ageing, hysteresis, memory effects, etc., just to name a few. See also Refs. [42, 44, 45] for some reviews on the topic.

Chapter 3

Simulation Methods

Statistical physics focuses on the study of systems which are constituted of a vast number of degrees of freedom. This in turn leads to the evaluation of large sums [see Eq. (2.4)] for the case of discrete degrees of freedom, or high-dimensional integrals for continuous degrees of freedom. These calculations are notably difficult and for most interesting physical systems an analytical solution is missing. Therefore, one has to utilise approximate methods, which can be of analytical or numerical character. Analytical methods such as series expansions or transfer matrix calculations, can provide approximate answers. On the other hand, numerical methods have played an important role in the progress of the field in connection with the continuous increase of computer power. For that a well-established process is the Monte Carlo method (MC).

3.1 Monte Carlo Simulations

3.1.1 Simple sampling

In order to describe the MC method, let us recall Eq. (2.4) which expresses the average value of an observable O,

$$\langle O \rangle = \frac{1}{Z} \sum_{\mu} O(\mu)\, e^{-\beta \mathcal{H}(\mu)}. \tag{3.1}$$

The goal then is to calculate the sum for the case of discrete degrees of freedom, or integral for the case of continuous degrees of freedom, of Eq. (3.1). In practice though this is not an easy process even for systems with moderate number of degrees of freedom. The rationale of this failure, is that the number of states μ increases exponentially with the number of degrees of freedom, and as one is interested in the thermodynamic limit the calculation of such a sum (integral) becomes impossible. Such difficulties can be alleviated by utilising an MC process, which provides *estimates* for quantities as in Eq. (3.1).

The basic idea behind the MC method is to estimate the sum of Eq. (3.1) by summing over a subset of the phase space, where the states are chosen from a *random* process, i.e., states are chosen according to some probability[1] $P(\mu)$. According to this, if M consecutive

[1] This is correct as long as the degrees of freedom are discrete. For continuous degrees of freedom one has to work with suitable probability densities instead.

states are generated, $M = \{\mu(1), \mu(2), \ldots, \mu(M)\}$ at time steps $i = 1, 2, \ldots, M$ respectively, then an estimate of $\langle O \rangle$ is given as

$$\overline{O} = \frac{\sum_{i=1}^{M} O\left[\mu(i)\right] e^{-\beta E[\mu(i)]} / P\left[\mu(i)\right]}{\sum_{i=1}^{M} e^{-\beta E[\mu(i)]} / P\left[\mu(i)\right]}, \tag{3.2}$$

where $\mu(i)$ is the state at time i, $P\left[\mu(i)\right]$ is probability that the state $\mu(i)$ is chosen, $O\left[\mu(i)\right]$ is the value of the observable O at the state $\mu(i)$ and $E\left[\mu(i)\right]$ is the energy of the state $\mu(i)$. Note that $P\left[\mu(i)\right]$ has to be strictly positive in order for Eq. (3.2) to hold. As the number of time steps M increases, Eq. (3.2) approaches $\langle O \rangle$ and in the limit of $M \to \infty$ we obtain

$$\lim_{M \to \infty} \overline{O} = \langle O \rangle. \tag{3.3}$$

The question that arises now is what probability distribution $P(\mu)$ one should choose. If states are chosen from a uniform distribution, then they are completely independent of each other, corresponding to a true random sampling. This is called *simple sampling* and it provides reasonable estimates for $\beta = 0$, i.e., when temperature is infinite and all states contribute equally to the sums of Eq. (3.1). On the other hand, at non-zero temperatures the Boltzmann distribution gives large weights only to a small region of the state space, thus making simple sampling not the optimal choice for exploring the representative region of the state space.

3.1.2 Importance sampling and the Metropolis algorithm

Contrary to simple sampling, *importance sampling* picks states according to some probability distribution (other than the uniform one), which for the case of a system in equilibrium is the Boltzmann distribution, i.e., $P_{\text{eq}}(\mu) = e^{-\beta E(\mu)}/Z$. Replacing $P(\mu)$ with $P_{\text{eq}}(\mu)$, Eq. (3.2) becomes

$$\overline{O} = \frac{1}{M} \sum_{i=1}^{M} O\left[\mu(i)\right], \tag{3.4}$$

which is just a simple average over the selected states. Thus, in order to utilise Eq. (3.4) one has to generate states according to the Boltzmann distribution. This can be achieved by using a *Markov process* (or Markov chain) $\mu(t)$ [57–60, 145, 146].

In a Markov process one generates a chain of random states, $\mu(1) \to \mu(2) \to \mu(3) \to \ldots$, according to some probability distribution, here the Boltzmann distribution. The restriction is that the current state depends only on the preceding state and not on the history of the hole trajectory in state space. Thus, the conditional (transition) probability for the system to be in state i at the time-step t, given that it was in state j at time-step $t-1$, etc., can be written as

$$P\left[\mu(t) = i \mid \mu(t-1) = j\right] = P\left[\mu(t) = i \mid \mu(t-1) = j,\ \mu(t-2), \ldots\ \mu(1)\right] \tag{3.5}$$

If we require that the Markov chain is homogeneous then the transition probabilities do not depend on time, i.e., $W\left(i \to j\right) \equiv P\left[\mu(t) = i \mid \mu(t-1) = j\right]$. From this property of the Markov chain and the normalisation of the probabilities W, i.e., $W\left(i \to j\right) \geq 0$ and

$\sum_j W(i \to j) = 1$, it can be shown that the probability of being in state μ at time-step t, i.e., $P(\mu, t)$, satisfies the so-called *Master equation* [58, 145]

$$P(\mu,t) - P(\mu,t-1) = \sum_{\mu'} \left[P(\mu',t) W\left(\mu' \to \mu\right) - P(\mu,t) W\left(\mu \to \mu'\right) \right], \tag{3.6}$$

where on the right-hand-side of Eq. (3.6) the first term of the sum accounts for all processes that reach μ while the second term corresponds to all processes leaving μ. Thus, Eq. (3.6) can be interpreted as a continuity equation, reflecting the fact that the probability is conserved.

If we want the distribution to be stationary, the left-hand-side of Eq. (3.6) should be zero. A sufficient, though not necessary, condition for the Boltzmann distribution to be a stationary probability $P(\mu, t) = P_{\text{eq}}(\mu)$, is given by the so-called *detailed balance*

$$P_{\text{eq}}(\mu') W\left(\mu' \to \mu\right) = P_{\text{eq}}(\mu) W\left(\mu \to \mu'\right). \tag{3.7}$$

Additionally to stationarity of the Boltzmann distribution, one has to guarantee the convergence of $P(\mu)$ to $P_{\text{eq}}(\mu)$. This is a more subtle issue, but it can be proved under the additional condition of ergodicity of the Markov chain. Ergodicity ensures that a Markov process can reach with a finite probability any state, irrespective of the starting state; for a discussion about convergence of the MC process see Ref. [147]. By substituting the Boltzmann weights to Eq. (3.7) we can rewrite it as

$$\frac{W\left(\mu \to \mu'\right)}{W\left(\mu' \to \mu\right)} = e^{-\beta(E(\mu') - E(\mu))}, \tag{3.8}$$

where $E(\mu), E(\mu')$ are the energies of states μ, μ' respectively.

Metropolis algorithm

There are many choices of transition probabilities that satisfy Eq. (3.8). One of the most commonly used choices is the Metropolis algorithm [52]. Here the new state is generated by updating a single degree of freedom, with a transition probability given as

$$W\left(\mu \to \mu'\right) = \begin{cases} e^{-\beta[E(\mu') - E(\mu)]}, & \text{if } E(\mu') > E(\mu) \\ 1, & \text{if } E(\mu') < E(\mu). \end{cases} \tag{3.9}$$

It is easy to check that this choice of transition probability of Eq. (3.9) satisfies the condition of detailed balance, see Eq. (3.8). Additionally, ergodicity is ensured as on a finite lattice any state could be reached given an initial state by updating one by one the degrees of freedom that these two states differ [57]. A practical implementation of the Metropolis algorithm for the Ising model is given below:

Metropolis algorithm

(1) Pick a spin i.

(2) Calculate the energy difference $\Delta E = E(\mu') - E(\mu)$ for flipping the spin i.

(3) Generate a random number r, with $r \in [0, 1)$.

(4) If $r < \exp[-\beta \Delta E]$, then flip the spin.

(5) Go to step **(1)** and repeat.

The Metropolis algorithm can be implemented for a variety of systems in statistical physics, such as lattice/off-lattice models, discrete/continuous symmetries, long-range/short-range interactions. Its simplicity and flexibility are the main reasons of considering it as one of the standards MC processes. Finally, similarly to Metropolis other single-spin-flip algorithms exist, e.g., heat-bath algorithm [148], Glauber algorithm [149].

3.2 Cluster Algorithms

Although single-spin-flip or local updates are applicable to essentially all models in statistical physics, their main drawback is that they perform quite poorly in the vicinity of a continuous phase transition, where the degrees of freedom are strongly correlated. This can be understood in terms of the autocorrelation time τ, which quantifies the minimum necessary number of time steps (sweeps) for two configurations to be statistically independent, see Appendix A.1. In the thermodynamic limit and close to the critical point the autocorrelation time τ scales as [57, 58]

$$\tau \sim \xi^z, \tag{3.10}$$

where $z \geq 0$ is the dynamical critical exponent. As we have seen in Chap. 2 correlation length scales as $\xi \sim |T - T_c|^{-\nu}$, and thus it diverges as the critical temperature is approached. Consequently the autocorrelation time also diverges as

$$\tau \sim |T - T_c|^{-z\nu}, \tag{3.11}$$

a phenomenon known as *critical slowing down* at a continuous phase transition. For finite systems ξ can not exceed the linear dimension of the lattice, say L, and near the critical point $\tau \sim L^z$. Thus if the size of the system increases, τ is rapidly growing and the rate at which statistically independent configurations are created decreases substantially, at least for reasonable computational times [57].

Specifically, for the case of the Metropolis algorithm for the two-dimensional Ising model at the critical temperature $z \approx 2.17$ [150, 151]; see also Ref. [152] for a review. Therefore, correlations among configurations become pronounced. In order to reduce such correlations non-local algorithms such as cluster algorithms have been introduced, which significantly reduce the dynamical critical exponent z. The corresponding caveat though is that such algorithms depend strongly on the studied system.

Swendsen-Wang algorithm

As we have seen in Chap. 2, Fortuin and Kasteleyn showed that the q-state Potts model is equivalent to a percolation process, in the sense that the partition function of the former can be written as a sum over all FK clusters on the lattice. Swendsen and Wang (SW) [27] based on the FK decomposition proposed a cluster algorithm for the q-state Potts model. The algorithm proceeds in two steps: First given the spin configuration, bonds are created among aligned spins with a probability $p_{\text{add}} = 1 - \exp(-2\beta J)$. Then, given the bond configuration, clusters are created from aligned spins that are connected with bonds. Under this construction spins belonging to different clusters are statistically independent and we can assign independently to each cluster a new spin value. For the Ising model the algorithm proceeds as follows:

Swendsen-Wang algorithm

(1) Construct the bond configuration: If neighbouring spins are aligned, form a bond with probability $p_{\text{add}} = 1 - \exp(-2\beta J)$.

(2) Identify all clusters: As clusters we consider spins that are connected directly or indirectly via bonds.

(3) Flip all clusters (even the ones with only one cite) independently with probability $1/2$.

(4) Delete all bonds, go to step **(1)** and repeat.

Thus, it is possible that neighbouring spins with the same orientation are not part of the same cluster as their bond could be deleted with probability $1 - p_{\text{add}}$. This results in clusters of smaller size compared to the geometrical ones where all neighbouring aligned spins are included in the same cluster. Only when $\beta \to \infty$, i.e., at zero temperature, the two cluster types coincide.

Hence, at each step of the SW algorithm, the whole lattice is decomposed into clusters which are then randomly assigned a spin value $+1$ or -1. It turns out that these clusters (FK) suppress significantly the temporal correlations, resulting in an exponent z sufficiently smaller compared to algorithms with single-spin-flip dynamics (values are given further down) [27, 153]. Although, this holds in the vicinity of the critical point (where much of the most interesting things are happening), away from this region, although correct, local-spin-flips updates perform slightly better [57].

Wolff algorithm

Soon after the SW algorithm had been suggested, Wolff [28] proposed a variant of it, where instead of the whole lattice decomposition a single cluster is flipped at a time. The implementation, again for the Ising model, is as follows:

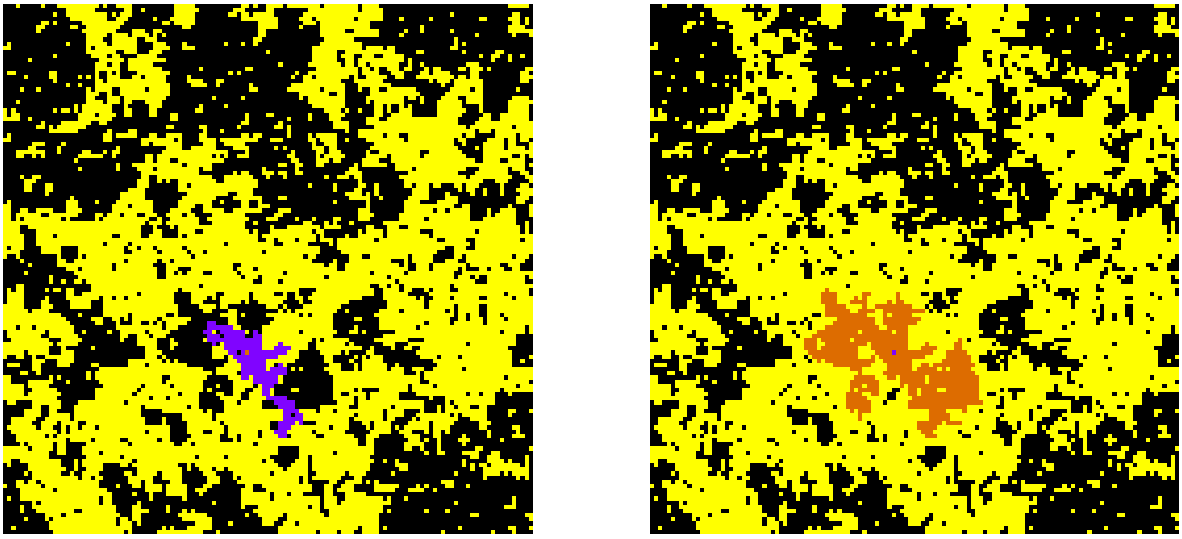

(a) Wolff cluster. (b) Geometrical cluster.

Figure 3.1: Spin configuration of the 2-dimensional Ising model near the critical temperature $T_c \approx 2.269185$ for a 128×128 lattice. (a) A Wolff cluster from down (black) spins is depicted in purple colour (b) The equivalent geometrical cluster is depicted is orange colour, where all aligned spins (black) are included in the cluster, which results in an apparent difference in sizes between the two cluster types.

Wolff algorithm

(1) Pick a spin at random.

(2) If its neighbours are aligned, add them to the cluster with probability $p_{\text{add}} = 1 - \exp(-2\beta J)$.

(3) For the new members of the cluster, repeat step **(2)**, until all members have checked their neighbours.

(4) Flip the cluster.

(5) Go to step **(1)** and repeat.

Similarly to the SW construction, the clusters created by the Wolff algorithm are smaller compared to the geometrical ones, and they coincide only at zero temperature. This is shown in Fig. 3.1, where the size of a typical Wolff cluster, see Fig. 3.1(a), is sufficiently smaller than the geometrical one, see Fig. 3.1(b), where all aligned spins (orange dots) are considered to be in the same cluster.

For both cluster algorithms temporal correlation are suppressed mainly through the flipping of the larger clusters. In the SW implementation though, the whole configuration is decomposed into clusters, which are flipped independent of their size. This means that a sig-

nificant part of effort, as well computational time, is dedicated to the construction of smaller clusters which do not contribute much. In contrast, Wolff's implementation picks on average larger clusters which are always flipped. Thus, if a large cluster is picked then the suppression of correlations is comparable with the SW and if a smaller cluster is picked nothing changes much but the computational effort is relatively small. Thus, correlations are suppressed even further than in the SW algorithm resulting to a smaller dynamical exponent z. This is true for the three-dimensional Ising model, where $z = 0.28(2)$ for the Wolff and $z = 0.50(3)$ for the SW algorithm [153], for the two-dimensional Ising the two methods give comparable results, i.e., $z \approx 0.26$ [153]. Lastly, similarly to SW the Wolff algorithm performs better in the vicinity of the critical point, while away from it local-spin-flips are expected to perform slightly better.

Finally, it is worth mentioning that both cluster algorithms can be implemented (with some modifications) for other systems too. For the q-state Potts model for example, where each spin can take values from 1 to q, the SW algorithm can proceed by decomposing the system into clusters[2] and assigning to each one of them a random value from 1 to q with probability $1/q$. Additionally, the Wolff algorithm can be extended to the case of the XY and Heisenberg models [28, 154–156].

3.3 Spin Glass Simulations

In Sec. 2.5 we saw that spin glasses are systems with rugged free-energy landscapes, where states in phase space are separated by large energy barriers with many local minima, which grow rapidly as the size of the system increases. Although for such systems conventional MC schemes, e.g., the Metropolis algorithm, work in principle, the time needed to equilibrate even the smallest system is extremely large, thus making them impractical. The reason is that at low temperatures such MC algorithms usually get "trapped" in local energy minima having not enough energy to overcome the energy barriers, thus not exploring the full, or at least a representative portion, of the phase space. In this section we discuss two methods that are able to overcome such large energy barriers, leading to a substantial reduction of the equilibration time: *(i)* Parallel tempering *(ii)* Houdayer's cluster algorithm.

3.3.1 Parallel tempering

In parallel tempering (PT) [157] several copies of the system are simulated at different temperatures, and at regular time intervals copies are exchanged. In this fashion copies which usually get stuck in a local minima at low temperatures can escape to higher temperatures where equilibration is faster. Thus, the diffusion of copies from lower to higher temperatures, and vice versa, allows for a better exploration of the phase space.

Let us consider M non-interacting copies (replicas) of a system, which we simulate in parallel using an MC process, e.g., Metropolis algorithm, for each copy, running at inverse temperatures $\beta_1, \beta_2, \ldots, \beta_M$ respectively. Since the copies are not interacting, the partition function of the whole system can be written as

[2] In that case the probability to form a bond between two spins with the same q value is $p_{\text{add}} = 1 - e^{-\beta J}$ [27].

$$Z = \prod_{j=1}^{M} \sum_{\mu^{(j)}} e^{-\beta_j \mathcal{H}^{(j)}}, \tag{3.12}$$

where $\mu^{(j)}$, $\mathcal{H}^{(j)}$ is the spin configuration and energy of the j-th replica, respectively. The probability to exchange copies j, k is given by

$$W\left(j, \beta_j \;\leftrightarrow\; k, \beta_k\right) = \min\left[1, e^{(\beta_k - \beta_j)(E_k - E_j)}\right]. \tag{3.13}$$

It can be shown that such transition probabilities satisfy detailed balance [157], while ergodicity is ensured if ergodic MC update schemes are performed in each replica. The exchange probability depends on the difference $\beta_k - \beta_j$ of inverse temperatures, and decreases exponentially as the temperature difference is increased. Thus, it is preferable to consider exchanges between neighbouring temperatures, i.e., $i \leftrightarrow i \pm 1$.

Although the idea of PT is relatively simple, a suitable choice of temperatures is essential for the performance of the algorithm. This can be understood from the energy histograms of the individual replicas. If two neighbouring temperatures $i, i+1$ are sufficiently away from each other such that the overlap of their respective energy histograms will be small, the exchange probability will be relatively small. Thus, these copies are highly unlikely to be exchanged and the round-trip of copies from the lowest to the highest temperature and back will stop. On the other hand, if the temperatures are very close to each other, resulting in a large overlap of the energy histograms, computational time is wasted without gaining much information about the system.

Thus, a suitable temperature schedule is required such that the overlap of the energy histograms is sufficiently large. There is a plethora of different temperature schedules in the literature, in order for the PT algorithm to perform optimally. Here we will firstly discuss the ones that are used in this thesis (see Chap. 6) and briefly comment on some of rest.

As the random walk of copies in the temperature space depends on the exchange events of copies, we have to assure a sufficient exchange probability for all temperatures involved. This can be guaranteed if exchange probabilities are approximately independent of temperature. For systems with not strong divergence of the specific heat, such as spin glasses, this can be achieved with a *geometric progression* schedule [158–160]. Given a range of temperatures $[T_1, T_M]$ the intermediate values $M-2$ can be computed via

$$T_j = T_1 \prod_{k=1}^{j-1} \sqrt[M-1]{\frac{T_M}{T_1}}. \tag{3.14}$$

With this schedule more replicas are placed at low temperatures, and fewer in the high temperature regime. However, if the specific heat has a strong divergence then the exchange probability drops in the vicinity of the critical point, leading to a non-optimal temperature schedule. In the case of the Ising model for example, where a phase transition occurs for dimensions greater than one, the geometrical schedule leads to poor performance as near the critical region the probability for replicas to be exchanged is sufficiently low, see Fig. 3.2. Finally, given a temperature range, the optimal number of temperatures for systems without a phase transition is of the order of $M \sim \sqrt{N}$, where N is the total number of spins. For systems with a continuous phase transition, however, it can been shown [157] that the optimal

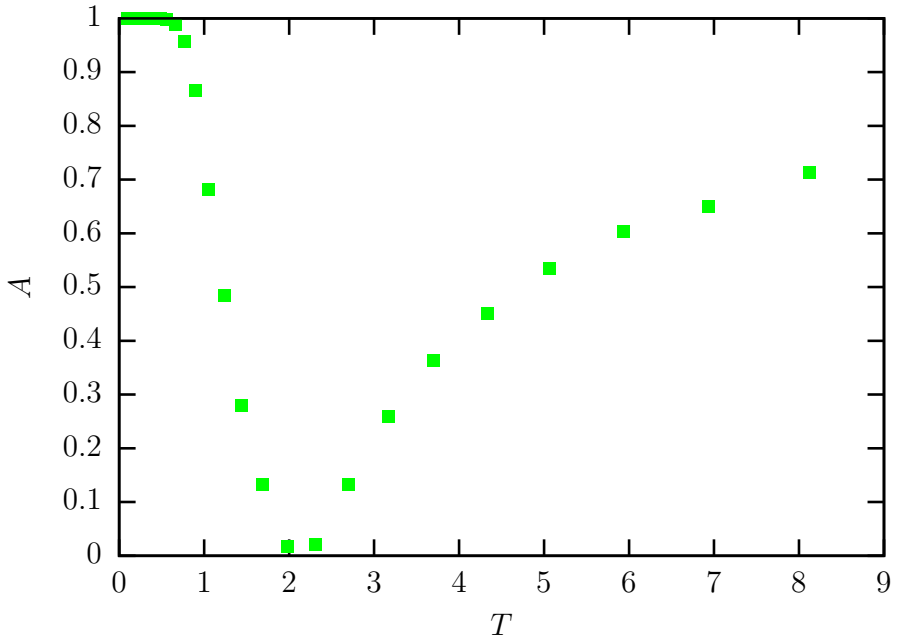

Figure 3.2: Acceptance probability as a function of temperature T, from simulations of the two-dimensional Ising ferromagnet for linear size $L = 20$, using a geometrical temperature schedule. In the vicinity of the critical point $A(T)$ is rather small (close to zero), leading to poor performance of the PT algorithm.

number of temperatures is $M \sim \sqrt{N^{1-d\nu/\alpha}}$ where d the dimensionality of the system, ν the critical exponent of the correlation length, and α the critical exponent of the specific heat.

The other temperature schedule that is implemented in this thesis is the inverse linear one. Here, inverse temperatures are equally spaced between the low and high inverse temperature regime.

A more elaborate technique called the feedback-optimized method [159], defines an optimal temperature schedule by maximizing the rate of the replicas' round trips in a given temperature range. Using a recursive readjustment of the temperatures the local diffusivity of the copies is maximized. However, the method is quite complicated and hard to control; especially since some numerical differentiation is involved.

Another method introduced in Ref. [161], suggested that the round trip of copies can be significantly increased by adjusting the number of MC sweeps in each copy to the autocorrelation time before a proposed exchange of the copies. Additionally, the temperatures were adjusted so that a constant overlap of the energy histogram was obtained (50% of exchange probability). Although, the method improves the performance of the algorithm, it comes with an additional cost of pre-runs in order to estimate the autocorrelation times.

Lastly, a recent parametric scheme was proposed in Ref. [162]. In this method the optimal temperature set is determined by the optimal choice of the involved parameters. For the optimal set of parameters pre-runs need be to be performed. Once the optimal parameters for some system sizes are known, by employing FSS, the temperature-schedule parameters for larger system sizes can be obtained. Again this method provides reliable temperature sets

with the additional cost of pre-runs. However, the fact that the parameters for larger system sizes can be indirectly determined from fit results and not from direct simulations is surely advantageous.

3.3.2 Houdayer's cluster algorithm

In Sec. 3.2 we discussed the cluster algorithms for the case of ferromagnetic systems and how efficiently they can be for simulations in the vicinity of the critical point. For spin glasses though, such algorithms cannot be applied because of frustration. Specifically, for ferromagnetic systems the spin-spin correlation function is equal to the probability that two sites belong to the same FK cluster [40]. Consequently, a phase transition in the spin system emerges from a percolation transition of the FK clusters, and vice versa. Unfortunately, this relation does not hold for spin glasses resulting in a transition temperature well above the transition temperature of the spin glass phase [41, 163, 164]. Over the years attempts have been made to construct a cluster algorithm for the spin glass problem [40, 48, 165–169]. However, a cluster algorithm for accessing larger system sizes especially in three dimensions is still missing.

For two-dimensional systems, however, the cluster algorithm proposed by Houdayer [48] can efficiently simulate the spin glass system at low temperatures, where the relaxation is sufficiently slow. The caveat of the method is that it is applicable only for lattice geometries where the percolation threshold p_c is above 0.5; below that, although correct, it becomes inefficient.

Houdayer's algorithm considers two independent copies of the system at the same temperature and with the same disorder realisation of the interactions among spins. Then, a q_i variable is defined as $q_i = s_i^{(1)} s_i^{(2)}$ which connects the lattice site i between the two copies. Under this construction domains with $q = 1$ and $q = -1$ are created, see Fig. 3.3. Then clusters in both copies are constructed by activating bonds between neighbouring spins with the same q value and a non-zero interaction. It can be easily checked that if we flip a cluster with $q = -1$ the energy of each of the two copies will change but not the total energy (the sum of the energies of the two copies). In the absence of a magnetic field the same holds for clusters with $q = 1$. Thus, such cluster moves trivially satisfy detailed balance and are always accepted. Additionally, to ensure that the algorithm is ergodic, Metropolis updates are introduced in each copy.

The idea of the algorithm is similar to the replica MC method [170], with the essential difference that there copies are at different temperatures. PT moves are also included to ensure fast equilibration. Thus, if one simulates M such pairs of copies at different temperatures one MC step consists of the following steps:[3]

1. For each of the $2M$ copies perform one Metropolis sweep.

2. For every temperature and pair pick a spin at random and perform one cluster update.

3. Perform one PT update for all pairs of copies at neighbouring temperatures.

[3] In the original paper of Houdayer [48] a large number of copies at each temperature is considered. However, as argued in Ref. [162] it is prudent to consider only two copies at each temperature and use the additional computational resources for simulation over additional disorder realisations.

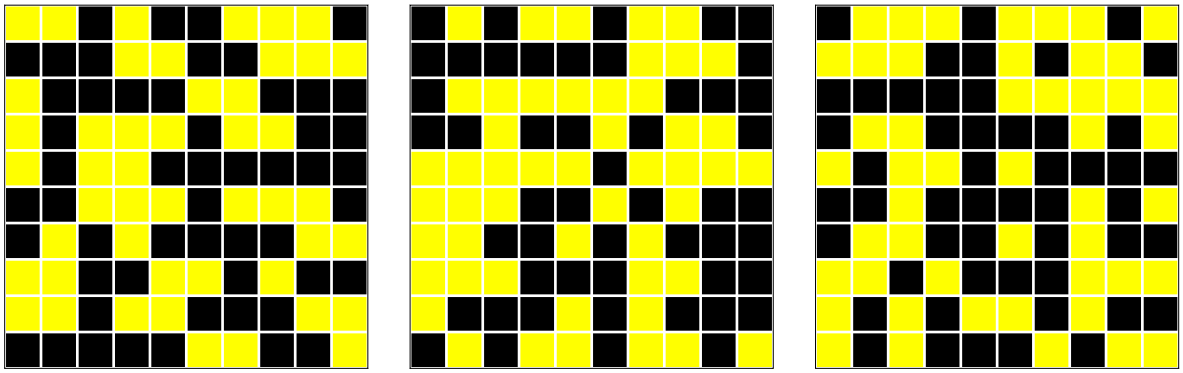

(a) System 1 (b) System 2 (c) Overlap

Figure 3.3: Illustrative example of a 10×10 grid for Houdayer's clusters. Yellow plaquettes represent $+1$ spins and black plaquettes -1 spins. Figs. 3.3(a) and 3.3(b) represent the spin configuration of the first and second copy respectively. Fig. 3.3(c) is the overlap of the two configurations.

As it was stated above, the algorithm is restricted to lattices where $p_c > 0.5$. Because the cluster update does not reject any aligned neighbouring spin, if $p_c < 0.5$ then even at high temperatures percolating clusters would occur in both replicas. Thus, a cluster update would result in just an exchange of replicas and the algorithm will be inefficient.

Chapter 4

Geometrical Clusters of the Ising Model

The properties of geometrical clusters of the Ising model have been studied extensively over the years by many researchers. As it was discussed in Sec. 2.4.2, such clusters cannot properly describe the phase transition of the Ising model in any dimension as, in general, they percolate at different temperatures from the thermal transition and their exponents do not coincide with the thermal ones. Nonetheless, in two dimensions geometrical clusters percolate at the critical temperature of the phase transition. Additionally, the connection of geometrical clusters of the two-dimensional Ising model with the site-diluted q-state Potts model, as well as an analytic description of their boundaries via the stochastic Loewner evolution method, still make them appealing (see Sec. 2.4.4). Besides, such clusters define an interesting percolation problem the properties of which are not completely understood.

In this chapter we investigate the percolation properties of such clusters for the two-dimensional Ising ferromagnet, with the help of Monte Carlo simulations. The behaviour of wrapping probabilities and their interlineations will first be discussed. Then the estimation of critical exponents of the average cluster size and percolation strength using FSS, and a comparison with the already known analytical values will be obtained. Since the critical temperature is known exactly, simulations will be performed precisely at this critical point for the estimation of the involved exponents. Additionally, special considerations, will be given to the estimation of critical exponents and the existence of finite-size corrections when observables are defined from different cluster sets.

Specifically, we have simulated the two-dimensional Ising model with periodic boundary conditions using the Swendsen-Wang algorithm [27]. We considered systems of linear size $L = 16, 32, 64, 128, 256, 512, 600, 1000, 1200, 1600$ and 2000, at the exact critical temperature $T_c = 2/\ln\left(1+\sqrt{2}\right)$ of the two-dimensional Ising model[1]. For each L the total number of simulation steps was $1.1 \times \tau_{\text{int, E}} \times 10^5$ sweeps, where $\tau_{\text{int, E}}$ is the integrated autocorrelation time of the energy (see Appendix A.1), and $\tau_{\text{int, E}} \times 10^4$ sweeps were discarded during equilibration. After every $\tau_{\text{int, E}}$ sweeps a measurement was taken, leading to up to 10^5 measurements per run. The estimates of $\tau_{\text{int, E}}$, rounded up to the next largest integer, in ascending order of the system size are: $\tau_{\text{int, E}} = 4, 5, 5, 6, 7, 9, 9, 10, 11, 11, 12$ sweeps. Statistical errors were

[1] The only exception is for the system of linear size $L = 256$, which was simulated at a temperature range $T = [1.5 - 3.8]$, see Sec. 4.1.

estimated by means of jackknife blocking, see Appendix A.2. We considered a cluster to percolate in one direction if it wraps around this direction and is connected back to itself. To identify the wrapping clusters, we employed the method of Machta et al. [171] (see also Ref. [172] for an alternative method).

4.1 Wrapping Probabilities

The spanning probability R, introduced in Sec. 2.4.1, gives the probability for a spanning cluster to emerge, in the limit of the infinite system. For ordinary percolation, R is given as a function of p, which expresses the fraction of occupied sites (or bonds) in a lattice, and by varying p we could observe the phase transition from a non-percolating to a percolating phase and vice versa. In the study of phase transitions of spin systems, the control parameter is the temperature T, whose variation signals the transition[2]. For the Ising model in particular, we expect that above the transition temperature, $T > T_c$, the probability of finding an infinite cluster is 0, i.e., $R(T > T_c) = 0$, while the ordering phase should be characterized by the appearance of an infinite cluster $R(T < T_c) = 1$. Thus, $R(T)$ is a step-function whose discontinuity marks the transition temperature.

For systems of finite size L, $R(T)$ varies continuously with temperature and approaches a step-function in the thermodynamic limit, i.e., $L \to \infty$. There are a variety of ways in which a cluster can span the system. For finite systems with periodic boundary conditions though, it is common to work with the so-called *wrapping probability*, which considers a cluster to percolate in one direction if it wraps around this direction and connects back to itself (closed loop). Even defining a percolating cluster as above, still percolation can occur in various ways. Here, and throughout this thesis, we will consider the following cases for the wrapping probabilities R:

1. $R_{\mathrm{x\ or\ y}}$ is the probability for a cluster to wrap around the horizontal *or* vertical direction (or both).
2. $R_{\mathrm{x\ and\ y}}$ is the probability for a cluster to wrap around the horizontal *and* vertical direction.
3. R_{x} is the probability for a cluster to wrap around the horizontal direction.
4. $R_{\mathrm{x\ and\ \bar{y}}}$ is the probability for a cluster to wrap around the horizontal *but not* the vertical direction.

On square lattices, i.e., $L \times L$, due to symmetry the horizontal and vertical directions are equivalent, meaning that $R_{\mathrm{x}} = R_{\mathrm{y}}$ and $R_{\mathrm{x\ and\ \bar{y}}} = R_{\mathrm{y\ and\ \bar{x}}}$.

These four wrapping probabilities satisfy the following inequalities [173]

$$R_{\mathrm{x\ and\ y}} \leq R_{\mathrm{x}} \leq R_{\mathrm{x\ or\ y}} \quad \text{and} \quad R_{\mathrm{x\ and\ \bar{y}}} \leq R_{\mathrm{x}}. \tag{4.1}$$

This is illustrated in Fig. 4.1, where the four wrapping probabilities introduced above are plotted as a function of temperature, for a system of linear size $L = 256$. Additionally, they satisfy the following equalities [173]

[2] Note that p is a number defined in $[0, 1]$, whereas T is defined in $[0, \infty)$.

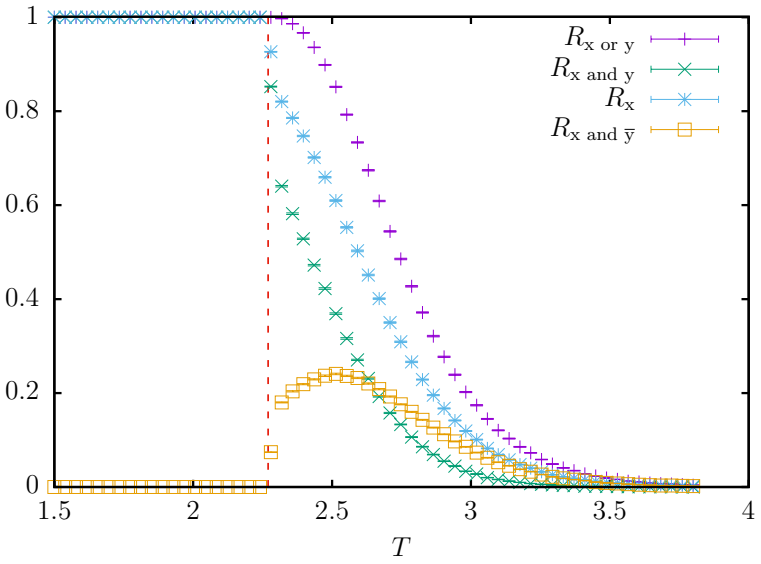

Figure 4.1: Wrapping probabilities as a function of temperature T for a system of linear size $L = 256$. The dashed vertical line marks the transition temperature of the two-dimensional Ising model.

$$R_{\text{x or y}} = R_{\text{x}} + R_{\text{y}} - R_{\text{x and y}} = 2R_{\text{x}} - R_{\text{x and y}}, \tag{4.2}$$

$$R_{\text{x and }\bar{\text{y}}} = R_{\text{x}} - R_{\text{x and y}} = R_{\text{x or y}} - R_{\text{x}} = \frac{1}{2}\left(R_{\text{x or y}} - R_{\text{x and y}}\right). \tag{4.3}$$

This means that by knowing two of them, we can calculate the rest of them. Equations (4.2) and (4.3) are plotted in Figs. 4.2(a) and 4.2(b) respectively, where one can visually verify that the equalities hold. Except $R_{\text{x and }\bar{\text{y}}}$, all probabilities are monotonous functions of temperature. In contrast, $R_{\text{x and }\bar{\text{y}}}$ exhibits a maximum which signals the transition, and as the system size increases this maximum shifts towards the asymptotic value of the temperature [173].

Finally, we note that in numerical studies of percolation wrapping probabilities are utilised to determine the percolation threshold p_c [173–177]. Similarly, they have also been used in the study of phase transitions of spin systems as they can provide estimates of the critical temperature [178–182]. In what follows in this chapter, however, we will not attempt to determine the critical temperature, since it is known that for the geometrical clusters of the two-dimensional Ising model it coincides with that of the thermal transition. Nonetheless, we note that the wrapping probabilities will be employed for finding the critical temperature for the multi-replica Ising model, as we will see in Chap. 5.

4.2 Average Cluster Size

As we have seen in Sec. 2.4.1, the average cluster size S diverges at the critical point with an exponent γ. For the Ising model, S is expected to diverge at the critical temperature T_c

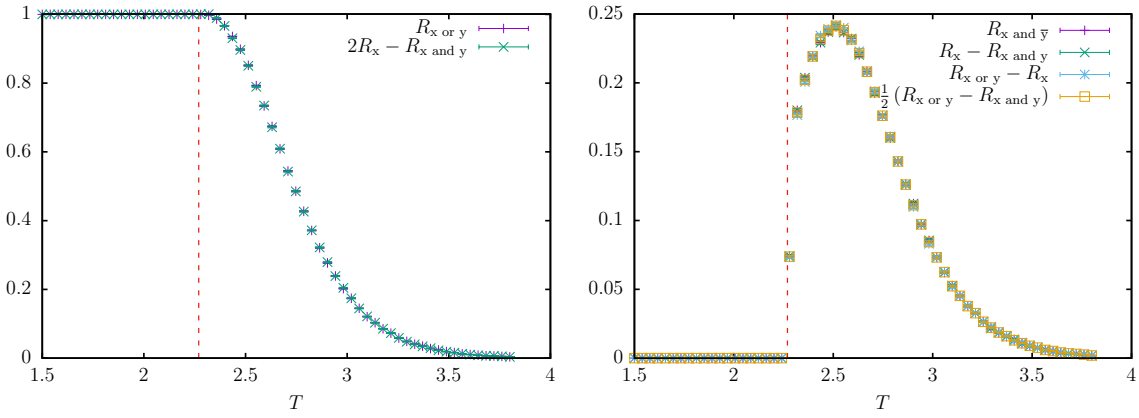

(a) (b)

Figure 4.2: Equality relations of wrapping probabilities as a function of temperature T for a system of linear size $L = 256$. (a) Eq. (4.2) (b) Eq. (4.3). The dashed vertical line marks the transition temperature of the two-dimensional Ising model.

as $S \sim |t|^{-\gamma}$, where $t \equiv |T - T_{\text{c}}| / T_{\text{c}}$ is the reduced temperature. Since the calculation of S considers only finite size clusters, its divergence can be understood as follows: In the non-percolating phase ($T > T_{\text{c}}$) many small clusters contribute to S and as the critical temperature is approached the size of the clusters, though finite, increases. On the other hand, in the percolating phase ($T < T_{\text{c}}$) most spins belong to the percolating cluster and clusters formed by the residual spins are relatively small and do not contribute much to S.

For finite systems of linear size L the average cluster size exhibits a maximum in the vicinity of the critical point and according to FSS it satisfies the following equation [19]

$$S(L, T) = L^{\gamma/\nu} \widetilde{S} \left[L^{1/\nu} (T - T_{\text{c}}) \right], \tag{4.4}$$

where ν is the critical exponent of the correlation length, and $\tilde{S}$ is a universal finite-size scaling function. Note, that the position of the maximum T^* of the average cluster size, defines a sequence of pseudo-critical points as a function of L and according to FSS it should scale as

$$T^*(L) = T_{\text{c}} + aL^{-1/\nu}, \tag{4.5}$$

where $a = \arg\max \widetilde{S}$, i.e., the argument that maximizes the scaling function $\widetilde{S}$, see, e.g., Ref. [74]. Thus, one can provide estimates of the critical temperature and the exponent ν from the location of the peaks using Eq. (4.5). Note that for thermal observables, T_{c} and ν are estimated from the maxima of the specific heat or magnetic susceptibility. Of course Eq. (4.5) is valid as long as we are close the critical region and for large enough system sizes [74].

In numerical studies of percolation the "standard" approach for estimating the average cluster size is to exclude the *largest cluster* in each measurement [19]. In that way S exhibits a maximum near the transition, as in the non-percolating phase there exist many small clusters, while in the percolating phase most sites belong to the largest (usually percolating) cluster which we exclude. Thus, the peaks S_{peak} should scale with the linear size of the system L as

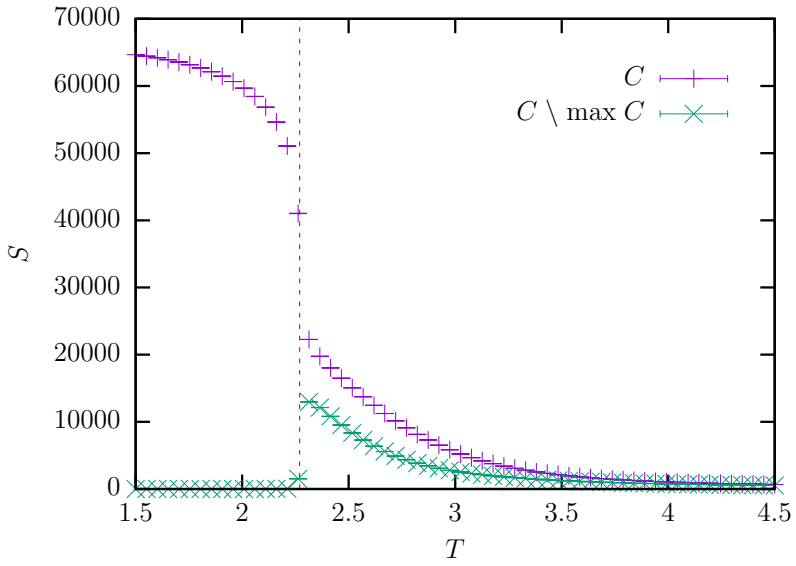

Figure 4.3: Average cluster size S as a function of temperature of the two-dimensional Ising ferromagnet for system of linear size $L = 256$. By excluding the largest cluster in each measurement ($C \setminus \max C$) S has a maximum around the critical point (red dashed line), whereas if all clusters all included (C) S is a monotonously increasing function as temperature decreases.

$S_{\text{peak}} \sim L^{\gamma/\nu}$, from where one can obtain the critical exponent. Nonetheless, we will extend this approach by considering different sub-sets of clusters. Specifically, we will estimate the average cluster size for the following cases:

1. All clusters are included: C.
2. Exclude the largest cluster in each measurement: $C \setminus \max C$.
3. Exclude all percolating clusters: $C \setminus P$.
4. Exclude all clusters percolating in horizontal and in vertical direction: $C \setminus P_{\text{x and y}}$.
5. Exclude all clusters percolating in one specific direction, e.g., horizontal: $C \setminus P_{\text{x}}$.
6. Exclude all clusters percolating in one but not the other direction, e.g., horizontal and not vertical: $C \setminus P_{\text{x and } \bar{\text{y}}}$.

Note that the inclusion of all clusters results in a monotonously increasing average cluster size as the temperature decreases, and at zero temperature S will be equal to the total number of spins, see Fig. 4.3. Even though S does not exhibit a maximum, Eq. (4.5) can be applied for the estimation of the critical temperature and the ν exponent by considering as $T^*(L)$ the inflection points of the function $S(L, T)$. However, this procedure is more complicated as for the estimation of such inflection points the numerical derivative should be applied which is prone to systematic errors [183].

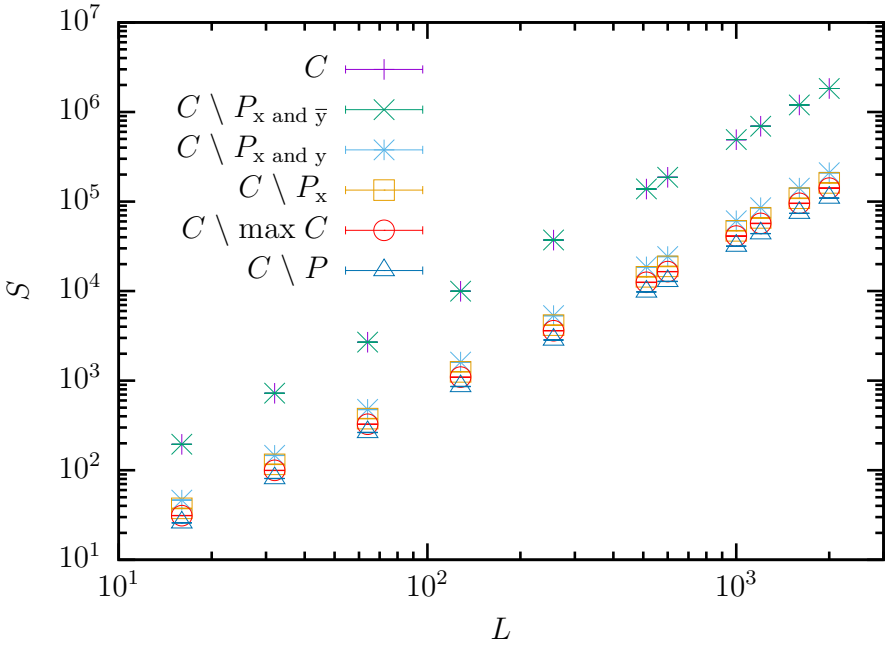

Figure 4.4: Log-log plot of the average cluster size as a function of L, for the different definitions, at the Ising critical temperature $T_{\mathrm{c}} = 2/\ln(1+\sqrt{2})$.

Nonetheless, since the percolation temperature is known analytically for the geometrical clusters of the two-dimensional Ising model, which coincides with that of the thermal phase transition [29–31], we performed simulation exactly at $T_{\mathrm{c}} = 2/\ln(1+\sqrt{2})$. Consequently for $T = T_{\mathrm{c}}$, $\tilde{S}(0) = \text{const.}$, and Eq. (4.4) becomes $S(L) \sim L^{\gamma/\nu}$, which allows an estimation of the exponent γ/ν. In Fig. 4.4 the average cluster size is plotted as a function of the system size and for all the definitions introduced above. For the definitions at hand, data seems to follow straight lines, parallel to each other. This implies that corrections to scaling are not prominent and that the γ/ν exponent is independent of the definitions been used. For the estimation of γ/ν we performed fits using the least-squares Levenberg-Marquardt algorithm[3] [183] for each of the different definitions. Fits performed in intervals $L_{\mathrm{min}} \leq L \leq L_{\mathrm{max}}$, where L_{min} was continuously increased while L_{max} was kept fixed at $L_{\mathrm{max}} = 2000$. By performing consecutive linear fits with an increasing value of L_{min}, we were also able to monitor the influence of corrections to scaling.

Figure 4.5 shows the estimates of γ/ν as a function of $1/L_{\mathrm{min}}$, and in Table B.1, shown in the Appendix, we report the estimates of γ/ν and the respective quality-of-fit parameters Q [183] for the different definitions. From the definitions used, C and $C \setminus P_{\mathrm{x\ and\ \bar{y}}}$ converge relatively quickly to the asymptotic value $\gamma/\nu = 91/48$ [89], which is denoted by the dashed horizontal line in Fig. 4.5. Additionally, from Table B.1 we observe that for the C and $C \setminus P_{\mathrm{x\ and\ \bar{y}}}$ with $L_{\mathrm{min}} \geq 64$ and $L_{\mathrm{min}} \geq 256$ respectively, the estimations of the exponent are less than 3 standard deviations (3σ) away from the asymptotic value, verifying the fact

[3] In general, the Levenberg-Marquardt algorithm is a common method for fitting to non-linear models. However, for the fits performed in this thesis we used the `gnuplot` program, where the Levenberg-Marquardt algorithm is the standard in-built option.

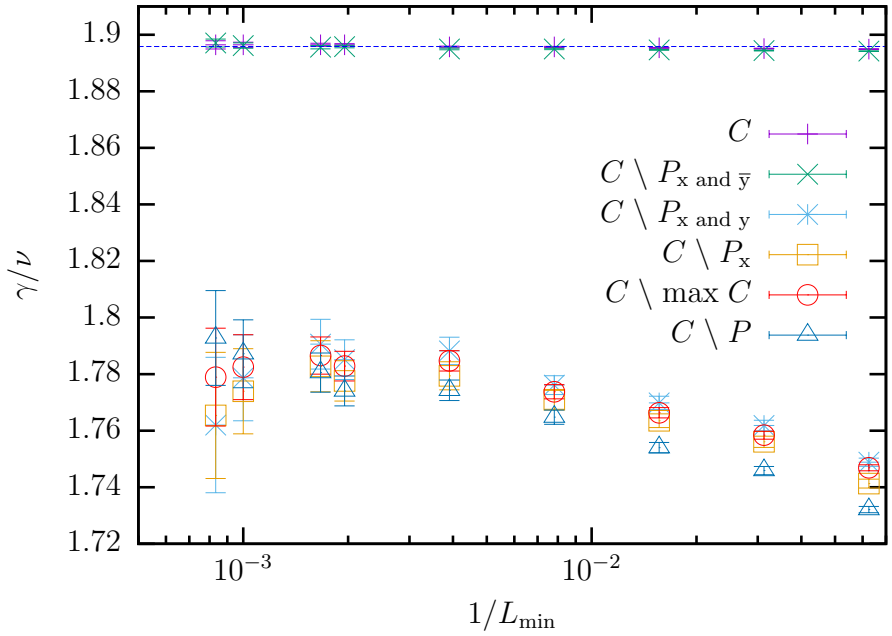

Figure 4.5: Exponent ratio γ/ν as a function of $1/L_{\min}$, for the different definitions, using linear fits. The dashed horizontal line marks the asymptotic value $91/48 \approx 1.896$ [89].

that corrections to scaling are not significant. In contrast, corrections to scaling are quite substantial for the rest of the definitions, i.e., $C \setminus P_{\text{x and y}}$, $C \setminus P_{\text{x}}$, $C \setminus \max C$, and $C \setminus P$, cf. Fig. 4.5. For example, even for the largest $L_{\min}$ value, i.e., $L_{\min} = 1200$, the deviation from the asymptotic value is greater than 5σ, see Table B.1.

Thus, we see that for the average cluster size the C and $C \setminus P_{\text{x and } \bar{\text{y}}}$ definitions lead to considerably smaller corrections to scaling compared to the rest of definitions. Finally, the fact that C and $C \setminus P_{\text{x and } \bar{\text{y}}}$ definitions give similar results can be explained as follows: Clusters that percolate in one but not the other direction are very scarce. Thus, excluding them from the sums of Eq. (2.60) will not alter the average cluster size significantly. Estimates of the exponent have been also reported in Ref. [184] using the $C \setminus P_{\text{x}}$ definition, and in Ref. [33] using the C definition.

4.3 Percolation Strength

The inclusion of different definitions can also be applied to the case of the percolation strength P_∞. As we discussed in Sec. 2.4.1, P_∞ is the probability of a site to belong to the infinite cluster, in the thermodynamic limit. For finite systems though, this is usually defined as the probability for a site to belong in the largest cluster, which can be estimated by the number of sites belonging to the largest cluster divided by the total number of sites. This is shown in Fig. 4.6, where P_∞ is plotted as a function of temperature for a system of linear size $L = 256$. As temperature goes to zero, P_∞ goes to 1, meaning that all spins belong to the same cluster. Exactly at zero temperature geometrical clusters are identical to the FK clusters. As temperature now increases the percolation strength will decrease, as the size of

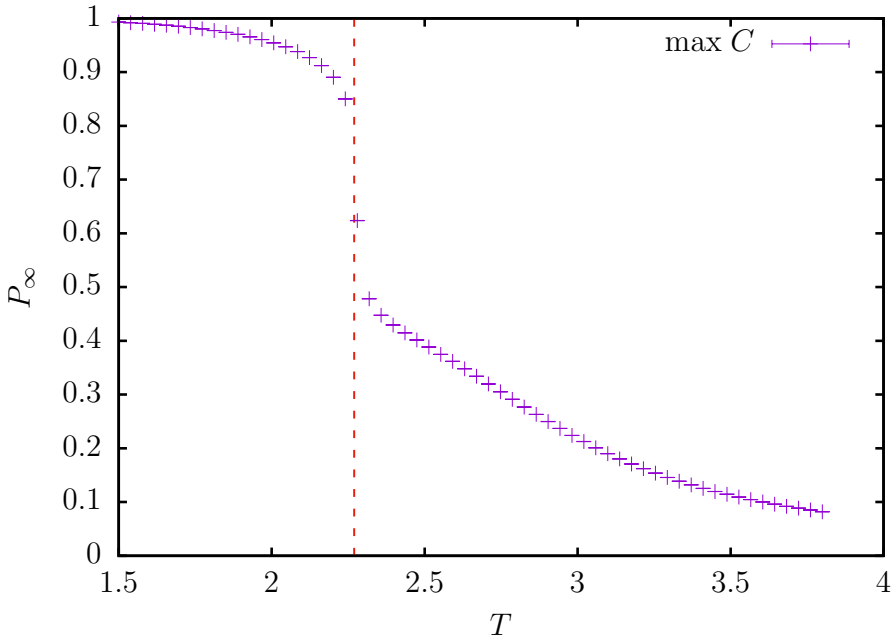

Figure 4.6: Percolation strength P_∞ as a function of temperature of the two-dimensional Ising ferromagnet for a system of linear size $L = 256$. In each measurement, the largest cluster is considered (max C). The dashed vertical line marks the transition temperature of the two-dimensional Ising model.

the percolating cluster (or the largest in that occasion) will decrease. According to FSS, in the vicinity of the critical point the percolation strength has the following scaling behaviour [19]

$$P_\infty\left(L,T\right) = L^{-\beta/\nu}\widetilde{P}_\infty\left[\left(T-T_\mathrm{c}\right)L^{1/\nu}\right], \tag{4.6}$$

where $\widetilde{P}_\infty$ is a universal scaling function.

Adapting now the idea of different cluster sets for the case of percolation strength we can obtain several definitions. Specifically, we consider in each configuration, the fraction of sites that belong to the:

1. Largest cluster: max C.
2. Largest percolating cluster: max P.
3. Largest cluster that percolates in horizontal and in vertical direction: max $P_{\mathrm{x\ and\ y}}$.
4. Largest cluster that percolates in one specific direction, e.g., horizontal: max P_x.
5. Largest cluster that percolates in one but not the other direction, e.g., horizontal and not vertical: max $P_{\mathrm{x\ and\ }\overline{\mathrm{y}}}$.

Depending on the definition it is possible that the percolation strength, given a configuration, could be zero as it is likely that none of the clusters percolate in the way that is dictated by

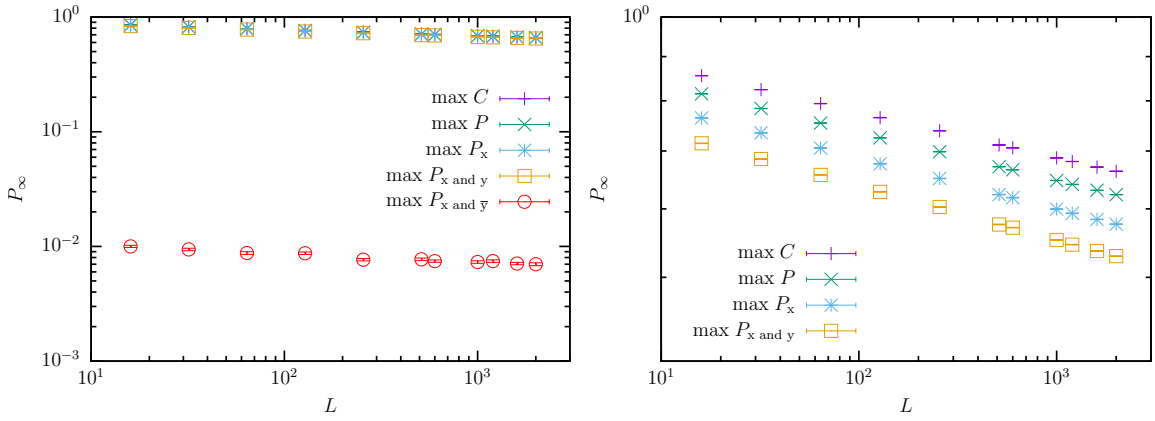

Figure 4.7: Log-log plot of the percolation strength as a function of L, at the Ising critical temperature $T_{\mathrm{c}} = 2/\ln(1+\sqrt{2})$ for (a) all definitions, (b) all definitions except max $P_{\mathrm{x\ and\ \bar{y}}}$. The data for the different definitions in panel (b) have been shifted downwards by: max P 0.04, max P_{x} 0.08, and max $P_{\mathrm{x\ and\ y}}$ 0.12, for clarity.

the definition. The only exception to that is the max C, where for each configuration the largest cluster is always considered.

As with the average cluster size, for simulations exactly at the critical temperature of the two-dimensional Ising model, $\widetilde{P}_\infty(0) = \text{const.}$, and Eq. (4.6) becomes $P_\infty(L) \sim L^{-\beta/\nu}$, which allows for the estimation of the involved exponent. In Fig. 4.7 P_∞ is plotted as a function of L on a log-log scale, for the different definitions considered. Data from different definitions seem to follow straight lines indicating small scaling corrections. In order to check the influence of scaling corrections, we follow the same procedure as with the average cluster size, by performing fits in intervals $L_{\min} \leq L \leq L_{\max}$, with varying $L_{\min}$, while $L_{\max} = 2000$ is fixed.

As we can see in Fig. 4.8 for all definitions, aside from max $P_{\mathrm{x\ and\ \bar{y}}}$, the asymptotic value $\beta/\nu = 5/96$ (dashed horizontal line) is approached relatively quickly indicating that corrections to scaling are not substantial. This is also verified in Table B.2 in the Appendix, where for $L_{\min} \geq 64$ the deviations from the asymptotic value is less than 3σ for all definitions, except for max $P_{\mathrm{x\ and\ \bar{y}}}$. Specifically, for max $P_{\mathrm{x\ and\ y}}$ deviations are less that 2σ for all values of $L_{\min}$. For the max $P_{\mathrm{x\ and\ \bar{y}}}$ definition, although the estimations are less than 3σ for all $L_{\min} \geq 16$, the respective error bars are quite large, see Table B.2. This is to be expected, as clusters percolating in one but not the other direction are relatively rare, which leads to poor statistics during the simulation process, and thus to large error bars in the estimation of the exponent.

4.4 Concluding Remarks

In this chapter we discussed the properties of the geometrical clusters of the two-dimensional Ising model. In particular, the properties of the wrapping probabilities and their interrelations, as well as the average cluster size and percolation strength along with their corre-

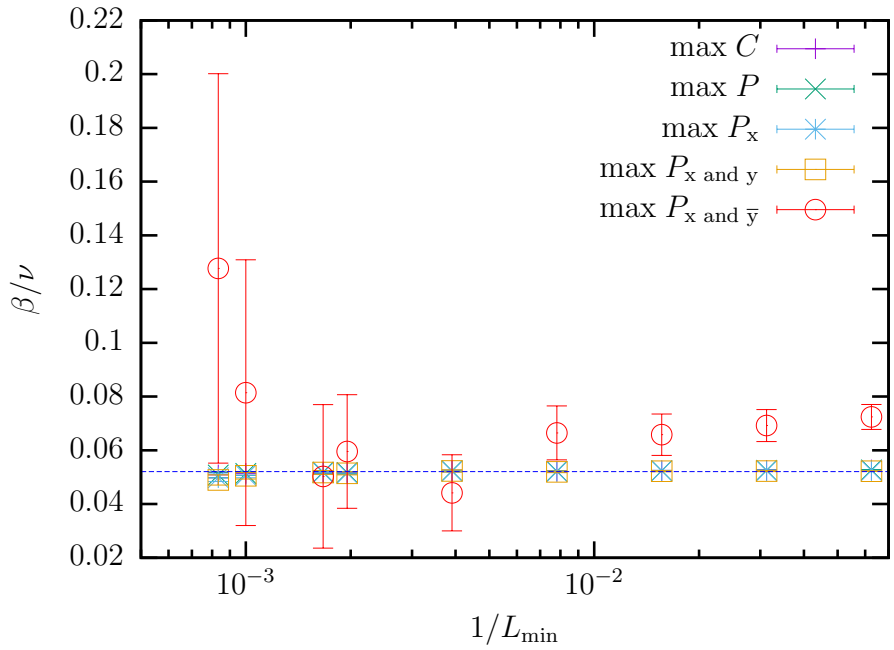

Figure 4.8: Exponent ratio β/ν as a function of $1/L_{\min}$, for the different definitions, using linear fits. The dashed horizontal line marks the asymptotic value $5/96 \approx 0.052$ [89].

sponding exponents were studied. As for the latter, we utilised different sets of clusters for the estimation of the critical exponents for the average cluster size and percolation strength. We also monitor the influence of corrections to scaling, via fits on intervals $L_{\min} \leq L \leq L_{\max}$ with increasing $L_{\min}$ while $L_{\max}$ was kept fixed at $L_{\max} = 2000$. The accuracy of our data reveals the existence of corrections to scaling for the different cluster-sets at hand, and for the sets where scaling corrections are not substantial our estimates are in good agreement with the theoretical values.

For the average cluster size, the convergence to the asymptotic value is relatively fast when (i) all clusters are included (ii) excluding clusters that percolate in one but not the other direction. For the rest of the definitions, i.e., excluding the largest cluster, clusters percolating in both directions, and clusters percolating in one direction, strong scaling corrections are observed.

The percolation strength does not exhibit a strong dependence on the cluster definitions used. All definitions, except max $P_{\mathrm{x\ and\ \bar{y}}}$, provide high accuracy estimates for the involved exponent. The discrepancy between max $P_{\mathrm{x\ and\ \bar{y}}}$ and the rest of the definitions relies on the poor statistics for the estimation of the percolation strength, as in that case clusters percolating in one but not the other direction are very rare.

The above analysis for the estimates of critical exponents using different sets of clusters revealed that strong scaling corrections can emerge when specific definitions are chosen (see also Ref. [185]). For example, excluding the largest cluster in the estimation of the average cluster size leads to substantial scaling corrections, nonetheless this is the usual definition used in percolation studies [19]. Hence, the above analysis will be also utilised in the next chapter, where the percolation properties of the multi-replica Ising model are discussed.

Chapter 5

The 2- 3- and 4-replica Ising Model

Ordinary percolation can be understood as one of the simplest models exhibiting a phase transition. Over the years many variants and modified percolation models have been introduced, finding applications in many and diverse fields (for reviews see, e.g., Refs. [26, 83, 186]). Specifically, in statistical physics the formulation introduced by Fortuin and Kasteleyn for the q-state Potts model as a site-bond correlated percolation process (see Sec. 2.4.2), where the limiting cases of $q \to 0$ and $q \to 1$ correspond to tree and uncorrelated percolation respectively [186], has greatly enhanced our understanding for the q-state Potts model. However, finding a well-defined percolation process for a general class of models, such as spin-models, is by no means a straightforward task, as the percolation process depends strongly, in general terms, on the specific system at hand. For example, the FK clusters for the q-state Potts model propagate the critical fluctuations of the system, as the spin correlation function is equal to the probability of finding two sites belonging in the same cluster in the FK representation [26]. Over the years attempts have been made to tackle other spin systems, such as spin glasses, by defining a suitable percolation process. Unfortunately, the FK representation does not properly describe the phase transition of the spin-glass system, with clusters percolating at a much higher temperature [40, 41].

For such a description, attempts have been made by studying the percolation properties of clusters defined from several non-interacting copies (replicas) of the initial system. Houdayer's algorithm [48] (see Sec. 3.3.2) as well as the proposed cluster algorithms by Machta et al., in Ref. [40] of the two-replica FK representation [49] and the spin-glass version of Chayes, Machta, and Redner (CMR) [50, 51], are in the right direction. Nonetheless, little attention has been paid to the percolation properties of such replicas for the ferromagnetic case. This can be beneficial as on one hand features of such cluster could potentially be utilised in the study of spin-glass systems, and on the other hand this defines an interesting percolation problem in its own right.

In this chapter, we will discuss such a percolation process for the two-dimensional Ising model, defined in terms of multiple replicas of the system, i.e. *multi-replica* Ising model. Specifically, we will consider the cases of two, three, and four replicas, where two types of clusters will be involved, namely the *soft constraint* and *hard constraint* clusters. For the two cluster types the critical behaviour will be studied, in terms of identifying the critical point and the set of critical exponents that characterize the transition.

5.1 Multi-replica Ising Model

In order to introduce the multi-replica Ising model, let us rewrite here the Hamiltonian of the Ising model in the absence of an external field, cf. Eq. (2.1),

$$\mathcal{H} = -J \sum_{\langle i,j \rangle} \sigma_i \sigma_j. \tag{5.1}$$

The multi-replica Ising model consists of k copies (replicas), all of which are described by Eq. (5.1). All replicas are at the same temperature T and do not interact with each other, thus being *statistically independent*. Consequently, one can write the partition function of the system as

$$Z = \sum_{\mu^{(1)}} \sum_{\mu^{(2)}} \cdots \sum_{\mu^{(k)}} e^{-\beta\left[\mathcal{H}^{(1)}+\mathcal{H}^{(2)}+\cdots+\mathcal{H}^{(k)}\right]}, \tag{5.2}$$

where $\mu^{(n)}$, $\mathcal{H}^{(n)}$ is the spin configuration and energy of the n-th replica respectively.

Assuming that all k replicas are defined on a lattice of linear size L, we can construct a new set of spin variables k, defined on a lattice of linear size L too, at the site i of which k_i takes the values ± 1 according to

$$k_i = \prod_{r=1}^{k} \sigma_i^{(r)}, \tag{5.3}$$

where the superscript r is used to distinguish between different replicas. On the k-plane, defined from Eq. (5.3), we identify the geometrical clusters, i.e., neighbouring spins pointing in the same direction, in two distinct ways:

1. From neighbouring spins i, j satisfying $k_i = k_j$: We refer to those as *soft constraint* clusters.

2. From neighbouring spins i, j satisfying $\sigma_i^{(r)} = \sigma_j^{(r)}, \quad \forall\, r = 1, 2, \ldots, k$: We refer to those as *hard constraint* clusters[1].

As it is illustrated in Fig. 5.1 for the case of two replicas, the hard constraint clusters are subsets of the soft constraint clusters. Additionally, note that the soft constraint clusters are the same as the ones of Houdayer's cluster algorithm, cf. Sec. 3.3.2. Having defined the multi-replica Ising model for the general case of k replicas we now proceed with the critical properties of the 2-replica Ising model in two dimensions.

5.2 The 2-replica Ising Model

In this section we will discuss the percolation properties of the 2-replica Ising model in two dimensions. Since the replicas are at the same temperature and do not interact with each other in the limit of infinite temperature every spin in each replica has equal probability of pointing up or down. This results in configurations in the k-plane, defined above, where

[1] It is easy to check that the definition of the hard constraint clusters immediately implies that $k_i = k_j$.

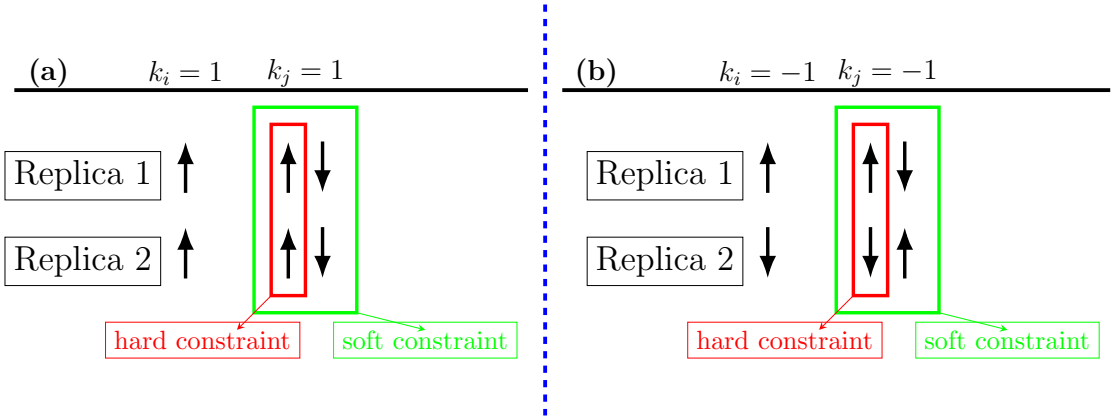

Figure 5.1: Schematic representation of the formation of soft and hard constraint clusters between two neighbouring spins, for the 2-replica case.

each spin is uncorrelated with each other, pointing in random directions, and consequently clusters will be of very small size. However, one has to be careful with such arguments since the existence of large or even percolating clusters strongly depends on the geometry of the lattice. For example, in lattice geometries where the percolation threshold (see Sec. 2.4) is not greater than 0.5, e.g., cubic lattices, percolating clusters will occur even in the infinite temperature limit. Nonetheless, since our simulations were performed on square lattices (to be discussed below), the percolation threshold is above[2] 0.5.

On the other hand, at temperatures sufficiently below the critical one, both replicas should be characterized by a large percolating cluster whose size is comparable with the size of the entire system. Thus, in the k-plane a percolating cluster should also occur at such temperatures. Consequently, there must be a critical temperature, such that an incipient spanning cluster in the k-space emerges. It is tempting and to some extent plausible, to assume that the critical temperature should be the critical temperature of the Ising model (or 1-replica Ising model, as we will address it from now on). This statement can be supported by looking at typical configurational snapshots as in Fig. 5.2, where configurations of the two replicas are shown (upper panel) along with the soft and hard constraint cluster (lower panel) for a system of linear size $L = 128$ at the critical temperature of the 1-replica model. In that case we see that replicas 1 and 2 have a large percolating cluster, whereas the soft and hard constraint clusters are just critical, with the appearance of an incipient percolating cluster for both soft and hard constraint clusters. Of course, the precise location of the critical temperature will be obtained in a more robust way (see Sec. 5.2.2), rather than simply looking at random equilibrium configurations, however it provides a qualitative picture for the behaviour of the system.

In what follows, we will discuss the percolation properties of the 2-replica Ising model in two dimensions. Specifically, we will obtain the transition temperature T_c, of the model as well as the set of critical exponents concerning the correlation length, average cluster size and percolation strength, i.e., ν, γ, and β, respectively. To this end, Monte Carlo simulations and a FSS analysis will be employed. In particular, we simulated the 2-replica Ising model

[2] An interesting case in two dimensions is also the triangular lattice, where the site-percolation threshold is exactly 0.5.

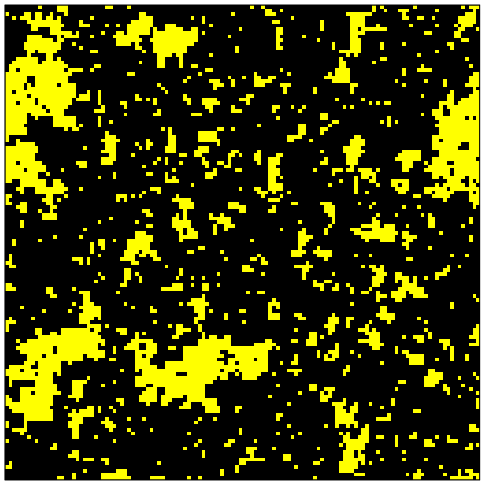

(a) Replica 1.

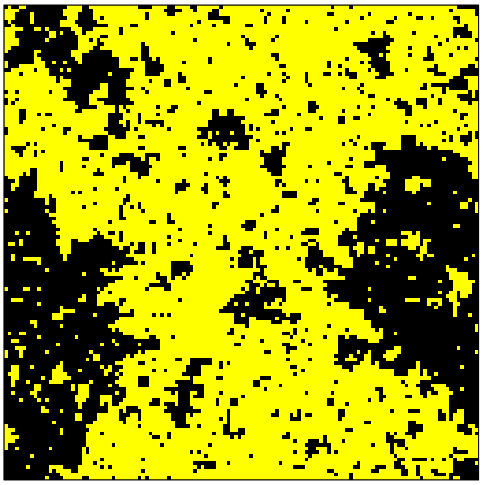

(b) Replica 2.

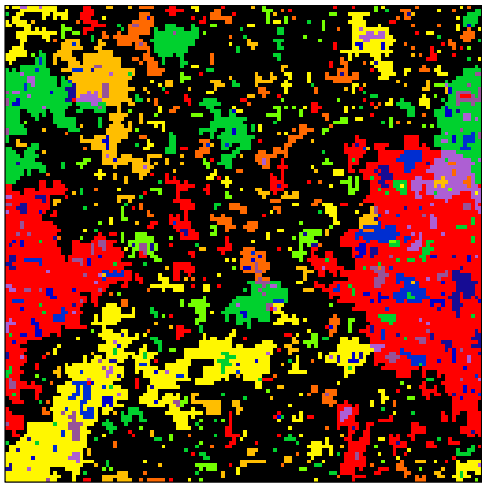

(c) Soft constraint clusters.

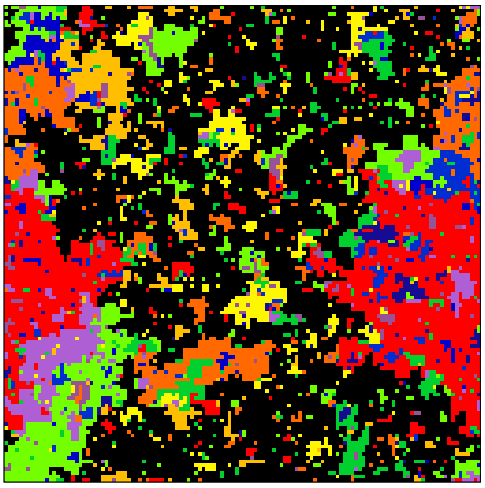

(d) Hard constraint clusters.

Figure 5.2: Snapshot configurations of the two-dimensional Ising model, at the critical temperature T_c. (a) First replica. (b) Second replica. (c) Soft constraint clusters. (d) Hard constraint clusters. In (c) and (d) all clusters, apart from the largest percolating one, are assigned colours at random. For the largest percolating cluster of both the soft and hard constraint definitions, the same colour (black) is assigned. Note that in our setup we allow the black colour to be assigned *only* to the largest percolating cluster.

in two dimensions on a square lattice using periodic boundary conditions for a range of system sizes and temperatures, including the critical temperature of the 1-replica model, i.e., $T_c = 2/\left(1+\sqrt{2}\right)$. Simulations were performed using the SW algorithm [27], for systems of linear size $L = 8$, 10, 16, 20, 32, 40, 50, 64, 80, 100, 128, 160, 200, 256, 320, 400, 512, 640, 800, 1024, 1280, 1600 and 2048. For each system size and each replica a total number of $1.1 \times \tau_{\text{int, E}} \times 10^5$ sweeps was considered, where $\tau_{\text{int, E}}$ is the integrated autocorrelation time of the energy (see Appendix A.1). The estimates of $\tau_{\text{int, E}}$, rounded up to the next largest integer, are varying from $\tau_{\text{int, E}} = 3$ sweeps for $L = 8$ to $\tau_{\text{int, E}} = 15$ sweeps for $L = 2048$. For each L the first $\tau_{\text{int, E}} \times 10^4$ sweeps were discarded during equilibration and a measurement was taken after $\tau_{\text{int, E}}$ sweeps, leading to a number of 10^5 measurements per run. On each measurement and for both cluster types, the full cluster profile of the configuration was recorded, i.e., size of *each* cluster, and whether it percolates. From that, we calculated the wrapping probabilities, average cluster size, and percolation strength, for the different definitions as introduced in Chap. 4. For the percolation (or wrapping due to the periodic boundary conditions) of the clusters we employed the method of Machta et al. [171] (see also Ref. [172] for an alternative method).

We will now proceed with a general description of the observables introduced above. As for each observable we will consider two cluster types, namely soft and hard constraint clusters (see Sec. 5.1), a superscript (s) and (h) will be used in all the quantities considered, in order to distinguish them.

5.2.1 Observables

Wrapping probabilities

Firstly, we consider the different types of wrapping probabilities R as introduced in Sec. 4.1, for the soft and hard constraint clusters of the 2-replica Ising model. In Figs. 5.3 and 5.4 the wrapping probabilities R are plotted as a function of temperature T for the different system sizes L of the soft and hard constraint clusters, respectively. Except for $R_{\text{x and }\bar{\text{y}}}$, the wrapping probabilities increase as the temperature decreases, signalling the existence of a percolating cluster. Additionally, for all R's (including $R_{\text{x and }\bar{\text{y}}}$), curves of different L seem to cross around a temperature which is close to that of the 1-replica Ising model which is denoted by the dashed vertical line, for both cluster types (see right panel of Figs. 5.3 and 5.4). In percolation studies such crossings denote the transition point from a non-percolating to a percolating phase, see, e.g., [173, 176]. More rigorous considerations about the estimation of the critical point will be given in Sec. 5.2.2, for now note that this observation is in agreement with the snapshots of Fig. 5.2.

The $R_{\text{x and }\bar{\text{y}}}$ case is of some importance since, as we discussed in Sec. 4.1, it exhibits a maximum that shifts towards the critical point as the size of the system increases. Additionally, as it was stated above such a function also exhibits a crossing point, for the soft and hard constraint clusters, respectively. Both, the position of the maxima as well the crossing points, are expected to converge to the critical point of the infinite system [173]. In numerical studies of ordinary percolation it has been observed that $R_{\text{x and }\bar{\text{y}}}$ exhibits both crossing points and maxima *only* in three dimensions [176], whereas in two dimensions there are no crossings among the curves [173, 176]. Thus, the existence of both crossing points and maxima for the two-dimensional Ising model is an interesting feature.

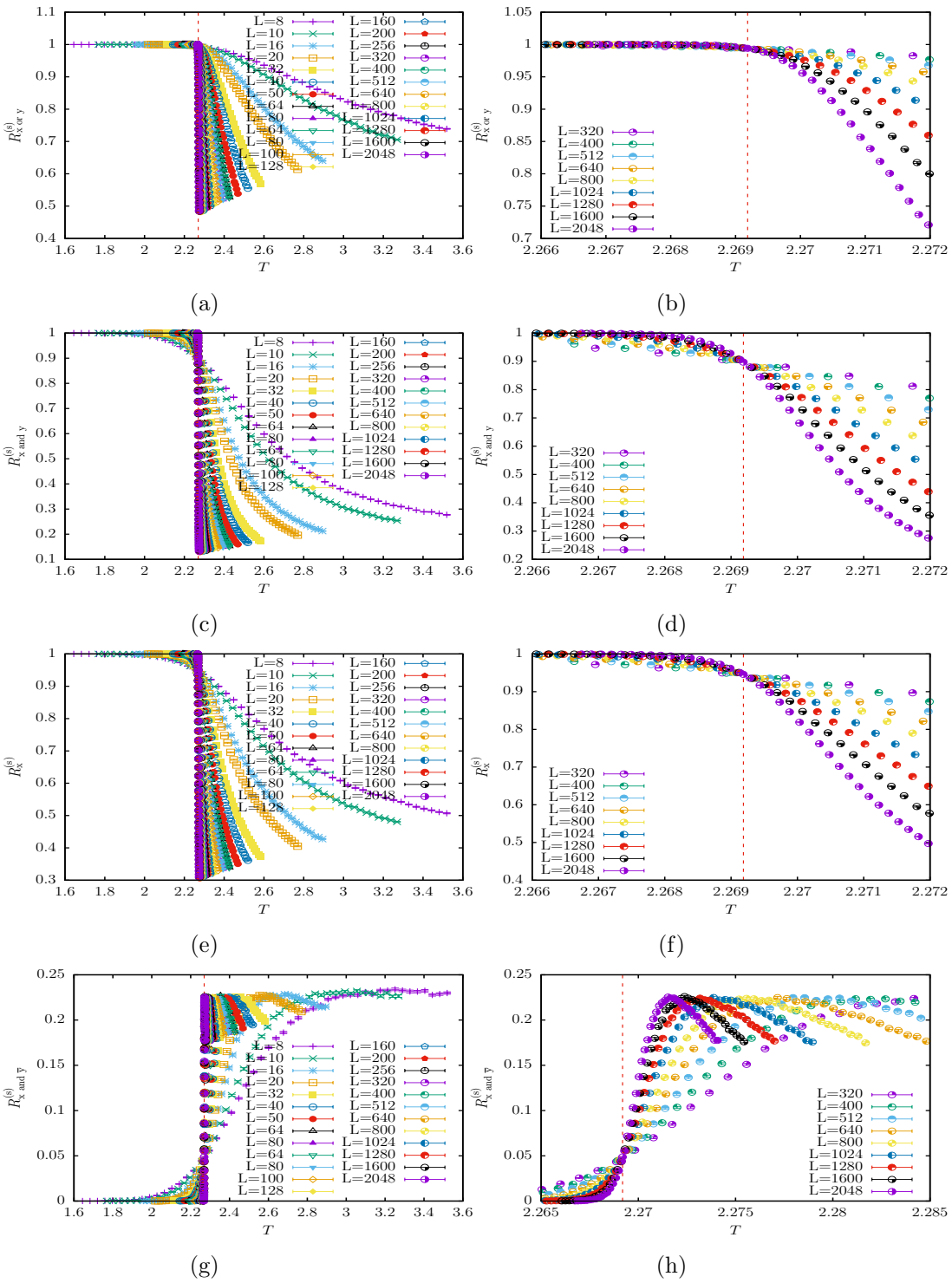

Figure 5.3: *Left column*: Wrapping probabilities of the soft constraint clusters, for the 2-replica Ising model as function of temperature T, for different system sizes L. *Right column:* Analogous to left column for the larger system sizes considered. The dashed vertical line marks the transition temperature of the 1-replica Ising model.

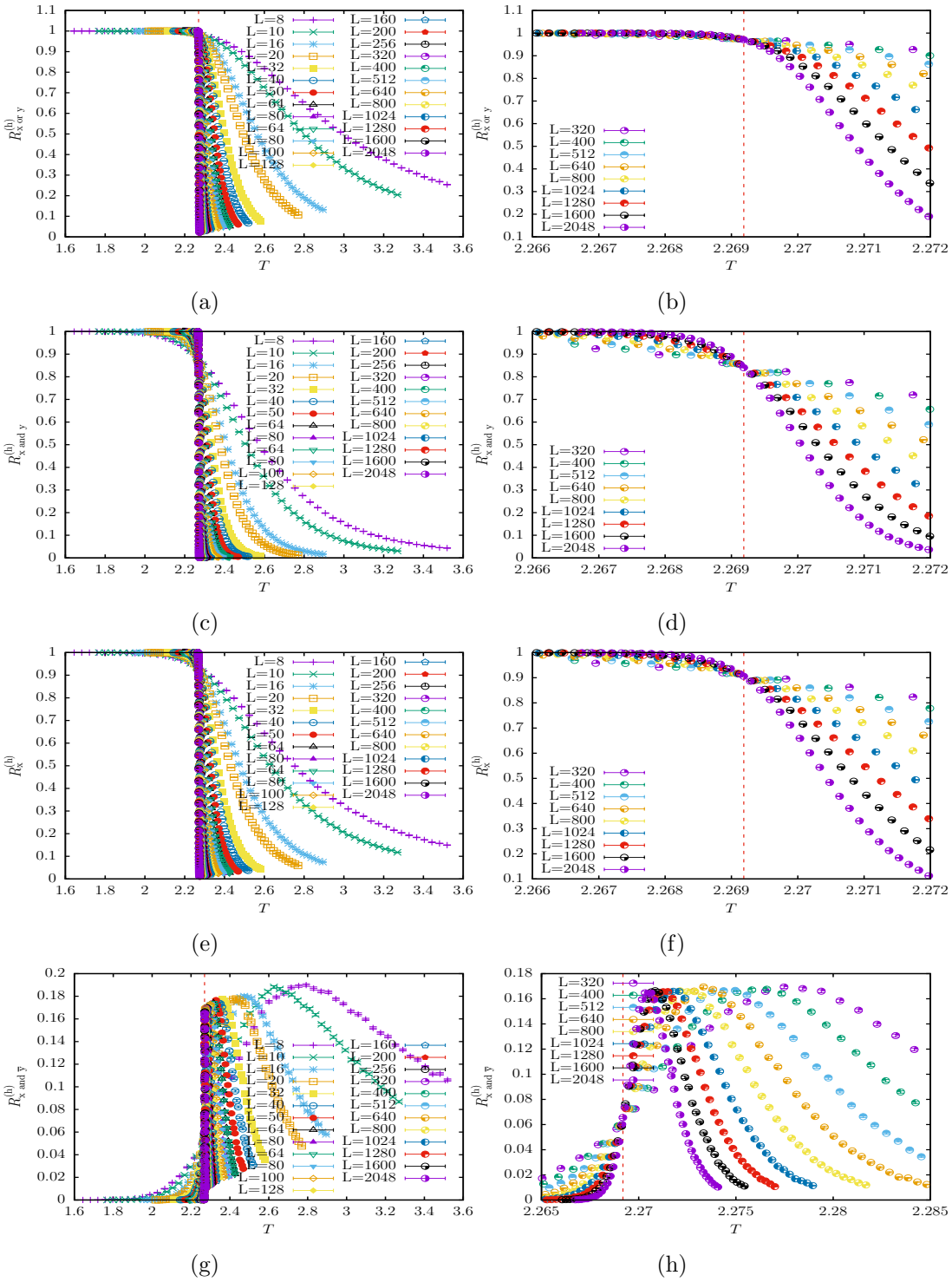

Figure 5.4: *Left column*: Wrapping probabilities of the hard constraint clusters, for the 2-replica Ising model as function of temperature T, for different system sizes L. *Right column:* Analogous to left column for the larger system sizes considered. The dashed vertical line marks the transition temperature of the 1-replica Ising model.

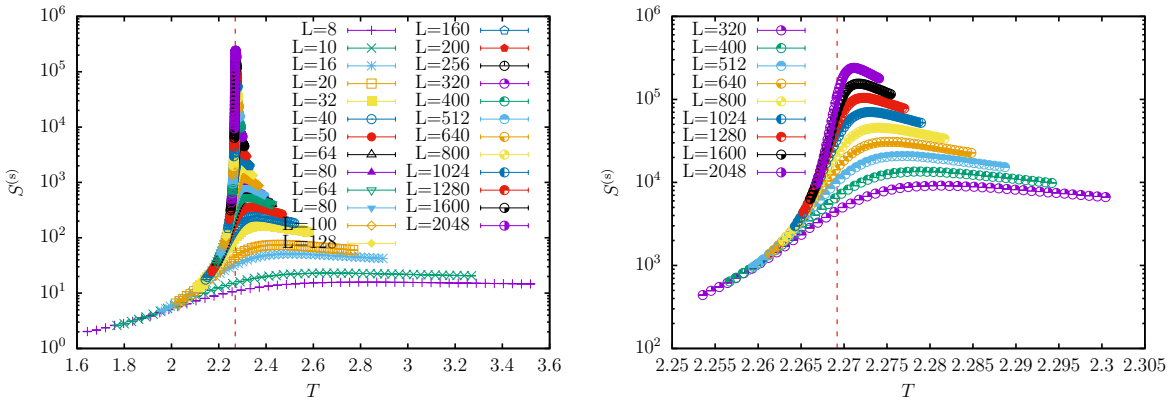

(a) (b)

Figure 5.5: (a) Average cluster size of the soft constraint clusters $S^{(s)}$ on a semi-log axis, for the 2-replica Ising model as a function of temperature T, for different system sizes L. (b) Analogous to panel (a) for the larger system sizes considered. The dashed vertical line marks the transition temperature of the 1-replica Ising model.

Average cluster size

Using the conventional definition of the average cluster size S, where the largest cluster is excluded from the sums of Eq. (2.60), such quantity should exhibit a maximum which increases as the size of the system increases, while the location of the maximum should be around the transition point, and shifted towards its asymptotic value with the increasing size of the system. This is shown in Figs. 5.5 and 5.6, where S is plotted as a function of temperature T for the different system sizes L of the soft and hard constraint clusters respectively. As the system size increases the maximum of S also increases, and the location of the peak shifts to lower temperatures, approaching (presumably) the transition point of the 1-replica Ising model, which is again denoted by the dashed vertical line (see Figs. 5.5(b) and 5.6(b) for the soft and hard constraint clusters, respectively). Additionally, from Figs. 5.5 and 5.6 we can observe that for a fixed temperature and system size, the soft constraint clusters are on average larger than the hard constraint clusters, e.g., for $L = 2048$ the peak of the hard constraint cluster is very close to 10^5 as shown in Fig. 5.6(b), while from Fig. 5.5(b) we see that the corresponding peak for the soft constraint clusters is around 2×10^5. This is to be expected, since as it was already mentioned in Sec. 5.1 the hard constraint clusters are a subset of the soft ones.

Percolation strength

The percolation strength P_∞ as a function of temperature T for different system sizes L of the soft and hard constraint clusters is shown in Figs. 5.7 and 5.8, respectively. In these plots we used the definition of P_∞, where the largest cluster is considered in each measurement, see Sec. 4.3. For both cluster types the percolation strength increases with decreasing temperature, and it approaches the value 1 as the temperature goes to zero, signalling the fact that all spins in their respective replicas are pointing in the same direction. As the temperature increases, the percolating clusters in each replica reduce their size, resulting in percolating

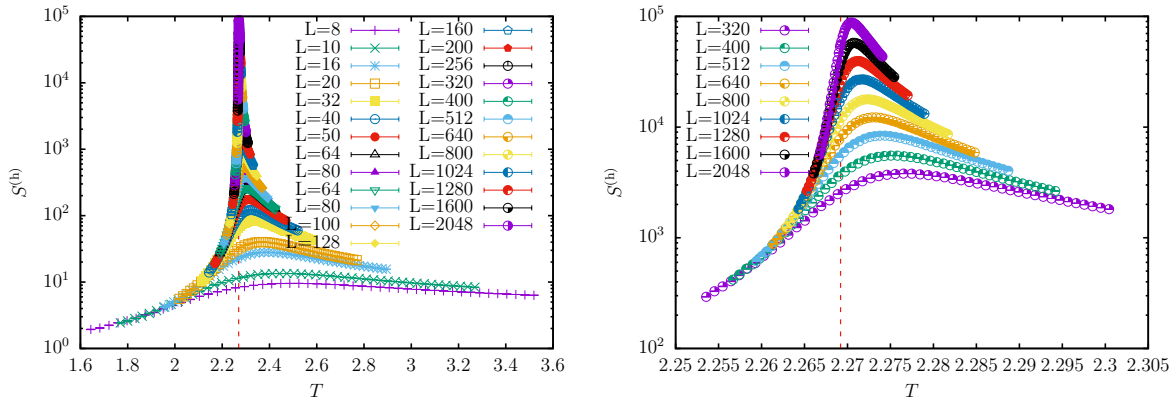

(a) (b)

Figure 5.6: (a) Average cluster size of the hard constraint clusters $S^{(\mathrm{h})}$ on a semi-log axis, for the 2-replica Ising model as a function of temperature T, for different system sizes L. (b) Analogous to panel (a) for the larger system sizes considered. The dashed vertical line marks the transition temperature of the 1-replica Ising model.

clusters in the k-plane of smaller size. Finally, at very high temperatures percolation strength will be essentially zero, as very small clusters occurs in both replicas, and consequently the percolation strength of the soft and hard constraint clusters for the 2-replica Ising model will be zero too, cf. Sec. 4.3.

Note that the behaviour of the above observables for the soft and the hard constraint clusters is, at least qualitatively, similar to that of the 1-replica Ising model. For the latter case we already discussed the scaling behaviour of the average cluster size and percolation strength, by performing simulations at the critical point of the 1-replica Ising model and determining the critical exponents γ/ν and β/ν, see Chap. 4. We will now proceed to the investigation of the critical behaviour of the 2-replica Ising model for the soft and hard constraint clusters, respectively.

5.2.2 Critical behaviour

The critical behaviour of the 2-replica Ising model will be discussed in this section. We will begin with the estimation of the critical exponent ν and critical temperature for the soft and hard constraint clusters, respectively, by utilising the wrapping probabilities. Subsequently, the critical exponents γ/ν and β/ν will be determined by utilising different sets of clusters, as introduced in Chap. 4.

Critical exponent ν

In Sec. 2.3 we discussed how the ν exponent can be determined from the maximum of derivatives of the Binder cumulant or the maximum of derivatives of logarithms of powers of the magnetisation, via Eqs. (2.52) and (2.54) respectively. In the FK representation percolation quantities correspond to observables of the physical system, e.g., the percolation strength of the FK clusters is equivalent to the magnetisation of the system. For geometrical clusters,

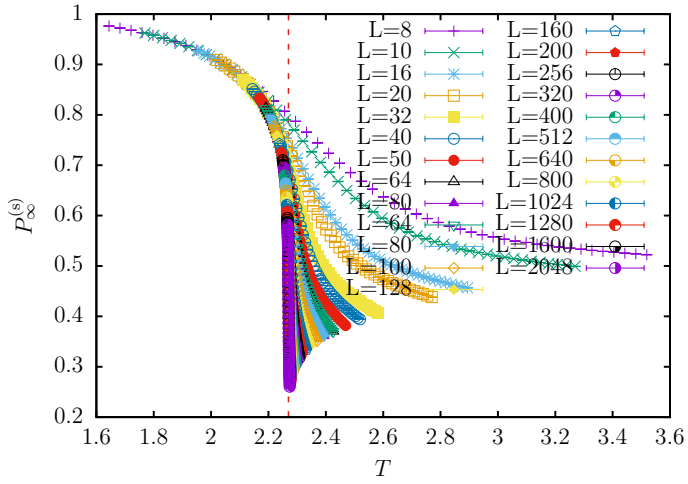

Figure 5.7: Percolation strength of the soft constraint clusters $P_\infty^{(s)}$, for the 2-replica Ising model as a function of temperature T, for different system sizes L. The dashed vertical line marks the transition temperature of the 1-replica Ising model.

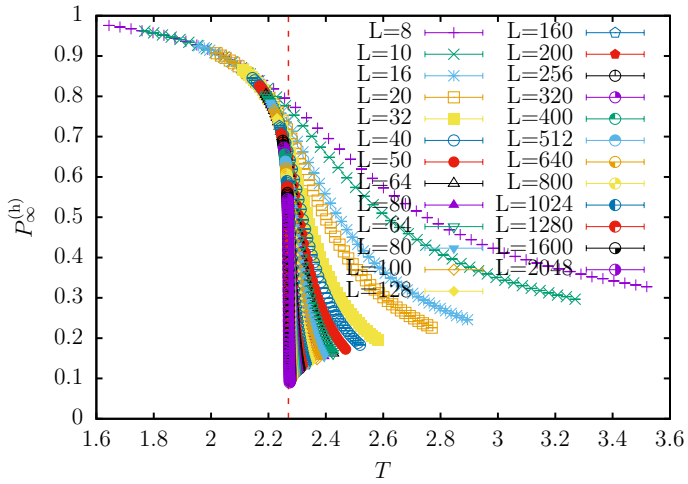

Figure 5.8: Percolation strength of the hard constraint clusters $P_\infty^{(h)}$, for the 2-replica Ising model as a function of temperature T, for different system sizes L. The dashed vertical line marks the transition temperature of the 1-replica Ising model.

however, such a correspondence is absent, thus one cannot utilise directly Eqs. (2.52) and (2.54) to determine the ν exponent.

Nonetheless, one can work with quantities similar to the Binder cumulant which are expected to exhibit the same scaling behaviour. As we have pointed out in Sec. 4.1, in numerical studies of percolation wrapping probabilities have been employed to estimate the critical exponent ν. These are dimensionless quantities which depend strongly on the geometry of the lattice, similar to the Binder cumulant (for the latter see, e.g., Refs. [148, 187–189]). Thus, in the vicinity of the critical point the maximum of the derivative of R with respect to temperature is expected to behave as [173, 176]

$$\left|\frac{dR}{dT}\right|_{\max} \sim L^{1/\nu}. \tag{5.4}$$

The absolute value in taken, as R is a monotonously decreasing function of temperature leading to a negative slope for all definitions, except $R_{\mathrm{x\ and\ \bar{y}}}$ which for temperatures below its maximum is an increasing function of temperature (positive slope) for both cluster types (see Figs. 5.3 and 5.4).

These maxima are numerically determined by finding the root of the second derivative of R with respect to temperature. For the evaluation of the derivative the symmetric-finite-difference approximation was used, and the root of the second derivative was estimated using the bisection method [183]. In order to minimize the effects of systematic errors coming from the numerical estimation of derivatives, the single histogram reweighting technique was employed (see Appendix A.4).

In Figs. 5.9 and 5.10 the maximum of the absolute values of the derivatives of the wrapping probabilities with respect to temperature are plotted as a function of the system size L, for the soft and hard constraint clusters, respectively. The seemingly straight lines for all definitions considered (on a log-log plot) for both soft and hard constraint clusters, indicate that Eq. (5.4) is valid, and that the slopes of such lines should provide estimates of the ν exponent.

To extract ν, we performed linear fits similar to the ones described in Sec. 4.2. Specifically, we considered intervals of $L_{\min} \leq L \leq L_{\max}$ where fits were performed by systematically increasing $L_{\min}$, while $L_{\max}$ was kept fixed at $L_{\max} = 2048$. Estimated values from fits for the ν exponent as a function of $1/L_{\min}$ are shown in Figs. 5.11 and 5.12 for the soft and hard constraint clusters respectively. For the soft constraint clusters and for L above a certain threshold around $L_{\min} = 100$, estimates of the exponent ν for the soft constraint clusters are consistent with a value around 1, i.e., $\nu^{(\mathrm{s})} \approx 1$. This can also be verified from Table B.3 in the Appendix, where we report the values of $\nu^{(\mathrm{s})}$ for different fit intervals, the deviation Δ_σ of the estimates from $\nu^{(\mathrm{s})} = 1$ in multiples of their estimated statistical errors, the number of degrees of freedom[3] (d.o.f.), the χ^2 per degree of freedom (χ^2/d.o.f.) and the respective quality-of-fit parameter Q. In particular, for $L_{\min} \geq 100$ and all definitions considered the estimated $\nu^{(\mathrm{s})}$ is less than 3σ away from $\nu^{(\mathrm{s})} = 1$ with acceptable values of χ^2/d.o.f. and Q [183, 190]. For the hard constraint clusters the convergence to the asymptotic value of the exponent ν for the hard constraint clusters, i.e., $\nu^{(\mathrm{h})}$, is slower except for the $R^{(\mathrm{h})}_{\mathrm{x\ and\ \bar{y}}}$ definition which approaches the $\nu^{(\mathrm{h})} = 1$ value faster. This can also be seen from Table B.4 in the Appendix, where for $L_{\min} \geq 800$ and all definitions considered, except $R^{(\mathrm{h})}_{\mathrm{x\ and\ \bar{y}}}$, the

[3] In the fitting context the number of degrees of freedom is defined as the number of the available data points minus the fitting parameters of the fitting function. See also Ref. [190] for a more detailed discussion.

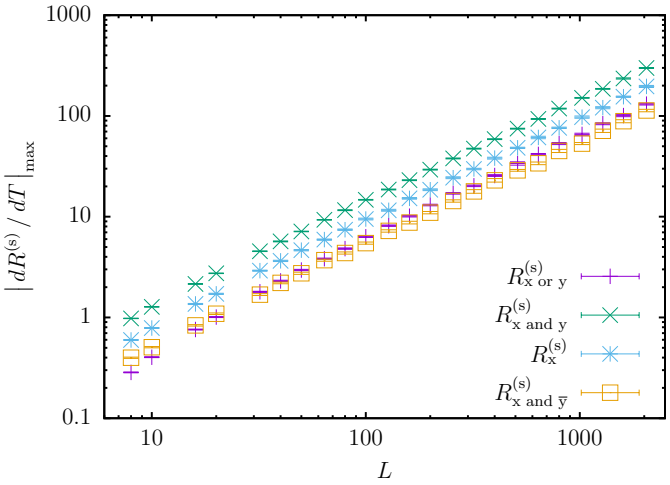

Figure 5.9: Log-log plot of $|dR/dT|_{\max}$ for the different definitions of the wrapping probabilities of the soft constraint clusters, for the 2-replica Ising model as a function of system size L.

estimated $\nu^{(\text{h})}$ is less than 3σ away from $\nu^{(\text{h})} = 1$ with acceptable values of χ^2/d.o.f. and Q. For $R^{(\text{h})}_{\text{x and }\overline{\text{y}}}$ all estimates are consistent with $\nu^{(\text{h})} = 1$ for all values of $L_{\min}$. Nonetheless, as fits are linear, precautions against unavoidable corrections to scaling dictate that estimates of $\nu^{(\text{h})}$ for small values of $L_{\min}$ (say $L_{\min} \leq 100$) should not be regarded as reasonable.

We can thus conclude, that the several estimates of ν resulting from the different definitions of the wrapping probabilities are in agreement with each other for both soft and hard constraint clusters. Additionally, estimates seems to indicate that soft and hard constraint clusters are characterized by the same critical exponent ν, i.e., $\nu^{(\text{s})} = \nu^{(\text{h})} = 1$, which in turn coincides with the critical exponent for the geometrical clusters of the 1-replica Ising model. We now turn our attention at the estimation of the critical temperature T_{c}.

Critical temperature

For the estimation of the critical temperature we will utilise the crossing method. As we discussed in Sec. 2.3 the crossing method considers the crossings of curves of the Binder cumulant of pairs of system sizes (L_1, L_2), which scale according to Eq. (2.55). In the absence of immediate correspondence between percolation quantities and observables of the system, we will work with the wrapping probabilities, which resemble the Binder cumulant.

We have already elaborated in Sec. 5.2.1 that the wrapping probabilities cross at a temperature close to the critical temperature of the 1-replica Ising model for both soft and hard constraint clusters (see Figs. 5.3 and 5.4 respectively). This is shown more clearly in Fig. 5.13, where $R_{\text{x or y}}$ is plotted as a function of temperature for the larger system sizes considered, i.e., $L = [512 - 2048]$, for the soft (top panel) and hard (bottom panel) constraint clusters, respectively. Even in this smaller temperature range (cf. Figs. 5.3 and 5.4), it is visually evident that the crossings occurs at (or very close) to the critical temperature of the 1-replica Ising model.

We applied Eq. (2.55) by considering the crossings of wrapping probabilities of pairs of

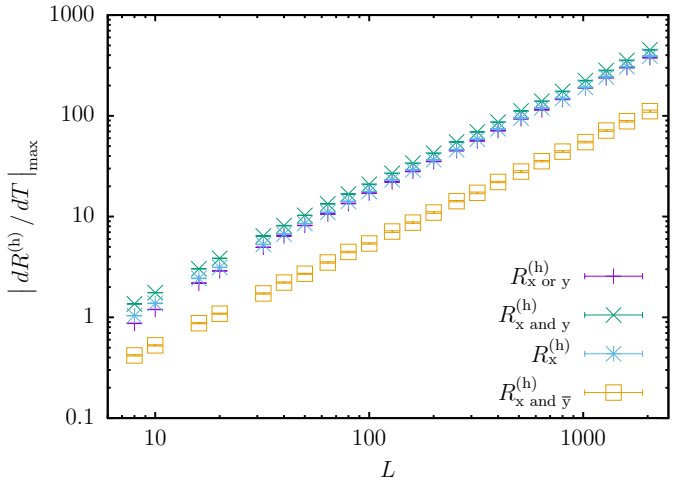

Figure 5.10: Log-log plot of $|dR/dT|_{\max}$ for the different definitions of the wrapping probabilities of the hard constraint clusters, for the 2-replica Ising model as a function of system size L.

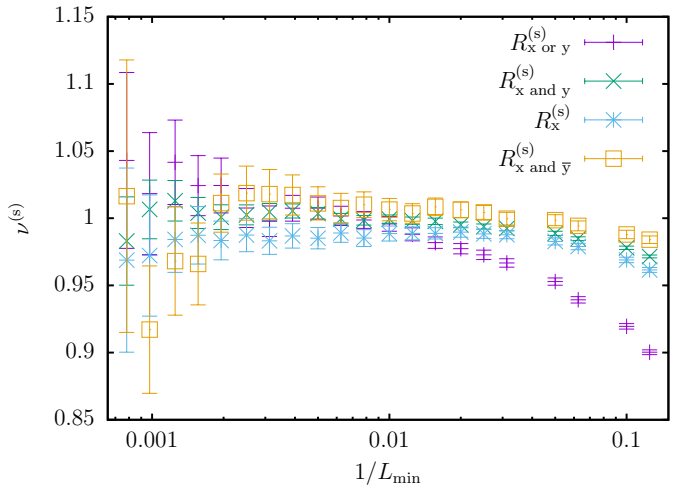

Figure 5.11: Estimates of the ν exponent of the soft constraint clusters, for the 2-replica Ising model as function of $1/L_{\min}$. Estimates extracted from linear fits (on a log-log scale) of $|dR/dT|_{\max}$ as a function of system size L.

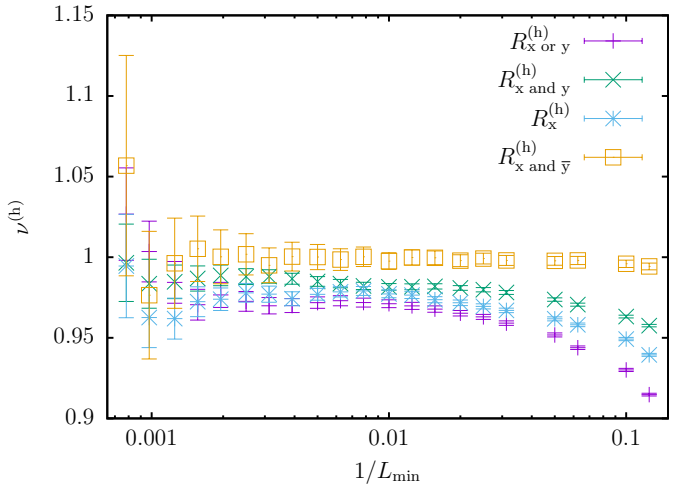

Figure 5.12: Estimates of the ν exponent of the hard constraint clusters, for the 2-replica Ising model as function of $1/L_{\min}$. Estimates extracted from linear fits (on a log-log scale) of $|dR/dT|_{\max}$ as a function of system size L.

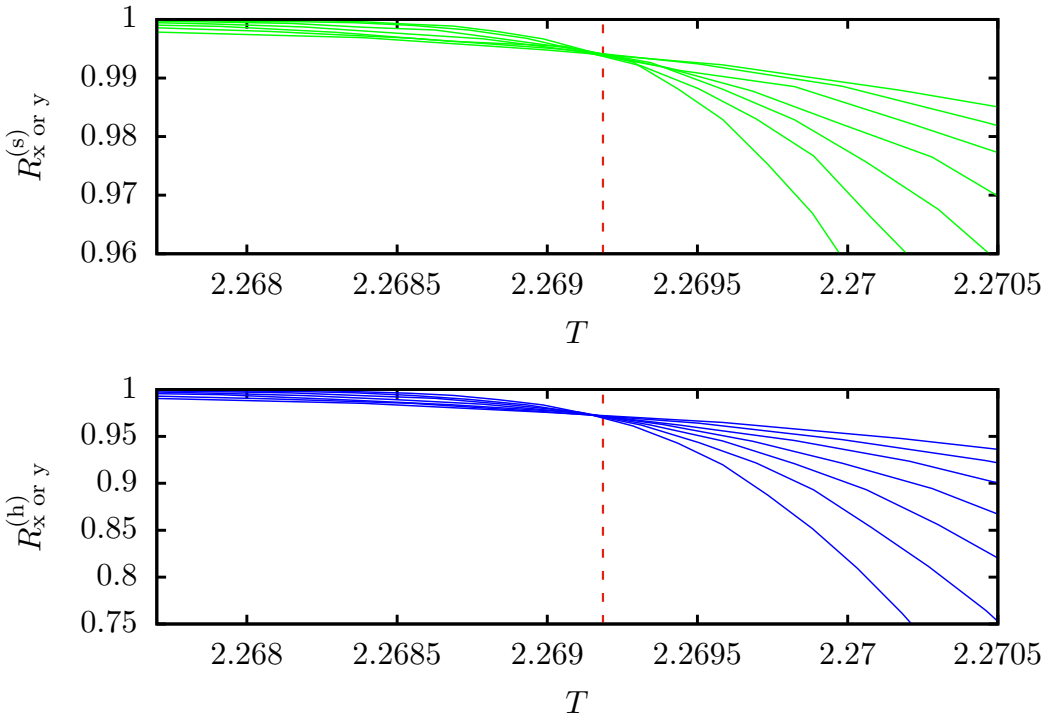

Figure 5.13: $R_{\text{x or y}}$ as a function of temperature for system sizes $L = [512 - 2048]$, for the soft (top panel) and hard (bottom panel) constraint clusters, of the 2-replica Ising model. The dashed vertical line marks the transition temperature of the 1-replica Ising model.

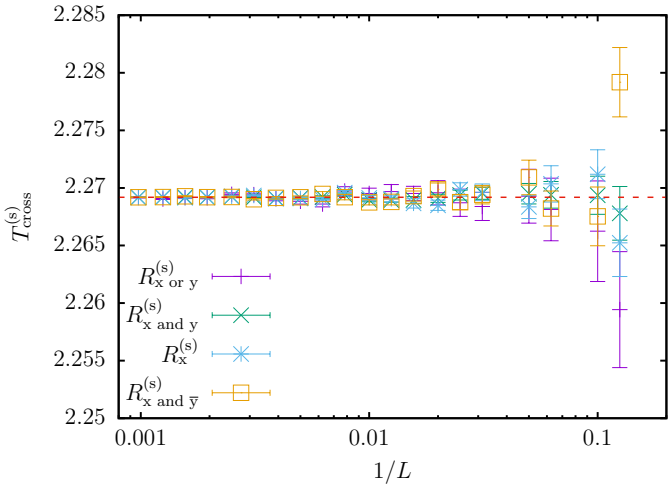

Figure 5.14: Estimates of the crossing temperatures of pairs $(L, 2L)$ from the wrapping probabilities of the soft constraint clusters, for the 2-replica Ising model as a function of $1/L$. The dashed horizontal line marks the transition temperature of the 1-replica Ising model.

system sizes $(L, 2L)$, for both soft and hard constraint clusters. The crossings were obtained using the bisection method [183], and in order to produce more accurate results for the position of the crossings, the single histogram reweighting technique was used (see Appendix A.4). In Figs. 5.14 and 5.15, the temperatures where the crossings of the pairs of the wrapping probabilities occur are plotted as a function of $1/L$ [we used the smaller system size of the pair $(L, 2L)$] for all definitions and for the soft and hard constraint clusters, respectively. For the larger system sizes, T_{cross} lies around the critical temperature of the 1-replica Ising model, indicated by the dashed vertical line. For obtaining more accurate estimates of the critical temperature, we first tried to perform fits according to Eq. (2.55). Unfortunately, the accuracy of the data resulted in fits of poor quality and consequently to unreliable estimates of the involved parameters. Note, that such non-linear fits are usually hard to control, even when some of the involved parameters, e.g., ν or ω, are known either analytically or from other works. As an alternative, we proceed by considering linear fits on intervals $L_{\text{min}} \leq L \leq L_{\text{max}}$ in the same fashion as before. This means that fits performed by setting the L-exponent of Eq. (2.55) equal to one, i.e., $1/\nu + \omega = 1$, which is a reasonable choice since estimates of the exponent ν, as discussed above, are in agreement with a value around 1 and assuming that the correction exponent ω is small. Thus, the fitting ansatz is of the form

$$T_{\text{cross}}(x) = T_{\text{c}} + ax, \tag{5.5}$$

where a is a non-universal scaling parameter and $x \equiv 1/L$.

For the soft constraint clusters fitting results are reported in Table B.5 in the Appendix. The estimates of the critical temperature $T_{\text{c}}^{(s)}$ are consistent with the critical temperature of the 1-replica Ising model, i.e., $T_{\text{c}} \approx 2.2691853$, with deviations of the estimates from T_{c} being less than 3σ for all L_{min} values and all definitions. The only exception is the estimate for the $R_{\text{x or y}}^{(s)}$ definition and $L_{\text{min}} = 320$, where the deviation is slightly larger than 3σ, namely 3.2σ from the critical temperature of the 1-replica Ising model. Note that for all definitions

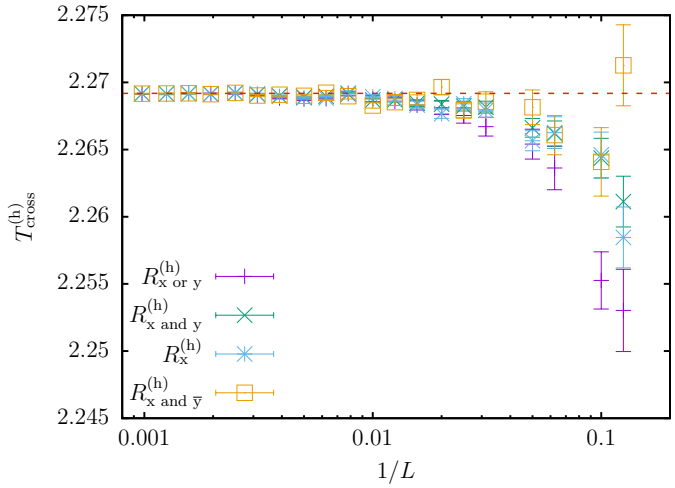

Figure 5.15: Estimates of the crossing temperatures of pairs $(L, 2L)$ from the wrapping probabilities of the hard constraint clusters, for the 2-replica Ising model as a function of $1/L$. The dashed horizontal line marks the transition temperature of the 1-replica Ising model.

and values of $L_{\rm min}$, the fitting parameter a is consistent with zero, as all estimates differ less than 3σ from it. This means that data are consistent with straight lines parallel to the $x \equiv 1/L$ axis. Nonetheless, not all definitions result in reasonable values of χ^2/d.o.f. and Q. The $R_{\rm x\ or\ y}^{\rm (s)}$ has relatively large values of χ^2/d.o.f. (greater than 1.7) and consequently poor Q values, for all the $L_{\rm min}$ values. Additionally, the $R_{\rm x}^{\rm (s)}$ definition has also relatively large values of χ^2/d.o.f., although for fewer $L_{\rm min}$ values compared to $R_{\rm x\ or\ y}^{\rm (s)}$. On the other hand, $R_{\rm x\ and\ y}^{\rm (s)}$ and $R_{\rm x\ and\ \overline{y}}^{\rm (s)}$ have at least acceptable χ^2/d.o.f. and Q values for the majority of the $L_{\rm min}$ values. For the hard constraint clusters results are reported in Table B.6 in the Appendix. Similarly to soft constraint clusters, the estimates of the critical temperature $T_{\rm c}^{\rm (h)}$ are consistent with that of the 1-replica Ising model, for the larger $L_{\rm min}$ values considered. For most of $L_{\rm min} \geq 320$ and for all definitions the values of χ^2/d.o.f. and Q are reasonable. All the above can be illustrated on Figs. 5.16 and 5.17, where the estimates of the critical temperature are plotted as a function of $1/L_{\rm min}$ for the soft and hard constraint clusters, respectively.

We note that by performing linear fits according to Eq. (5.5) and obtaining reasonable estimates and quality of fits (in most of the cases), does not imply that corrections to scaling are *absent*, but rather that they are *not accessible* within the accuracy of our data. Additionally, we checked if the estimates of the critical temperature of the soft and hard constraint clusters are affected when the exponent $1/\nu + \omega$ of Eq. (2.55) is close but different from one. In particular we performed fits (not presented here) using Eq. (2.55) for three different (fixed) values of the exponent, i.e., $1/\nu + \omega = 0.9, 1.1,$ and, 1.2. For each definition and value of $L_{\rm min}$ the estimated fitting parameters, resulting from the three different values of the exponent, are consistent with each other and in agreement with the ones obtained from Eq. (5.5), for the soft and hard constraint clusters, respectively. Thus, we see that our estimates for the critical temperature of the soft and hard constraint clusters are stable since no systematic shift appears upon varying the exponent $1/\nu + \omega$ of Eq. (2.55).

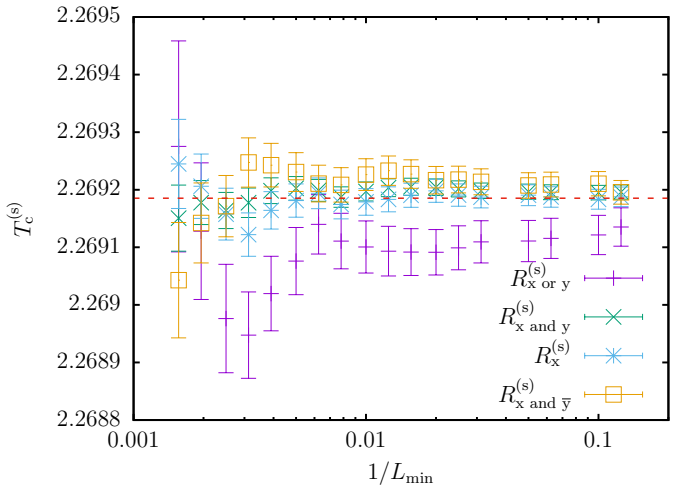

Figure 5.16: Estimates of the critical temperature of the soft constraint clusters, for the 2-replica Ising model as a function of $1/L_{\min}$. Estimates extracted from the linear fits of Eq. (5.5). The dashed horizontal line marks the transition temperature of the 1-replica Ising model.

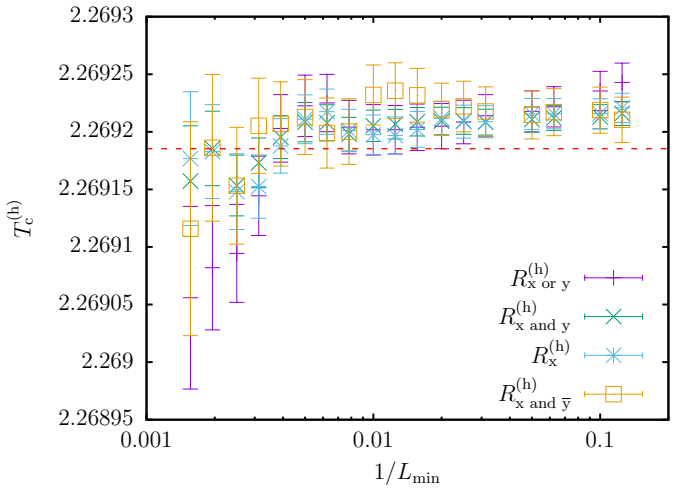

Figure 5.17: Estimates of the critical temperature of the hard constraint clusters, for the 2-replica Ising model as a function of $1/L_{\min}$. Estimates extracted from the linear fits of Eq. (5.5). The dashed horizontal line marks the transition temperature of the 1-replica Ising model.

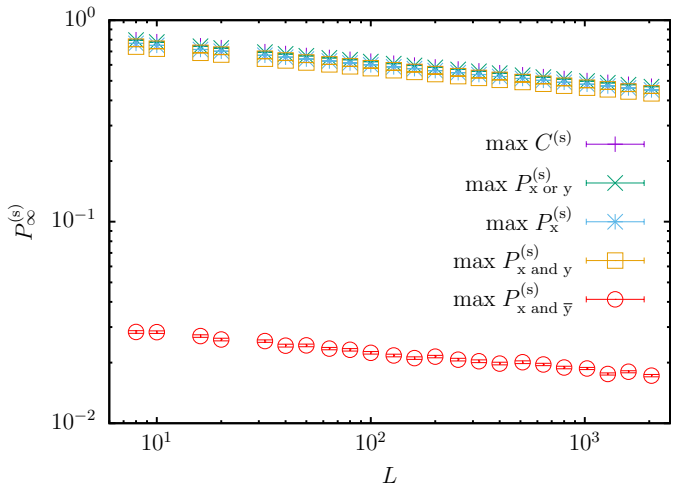

Figure 5.18: Log-log plot of the percolation strength for the different definitions of the soft constraint clusters $P_\infty^{(s)}$, for the 2-replica Ising model as a function of the system size L, at the critical temperature of the 1-replica Ising model.

We can conclude that, given the accuracy of our data and the size of the systems considered, both soft and hard constraint clusters have the same critical temperature which coincides with that of the 1-replica Ising model. Although our simulations were of reasonable length and for sufficiently large system sizes, we cannot exclude the possibility that deviations from the above behaviour could become visible for even larger system sizes. We will now proceed with the estimate of the critical exponents for the average cluster size and percolation strength. Having determined the critical temperature of the system, or at least a reasonable value close to it, we performed simulations at that temperature., i.e., the critical temperature of the 1-replica Ising model, for the estimation of the aforementioned exponents.

Percolation strength

For the percolation strength P_∞, we will use the definitions as of Sec. 4.3, for the case of the 1-replica Ising model. In Figs. 5.18 and 5.19 the percolation strength is plotted as a function of system size for the different definitions considered, as computed at the critical temperature of the 1-replica Ising model for the soft and hard constraint clusters, respectively. For both cluster types and all definitions the data seem to follow straight lines, indicating that corrections to scaling are small and that the involved exponent is independent of the definition used. The scaling behaviour of P_∞ should follow Eq. (4.6), and as simulations are performed at the critical temperature the scaling function is constant, i.e., $P_\infty \sim L^{-\beta/\nu}$, thus allowing the determination of the exponent, cf. Sec. 4.3.

For that we performed linear fits (on a log-log scale) on varying intervals $L_{\min} \leq L \leq L_{\max}$, in the same fashion as described before, e.g., see Sec. 4.2. In Figs. 5.20 and 5.21 the estimated exponent β/ν is shown as a function of $1/L_{\min}$ for the soft and hard constraint clusters, respectively. Similarly to the 1-replica case (see Sec. 4.3), the max $P_{\text{x and }\bar{\text{y}}}$ definition provides unreliable estimates of the exponent for both cluster types, as clusters percolating in one but

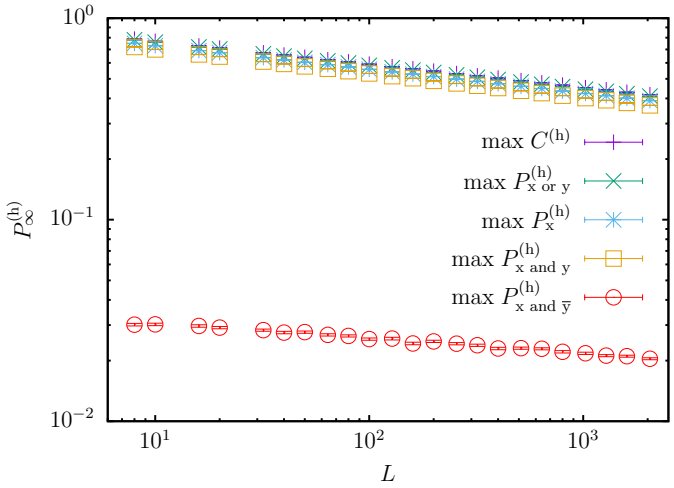

Figure 5.19: Log-log plot of the percolation strength for the different definitions of the hard constraint clusters $P_\infty^{(h)}$, for the 2-replica Ising model as a function of the system size L, at the critical temperature of the 1-replica Ising model.

not the other direction are very rare, leading to poor statistics for the involved observable, i.e., P_∞. The rest of the definitions provide estimates of the exponent which are in agreement with each other in between error bars, at least for the larger $L_{\min}$ values. Additionally, in order to include smaller system sizes for the estimation of the exponent non-linear fits, including one correction term, were performed. Unfortunately, the resulting fits where of poor quality (large values of χ^2/d.o.f.) resulting in unreliable estimates of the involved fitting parameters. Hence, as a *trade-off* between unavoidable corrections to scaling and values of χ^2/d.o.f. close to one, our estimates for the percolation strength exponent of the soft and hard constraint clusters are

$$\left(\frac{\beta}{\nu}\right)^{(s)} = 0.0950(7), \qquad \chi^2/\text{d.o.f.} \approx 0.96, \qquad L_{\min} = 320, \qquad \max P^{(s)}_{x\text{ and }y}, \tag{5.6}$$

$$\left(\frac{\beta}{\nu}\right)^{(h)} = 0.1184(11), \qquad \chi^2/\text{d.o.f.} \approx 0.82, \qquad L_{\min} = 512, \qquad \max P^{(h)}_{x}. \tag{5.7}$$

For more details regarding the fitting results of the exponent β/ν for the soft and hard constraint clusters see Tables B.7 and B.8 in the Appendix, respectively.

Average cluster size

As with the percolation strength discussed above, we will utilise the different definitions of the average cluster size as introduced in Sec. 4.2. Figs. 5.22 and 5.23 show the average cluster size as a function of system size for the different cluster-set definitions considered evaluated at the critical temperature of the 1-replica Ising model, and for the soft and hard constraint clusters, respectively. As with P_∞, the straight lines indicate that corrections to scaling should be small and that the exponent should be independent of the definition. Nonetheless,

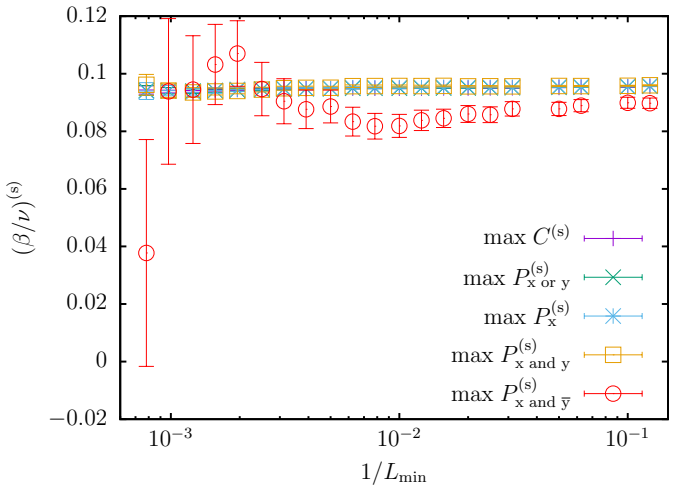

Figure 5.20: Exponent ratio for the different definitions of the soft constraint clusters $(\beta/\nu)^{(s)}$, for the 2-replica Ising model as a function of $1/L_{\min}$.

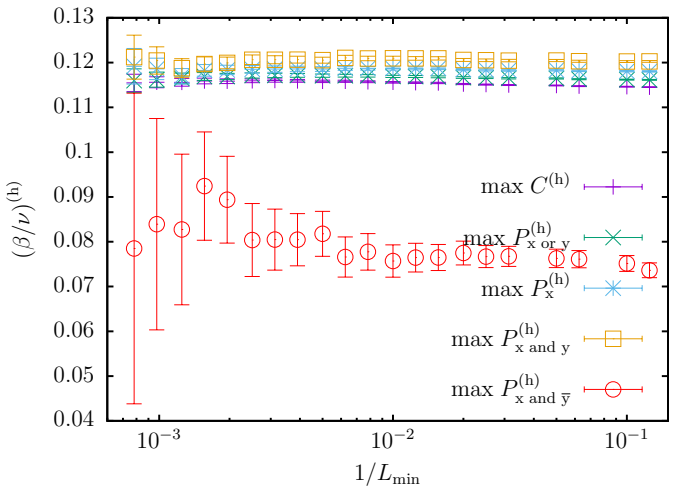

Figure 5.21: Exponent ratio for the different definitions of the hard constraint clusters $(\beta/\nu)^{(h)}$, for the 2-replica Ising model as a function of $1/L_{\min}$.

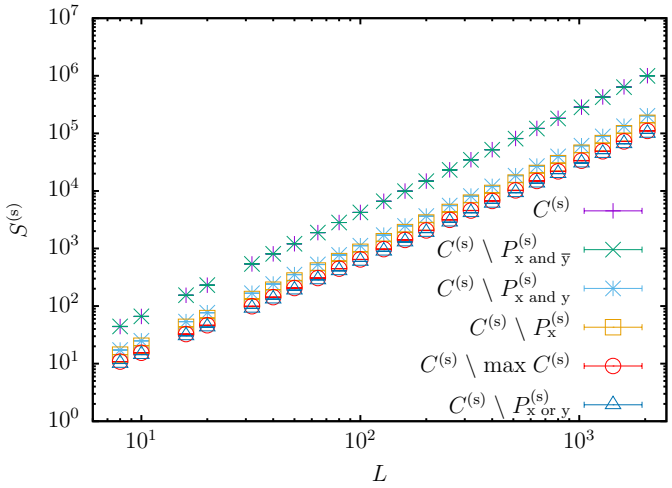

Figure 5.22: Log-log plot of average cluster size for the different definitions of the soft constraint clusters $S^{(s)}$, for the 2-replica Ising model as a function of the system size L , at the critical temperature of the 1-replica Ising model.

this is only a crude observation; recall that the same behaviour occurred for the 1-replica case but as it turned out the involved exponent strongly depended on the definition that was used, see Sec. 4.2. Having performed simulations at the critical temperature, the scaling equation of the average cluster size, see Eq. (4.4), can be written as $S \sim L^{\gamma/\nu}$, allowing for the estimation of the involved exponent.

Again, linear fits (on a log-log scale) were performed on alternating intervals $L_{\min} \leq L \leq L_{\max}$, and the estimated exponents for the soft and hard constraint clusters as a function of $1/L_{\min}$ for all definitions considered are shown in Figs. 5.24 and 5.25 respectively. For both soft and hard constraint clusters the C and $C \setminus P_{x \text{ and } \bar{y}}$ definitions, converge quickly to a value around $(\gamma/\nu)^{(s)} \approx 1.81$ and $(\gamma/\nu)^{(h)} \approx 1.77$, respectively, indicating that corrections to scaling are not substantial. In contrast, the rest of the definitions seem to have strong scaling corrections, and the convergence to the asymptotic value is quite slow. As in the case of the 1-replica model, C and $C \setminus P_{x \text{ and } \bar{y}}$ yield similar results, since the exclusion of clusters wrapping in one but not the other direction will not change the sums of Eq. (2.60) significantly as such clusters are very rare, cf. Sec. 4.2. The results from the linear fits to the average cluster size are reported in Tables B.9 and B.10 in the Appendix for the soft and hard constraint clusters, respectively.

In order to obtain more reliable estimates of the exponent concerning the average cluster size, we would like to incorporate correction-to-scaling terms. Since the asymptotic behaviour of the involved exponent should be independent of the definition used, we performed joint fits [191] using all definitions considered, for the soft and hard constraint clusters, respectively. The fitting ansatz is of the form

$$S = aL^{\gamma/\nu}\left(1 + bL^{-\omega}\right), \tag{5.8}$$

and the fits below have been performed by treating γ/ν and ω as shared (common) parameters for all definitions, whereas a and b as dependent on the specific data-set (different definition)

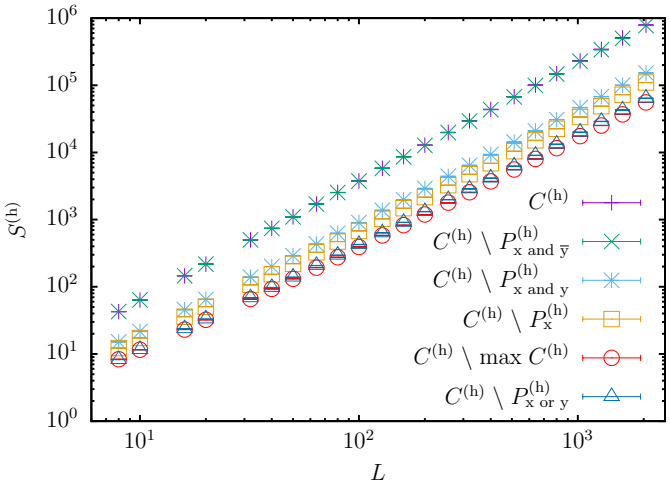

Figure 5.23: Log-log plot of average cluster size for the different definitions of the hard constraint clusters $S^{(h)}$, for the 2-replica Ising model as a function of the system size L , at the critical temperature of the 1-replica Ising model.

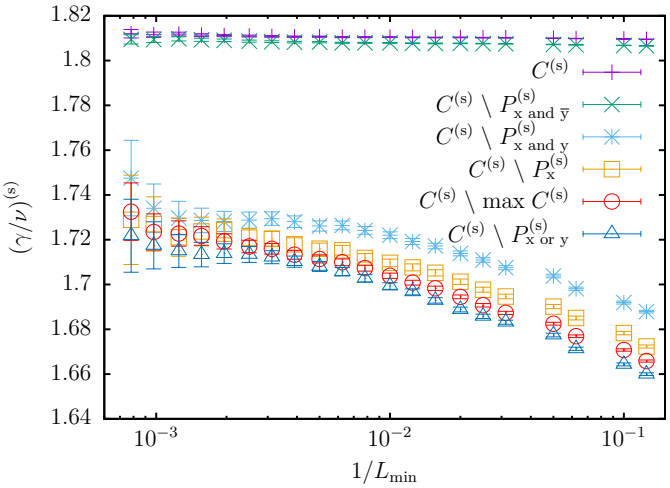

Figure 5.24: Exponent ratio for the different definitions of the soft constraint clusters $(\gamma/\nu)^{(s)}$, for the 2-replica Ising model as a function of $1/L_{\min}$.

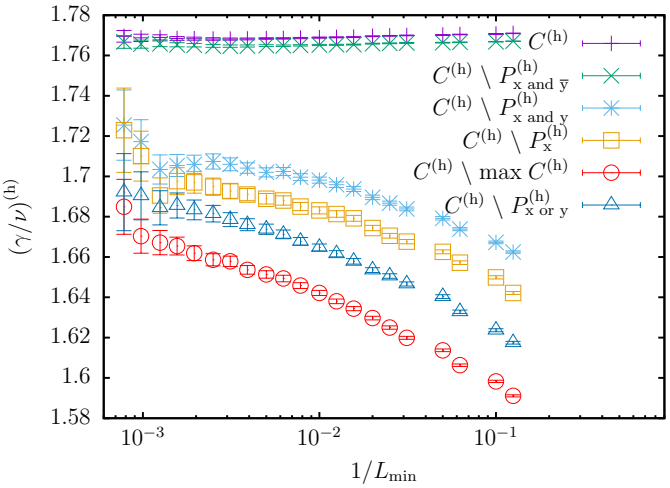

Figure 5.25: Exponent ratio for the different definitions of the hard constraint clusters $(\gamma/\nu)^{(h)}$, for the 2-replica Ising model as a function of $1/L_{min}$.

used. Since data from different definitions are not statistically independent, as they result from the same MC series, a naive implementation of the above fitting procedure will result in wrong estimates of the errors for the involved parameters. Thus, in order to provide reliable estimates for the errors of the involved parameters, the jackknife method was employed (see Appendix A.2). The fitting results from the joint fits are reported in Tables B.11and B.12 in the Appendix for the soft and hard constraint clusters, respectively.

In Figs. 5.26 and 5.27, the exponent γ/ν is plotted as a function of $1/L_{min}$, resulting from the joint fits described above, for the soft and hard constraint clusters respectively. For the different values of L_{min}, the estimates of the exponent are consistent with each other, in between error bars, while as L_{min} increases the respective errors increase as a consequence of the decreasing d.o.f.. Additionally, the estimates of the exponent ω up to a certain value of $L_{min} = 256$ are consistent with each other for both cluster sets. Nonetheless, for $L_{min} = 320$ and above the error bars of the ω are quite large, resulting in unsatisfactory estimates. This is shown in Figs. 5.28 and 5.29 for the soft and hard constraint clusters respectively. Note, that the estimated ω exponent is relatively small for both cluster types (around 0.3), which is consistent with the strong scaling corrections observed for the average cluster size for some of the definitions employed.

Fractal dimension

At the percolation threshold p_c, the incipient spanning cluster is a fractal object, with its mass M (number of sites belonging to the infinite cluster) characterized by a critical exponent D, i.e., the fractal dimension, see Sec. 2.4.1. In numerical studies of percolation D is estimated from the mass of the largest cluster, which scales as $M \sim L^D$ [19]. Additionally, the fractal dimension is related to the other exponents according to Eqs. (2.68) and (2.69), i.e., $D = (\beta + \gamma)/\nu$ and $D = 2 - \beta/\nu$. Since we have already obtained estimates for the β/ν, γ/ν we will determine D by using these relations. Specifically, from Eqs. (5.6) and (5.7) we have $(\beta/\nu)^{(s)} = 0.0950 \pm 0.0007$ and $(\beta/\nu)^{(h)} = 0.1184 \pm 0.0011$, and according to Tables B.11

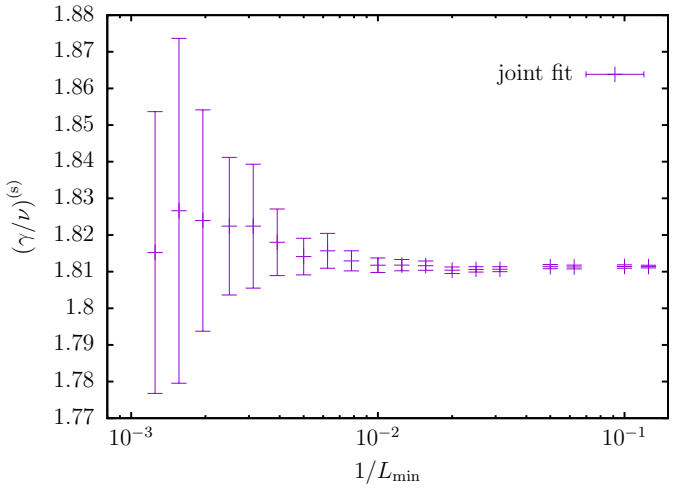

Figure 5.26: Exponent ratio resulting from the joint fit of all definitions of the soft constraint clusters $(\gamma/\nu)^{(s)}$, for the 2-replica Ising model as a function of $1/L_{\min}$.

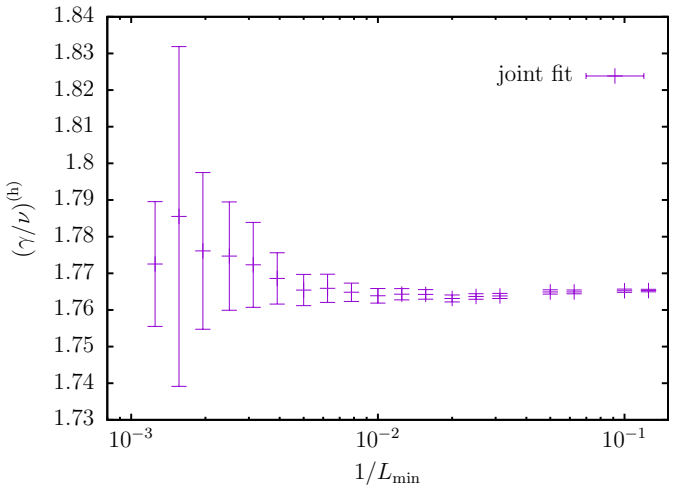

Figure 5.27: Exponent ratio resulting from the joint fit of all definitions of the hard constraint clusters $(\gamma/\nu)^{(h)}$, for the 2-replica Ising model as a function of $1/L_{\min}$.

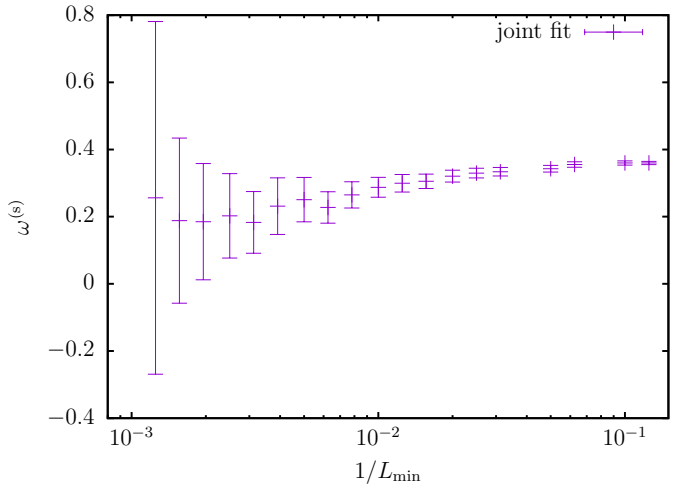

Figure 5.28: Correction-to-scaling exponent resulting from the joint fit of all definitions of the soft constraint clusters $\omega^{(s)}$, for the 2-replica Ising model as a function of $1/L_{\min}$.

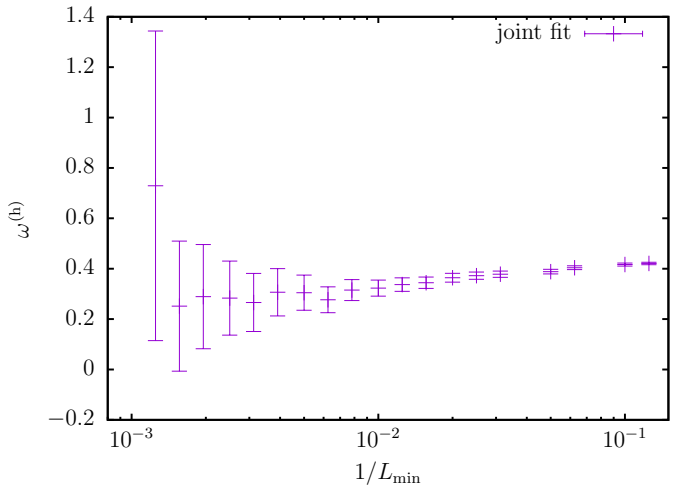

Figure 5.29: Correction-to-scaling exponent resulting from the joint fit of all definitions of the hard constraint clusters $\omega^{(h)}$, for the 2-replica Ising model as a function of $1/L_{\min}$.

and B.12 we choose $(\gamma/\nu)^{(\mathrm{s})} = 1.814 \pm 0.005$ and $(\gamma/\nu)^{(\mathrm{h})} = 1.765 \pm 0.004$. Thus, the fractal dimensions for the two cluster types are listed below

$$D^{(\mathrm{s})} = 1.909 \pm 0.005, \qquad D^{(\mathrm{h})} = 1.883 \pm 0.004, \qquad \text{using} \qquad D = \frac{\beta+\gamma}{\nu} \tag{5.9}$$

$$D^{(\mathrm{s})} = 1.9050 \pm 0.0007, \qquad D^{(\mathrm{h})} = 1.8816 \pm 0.0011, \qquad \text{using} \qquad D = d - \beta/\nu. \tag{5.10}$$

Note that the above estimates are smaller than $D = 187/96 \approx 1.9479$, which is the fractal dimension of the geometrical clusters of the 1-replica Ising model [89]. Additionally, the estimates resulting from the two different relations of the fractal dimension are consistent with each other, for the soft and hard constraint clusters, respectively. As mentioned in Sec. 2.4.1 the $(\beta+\gamma)/\nu$ holds for all dimensions, while the $D = d - \beta/\nu$ is a hyperscaling relation, valid only below the upper critical dimension. From, that we can conclude that hyperscaling holds for both cluster types. Note that $D^{\mathrm{s}} > D^{\mathrm{h}}$, indicating that the soft constraint clusters are more dense than the hard ones, in good agreement with the configurational snapshots of the two cluster types in Fig. 5.2.

5.2.3 Concluding remarks

In this section we discussed the percolation properties of the 2-replica Ising model, in terms of the soft and hard constraint clusters. After a short exposition of the main observables considered, we proceeded to the determination of the critical behaviour for both cluster types.

Firstly, an estimate of the correlation length exponent ν was obtained with the use of the wrapping probabilities. Specifically, one can obtain estimates of the ν exponent from the wrapping probabilities, since the maximum of the absolute value of the derivative of the wrapping probability with respect to temperature should scale as $\sim L^{1/\nu}$. The location of the maximum of the derivative was obtained by identifying the temperature where the second derivative becomes zero. For the numerical estimation of the second derivative the symmetric-finite-difference approximation was used and the root of the second derivative was estimated using the bisection method. Additionally, in order to avoid, as far as possible, the systematic errors arising from the numerical derivatives, the single-histogram reweighting technique was used. The estimates of ν, resulting from the fits, indicate that $\nu = 1$ for both soft and hard constraint clusters, which coincides with the exponent of the 1-replica Ising model.

Subsequently, the critical temperature was obtained using the crossing technique for pairs $(L, 2L)$ of the wrapping probabilities. Again, for more refined results the temperature where the curves cross was obtained using the single-histogram reweighting technique. The obtained results agree with a temperature similar for the soft and hard constraint clusters, which again coincides with that of the 1-replica Ising model. Nonetheless, we stress again the fact that the critical temperatures obtained are subjected to the given accuracy of our data, and we cannot exclude the possibility that the true asymptotic value can be slightly shifted away from the critical temperature of the 1-replica Ising model, which could only be revealed by more extensive simulations.

We then proceeded with the estimations of the critical exponents for the percolation strength and average cluster size, where we utilised the sets of different definitions as discussed in Sec. 4.1. For the percolation strength the associated exponent is independent of the definition used and different for the two types of clusters. Similarly to the 1-replica case

Table 5.1: Critical exponents of the soft and hard constraint clusters for the 2-replica Ising model and the exact values (last column) of the critical exponents for the 1-replica model, in two dimensions respectively.

	2-replicas		1-replica
Exponent \ Constraint	soft	hard	–
ν	1.005(5)	1.00(3)	1
β/ν	0.0950(7)	0.1184(11)	$5/96 \approx 0.0521$
γ/ν	1.814(5)	1.765(4)	$91/48 \approx 1.8958$
$D = \gamma/\nu + \beta/\nu$	1.909(5)	1.883(4)	$187/96 \approx 1.9479$
$D = d - \beta/\nu$	1.9050(7)	1.8816(11)	187/96

(see Sec. 4.3), the definition where the largest cluster percolating in one but not the other direction is considered in each measurement, provide poor estimates of the exponent, for both cluster types, as such clusters are very rare leading to pure statistics.

The average cluster size is more sensitive to the definition being used, with C and $C \setminus P_{\mathrm{x\ and\ \overline{y}}}$ exhibiting small scaling corrections, while the rest of the definitions have strong corrections to scaling, both for the soft and hard constraint clusters, respectively. Again, the C and $C \setminus P_{\mathrm{x\ and\ \overline{y}}}$ definitions give similar results as clusters that percolate in one but not the other direction are very rare and do not alter significantly the sums of Eq. (2.60). In order to obtain more accurate estimates of the exponent we performed joint fits using all definitions and including a correction term for the two cluster types, respectively. The exponents are in agreement with the estimates obtained from the individual fits using the C and $C \setminus P_{\mathrm{x\ and\ \overline{y}}}$, and different for the soft and hard constraint clusters. Also, the correction-to-scaling exponent is relatively small for both cluster types, indicating that corrections cannot be neglected. Lastly, via the scaling relations we obtained the fractal dimension of the soft and hard constraint clusters. All the estimated exponents for the 2-replica Ising model, along with the analytical values of the 1-replica case, are reported in Table 5.1. It is clear that the respective critical exponents for the soft and hard constraint clusters are different from each other, as well as from them of the 1-replica case; except for the exponent ν.

5.3 The 3-replica Ising Model

We continue our discussion with the percolation properties of the 3-replica Ising model in two dimensions considering the soft and hard constraint clusters as introduced in Sec. 5.1. Similarly to the 2-replica case (see Sec. 5.2), we will focus our attention on the estimation of the critical temperature T_{c}, and the critical exponents ν, β, γ concerning the correlation length, average cluster size, and percolation strength, respectively. These estimations were obtained with the help of Monte Carlo simulations and subsequently by applying the FSS analysis. The simulation details concerning the 3-replica case are similar to those of the 2-

replica runs (see Sec. 5.2) with the obvious difference that three instead of two replicas are simulated for each temperature and system of linear size L.

On a more qualitative basis now we expect that the 3-replica Ising model should exhibit a critical behaviour. Well below the critical temperature of the 1-replica Ising model all three replicas have a percolating cluster of a size comparable to that of the system, thus in the k-plane a percolating cluster should also occur (for both soft and hard constraint cluster). In contrast, in the limit of infinite temperature spins on each replica point in random directions and one should expect that in the k-plane there is no percolating cluster. Consequently, there should be a finite temperature where an incipient percolating cluster in k-space appears for the first time. This can be visually realised in Fig. 5.30, where in the upper panel configurations of the three replicas are shown, and in the lower panel the soft and hard constraint clusters are presented. We see that both cluster types are characterized by a percolating cluster, where the size of the soft constraint one is larger than that of the hard constraint one. Additionally, note that the temperature from where these configurations were taken is below the critical point of the 1-replica Ising model. As it will become apparent in the next sections the transition temperature for the soft and hard constraint clusters is below that of the 1-replica Ising model, as well as different between the two cluster types. For the configurational snapshots of Fig. 5.30 in particular, we choose a temperature which lies in between the critical temperatures of the soft and hard constraint clusters, cf. Fig. 5.43. We will now proceed with a general description of the aforementioned observables, before discussing their critical behaviour in Sec. 5.3.2.

5.3.1 Observables

Wrapping probabilities

In Figs. 5.31 and 5.32 the wrapping probabilities R are plotted as a function of temperature T for the different system sizes L of the soft and hard constraint clusters, respectively. The situation here is different from the 2-replica case, as the wrapping probabilities cross at temperatures not very close the critical point of the 1-replica Ising model, which is denoted by the dashed vertical line; see the right panels of Figs. 5.31 and 5.32 respectively and cf. Figs. 5.3 and 5.4. Additionally, the deviation of the crossings from the critical temperature of the 1-replica Ising model for the hard constraint clusters appear larger than the one for the soft constraint, indicating that the transition point of the two cluster types is potentially different. This issue will be discussed in greater detail in Sec. 5.3.2, where the estimation of the critical point for both cluster types will be considered. For now note that this is in agreement with Fig. 5.30, where the soft and hard constraint clusters appear critical for a temperature below that of the 1-replica Ising model. Lastly, note that similarly to the 2-replica case, $R_{\mathrm{x\ and\ }\overline{\mathrm{y}}}$ exhibits a maximum and a crossing point, which should converge to the same critical point as the size of the system becomes infinite [173].

Average cluster size

The average cluster size S is plotted as a function of temperature T for the different system sizes L considered, of the soft and the hard constraint clusters in Figs. 5.33 and 5.34, respectively. Here we used again the conventional definition, where on each measurement the largest cluster is excluded, which results in the appearance of a maximum in the vicinity of

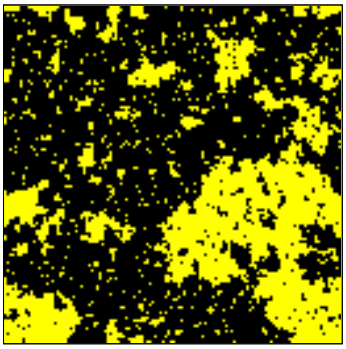

(a) Replica 1.

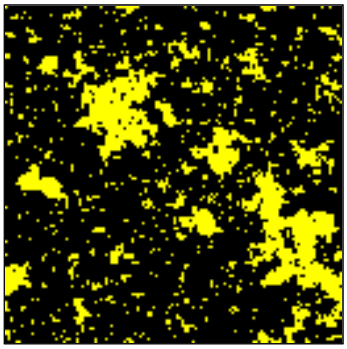

(b) Replica 2.

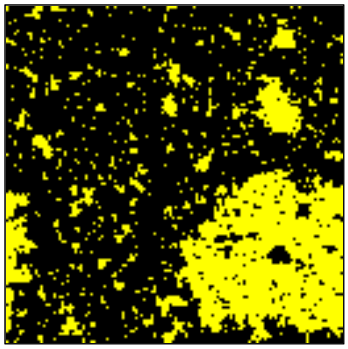

(c) Replica 3.

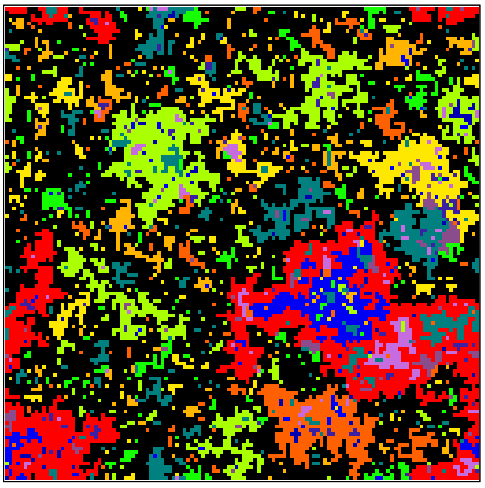

(d) Soft constraint clusters.

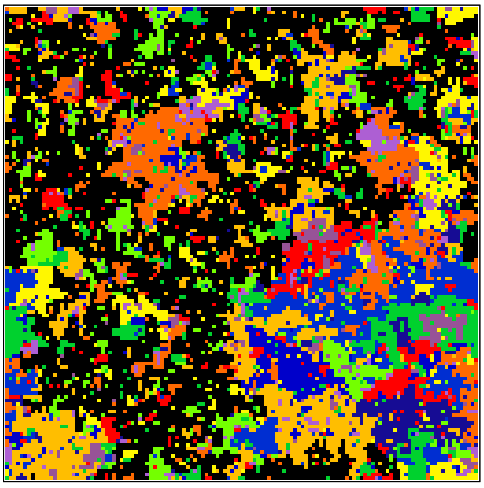

(e) Hard constraint clusters.

Figure 5.30: Snapshot configurations of the two-dimensional Ising model, at temperature $T = 2.26884$. (a) First replica. (b) Second replica. (c) Third replica. (d) Soft constraint clusters. (e) Hard constraint clusters. In (d) and (e) all clusters, apart from the largest percolating one, are assigned colours at random. For the largest percolating cluster of both the soft and hard constraint definitions, the same colour (black) is assigned. Note that in our setup we allow the black colour to be assigned *only* to the largest percolating cluster.

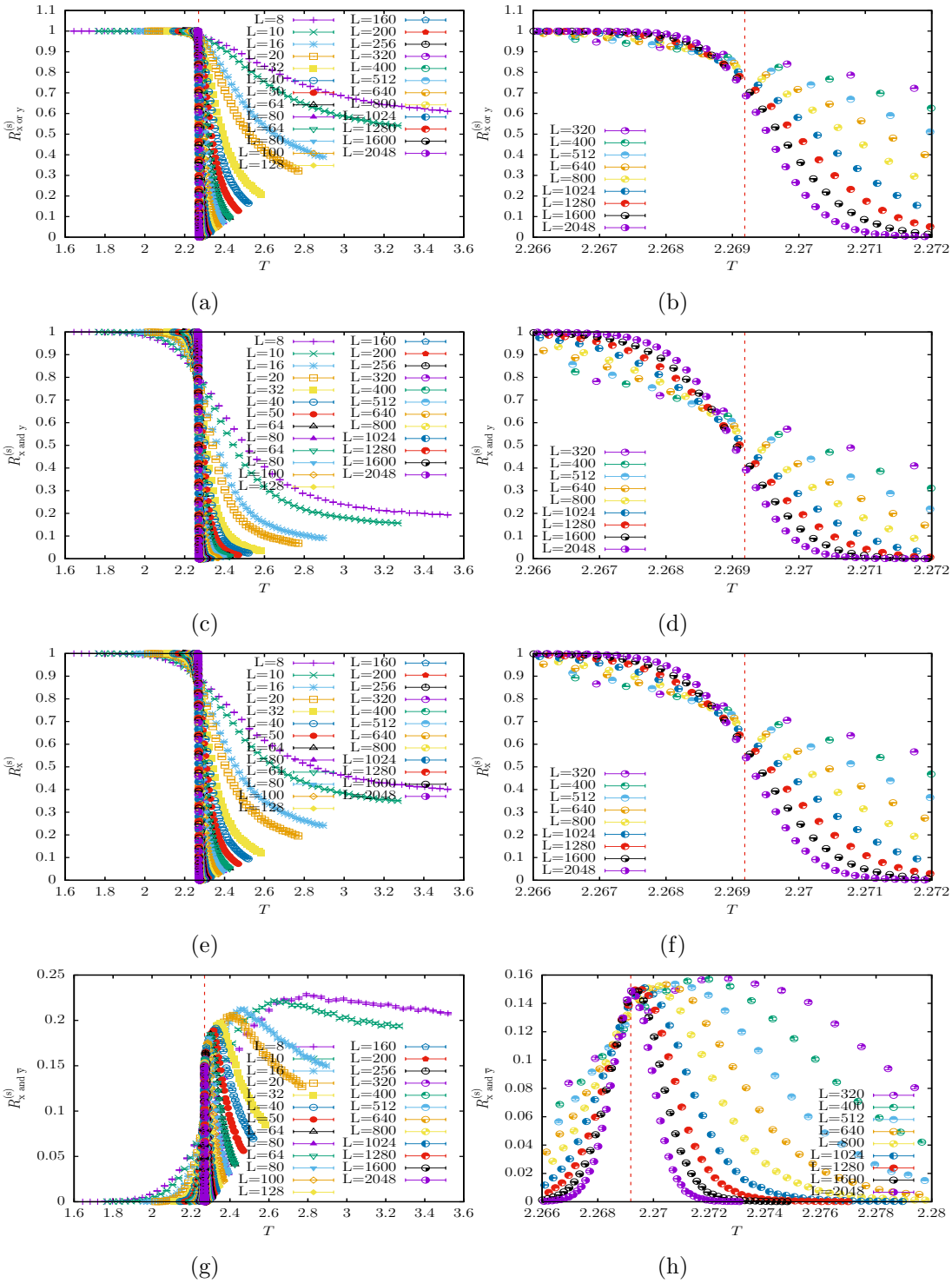

Figure 5.31: *Left column*: Wrapping probabilities of the soft constraint clusters, for the 3-replica Ising model as function of temperature T, for different system sizes L. *Right column:* Analogous to left column for the larger system sizes considered. The dashed vertical line marks the transition temperature of the 1-replica Ising model.

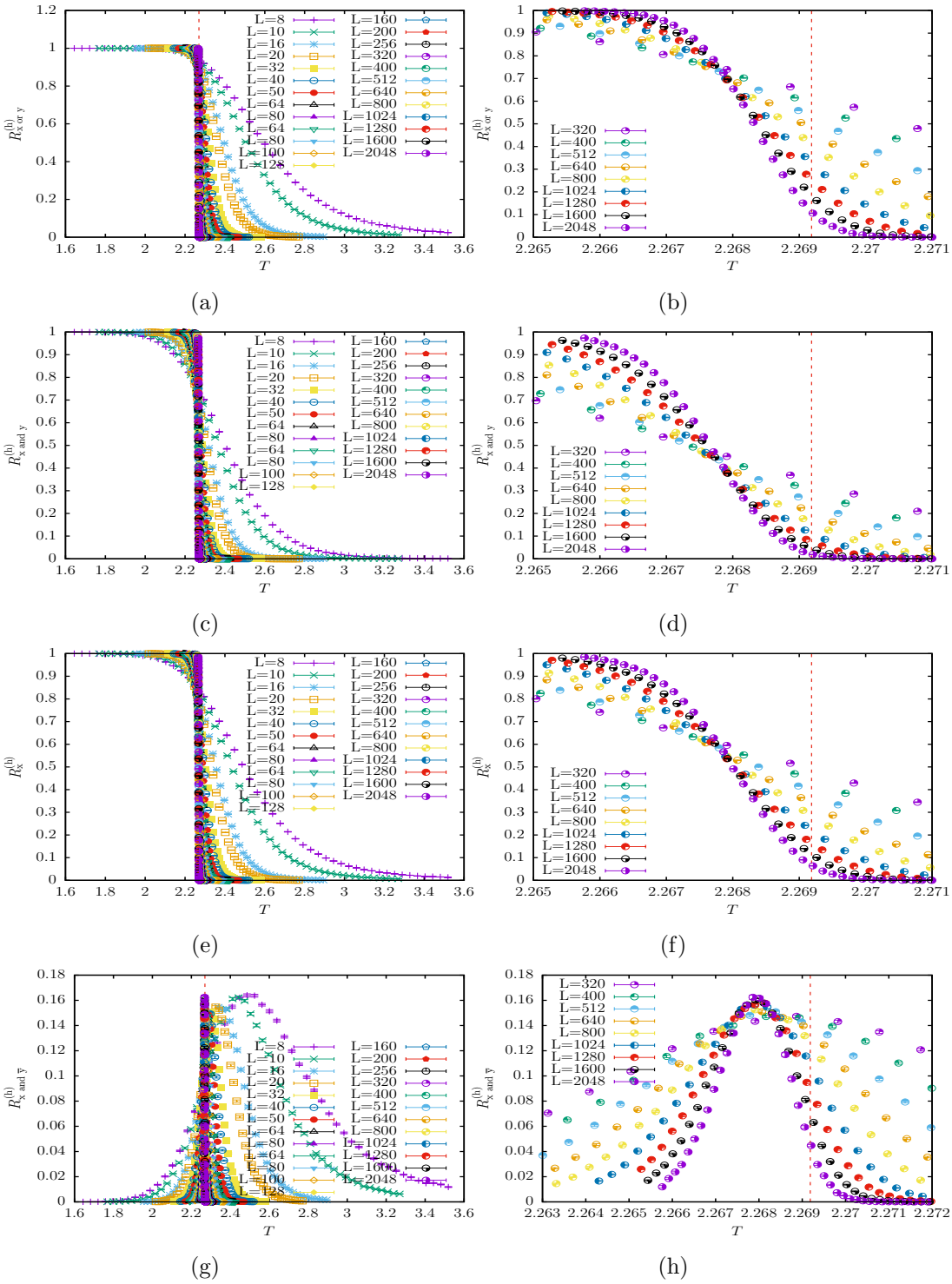

Figure 5.32: *Left column*: Wrapping probabilities of the hard constraint clusters, for the 3-replica Ising model as function of temperature T, for different system sizes L. *Right column:* Analogous to left column for the larger system sizes considered. The dashed vertical line marks the transition temperature of the 1-replica Ising model.

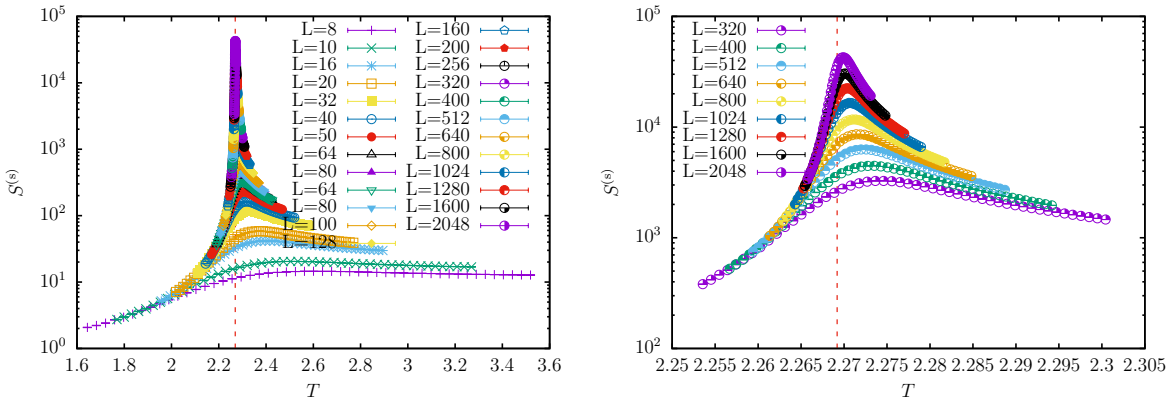

(a) (b)

Figure 5.33: (a) Average cluster size of the soft constraint clusters $S^{(s)}$ on a semi-log axis, for the 3-replica Ising model as a function of temperature T, for different system sizes L. (b) Analogous to panel (a) for the larger system sizes considered. The dashed vertical line marks the transition temperature of the 1-replica Ising model.

the critical point. We note again that S for the same system size and temperature is larger for the soft constraint clusters in comparison with the hard constraint ones. For example, the peak of the average cluster size for $L = 2048$ is around 4×10^4 for the soft constraint clusters whereas for the hard constraint ones around 2×10^4, see Figs. 5.33(b) and 5.34(b) for the soft and the hard constraint clusters, respectively.

Percolation strength

The percolation strength P_∞ is plotted as a function of temperature T for the different system sizes L of the soft and hard constraint clusters in Figs. 5.35 and 5.36, respectively. The definition that has been used here is, again, that of the largest cluster considered in each measurement. For both cluster types P_∞ is a decreasing function of temperature, and as temperature approaches 0 it goes to 1, signalling that all spins in the k-plane are aligned. In contrast, for very high temperatures (approaching infinity) the percolation strength is essentially zero, reflecting the fact that in all replicas spins are pointing in random directions, cf. Sec. 5.2.1. Note that the percolation strength decreases faster as a function of temperature, for the 3-replica case in comparison with the 2-replica case, for the respective cluster type and system size L, cf. Figs. 5.7 and 5.8.

5.3.2 Critical behaviour

In this section the critical behaviour of the 3-replica Ising model will be discussed, where we will follow the same path as for the case of the 2-replica Ising model (see Sec. 5.2.2). Namely, the critical exponent ν will first be discussed, followed up by the determination of the critical point, for the soft and hard constraint clusters, respectively. Subsequently, the critical exponents β/ν and γ/ν will be considered.

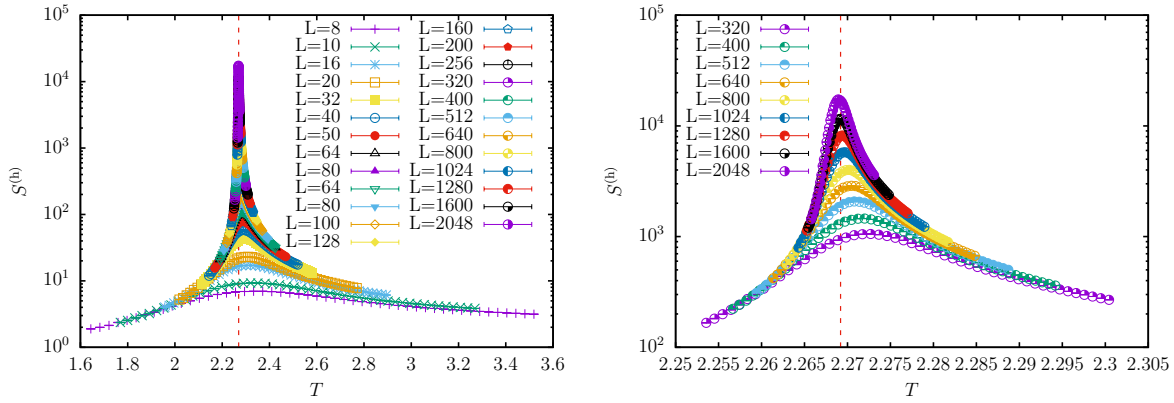

(a) (b)

Figure 5.34: (a) Average cluster size of the hard constraint clusters $S^{(s)}$ on a semi-log axis, for the 3-replica Ising model as a function of temperature T, for different system sizes L. (b) Analogous to panel (a) for the larger system sizes considered. The dashed vertical line marks the transition temperature of the 1-replica Ising model.

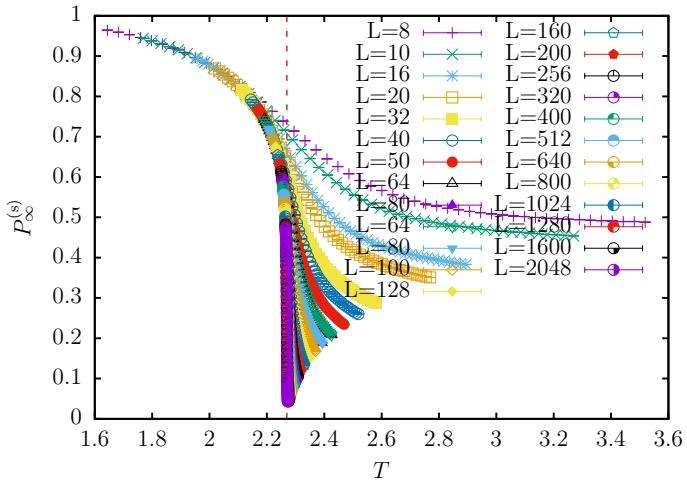

Figure 5.35: Percolation strength of the soft constraint clusters $P_\infty^{(s)}$, for the 3-replica Ising model as a function of temperature T, for different system sizes L. The dashed vertical line marks the transition temperature of the 1-replica Ising model.

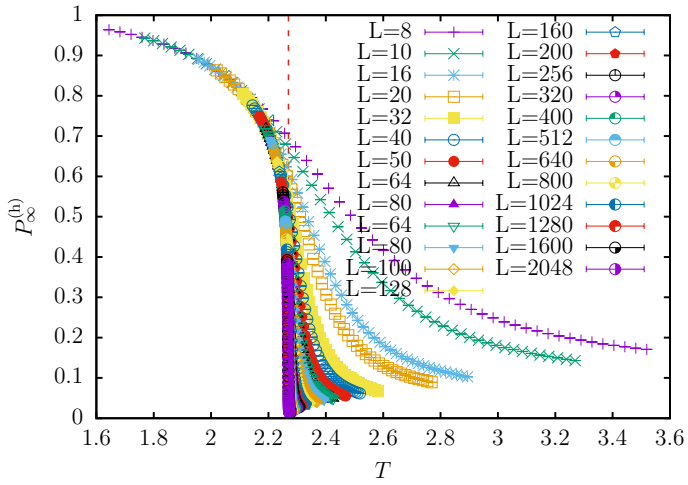

Figure 5.36: Percolation strength of the hard constraint clusters $P_\infty^{(s)}$, for the 3-replica Ising model as a function of temperature T, for different system sizes L. The dashed vertical line marks the transition temperature of the 1-replica Ising model.

Critical exponent ν

For the estimation of the ν exponent, we will utilise the absolute value of the derivatives of the various wrapping probabilities with respect to temperature for the soft and hard constraint clusters, which their maxima scale with system size L according to Eq. (5.4), cf. Sec. 5.2.2. The maxima of the aforementioned derivates are plotted as a function of system size L (on a log-log scale) in Figs. 5.37 and 5.38, for the soft and hard constraint clusters, respectively. These maxima are obtained from the root of the second derivative of R with respect to temperature, where the derivative is evaluated numerically using the symmetric-finite-difference approximation, and the root of the second derivative is estimated using the bisection method [183]. Additionally, the single histogram reweighting technique is employed (see Appendix A.4), in order to minimize the effect of systematic errors, coming from the numerical estimation of the derivatives.

In order to utilise Eq. (5.4), we will perform linear-fits (on a log-log scale) on varying intervals $L_{\min} \leq L \leq L_{\max}$, similarly to the 2-replica case, see Sec. 5.2.2. The estimates of the involved exponent as a function of $1/L_{\min}$ are shown in Figs. 5.39 and 5.40 for the soft and hard constraint clusters, respectively. For the ν exponent of the soft constraint clusters, $\nu^{(s)}$, estimates resulting from different definitions are quite distinct from each other, for small and intermediate values of $L_{\min}$, while they seem to approach a common value which is close to 1 only for the two largest values of $L_{\min}$, i.e., $L = 1024$ and 1280. Additionally, for the hard constraint clusters $\nu^{(h)}$ does not seem to have approached its asymptotic value as it increases as the $L_{\min}$ increases, for all definitions except $R^{(h)}_{x \text{ and } \bar{y}}$. For the latter definition $\nu^{(h)}$ behaves inconsistently, as it is close to a value around 1.02 for all $L_{\min} \leq 200$, whereas above that it increases as $L_{\min}$ increases, with the exception of the second- and third-to-last points which are consistent with a value around 1.

Such behaviour of the involved exponent for the two cluster types is a strong indication that corrections to scaling are present, which in turn influence the behaviour of the exponent.

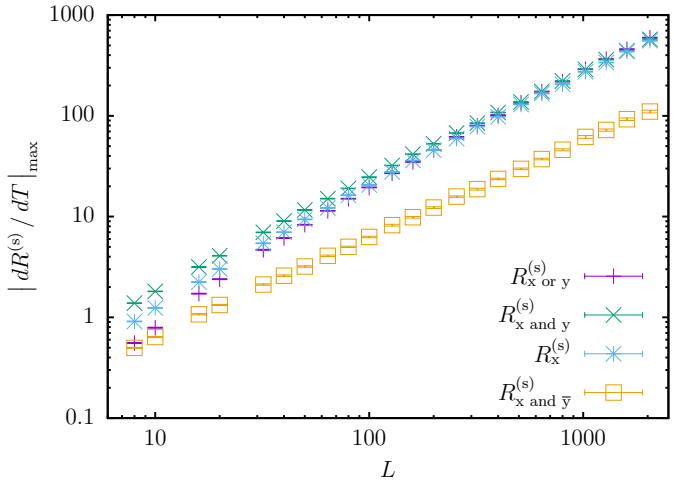

Figure 5.37: Log-log plot of $|dR/dT|_{\max}$ for the different definitions of the wrapping probabilities of the soft constraint clusters, for the 3-replica Ising model as a function of system size L.

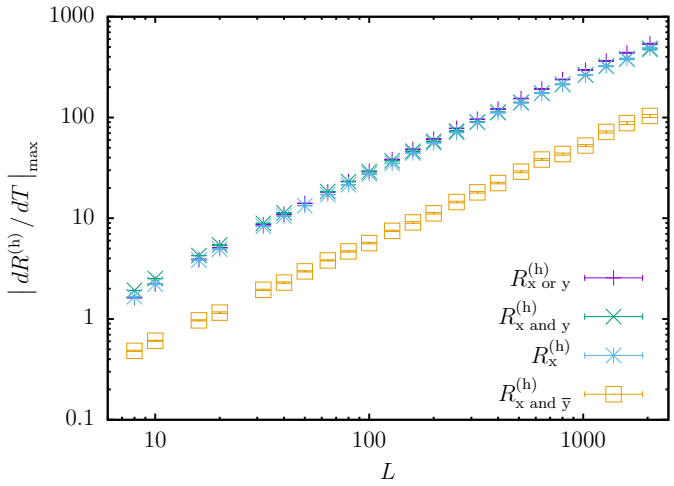

Figure 5.38: Log-log plot of $|dR/dT|_{\max}$ for the different definitions of the wrapping probabilities of the hard constraint clusters, for the 3-replica Ising model as a function of system size L.

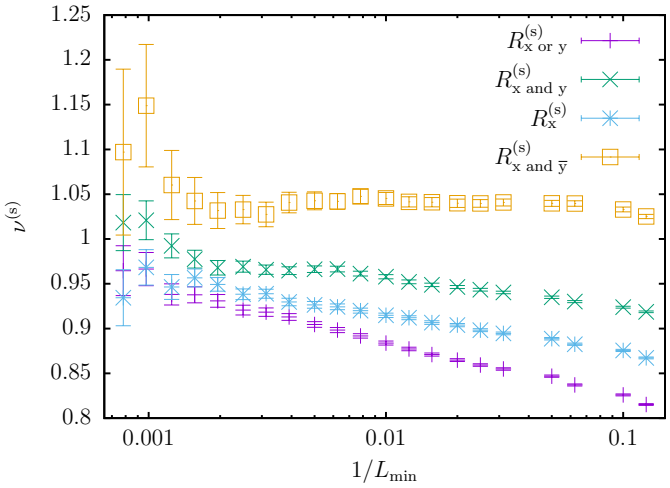

Figure 5.39: Estimates of the ν exponent of the soft constraint clusters, for the 3-replica Ising model as function of $1/L_{\min}$. Estimates extracted from linear fits (on a log-log scale) of $|dR/dT|_{\max}$ as a function of system size L.

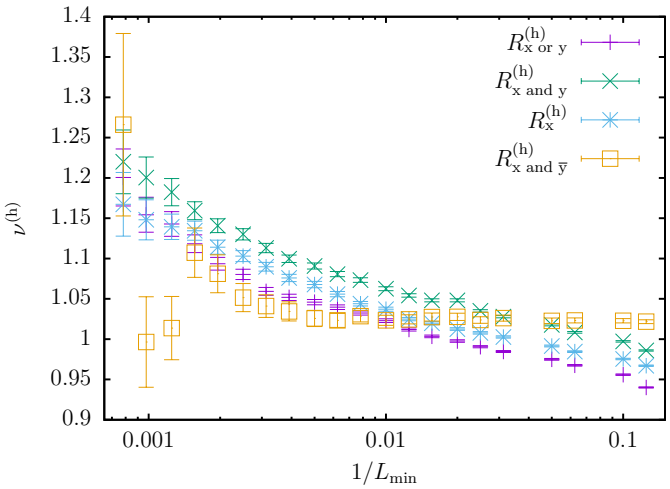

Figure 5.40: Estimates of the ν exponent of the hard constraint clusters, for the 3-replica Ising model as function of $1/L_{\min}$. Estimates extracted from linear fits (on a log-log scale) of $|dR/dT|_{\max}$ as a function of system size L.

To incorporate that we performed fits including a correction term as in Eq. (2.58). Unfortunately, such fits were unreliable, with quite large error estimates on the involved fitting parameters. As an alternative we tried fits including a logarithmic correction term of the form:

$$f(L) = a_1 L^{1/\nu} \left(1 + a_2 / \log L\right), \tag{5.11}$$

where a_1, a_2 are non-universal scaling parameters. We note that there is no obvious reason for such corrections to appear here, given that such logarithmic corrections usually emerge at the upper critical dimension. Thus, since an ansatz like Eq. (2.58) do not provide reliable estimates for the involved parameters, our choice for logarithmic corrections to scaling can only be seen as an alternative on a speculative basis.

In Figs. 5.41 and 5.42 the estimates of the exponent ν are plotted as a function of $1/L_{\min}$ for the soft and hard constraint clusters, respectively. For the soft constraint clusters, $\nu^{(\mathrm{s})}$ is compatible with a value around 1, for all definitions considered (with two exceptions which will be discussed shortly). However, for the larger values of $L_{\min}$ there is a trend of increasing values, especially for the $R^{(\mathrm{s})}_{\mathrm{x\ and\ \overline{y}}}$ definition, but still consistent with the value 1 in between error bars. Additionally, note that for $L_{\min} = 40$ and 50 the estimations of $\nu^{(\mathrm{s})}$ for $R_{\mathrm{x\ and\ y}}$, significantly deviate from $\nu^{(\mathrm{s})} = 1$, especially for $L = 50$. In general, the estimates of the fitting parameters correspond to the minimization of χ^2 in the space of the parameters [183, 190]. This parameter-space, especially for non-linear fits[4] as the one here, could have rugged landscapes with many local-minima, and it is likely that the minimization process could get "stuck" in one of those, resulting in a non-optimal set of parameters. In order to overcome such issues different initial starting values of the parameters should be tried, in order to assure that the global minimum has been reached; of course there is no *a priori* guarantee that this should happen. For our case we tried several initial values, but the resulting parameters did not change significantly. In any case, though, since such estimates correspond to values of $L_{\min}$ which are relatively small in comparison with the rest that we consider, as a precaution against unavoidable corrections to scaling we will not take them into account. Finally, note that the estimates of $\nu^{(\mathrm{s})}$ corresponding to $L_{\min} = 1024$ for all definitions have been omitted, as the error bars were *extremely* large, making them unreliable, however, these values along with the fitting results for the rest of the definitions have been reported in Table B.13 in the Appendix.

The estimates of the ν exponent for the hard constraint clusters, $\nu^{(\mathrm{h})}$, increase for $L_{\min} \leq 400$, where after that point it reaches a plateau which is around the value of $\nu^{(\mathrm{h})} \approx 1.5$. For the largest $L_{\min}$, i.e., $L_{\min} = 1024$, however, the error bars of the estimates for the different definitions are quite large making them unreliable. Note that the estimates for $L_{\min} = 512$ and 640, have been omitted from Fig. 5.42 as their error bars are extremely large resulting to unreliable estimates, while for $L_{\min} = 1024$ the fitting routine could not provide any result, as it did not converged. All the fitting results have been reported in Table B.14 in the Appendix.

[4] Note that the minimization routine could also get "stuck" even for linear fits. This might happen as some regions of the parameter space could be quite flat and during the minimization process of χ^2, which is usually implemented by the gradient descent method, the routine might not be able to reach the minimum value of χ^2.

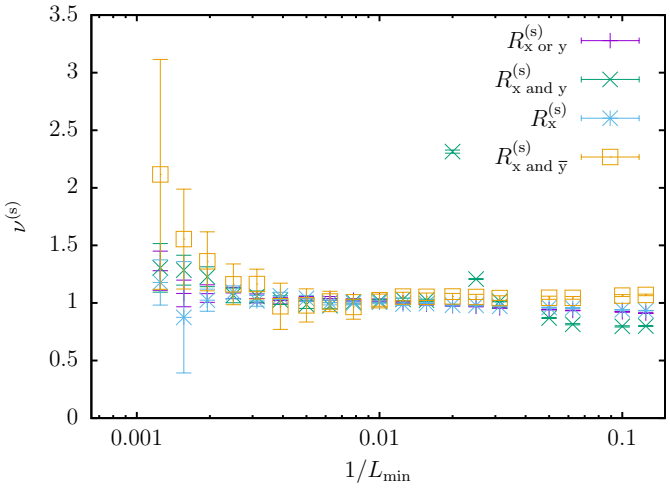

Figure 5.41: Estimates of the ν exponent of the soft constraint clusters, for the 3-replica Ising model as function of $1/L_{\rm min}$. Estimates extracted from fits using a logarithmic correction term [see Eq. (5.11)] of $|dR/dT|_{\rm max}$ as a function of system size L.

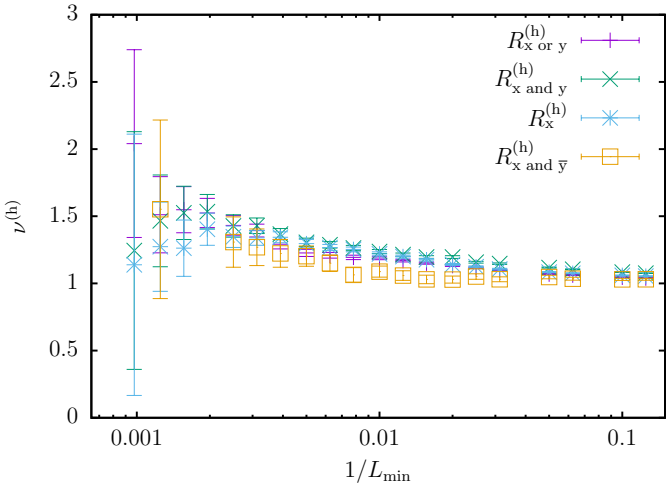

Figure 5.42: Estimates of the ν exponent of the hard constraint clusters, for the 3-replica Ising model as function of $1/L_{\rm min}$. Estimates extracted from fits using a logarithmic correction term [see Eq. (5.11)] of $|dR/dT|_{\rm max}$ as a function of system size L.

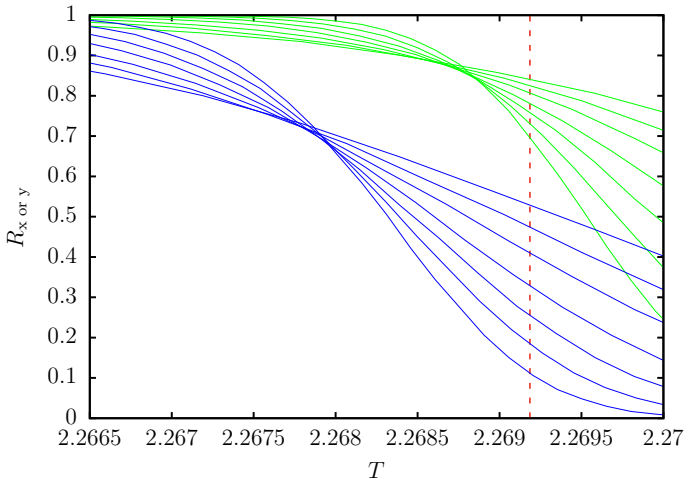

Figure 5.43: $R_{\mathrm{x\ or\ y}}$ as a function of temperature for system sizes $L = [512 - 2048]$, for the soft (green colour) and hard (blue colour) constraint clusters, of the 3-replica Ising model. The dashed vertical line marks the transition temperature of the 1-replica Ising model.

Critical temperature

Similarly to the 2-replica case, the estimation of the critical temperature of the soft and hard constraint clusters for the 3-replica Ising model will be obtained via the crossing method. As in Sec. 5.2.2, the location of the crossings of the wrapping probabilities of pairs of system sizes $(L, 2L)$ were obtained using the bisection method [183], along with the single histogram reweighting technique, in order to produce more accurate estimates, see Appendix A.4. In Fig. 5.43 the $R_{\mathrm{x\ or\ y}}$ is plotted as a function of temperature T for the larger system sizes considered, i.e., $L = [512 - 2048]$, for the soft (green colour) and hard (blue colour) constraint clusters, respectively. In contrast to the 2-replica case, curves of soft and hard constraint clusters cross at different temperatures, which are both below the critical temperature of the 1-replica Ising model (dashed vertical line), cf. Fig. 5.13.

In Figs. 5.44 and 5.45 the positions of the crossings are plotted as a function of $1/L$, where we again considered the smaller system size of the pair $(L, 2L)$, for all definitions and for the soft and hard constraint clusters, respectively. For the soft constraint clusters we see that crossings for the larger system sizes [see Fig. 5.44(b)] seem to approach a temperature different, but quite close, to that of the 1-replica Ising model. Nonetheless, one cannot exclude the possibility that such crossings could approach the critical temperature of the 1-replica Ising model, if larger system sizes will be considered. For the hard constraint clusters, the situation is somewhat more clear, as the deviation from the critical temperature of the 1-replica Ising model is quite pronounced, especially for the largest system sizes, and we can expect that the asymptotic value must be different from that of the 1-replica Ising model, see Fig. 5.45(b).

To determine the critical temperature we performed fits according to Eq. (2.55), where we accumulate the exponent $1/\nu + \omega$ in a single parameter ϵ, i.e.,

$$T_{\mathrm{cross}}(x) = T_{\mathrm{c}} + a x^{\epsilon}, \tag{5.12}$$

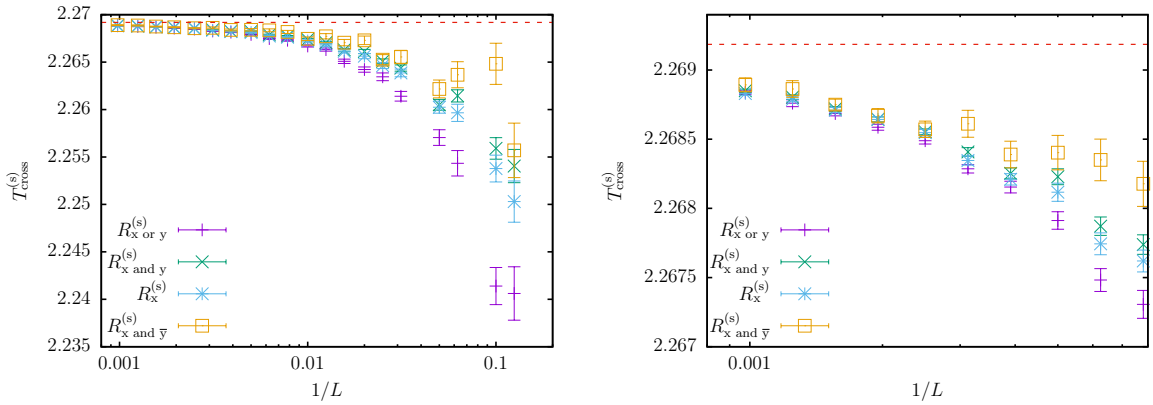

(a) (b)

Figure 5.44: (a) Estimates of the crossing temperatures of pairs $(L, 2L)$ from the wrapping probabilities of the soft constraint clusters, for the 3-replica Ising model as a function of $1/L$. The dashed horizontal line marks the transition temperature of the 1-replica Ising model. (b) Analogous to panel (a) for the larger system sizes considered. The x-axis is in a log-scale for a better presentation of the results.

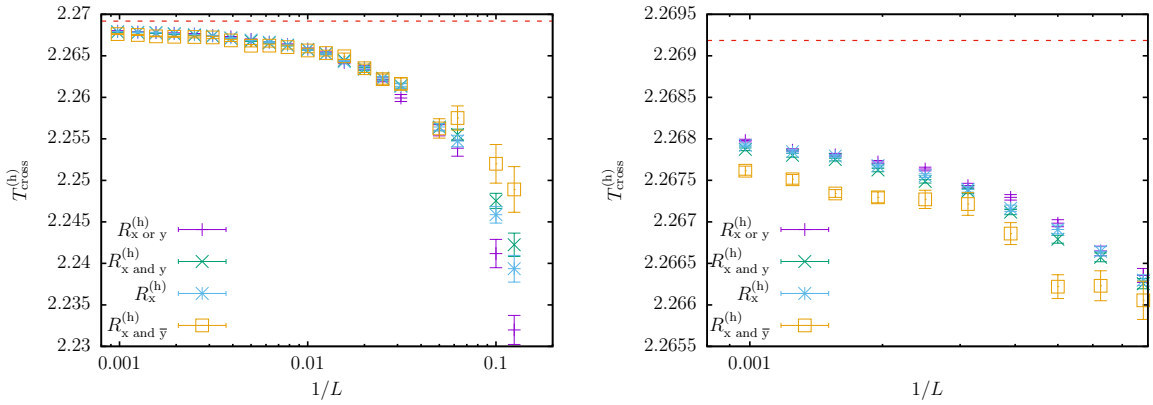

(a) (b)

Figure 5.45: (a) Estimates of the crossing temperatures of pairs $(L, 2L)$ from the wrapping probabilities of the hard constraint clusters, for the 3-replica Ising model as a function of $1/L$. The dashed horizontal line marks the transition temperature of the 1-replica Ising model. (b) Analogous to panel (a) for the larger system sizes considered. The x-axis is in a log-scale for a better presentation of the results.

where $x \equiv 1/L$, $\epsilon \equiv 1/\nu + \omega$, and a is a non-universal scaling parameter. Once again fits were performed on varying intervals $L_{\min} \leq L \leq L_{\max}$, in the same fashion as before (see, e.g., Sec. 5.2.2). We note that fits using Eq. (5.12) were also performed initially for the estimation of the critical temperature for the soft and hard constraint clusters of the 2-replica Ising model. However, as discussed in Sec. 5.2.2, the accuracy of our data resulted in fits of poor quality and consequently to unreliable estimates of the involved parameters. Thus, fits using Eq. (5.5) were performed instead.

In Figs. 5.46 and 5.47 the estimates of the critical temperature are plotted as a function of $1/L_{\min}$ for the soft and hard constraint clusters, respectively. Note that data points corresponding to $L_{\min} = 128$, 160, 200, 256, and 320 for the $R^{(\mathrm{s})}_{\mathrm{x\ and\ }\overline{\mathrm{y}}}$ definition, have been omitted from Fig. 5.46, as the estimated errors of the critical temperature were extremely large, leading to unreliable estimates of the involved parameter. For values of $L_{\min} = 100$ and above, estimates of the $T_{\mathrm{c}}^{(\mathrm{s})}$ are consistent with the critical temperature of the 1-replica Ising model, which is indicated by the dashed horizontal line; this is also supported from Table B.15 in the Appendix, where the fitting results are reported. Nonetheless, from Fig. 5.43 we see that the position of the crossings of $R_{\mathrm{x\ or\ y}}$ (green lines) are in a temperature range $[2.2685 - 2.269]$, which is also in agreement with the estimated values of the critical temperature from Fig. 5.46; the same holds for the rest of the wrapping probabilities considered, though not presented here, i.e., the crossings for the rest of the definitions are in a temperature range $[2.2685 - 2.269]$. Thus, although our estimates are consistent with a critical temperature equal to the 1-replica Ising model, we cannot exclude the possibility that the asymptotic value might be different, but quite close, from that. To clarify this issue simulations on larger system sizes have to be performed. For the hard constraint clusters estimates of $T_{\mathrm{c}}^{(\mathrm{h})}$, see Fig. 5.47, clearly show that the critical temperature is below that of the 1-replica Ising model, and close to a value around $T_{\mathrm{c}}^{(\mathrm{h})} \approx 2.268$. Here the data points for $L_{\min} = 400$ and 512 for $R_{\mathrm{x\ or\ y}}$ and $L_{\min} = 256$, 320, 400, and 512 for $R^{(\mathrm{s})}_{\mathrm{x\ and\ }\overline{\mathrm{y}}}$, are excluded for the same reason as with the soft constraint clusters discussed above, see also Table B.16 in the Appendix. Additionally, from Fig. 5.43, we see that the position of the crossings for the hard constraint clusters (blue lines) lies around $[2.2675 - 2.2682]$, which is also compatible with the results from the fits obtained above.

Furthermore, for relatively large values of $L_{\min}$, say $L_{\min} \geq 160$, the exponent ϵ is consistent with the value 1 for the soft and hard constraint clusters, respectively, see Tables B.15 and B.16; the only exception is for $R^{(\mathrm{s})}_{\mathrm{x\ and\ y}}$ where this is valid for $L_{\min} \geq 256$. Of course this is subject to the fact that a reasonable estimate has been obtained, e.g. for $R^{(\mathrm{s})}_{\mathrm{x\ and\ y}}$ and $L_{\min} = 400$ the exponent is 0.660 ± 0.483, which is not a reliable estimate since its error is comparable with the estimated value. Nonetheless, for other values of $L_{\min}$ and definitions of wrapping probabilities, results provide reasonable estimates of the involved exponent. From the estimation of the ν exponent using logarithmic fits, results are consistent with a value around 1 for the soft and 1.5 for the hard constraint clusters, respectively, i.e., $\nu^{(\mathrm{s})} \approx 1$ and $\nu^{(\mathrm{h})} \approx 1.5$. However, as the estimates of the accumulated parameter ϵ are consistent with a value around 1 too, this is clearly a *contradiction*. For example for the hard constraint clusters we have $\nu^{(\mathrm{h})} \approx 1.5$, which implies that the correction exponent is negative, which is certainly unreasonable as this in turn would suggest that corrections to scaling become important as the size of the system increases. Additionally, for the soft constraint clusters one can argue that presumably the correction exponent is quite small such that $\epsilon^{(\mathrm{s})} \approx \nu^{(\mathrm{s})}$, however, the

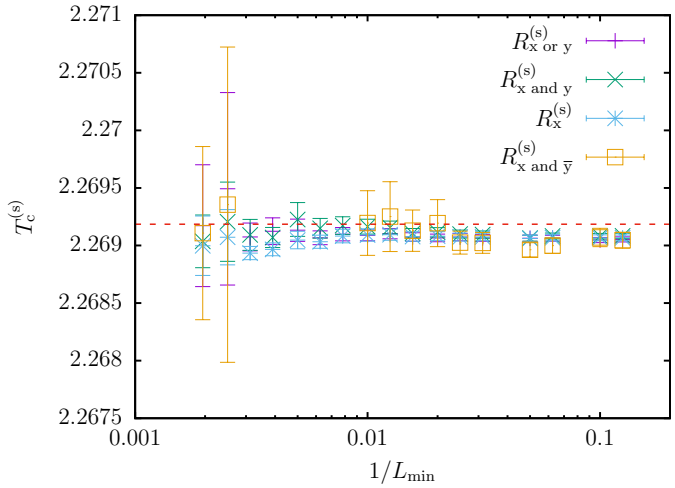

Figure 5.46: Estimates of the critical temperature of the soft constraint clusters, for the 3-replica Ising model as a function of $1/L_{\min}$. The dashed horizontal line marks the transition temperature of the 1-replica Ising model.

correction-to-scaling exponent needs to be determined in order to check the validity of that argument.

From the discussion thus far, it is clear that the estimates of the exponent ν, and critical temperature of the soft and hard constraint clusters for the 3-replica Ising model, are not as concrete as the ones obtained for the 2-replica Ising model; we will further elaborate on this issue in the concluding part of this section, see Sec. 5.3.3, where a possible explanation for the existence of possibly strong corrections to scaling based on qualitative arguments will be given. However, we continue our discussion with the estimation of the critical exponents concerning the average cluster size and percolation strength. For the 2-replica Ising model, the estimation of the critical temperature for the soft and hard constraint clusters, allowed us to perform simulations exactly at this temperature and study the scaling behaviour of the percolation strength and average cluster size as a function of system size, from which we extracted the respective exponents. In the lack of such concrete estimates of the critical temperature for the two cluster types of the 3-replica Ising model, one has to find a different strategy. As discussed in Sec. 2.3, the sequence of pseudo-critical points $T^*(L)$, which can be obtained from, e.g., the position of the maxima of the magnetic susceptibility, or the crossings of the Binder cumulant, can be further utilised to extract the critical exponents of the observables of interest. In our case we will use the crossing points of $R_{\text{x or y}}$ of the soft and hard constraint clusters, respectively, as such sequence of pseudo-critical points, and calculate the observables of interest at these temperatures[5]. Additionally, the single histogram reweighting method (see Appendix A.4) will be utilised, in order to have more accurate estimates of the involved observables. We begin our discussion by considering the percolation strength.

[5]Note, that two sequences of such pseudo-critical points will be utilised, namely one for the soft and the other for the hard constraint clusters.

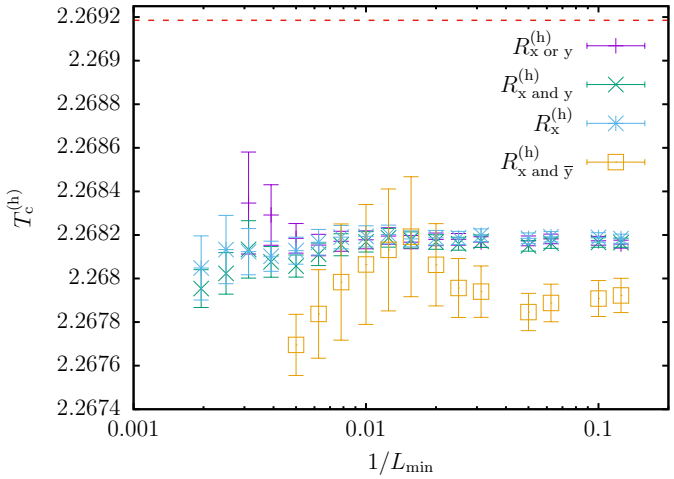

Figure 5.47: Estimates of the critical temperature of the hard constraint clusters, for the 3-replica Ising model as a function of $1/L_{\min}$. The dashed horizontal line marks the transition temperature of the 1-replica Ising model.

Percolation strength

In Figs. 5.48 and 5.49 the percolation strength P_∞ is plotted as a function of system size, for the different definitions considered, evaluated at the crossing points of $R_{\text{x or y}}$, for the soft and hard constraint clusters, respectively. Contrary to the 2-replica case, the different definitions seem to follow straight lines but *not* parallel to each other, indicating that they would result in different estimates of the involved exponent, cf. Figs. 5.18 and 5.19. As discussed above, utilising the sequence of pseudo-critical points of $R_{\text{x or y}}$ results in a constant scaling function of Eq. (4.6), i.e., $P_\infty \sim L^{-\beta/\nu}$, which allows the determination of the exponent, cf. Sec. 4.3.

In order to extract the critical exponent we performed linear fits (on a log-log scale) on varying intervals $L_{\min} \leq L \leq L_{\max}$ as in the 2-replica Ising model, cf. Sec. 5.2.2. In Figs. 5.50 and 5.51 the estimated exponent β/ν is plotted as a function of $1/L_{\min}$ for the soft and hard constraint clusters, respectively. As mentioned above the different definitions, indeed, result in different estimations of the involved exponent, which do not seem to converge to a common value as $L_{\min}$ increases. Specifically, for all definitions (except max $P_{\text{x and }\bar{\text{y}}}$) their estimates increase with $L_{\min}$, and are quite distinct from each other for any value of $L_{\min}$, for the soft and hard constraint clusters, respectively. This is inconsistent with what we have seen so far for the percolation strength of the 1- and 2-replica Ising model, where the exponent is independent of the definition used, cf. Secs. 4.3 and 5.2.2. One possible explanation for this behaviour is the existence of strong scaling corrections, that do not allow us to observe the true asymptotic value of the exponent, and can only be revealed if we consider larger system sizes. For max $P_{\text{x and }\bar{\text{y}}}$, estimates result in quite small values of the exponent, in comparison with the rest of the definitions, and for the larger values of $L_{\min}$ they are even consistent with 0, leading to unreliable estimates, for the soft and hard constraint clusters, respectively. Of course the fact that max $P_{\text{x and }\bar{\text{y}}}$ is not consistent with the rest of definitions, is something that has been observed again for the 1- and 2-replica Ising model, resulting from the rare appearance of such clusters.

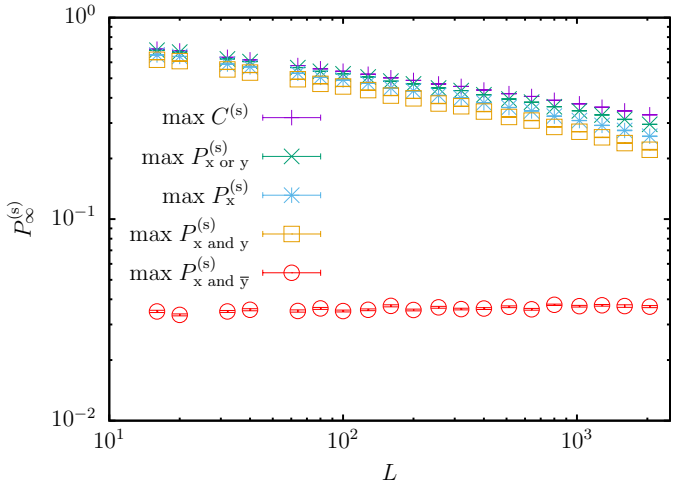

Figure 5.48: Log-log plot of the percolation strength for the different definitions of the soft constraint clusters $P_\infty^{(s)}$, for the 3-replica Ising model as a function of the system size L , evaluated at the pseudo-critical temperatures of $R^{(s)}_{\text{x or y}}$.

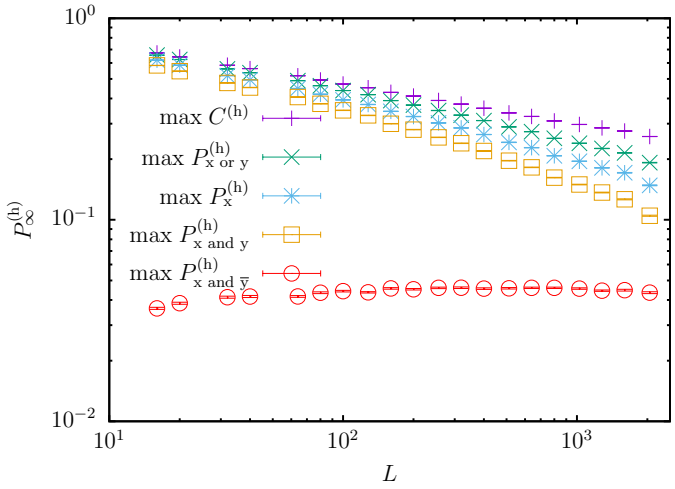

Figure 5.49: Log-log plot of the percolation strength for the different definitions of the hard constraint clusters $P_\infty^{(h)}$, for the 3-replica Ising model as a function of the system size L, evaluated at the pseudo-critical temperatures of $R^{(h)}_{\text{x or y}}$.

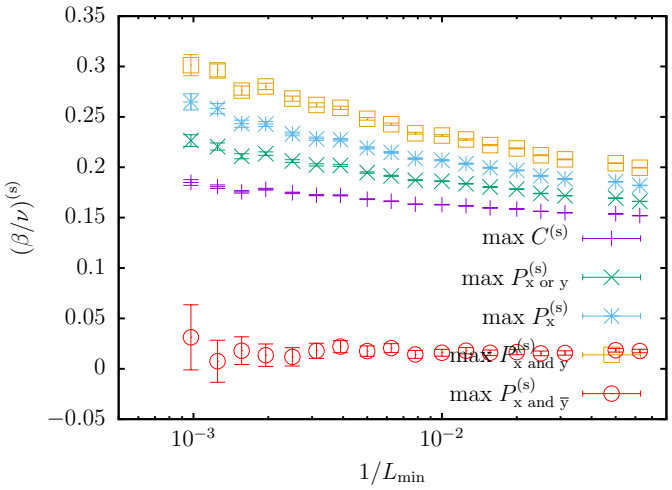

Figure 5.50: Exponent ratio for the different definitions of the soft constraint clusters $(\beta/\nu)^{(s)}$, for the 3-replica Ising model as a function of $1/L_{\min}$.

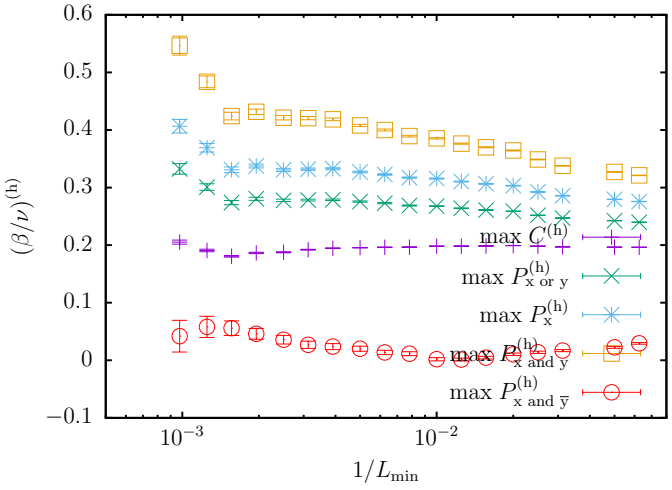

Figure 5.51: Exponent ratio for the different definitions of the hard constraint clusters $(\beta/\nu)^{(h)}$, for the 3-replica Ising model as a function of $1/L_{\min}$.

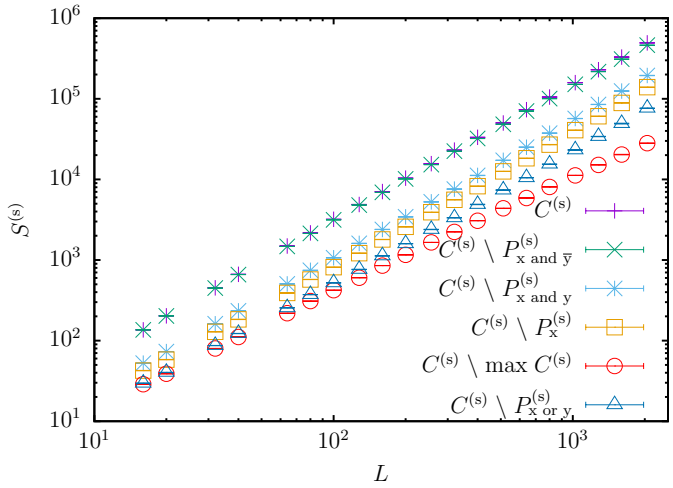

Figure 5.52: Log-log plot of average cluster size for the different definitions of the soft constraint clusters $S^{(s)}$, for the 3-replica Ising model as a function of the system size L , evaluated at the pseudo-critical temperatures of $R^{(s)}_{x \text{ or } y}$.

Average cluster size

In Figs. 5.52 and 5.53 the average cluster size S is plotted as a function of system size, for the different definitions considered evaluated at the crossing points of $R_{x \text{ or } y}$, for the soft and hard constraint clusters, respectively. Similarly to the percolation strength discussed above, utilising the sequence of pseudo-critical points of $R_{x \text{ or } y}$ results in a constant scaling function of Eq. (4.4), i.e., $S \sim L^{\gamma/\nu}$, which allows the determination of the exponent, cf. Sec. 4.2.

Once again, we performed linear fits (on a log-log scale) on varying intervals $L_{\min} \leq L \leq L_{\max}$ as in the 2-replica Ising model, cf. Sec. 5.2.2. The estimated exponent γ/ν is plotted as a function of $1/L_{\min}$ for the soft and hard constraint clusters in Figs. 5.54 and 5.55, respectively. As with the percolation strength, different definitions result in different estimates of the involved exponent. In particular for the soft constraint clusters, we see that the estimates of $C^{(s)} \setminus P^{(s)}_{x \text{ or } y}$, $C^{(s)} \setminus P^{(s)}_{x \text{ and } y}$, and $C^{(s)} \setminus P^{(s)}_{x}$ increase with $L_{\min}$ and for the larger system sizes considered they agree with each other, in between error bars, while the rest of definitions decrease with $L_{\min}$, with estimates being quite distinct from each other especially for the definition where the largest cluster is excluded in each measurement. For the hard constraint clusters the $C^{(h)} \setminus P^{(s)}_{x \text{ or } y}$, $C^{(h)} \setminus P^{(s)}_{x \text{ and } y}$, $C^{(h)} \setminus P^{(h)}_{x}$ and $C^{(h)} \setminus \max C^{(h)}$ increases with $L_{\min}$, but their values do not agree with each other especially for the larger values of $L_{\min}$; for $C^{(h)} \setminus \max C^{(h)}$ this is valid for all values of $L_{\min}$. The $C^{(h)}$ and $C^{(h)} \setminus P^{(h)}_{x \text{ and } \bar{y}}$ have a peak around $L_{\min} = 640$, and as $L_{\min}$ increases further they decrease. Note that C and $C \setminus P_{x \text{ and } \bar{y}}$ provide estimates of the involved exponent close to each other for all values of $L_{\min}$, in comparison to the rest of the definitions, as exclusion of clusters that percolate in one but not the other direction are very rare and they do not alter the average cluster size significantly; this has also been observed for the 1- and 2-replica Ising model, cf. Secs. 4.2 and 5.2.2, respectively.

Finally, it is clear that the estimates of the exponent provided here, are not sufficient to draw any conclusion regarding its asymptotic value. Similarly to the percolation strength,

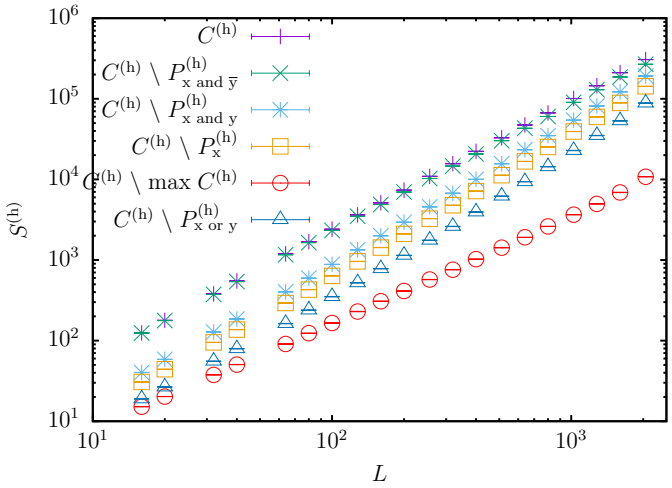

Figure 5.53: Log-log plot of average cluster size for the different definitions of the hard constraint clusters $S^{(h)}$, for the 3-replica Ising model as a function of the system size L , evaluated at the pseudo-critical temperatures of $R^{(h)}_{x \text{ or } y}$.

this might be caused by the existence of strong corrections to scaling, and simulations on larger system sizes would overcome such obstacles. We refer to this point in the next section which summarizes the results obtained for the 3-replica Ising model.

5.3.3 Concluding remarks

The percolation properties of the 3-replica Ising model in terms of the soft and hard constraint clusters were discussed, where the analysis and the path that we followed was similar to the case of the 2-replica Ising model. Specifically, we first examine the general behaviour of the main observables, and then proceed to the study of the critical behaviour of the system for both cluster types.

For the estimation of the exponent ν we utilised the wrapping probabilities, as introduced in Sec. 4.1. By calculating the maximum of the absolute value of the derivative with respect to temperature of the wrapping probabilities, we provided estimates of the exponent ν, for the soft and hard constraint clusters, respectively. At first we performed linear fits (on a log-log scale) and observed that for the soft constraint clusters the estimates resulting from the different definitions converged to a value close to 1 only for the two larger values of $L_{\min}$, whereas for the hard constraint clusters the estimates were increasing with $L_{\min}$, except from the second- and third-to-last points of $R^{(h)}_{x \text{ and } \bar{y}}$, see Fig. 5.40. Attempts to perform fits including a correction term, led to unsatisfactory estimates of the exponent. As an alternative method in order to tackle corrections to scaling, fits including a logarithmic term were considered. The performed fits were of reasonable quality for most of the larger values of $L_{\min}$, and the obtained results suggest that the exponent is consistent with a value $\nu^{(s)} \approx 1$ for the soft constraint clusters, and $\nu^{(h)} \approx 1.5$ for the hard constraint clusters. However, since logarithmic corrections to scaling usually emerge for systems at the upper critical dimension (see, e.g., Ref. [71] and references therein, and Ref. [109] for the case of percolation), we are not able to provide a concrete explanation of why such corrections could emerge here, since

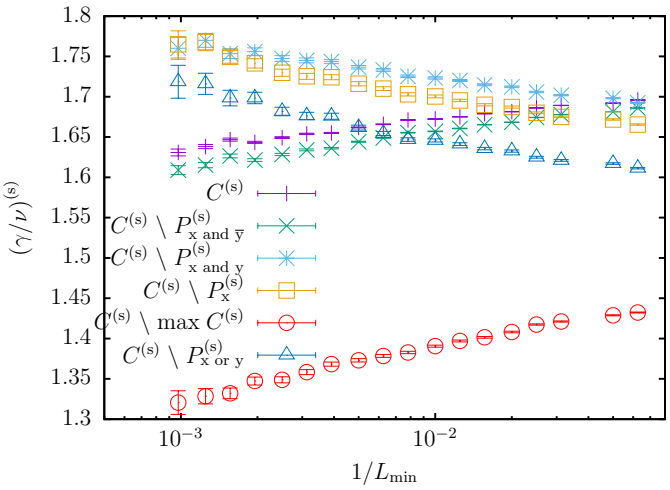

Figure 5.54: Exponent ratio for the different definitions of the soft constraint clusters $(\gamma/\nu)^{(s)}$, for the 3-replica Ising model as a function of $1/L_{\min}$.

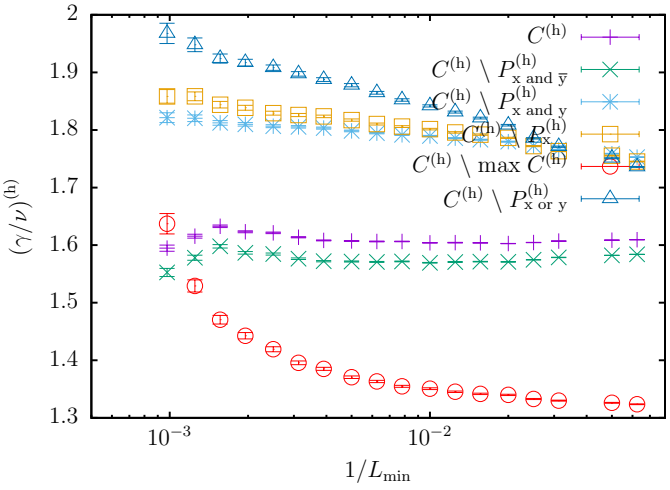

Figure 5.55: Exponent ratio for the different definitions of the hard constraint clusters $(\gamma/\nu)^{(h)}$, for the 3-replica Ising model as a function of $1/L_{\min}$.

the upper critical dimension of the Ising model is four.

Subsequently, the critical temperature for the soft and hard constraint clusters, was studied by utilising the crossing technique of pairs $(L, 2L)$ of the wrapping probabilities. For that we performed fits according to Eq. (2.55), where we accumulate the exponent $1/\nu + \omega$ into a single parameter ϵ. For the soft constraint clusters results indicate that the critical temperature in consistent with that of the 1-replica Ising model, however, from Fig. 5.43 the location of the crossings of $R^{(\mathrm{s})}_{\mathrm{x\ or\ y}}$ for the larger system sizes considered (green colour lines) is in a temperature range $[2.2685 - 2.269]$, which can also be supported from these estimates. For the hard constraint clusters, results are consistent with a temperature below that of the 1-replica Ising model, and as is shown in Fig. 5.43 this is in agreement with the location of the crossings of $R^{(\mathrm{h})}_{\mathrm{x\ or\ y}}$ for the larger system sizes considered (blue colour lines) which lies around $[2.2675 - 2.2682]$. Additionally, the accumulated exponent ϵ is consistent with a value around 1 for the soft and hard constraint clusters, respectively. For the hard constraint clusters this is inconsistent with the obtained value of $\nu^{(\mathrm{h})} \approx 1.5$, as this implies a negative correction-to-scaling exponent. For the soft constraint clusters, on the other hand, this implies that corrections to scaling are negligible, as $\nu^{(\mathrm{s})} \approx 1$, which still needs further investigation.

Having not obtained accurate estimates for the critical temperature, the estimation of the critical exponents concerning the percolation strength and average cluster size, were determined by utilising the sequence of pseudo-critical points resulting from the crossings of $R_{\mathrm{x\ or\ y}}$ for the soft and hard constraint clusters, respectively. Additionally, in order to provide more accurate estimates the single histogram reweighting technique was utilised. For the percolation strength estimates of the involved exponent coming from different definitions are quite distinct from each other for the soft and hard constraint clusters, respectively. For the exponent of the average cluster size, results also show that the exponent approaches different values depending on the definition being used, with estimates using C and $C \setminus P_{\mathrm{x\ and\ \bar{y}}}$ being closer to each other, only because excluding clusters percolating in one but not the other direction are very rare and do not alter significantly the average cluster size.

It is obvious that the above results do not allow the extraction of any firm conclusions regarding the critical properties of the soft and hard constraint clusters of the 3-replica Ising model, in opposition to the 1- and 2-replica Ising model, cf. Chap. 4 and Sec. 5.2. One possible explanation for that is the existence of strong scaling corrections, that do not allow the extraction of the asymptotic behaviour. For that we have come up with a possible explanation, which we outline here. Let us denote as $T^{(3)}$ the asymptotic critical temperature of the clusters for the 3-replica Ising model; here we will not distinguish between soft and hard constraint clusters. We assume that $T^{(3)}$ is different but quite close to that of the 1-replica Ising model, i.e., $T^{(1)}$, which is a valid assumption for both cluster types, cf., Fig. 5.43. For each of the three replicas the correlation length of the geometrical clusters ξ diverge at $T^{(1)}$ and takes finite values at $T^{(3)}$; remember that the geometrical clusters of the 2-dimensional Ising model (1-replica) percolate at the thermal transition point, see Sec. 2.4.2. On the other hand, $T^{(3)}$ is close to $T^{(1)}$, thus the correlation length is expected to be relatively large, though finite. This in turn defines an effective length scale L^*, as $L^* = \xi\left(T^{(3)}\right)$ that enters the problem of the 3-replica Ising model in the following fashion: If we study systems with $L < L^*$ each replica would appear as if it is in the critical phase, and consequently we are looking at the overlap of three *incipient* percolating clusters. For $L > L^*$ each of the three

replicas should be in the percolating phase, which in turns means that we are looking at the overlap of three *non-critical* percolating clusters. Thus, it is expected that the critical behaviour must change substantially in the vicinity of L^*. Consequently, if L^* is relatively large, say $L^* \gtrsim 500$, this could justify the presence of strong corrections to scaling, which in turn explains the unsatisfactory results obtained for the 3-replica Ising model. Lastly, we note that L^* can be estimated from the definition of the second moment correlation length [see Eq. (2.62)], or alternatively by utilizing the average radius of the clusters which is directly connected with the correlation length ξ; for the latter see, e.g., Ref. [19].

5.4 The 4-replica Ising Model: Preliminary Results

In the final section of this chapter we will discuss some preliminary results concerning the percolation properties of the 4-replica Ising model for the soft and hard constraint clusters as introduced in Sec. 5.1. The simulation details are similar to the ones introduced in Sec. 5.2 for the 2-replica case, with the difference that the largest system considered here is of linear size $L = 1600$, as opposed to the 2- and 3-replica Ising model which was $L = 2048$, and we did not perform simulations exactly at the critical temperature of the 1-replica Ising model, cf. Secs. 5.2 and 5.3.

5.4.1 Observables

Wrapping probabilities

In Figs. 5.56 and 5.57 the wrapping probabilities R are plotted as a function of temperature T for the different system sizes L of the soft and hard constraint clusters, respectively. The crossings of the wrapping probabilities are quite below the critical temperature of the 1-replica Ising model which is denoted by the dashed vertical line; see the right panels of Figs. 5.56 and 5.57, respectively. This is also supported in Fig. 5.58, where $R_{\text{x or y}}$ is plotted as a function of temperature T for the larger system sizes considered, i.e., $L = [400 - 1600]$, for the soft (green colour) and hard (blue colour) constraint clusters, respectively. According to that, the critical temperature of the soft constraint clusters is around $[2.263 - 2.267]$, whereas for the hard constraint clusters is around $[2.253 - 2.257]$. These temperature ranges are below the ones obtained for the soft and hard constraint clusters of the 3-replica Ising model; we remind here that for the soft constraint clusters the temperature range was $[2.2685 - 2.269]$ and for the hard constraint clusters $[2.2675 - 22682]$. Consequently, we see that as the number of replicas increases the critical temperature shifts to lower values, for the soft and the hard constraint clusters, respectively. Of course for more precise conclusions accurate estimates of the critical temperature as the ones for the 2-replica Ising model should be obtained, see Sec. 5.2.2.

Average cluster size

In Figs. 5.59 and 5.60 the average cluster size S is plotted as a function of temperature T for the different system sizes L considered of the soft and the hard constraint clusters, respectively. Here we used again the conventional definition of the average cluster size, where on each measurement the largest cluster is excluded, which results in the appearance of a maximum in the vicinity of the critical point. From Fig 5.59(b) we see that the chosen

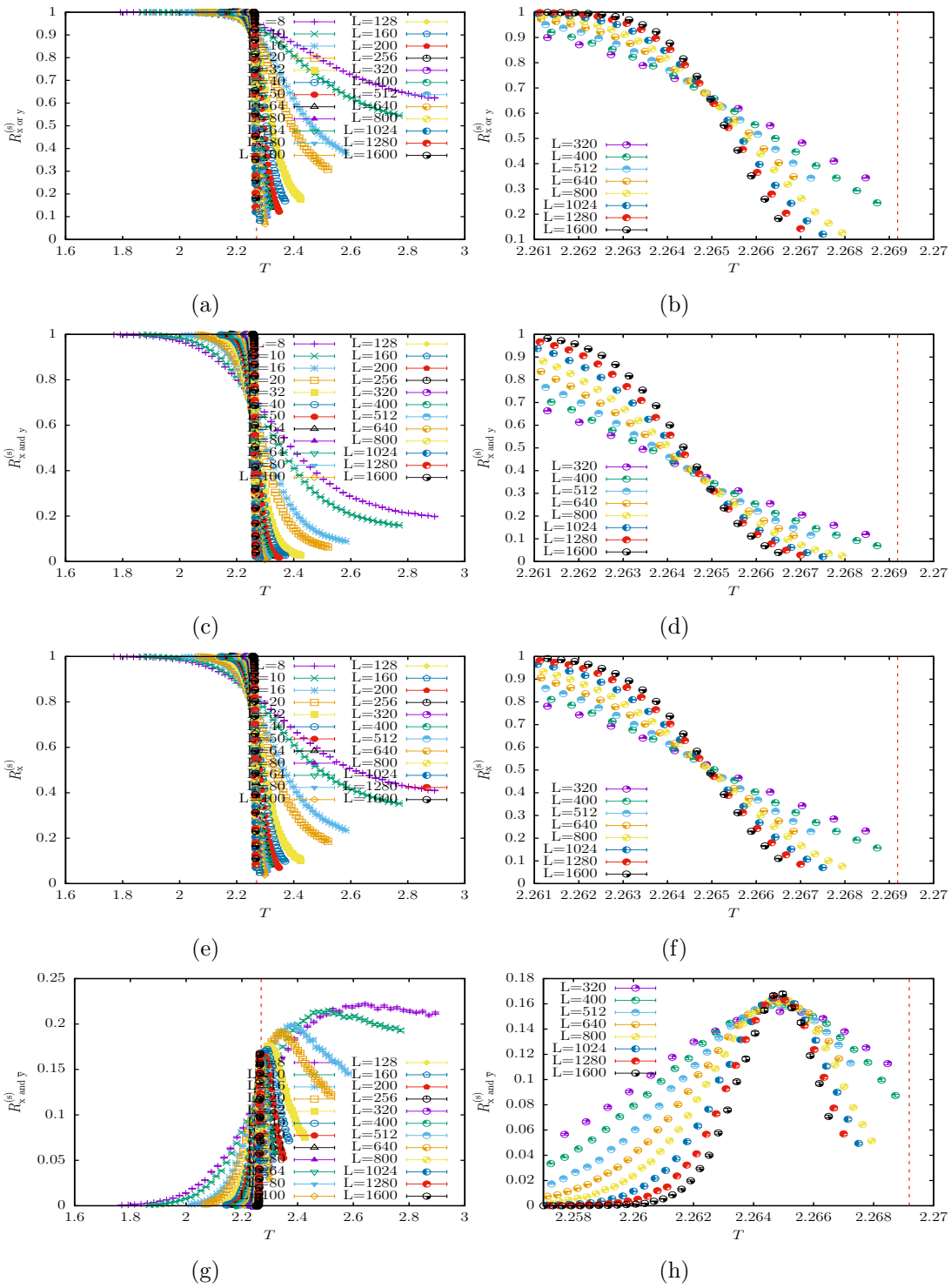

Figure 5.56: *Left column*: Wrapping probabilities of the soft constraint clusters, for the 4-replica Ising model as function of temperature T, for different system sizes L. *Right column:* Analogous to left column for the larger system sizes considered. The dashed vertical line marks the transition temperature of the 1-replica Ising model.

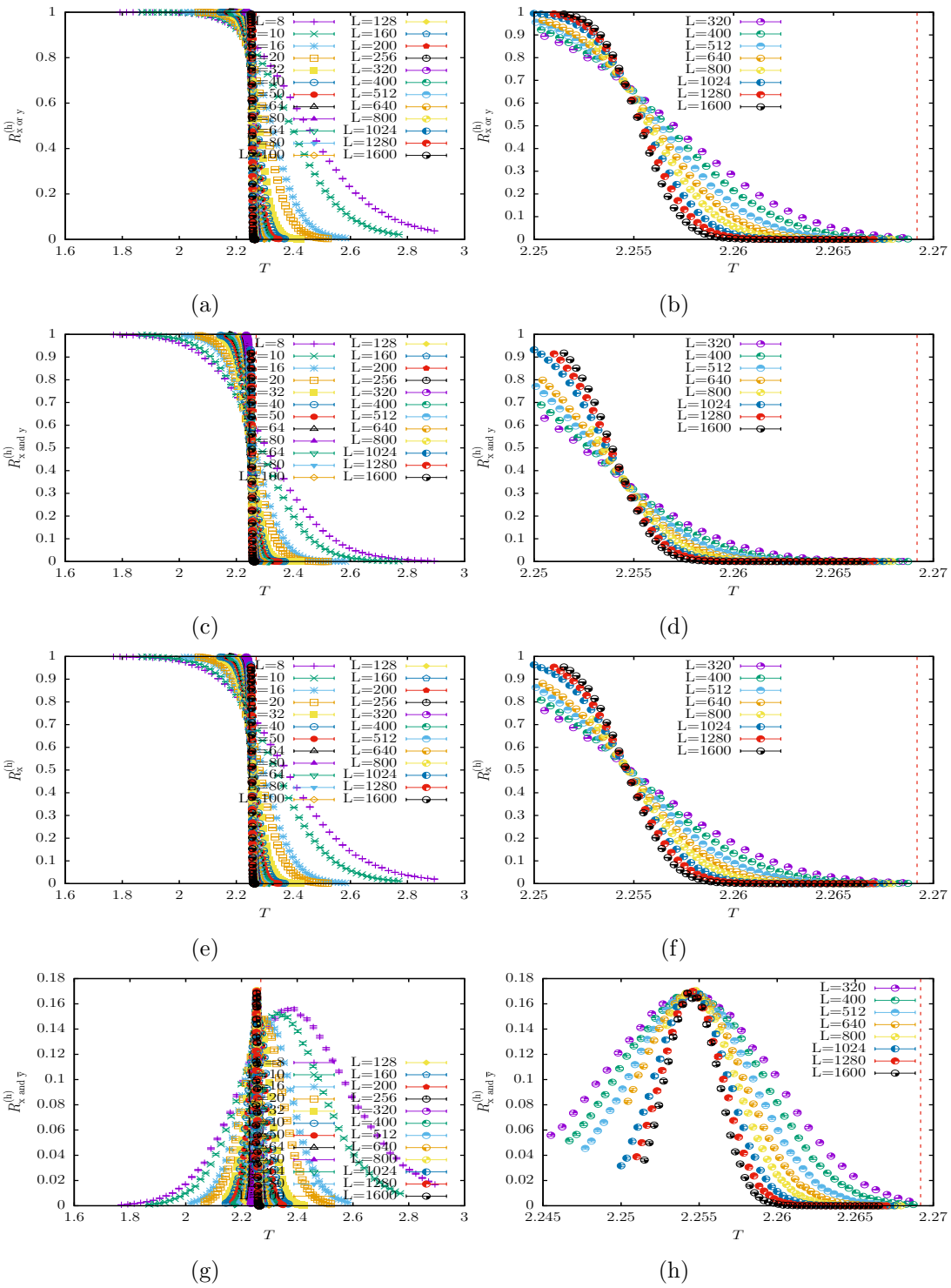

Figure 5.57: *Left column*: Wrapping probabilities of the hard constraint clusters, for the 4-replica Ising model as function of temperature T, for different system sizes L. *Right column:* Analogous to left column for the larger system sizes considered. The dashed vertical line marks the transition temperature of the 1-replica Ising model.

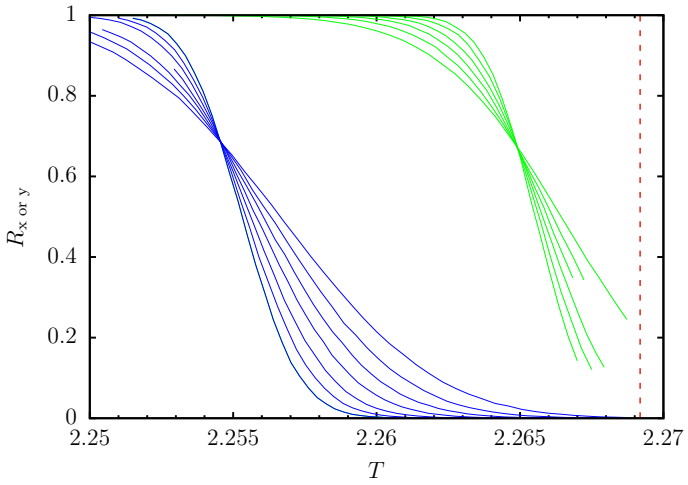

Figure 5.58: $R_{\text{x or y}}$ as a function of temperature for system sizes $L = [400 - 2048]$, for the soft (green colour) and hard (blue colour) constraint clusters, of the 4-replica Ising model. The dashed vertical line marks the transition temperature of the 1-replica Ising model.

temperature range for the soft constraint clusters dose not allow to clearly observe the peak of the average cluster size, as opposed to the 2- and 3-replica case, cf. Figs 5.5(b) and 5.33(b), respectively. Since the discussion for the 4-replica Ising model is on a more qualitative basis the relative poor choice of temperature range for the average cluster size of the soft constraint clusters does not raise further concerns, however, for a more detailed analysis simulations need to be performed for higher temperature values. For the hard constraint clusters though we see that the peaks of S for the different system sizes are below the critical temperature of the 1-replica Ising model, see Fig. 5.60(b).

Percolation strength

The percolation strength P_∞ is plotted as a function of temperature T for the different system sizes L of the soft and hard constraint clusters, in Figs. 5.61 and 5.62, respectively. The definition that has been used here is, again, that of the largest cluster considered in each measurement. Qualitatively, the behaviour of P_∞ is similar to the 2- and 3-replica Ising model, namely it decreases as function of temperature T, and as temperature goes to 0 it approaches the value 1, meaning that all spins in the k-plane are aligned. As the temperature approaches infinity the percolation strength is essentially zero, reflecting the fact that spins in their respective replicas are pointing in random directions.

5.4.2 Concluding remarks

In this section we presented some preliminary results regarding the percolation properties of the soft and hard constraint clusters for the 4-replica Ising model. As the discussion was on a more qualitative basis no firm conclusions can be made. Nonetheless, existing results indicate that, as in the 3-replica Ising model, the hard constraint clusters percolate at a temperature lower than that of the soft constraint clusters. Additionally, the critical temperature seems to

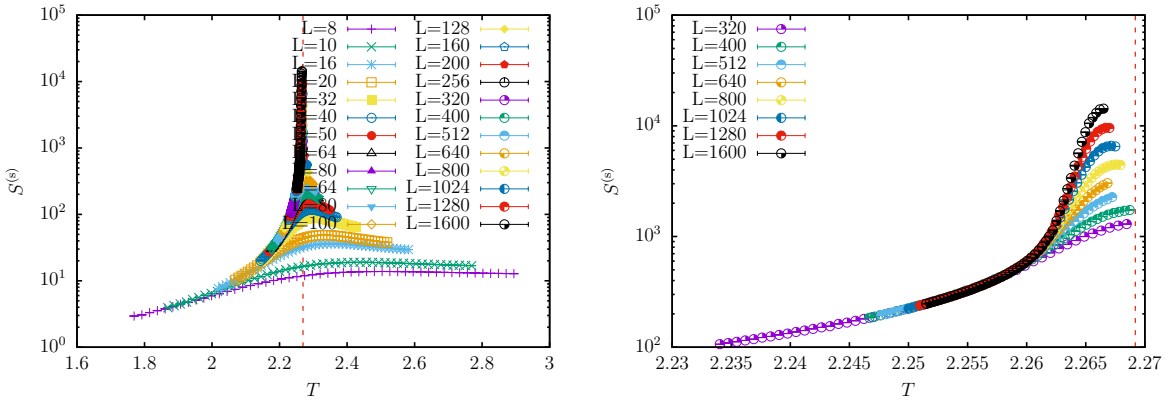

(a) (b)

Figure 5.59: (a) Average cluster size of the soft constraint clusters $S^{(s)}$ on a semi-log axis, for the 4-replica Ising model as a function of temperature T, for different system sizes L. (b) Analogous to panel (a) for the larger system sizes considered. The dashed vertical line marks the transition temperature of the 1-replica Ising model.

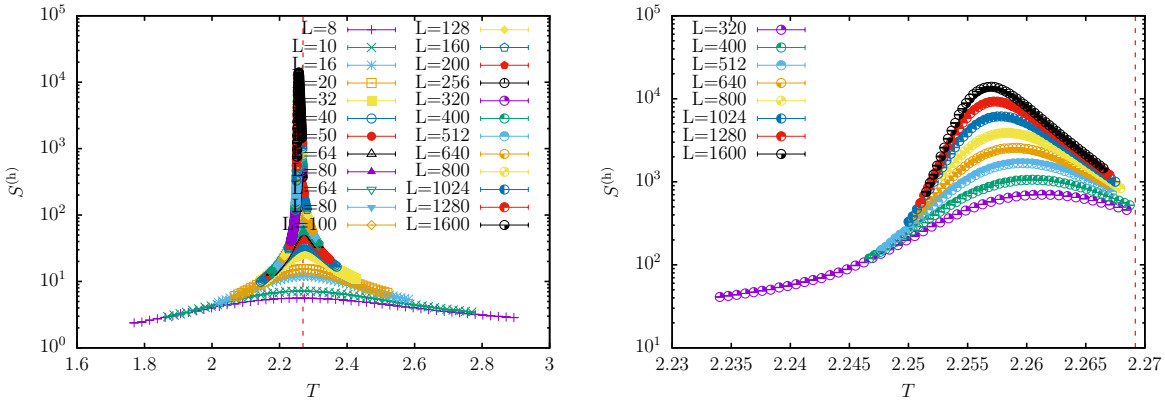

(a) (b)

Figure 5.60: (a) Average cluster size of the hard constraint clusters $S^{(s)}$ on a semi-log axis, for the 4-replica Ising model as a function of temperature T, for different system sizes L. (b) Analogous to panel (a) for the larger system sizes considered. The dashed vertical line marks the transition temperature of the 1-replica Ising model.

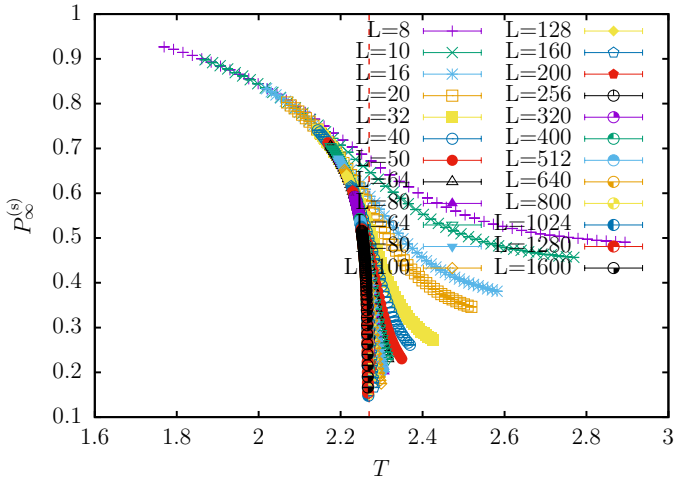

Figure 5.61: Percolation strength of the soft constraint clusters $P_\infty^{(s)}$, for the 4-replica Ising model as a function of temperature T, for different system sizes L. The dashed vertical line marks the transition temperature of the 1-replica Ising model.

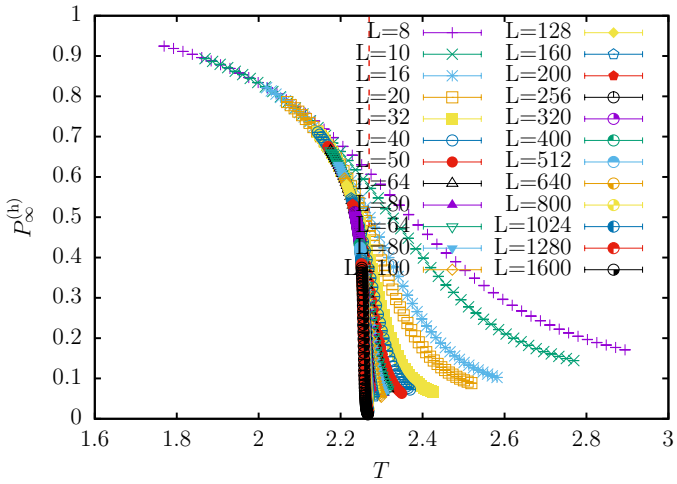

Figure 5.62: Percolation strength of the hard constraint clusters $P_\infty^{(s)}$, for the 4-replica Ising model as a function of temperature T, for different system sizes L. The dashed vertical line marks the transition temperature of the 1-replica Ising model.

shift to lower temperatures as the number of replicas increases for the soft and hard constraint clusters, respectively; cf. Figs. 5.43 and 5.58.

Lastly, we note that if our explanation for the existence of strong scaling corrections for the 3-replica Ising model is correct (see Sec. 5.3.3), then not such strong corrections are expected for the 4-replica case. This can be understood as follows: Let us denote as $T^{(4)}$ the asymptotic critical temperature of the clusters for the 4-replica Ising model (again we do not distinguish between soft and hard constraint clusters). From the above discussion it seems plausible to assume that $T^{(4)} < T^{(3)}$. Thus, since we are below the critical temperature of the 1-replica Ising model, each of the four replicas will satisfy $\xi\left(T^{(4)}\right) < \xi\left(T^{(3)}\right)$, which in turn means that the effective length scale L^* of the 4-replica Ising model will be smaller than that of the 3-replica Ising model.

Chapter 6

Spin Glasses

Until now it should have become clear that graphical representations have greatly enhanced our understanding in the study of phase transitions. Rigorous conclusions exist only for the case of the Ising, and Potts in general, ferromagnet, however, attempts of such a description for the spin glass problem have been made, although to certain extent incomplete. In Chap. 5 the multi-replica Ising model was introduced and the critical behaviour of the 2- and 3-replica case were studied. As it was also mentioned there, the soft constraint clusters are the same as the ones of Houdayer's algorithm, with the exception that in the latter interactions among spins are random. Thus, the percolation properties of Houdayer's clusters presented here can be understood as a continuation of the discussion in Chap. 5. Of course simulating a spin glass system is challenging on its own terms and thus we will first discuss the issue of equilibration.

6.1 Temperature-Schedule Comparisons

Here we study the two-dimensional Edwards-Anderson model, see Eq. (2.82), in the absence of a magnetic field $h = 0$, where the interactions J_{ij} are drawn from a Gaussian distribution with mean zero and variance one. The system was simulated using Houdayer's cluster algorithm, as described in Sec. 3.3.2, for a range of temperatures and systems of linear sizes $L = 10$, 20, 30 and 40. At each temperature two replicas of the system were considered, and a Monte Carlo step (sweep) consists of the following moves: *(i)* One Metropolis sweep for each replica. *(ii)* One Houdayer cluster update for each pair of replicas at the same temperature. *(iii)* One PT update for all pairs of replicas at neighbouring temperatures. The number of disorder realisations was 100 for all system sizes.

As already discussed in Sec. 3.3 spin-glass systems are hard to equilibrate at low temperatures, as the system is usually trapped in local energy minima and thus does not explore the phase space fully. Parallel tempering (PT) is used to alleviate this problem, by utilising parallel simulations of several replicas of the system at different temperatures, and attempting swaps between adjacent replicas. In order to assure equilibration we monitor the time series of the spin overlap q, which is the order parameter of the system [124, 192] and is defined as

$$q = \frac{1}{N} \sum_{i=1}^{N} \sigma_i^{(1)} \sigma_i^{(2)}, \tag{6.1}$$

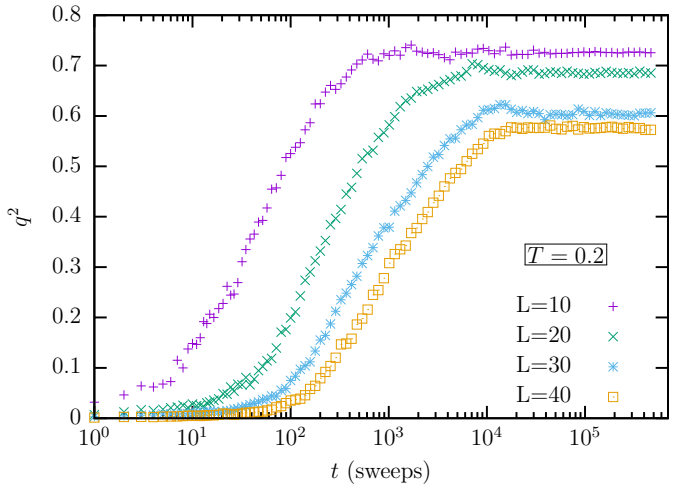

Figure 6.1: Logarithmically binned time series of q^2 as a function of time t, at temperature $T = 0.2$ and for the different system sizes L considered.

where $\sigma_i^{(1)}$, $\sigma_i^{(2)}$ refers to the spin i in the first and second replica, respectively, and N is the total number of spins in each replica.

The time series of q^2, averaged over all disorder realisations considered, is plotted in Fig. 6.1, for a relative low temperature $T = 0.2$, where the logarithmic binning procedure has been employed in order to ensure equilibration. For the two largest system sizes equilibration is achieved for $t > 10^5$ sweeps, while for $L = 10$ and 20 equilibration is achieved for $t > 10^4$ sweeps. Additionally, note that the mean of q^2 decreases as the size of the system increases. This is consistent with the fact that in two dimensions, there is strong evidence of a spin-glass phase at zero temperature only (see, e.g., Ref. [47] and references therein), thus the spin overlap should be zero for all non-zero temperatures in the thermodynamic limit. Of course for finite system sizes q^2 takes non-zero values.

An alternative criterion for equilibration of a system with Gaussian couplings was proposed in Ref. [193], which resorts to an identity introduced in Ref. [194] for the Sherrington and Kirkpatrick spin-glass model [116], which is defined through the Hamiltonian in Eq. (2.87). For this purpose let us introduce the *link overlap* q_l, which is defined as [193]

$$q_l = \frac{1}{N_l} \sum_{\langle i,j \rangle} \sigma_i^{(1)} \sigma_j^{(1)} \sigma_i^{(2)} \sigma_j^{(2)}, \tag{6.2}$$

where N_l is the number of links (bonds) in the system; for a regular cubic lattice with periodic boundary conditions $N_l = Nz/2$, where z is the *coordination number*, i.e., number of neighbours per site. The average energy per site e can be written as

$$\langle e \rangle = -\frac{1}{N} \sum_{\langle i,j \rangle} \overline{J_{ij} \langle \sigma_i \sigma_j \rangle_T}, \tag{6.3}$$

where $\langle \dots \rangle_T$ and the over-bar denotes thermal and disorder average, respectively. It can be shown that the thermal and disorder average of the link overlap $\langle q_l \rangle$ is related to $\langle e \rangle$ as [193, 194]

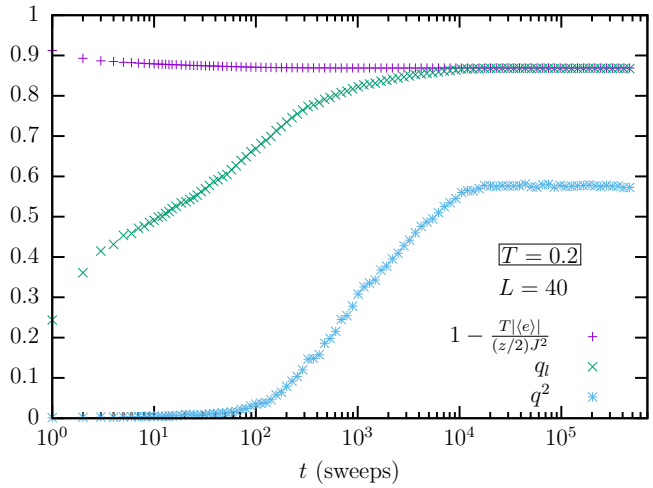

Figure 6.2: Logarithmically binned time series of $q^2, \langle q_l \rangle, 1 - \frac{T|\langle e\rangle|}{(z/2)J^2}$, as a function of time t, at temperature $T = 0.2$ and for system of linear size $L = 40$.

$$\langle q_l \rangle \equiv \frac{1}{N_l} \sum_{\langle i,j \rangle} \overline{\langle \sigma_i \sigma_j \rangle_T^2} = 1 - \frac{T\,|\langle e \rangle|}{(z/2)J^2}, \tag{6.4}$$

where J is the variance of the interaction distribution, which is set to 1 here. Equation (6.4) holds as long as the system is in equilibrium. Assuming that all replicas start with spins pointing in random directions, if the systems are not equilibrated $\langle q_l \rangle$ is expected to be relatively small, as spins are exploring, initially, quite distinct parts of the configuration space, in comparison with equilibrium. Thus, as the number of sweeps increases $\langle q_l \rangle$ is an increasing function of time, where for times greater than the equilibrium time it fluctuates around its mean value. Contrary to $\langle q_l \rangle$, the right-hand-side of Eq. (6.4) will be a decreasing function for times lower than the equilibration time, since for that case $\langle e \rangle$ is a deceasing function. Consequently, when both sides of Eq. (6.4) agree the system is in equilibrium [193]; see also Ref. [195] for the case where an external magnetic field is applied. This is shown in Fig. 6.2, where q^2 and the two terms of Eq. (6.4) are plotted as a function of time, for a system of linear size $L = 40$ at temperature $T = 0.2$. According to that, for $t > 10^5$ sweeps $\langle q_l \rangle$ and $1 - T\,|\langle e \rangle|\,/(z/2)J^2$ are equal indicating that the system is in equilibrium, which is in agreement with the result obtained from Fig. 6.1. The above reported equilibration times have been obtained using the optimal temperature schedule and set of parameters for the PT procedure; in what follows we discuss how we determined such parameters.

In Sec. 3.3.1, we mentioned that the geometric progression schedule is appropriate for systems that do not exhibit a strong divergence of the specific heat [158–160]. Since two-dimensional spin glasses do not possess a phase transition at any non-zero temperature, geometric progression seems a plausible temperature schedule. In Fig. 6.3 the probability A for replicas to be exchanged is plotted as a function of temperature T for different numbers of temperatures N_T, and system sizes $L = 10 - 40$. Given a system size L we see that A increases as the number of temperatures N_T increases, for all T. Consequently, if we want the probability for replicas to be exchanged relatively high, we have to include more replicas

Table 6.1: Tunnelling times for the different number of temperatures N_T and system sizes L considered, using the geometric progression schedule for the PT algorithm. The asterisk (*) corresponds to a temperature range [0.2 : 1.5], while the rest to [0.2 : 2.0]. Cells with N/A represent no tunnelling event.

L \ N_T	10	15	20	25	30	35
10	229 ± 1	255 ± 1	302 ± 1	353 ± 1	–	–
20	1903 ± 13	995 ± 3	918 ± 2	959 ± 2	–	–
30	29960 ± 318	3848 ± 17	2361 ± 6	2079 ± 3 $1509 \pm 3^*$	$1550 \pm 3^*$	–
40	N/A	19486 ± 110	6537 ± 21	4441 ± 9 $2900 \pm 6^*$	$2695 \pm 8^*$	$2680 \pm 4^*$

as the size of the system increases.

As argued in Ref. [159], for a speed-up of equilibration, besides a high probability for replicas to be swapped, one has to ensure that each system passes on average the same time in each temperature. For that we measure the time needed for a replica to travel from the lowest to highest temperature and back. Such a round trip is called *tunnelling* and the required time for that *tunnelling time*. Note that, since each replica performs a random walk in the temperature space, the minimum tunnelling time corresponds to that of an unbiased random walker [159, 161]. In Table 6.1 we report the tunnelling times for the corresponding system sizes and number of temperatures N_T of Fig. 6.3. One could naively think that the more replicas considered the smaller the tunnelling time would be. However, we see that the smaller tunnelling time does not necessarily correspond to the highest number of temperatures, e.g., for $L = 20$ the optimal number of temperatures is $N_T = 20$ which results the lowest tunnelling time of 918 ± 2 sweeps. Additionally, cells in Table 6.1 with an asterisk (*) correspond to a temperature range [0.2 : 1.5] while the rest to [0.2 : 2.0], from where we see that the maximum and minimum temperatures can also affect the tunnelling times. For example the optimal tunnelling time for $L = 30$ corresponds to $N_T = 25$ and temperature range [0.2 : 1.5], i.e., 1509 ± 3 sweeps.

The other temperature schedule that we have considered is the inverse linear, see Sec. 3.3.1. Similarly to Fig. 6.3, the probability for replicas to be exchanged A as a function of temperature T for different number of temperatures N_T, and system sizes $L = 10 - 40$ for the inverse linear schedule is plotted in Fig. 6.4. Additionally, the tunnelling times are reported in Table 6.2. It is clear that the geometrical schedule *outperforms* the inverse linear one, in both the probabilities for replica swapping and tunnelling times. For the former as it is shown in Fig. 6.4, A decreases as the temperature increases and for the two largest system sizes the probability is very close to zero. This is also reflected in the tunnelling times, where for some system sizes and values of N_T there is no tunnelling event (N/A entries). Additionally, we see that for a fixed system size tunnelling events, if at all happening, correspond to considerably larger tunnelling times in comparison with the geometric progression schedule. Of course increasing the number of temperatures could lead to smaller tunnelling times, but this comes with an additional computing cost as one has to simulate more replicas. Thus, the geometric progression schedule is preferred, in order for the PT algorithm to perform optimally.

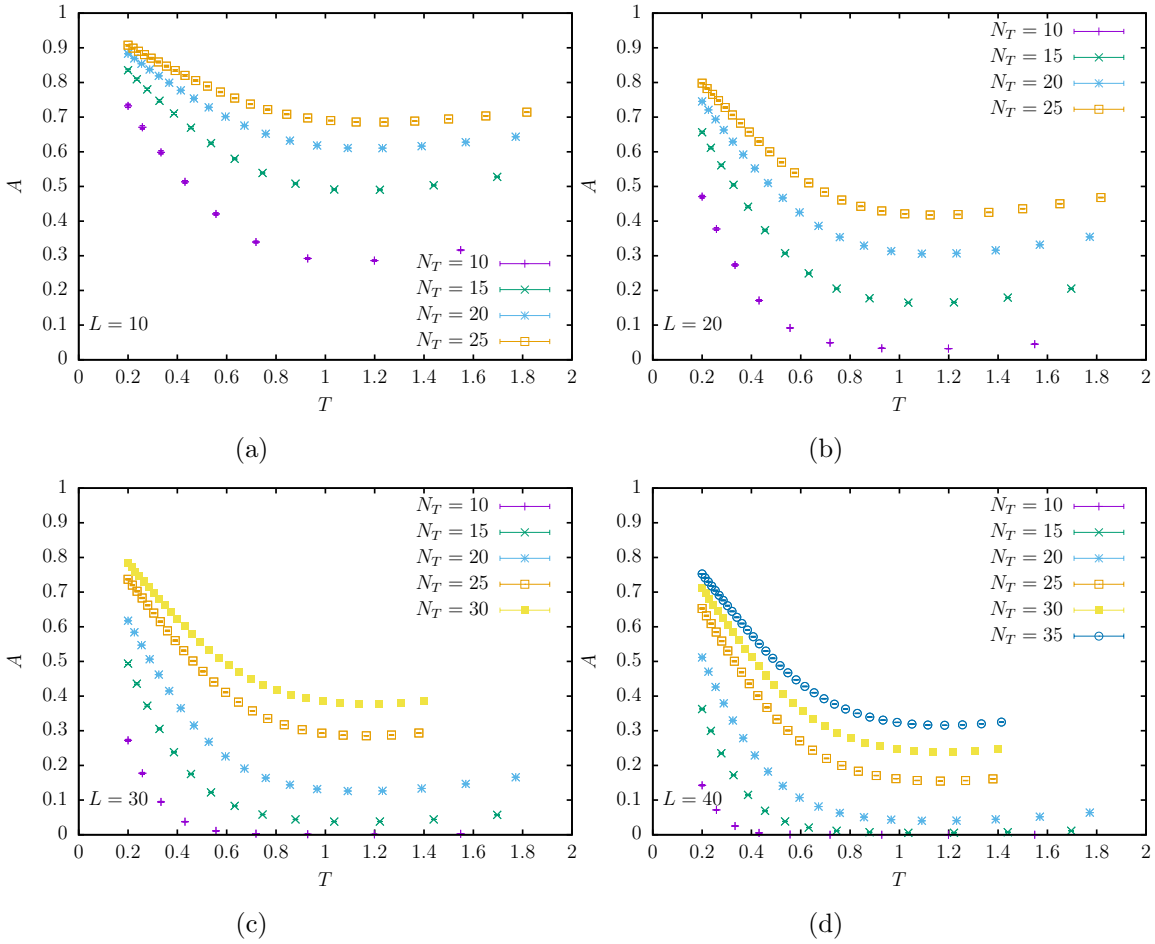

Figure 6.3: Acceptance probability of replica-swapping A as a function of temperature T, for different number of temperatures N_T, using the geometric progression schedule. Figs. (a), (b), (c), (d) correspond to systems of linear size $L = 10$, 20, 30, and 40 respectively.

Table 6.2: Tunnelling times for the different number of temperatures N_T and system sizes L considered, using the inverse linear schedule for the PT algorithm. The asterisk (*) corresponds to a temperature range [0.2 : 1.5], while the rest to [0.2 : 2.0]. Cells with N/A represent no tunnelling event.

L \ N_T	10	15	20	25
10	2580 ± 76	640 ± 7	499 ± 3	499 ± 2
20	N/A	299936 ± 11555	13386 ± 260	4106 ± 43
30	N/A	N/A	N/A	190467 ± 3948
40	N/A	N/A	N/A	N/A

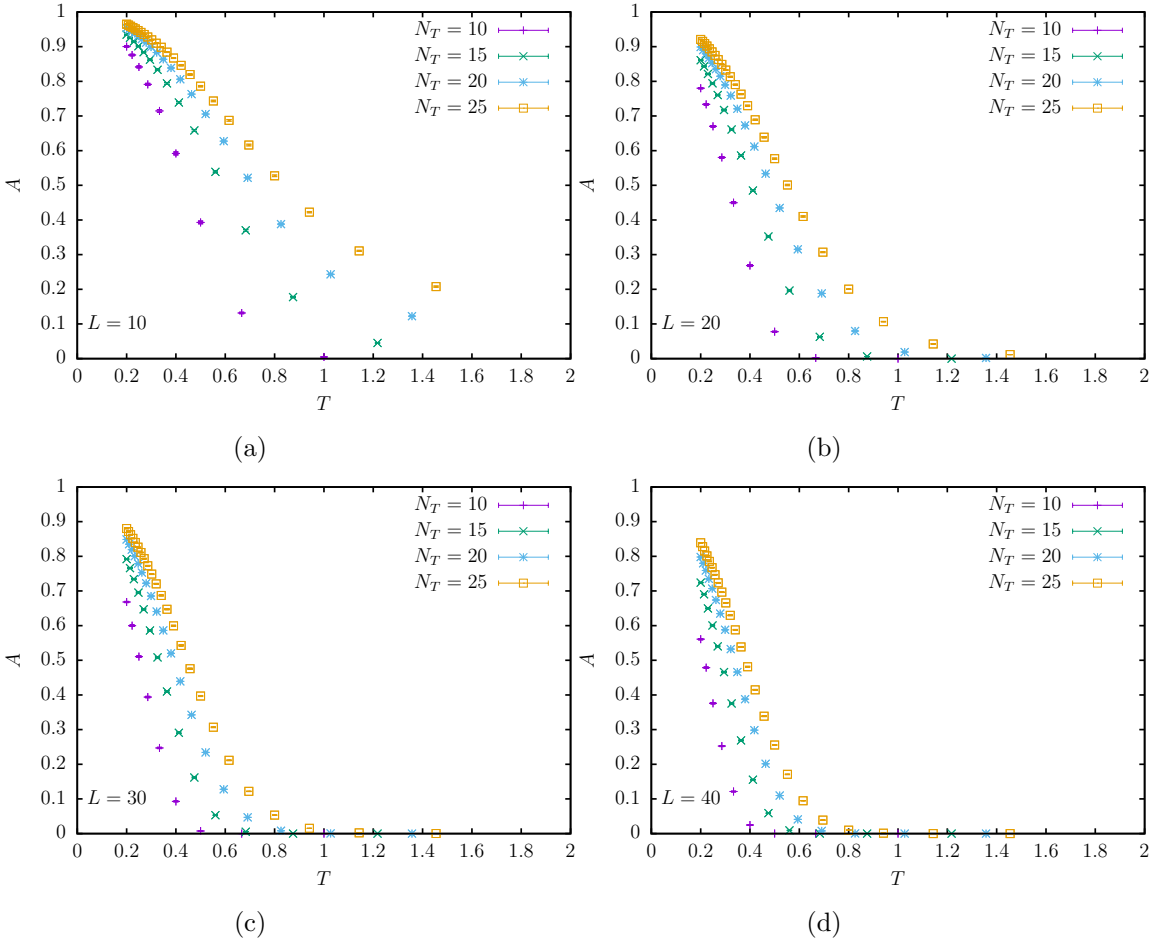

Figure 6.4: Acceptance probability of replica-swapping A as a function of temperature T, for different number of temperatures N_T, using the inverse linear schedule. Figs. (a), (b), (c), (d) correspond to systems of linear size $L = 10$, 20, 30, and 40 respectively.

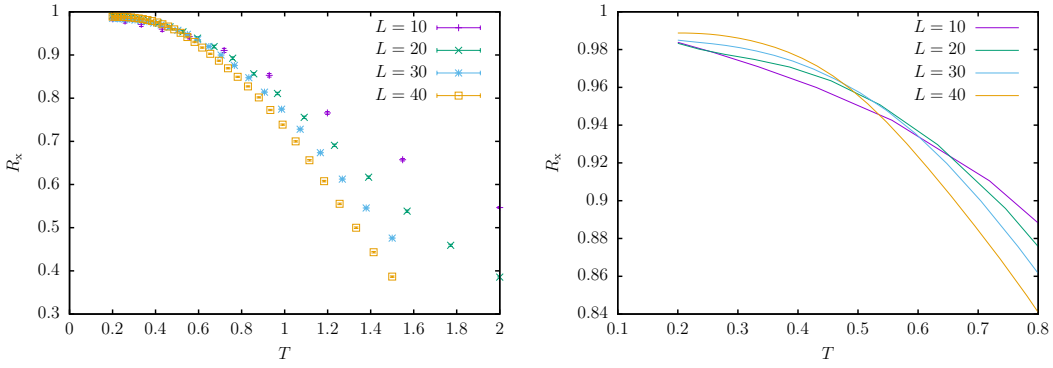

Figure 6.5: (a) Wrapping probability of clusters percolating in horizontal direction R_x as a function of temperature T for the different system sizes L, of the two-dimensional Ising spin-glass. (b) Enlarged region of (a).

6.2 Percolation Analysis

After determining the optimal temperature schedule and parameters for PT and ensuring equilibration of the system, we continue our discussion with the percolation properties for the clusters of the overlap as defined in Sec. 3.3.2. As already mentioned in Sec. 5.1, the overlap clusters for the spin-glass model are constructed in a similar way as the soft constraint clusters of the 2-replica Ising ferromagnet, with the essential difference that the interactions are now chosen at random. Our analysis here will not be as thorough as it was for the case of the ferromagnet (see Chap. 4 and 5) but we will rather restrict ourselves to a more qualitative description of the percolation properties of the cluster overlap. For the possible extension of the work presented in the Chaps. 4 and 5 to the spin-glass problem see the discussion in Chap. 7.

In Fig. 6.5(a) the wrapping probability of clusters percolating in the horizontal direction R_x is plotted as a function of temperature T for the different system sizes L considered. Curves should cross at the transition point, which for the two-dimensional Ising spin-glass is at $T_c = 0$. Nonetheless, from Fig. 6.5(b) the R_x curves appear to cross at finite temperatures, still the crossing point shifts to lower temperatures with increasing system size. This is an indication that there is no phase transition at finite temperature at the thermodynamic limit.

In Fig. 6.6 the average cluster size S is plotted as a function of temperature T for the different system sizes L considered. Since our analysis for the spin-glass problem at this point is more qualitative, as we discussed in the beginning of this section, we used only the definition where the largest cluster is excluded in each measurement, i.e., $C \setminus \max C$. With this definition, S has a maximum the location of which shifts towards the transition point as the size of the system increases. For the two-dimensional spin-glass the transition point is at $T = 0$ and it is clear even for this relatively small system sizes that the location of the maximum moves to zero as the system size increases.

Lastly, in Fig. 6.7 the percolation strength P_∞ is plotted as a function of temperature T for the different system sizes L considered. Here we see that as the temperature decreases the number of sites belonging to the largest cluster increases, indicating that the system

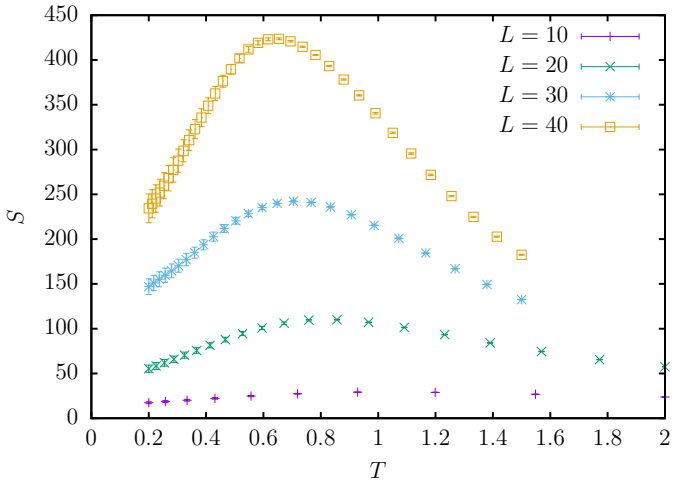

Figure 6.6: Average cluster size S as a function of temperature T for the different system sizes L, of the two-dimensional Ising spin-glass. The definition for S considered here is the exclusion of the largest cluster in each measurement, i.e., $C \setminus \max C$.

is approaching its critical point. Of course since $T_c = 0$ here, a percolating cluster in the thermodynamic limit will appear only at that temperature, for finite size systems though percolating clusters can occur even at non-zero temperatures.

6.3 Concluding Remarks

In this chapter the percolation properties of Houdayer's clusters for the two-dimensional Edwards-Anderson spin-glass model with Gaussian interactions were discussed. At first the issue of equilibration was presented, along with a comparison of different temperature schedules, which led to the determination of an optimal set of parameters for the PT algorithm. Subsequently, the percolation properties of the system were discussed.

Specifically, for the equilibration of the system we monitored the time series of the order parameter q^2 at a relatively low temperature $T = 0.2$, by utilising the logarithmic binning procedure. We observed that equilibration is achieved for $L = 10$ and 20 after $t > 10^4$ sweeps, while for $L = 30$ and 40 the system is in equilibrium after $t > 10^5$ sweeps. As we considered Gaussian interactions, we employed an alternative criterion for equilibration, as outlined in Ref. [193]. The latter method provided similar results to the one from the time series of q^2. For the PT algorithm the geometric progression and the inverse linear temperature schedules were compared. From the probabilities of replicas to be exchanged A and tunnelling times we concluded that geometric progression outperforms the inverse linear schedule, for all system sizes considered, cf. Tables 6.1 and 6.2. Additionally, for the geometric progression, we observed that for a given system of linear size L the minimum tunnelling time do not necessarily correspond to the maximum number of temperatures considered. This is to be expected, as PT works optimally if replicas perform an unbiased random walk in the temperature space.

Having obtained the optimal parameters for the PT algorithm, and assured equilibration we discussed the percolation properties of Houdayer's clusters, which are constructed in the

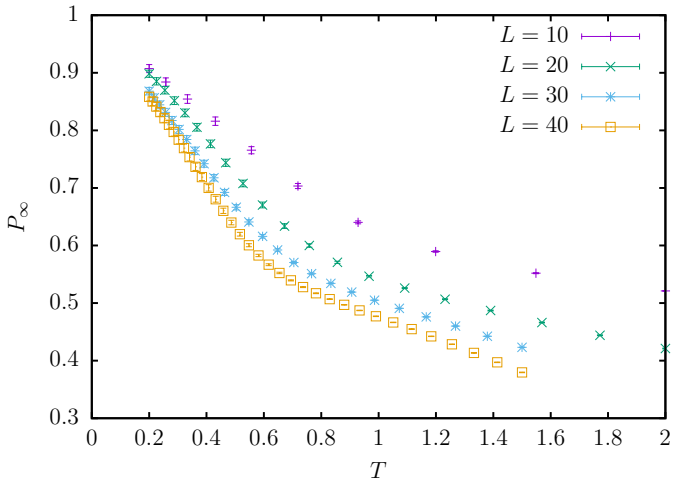

Figure 6.7: Percolation strength P_∞ as a function of temperature T for the different system sizes L, of the two-dimensional Ising spin-glass. The definition for P_∞ considered here is the inclusion of the largest cluster in each measurement, i.e., max C.

same way as the soft constraint clusters for the 2-replica Isng model, see Sec. 5.2. For that the average cluster size, percolation strength, and wrapping probability in the horizontal direction, for the different system sizes L as a function of temperature T, were presented. The crossings of the curves of different system sizes of the wrapping probability shifts to lower temperatures as the size of the system increases, indicating the absence of a spin-glass phase for any non-zero temperature. This is also supported from the location of the peaks for the average cluster size, which shifts to lower temperatures as the size of the system increases. The percolation strength increases as the temperature decrease, indicating that the size of the largest cluster is increasing. Of course, a spanning cluster should appear only at $T = 0$, when the thermodynamic limit in approached. Clearly, more concrete results would be welcome at this point and a detailed analysis of the percolation properties of such clusters is called for; some considerations in this direction are discussed in Chap. 7.

Chapter 7

Conclusions and Outlook

In this thesis, we studied the percolation properties of the geometrical clusters for the ferromagnetic and frustrated (spin-glass) multi-replica two-dimensional Ising model. For the ferromagnet we performed large scale Monte Carlo simulations, on relatively large system sizes up to $L_{\max} = 2048$. The critical behaviour in terms of critical temperature and the set of critical exponents characterizing the transition were obtained from FSS analysis. For the spin-glass system more qualitative arguments were given, based again on numerical simulations.

For the case of the 1-replica Ising model, the critical exponents of the average cluster size and percolation strength were obtained by utilising different cluster sets for the involved observables. For the percolation strength, the corresponding exponent β/ν does not strongly depend on the definition used, with estimates being in very good agreement with the analytical value [89], except for the max $P_{\mathrm{x\ and\ \bar{y}}}$ definition. The latter can be understood as clusters percolating in one but not the other direction are very rare, leading to poor statistics for the estimation of the involved exponent. On the other hand, the average cluster size strongly depends on the definition used. The definitions where all clusters are included and excluding clusters that percolate in one but not the other direction lead to estimates of the γ/ν exponent, which have small scaling corrections and are in good agreement with the analytical value [89]. If percolating clusters are excluded (except clusters percolating in one but not the other direction) or the largest cluster, however, strong scaling corrections are observed with deviations from the asymptotic value being considerably large even when fits are performed on the larger system sizes. This is of special importance as the exclusion of the largest cluster is one of the most commonly used definitions in the numerical studies of percolation [19]. Since the inclusion of different cluster sets could lead to estimations of exponents which suffer less from scaling corrections, an interesting exercise could be the inclusion of such cluster sets for the estimation of the critical exponents for the FK clusters. Consequently, as the critical exponents of the FK clusters coincide with those of the thermal phase transition for the q-state Potts model, estimates of the exponents using such cluster sets could lead to improvement of the already existing results, especially in three dimensions and for values of q other than two[1].

The multi-replica Ising model was then discussed, as a system of non-interacting copies

[1] Note that in the case of the three-dimensional Ising ($q = 2$) model critical exponents are known to very high accuracy from MC simulation [81] and the conformal bootstrap method [196–199]

(replicas) at the same temperature, for the two-dimensional case. The inclusion of replicas introduces a k-plane, on which we defined and studied two clusters types, namely the soft and hard constraint clusters. As far as percolation is concerned, the study of such clusters in the k-plane defines a correlated percolation process, the properties of which are beyond from trivial. On the other hand, and specifically the soft constraint clusters are the same as the ones of Houdayer's clusters [48] defined for the spin-glass problem. In order to investigate the critical behaviour of the model we employed different wrapping probabilities and sets of clusters in the definitions of the average cluster size and percolation strength that were introduced in Chap. 4. Additionally, in order to obtain more accurate estimates of the involved parameters, the single histogram reweighting technique was employed.

For the case of the 2-replica Ising model, our results suggest that the soft and hard constraint clusters percolate at the transition temperature of the 1-replica Ising model. However, the possibility that simulations on larger system sizes could show that the asymptotic value of the critical temperature is different from that of the 1-replica Ising model cannot be excluded. In the lack of correspondence between percolation quantities of the geometrical clusters and that of the physical system, the estimation of the ν exponent for the geometrical clusters cannot be obtained by using the, somewhat, standard procedures in the study of phase transitions, i.e., the maximum of derivatives of the Binder cumulant or the maximum of derivatives of logarithms of powers of the magnetisation [74]. Consequently, for the estimation of the involved exponent the wrapping probabilities were utilised, as their maximum of the absolute value of the derivative with respect to temperature scale as $\sim L^{1/\nu}$. The exponent was found to be the same for the soft and hard constraint clusters, and equal to that of the 1-replica Ising model, i.e., $\nu^{(\mathrm{s})} = \nu^{(\mathrm{h})} = 1$. For the critical exponents β/ν and γ/ν, concerning the percolation strength and average cluster size, respectively, simulations performed at the critical temperature of the soft and hard constraint clusters, i.e., the transition temperature of the 1-replica Ising model. For the percolation strength, the estimated exponents for the soft and hard constraint clusters respectively, are different from that of the 1-replica case, as well as from each other. Similarly to the 1-replica case, estimates from the different definitions agree with each other and corrections to scaling are not substantial. However, the definition where the largest clusters that percolate in one but not the other direction is considered results to unreliable estimates of the exponent, for the same reason as in the 1-replica case described above. On the other hand, the average cluster size strongly depends on the definition used, with the inclusion of all clusters and the exclusion of clusters that percolate in one but not the other direction exhibiting smaller corrections to scaling, in comparison with the rest of the definitions. For obtaining more accurate estimates of the involved exponent we performed joint fits, including a correction term, and using all the definitions considered, for the soft and the hard constraint clusters, respectively. The estimates of γ/ν from the joint fits were in agreement with the ones obtained from the individual fits using the C and $C \setminus P_{\mathrm{x\ and\ \overline{y}}}$, for the soft and hard constraint clusters, respectively. Additionally, the critical exponents for the two cluster types are different from the respective exponent of the 1-replica model, as well as from each other. The correction-to-scaling exponent was found to be relatively small for both cluster types; a fact that justifies the strong scaling corrections that we observed in the esimation of γ/ν, when certain types of percolating clusters were excluded in the definition of the average cluster size. Finally, utilising the scaling relations we obtained the fractal dimension for the two cluster types. The soft constraint clusters have a larger fractal dimension from the hard constraint ones, meaning that they are more dense. This is in agreement also with

the configurational snapshots of Fig. 5.2, as well as with the fact that the hard constraint clusters are a subset of the soft constraint ones. The set of critical exponents concerning the 2-replica ising model, are reported in Table 5.1.

For the 3-replica Ising model the obtained results are not as thorough as the ones obtained for the 2-replica Ising model, nonetheless some "*crude*" conclusions on the basis of the current analysis can be obtained. For the critical exponent ν results obtained from fits including a logarithmic correction term, seem to be consistent with a value $\nu^{(\mathrm{s})} \approx 1$ for the soft constraint clusters and $\nu^{(\mathrm{h})} \approx 1.5$ for the hard constraint clusters. However, we are not able to provide any plausible explanation of why such type of corrections should apply here, as these are usually present for systems at their upper critical dimension. We also highlight that fits including a logarithmic-correction term were utilised, only after attempting fits that include a correction exponent which, however, did not provide any reasonable estimate for the involved exponent. For the critical temperature, results for the soft constraint clusters are vague. On one hand, the estimates of the critical point resulting from the fits agree with a temperature similar to that of the 1-replica Ising model. The crossings, on the other hand, of $R^{(\mathrm{s})}_{\mathrm{x\ or\ y}}$ suggest that the critical temperature lies on the interval $[2.2685 - 2.269]$, which can also be supported from the fitting results. Consequently, we conclude that the critical temperature could be the same as that of the 1-replica Ising model, or if not, quite close to it. For the hard constraint clusters results suggest that the critical temperature is below that of the 1-replica Ising model, which also agrees with the location of the crossings of $R^{(\mathrm{s})}_{\mathrm{x\ or\ y}}$ for the hard constraint clusters. Additionally, the accumulated exponent ϵ of Eq. (5.12) is consistent for both clusters types with a value around 1. For the hard constraint clusters, this implies a negative correction exponent, provided that $\nu^{(\mathrm{h})} \approx 1.5$, which obviously is wrong. For the soft constraint clusters, if $\nu^{(\mathrm{s})} \approx 1$, we can conclude that the correction exponent is sufficiently small and cannot be obtained given the accuracy of our data; of course such statement needs further investigation. For the critical exponents concerning the percolation strength and average cluster size, in the lack of precise estimates of the critical temperature, we utilised the sequences of pseudo-critical points of the crossings of $R_{\mathrm{x\ or\ y}}$, for the soft and hard constraint clusters, respectively. Depending on the definition used, estimates approach different values, and thus any conclusion regarding the values of the involved exponents is inadequate. A possible explanation, for such unsatisfactory results is the presence of strong corrections to scaling which, as discussed in the last part of Sec. 5.3.3, can be deduced from the presence of an effective length scale L^* in the vicinity of which the scaling behaviour changes substantially. Thus, if L^* is relatively large, say $L^* \gtrsim 500$, this can explain the presence of such strong scaling corrections. Unfortunately, given the time restrictions for the thesis to be delivered, we were not able to perform such calculations. Still we are currently working in this direction.

For the 4-replica Ising model we presented some preliminary results, concerning the general behaviour of the wrapping probabilities, average clusters size, and percolation strength. Of some importance is the qualitative observation that the positions of the crossings of the wrapping probabilities of the soft and hard constraint clusters are at temperatures below the ones obtained for the 3-replica Ising model, and consequently from that of the 2- and 1-replica Ising model, respectively.

A continuation of the work presented in this thesis concerning the percolation properties of the ferromagnetic multi-replica Ising model is the determination of the critical exponents

for the 3-replica Ising model. For that we need to first understand, though, the existence and role of the possible strong scaling corrections which affect the determination of the exponents; we have already proposed a strategy to identify that, which we are currently working on. Subsequently, the critical behaviour of the 4-replica Ising model needs to be determined in terms of the critical temperature and critical exponents of the soft and hard constraint clusters, respectively. Having such information we can shed light in questions like: How the critical temperature and critical exponents depend on the number of replicas? Does a relation connecting the critical exponents with the number of replicas exist? What can we expect if we take the number of replicas to infinity? Finally, a possible outlook of this work is to study the Fortuin Kasteleyn clusters in the multi-replica framework. This is an interesting research path as the FK clusters have the same set of exponents with those of the thermal system and thus it would be beneficial to study how the inclusion of replicas will affect (or not) the critical behaviour of the system.

Based on a more qualitative analysis, some aspects regarding the percolation properties of Houdayer's clusters were presented, for the two-dimensional Edwards-Anderson spin-glass using Gaussian random interactions. Since spin glasses are hard to equilibrate at low temperatures we first presented evidence, based on the time series of the order parameter, that all system sizes considered have reached their stationary distribution. As interactions were Gaussian, we also cross-checked equilibration by using the method outlined in Ref. [193], with results found to be in agreement with the former method. For our simulations, we utilised the PT algorithm for which a comparison between two temperature schedules, namely the geometric progression and the inverse linear, was performed. The comparison was based on the probability of replicas to be exchanged and the tunnelling time, and showed that geometric progression outperforms the inverse linear schedule for all system sizes considered. Having ensured equilibration and defined the optimal set of parameters for the PT algorithm, we proceeded with the study of the percolation properties of the system. In particular, we considered the average cluster size, percolation strength, and wrapping probability in the horizontal direction as a function of temperature. The shift of the crossings of the wrapping probability and of the peak of the average cluster size to lower temperatures as the system size increases, supports, at least qualitatively, a zero critical temperature for the two-dimensional spin glass; this is also supported from other studies on more firm grounds, see, e.g., Ref. [47] and references therein.

Throughout this thesis, the importance of graphical representation as a method which enhances our understanding in the study of phase transitions was revealed. From that perspective, an analysis similar to the multi-replica Ising model for the percolation properties of Houdayer's clusters, sounds very promising towards the way of deepen our understanding for the spin-glass problem. Additionally, such analysis can also be applied to other graphical representation approaches for the spin-glass problem, such as the one proposed from Machta, et al. [40]; for the latter a study already exists [53].

Appendix A

Statistical Analysis of Monte Carlo Data

A.1 Autocorrelation Time

From the discussion in Chap. 3, it is obvious that in a Markov process the generated states of the chain will be *statistically dependent*, as the next state depends on the preceding one. In order to quantify the degree of correlations between two states at time steps t and t', for an observable O, we define the *unnormalized autocorrelation function* as

$$C_O\left(t', t\right) = \left\langle O(t')O(t)\right\rangle - \left\langle O(t')\right\rangle \left\langle O(t)\right\rangle, \tag{A.1}$$

where $O(t)$ is the value of the obervable O at time step t, with $t' < t$. Assuming that the process is stationary then, $\langle O\left(t'\right) O(t)\rangle = \langle O(0)O(t-t')\rangle$, and thus we can write $C_O\left(t', t\right) = C_O\left(0, t'-t\right) \equiv C_O(t)$. Note that $C_O(0)$ is equivalent to the variance $\sigma^2(O)$ of O. Typically $C_O(t)$ decays exponentially for large t [200]

$$C_O(t) \sim e^{-t/\tau_{\text{exp},\,O}}, \tag{A.2}$$

where $\tau_{\text{exp},\,O}$ defines the *exponential autocorrelation time*, which depends on the specific observable O and on the dynamics of the process. In general, a MC process is characterized by a number of different correlation times. The exponential autocorrelation time for the particular observable O, is then defined as the largest of the correlation times, i.e.,

$$\tau_{\text{exp},\,O} = \lim_{t\to\infty} \sup \frac{t}{-\ln \rho_O(t)}, \tag{A.3}$$

where $\rho_O(t) \equiv C_O(t)/C_O(0)$ is the *normalized autocorrelation function*.

Now if the observable O is appearing according to a probability distribution $P(O)$, then its *expectation value* is given as

$$\langle O\rangle = \int dO P(O) O. \tag{A.4}$$

In a MC process one generates a time series of states $\{O(1), O(2), \ldots, O(N)\}$ according to $P(O)$. An unbiased estimator of $\langle O\rangle$ is then given by the time average (mean) $\overline{O}$ as

$$\overline{O} = \frac{1}{N}\sum_{t=1}^{N} O(t), \tag{A.5}$$

where N is the length of the time series. Note that the estimator $\overline{O}$ is a random number fluctuating around the expectation value, and coincides with $\langle O \rangle$ only in the limit $N \to \infty$. Attention should be paid to the fact that although the distribution of the individual measurements $P(O)$ can be chosen arbitrarily[1], the distribution of the average $\overline{O}$ must be Gaussian, at least for uncorrelated data and in the limit of $N \to \infty$, according to the central limit theorem [201]. This means that the variance of $\overline{O}$, i.e., $\sigma^2\left(\overline{O}\right) \equiv \langle \overline{O}^2 \rangle - \langle \overline{O} \rangle^2$, is sufficient to describe the fluctuations of $\overline{O}$. It is easy to check that for uncorrelated data

$$\sigma^2\left(\overline{O}\right) = \frac{C_O(0)}{N} = \frac{\sigma^2(O)}{N}, \tag{A.6}$$

which means that the variance of the mean reduces with the number of measurements.

If the data are correlated, then the variance is given as follows [201]

$$\sigma^2\left(\overline{O}\right) = \frac{2\sigma^2(O)}{N}\left[\frac{1}{2} + \sum_{t=1}^{N}\left(1 - \frac{t}{N}\right)\rho_O(t)\right]. \tag{A.7}$$

Note that for the case of uncorrelated data $\rho_O(t) = 0$ and from Eq. (A.7) one recovers Eq. (A.6). If the decay of the correlation function is exponential, then for any meaningful MC process where $N \gg \tau_{\text{exp},\,O}$, the factor $(1 - t/N)$ will not contribute much to the summation and it can be neglected [201, 202]. Then one can define the *integrated autocorrelation time* as

$$\tau_{\text{int},\,O} \equiv \frac{1}{2} + \sum_{t=1}^{N} \rho_O(t). \tag{A.8}$$

By adopting Eq. (A.8) into Eq. (A.7) one gets

$$\sigma^2\left(\overline{O}\right) = \frac{\sigma^2(O)}{N/2\tau_{\text{int},\,O}}. \tag{A.9}$$

This means that similarly to uncorrelated data, the variance of the mean reduces with the number of measurements, but compared to Eq. (A.6) the number of uncorrelated measurements have now been reduced by a factor of $2\tau_{\text{int},\,O}$.

In general $\tau_{\text{int},\,O}$ is different from $\tau_{\text{exp},\,O}$, and one can show that $\tau_{\text{int},\,O} \leq \tau_{\text{exp},\,O}$ [203]. Only when the the decay is purely exponential (one correlation time), then $\tau_{\text{int},\,O}$ and $\tau_{\text{exp},\,O}$ are, apart from minor corrections, equal [201, 204].

A.2 The Binning and Jackknife Methods

A.2.1 The Binning method

As $\overline{O}$ is a random number fluctuating around the expectation value $\langle O \rangle$, the complete answer is provided only if the variance of $\overline{O}$, i.e., $\sigma^2\left(\overline{O}\right)$ is calculated. For uncorrelated data this

[1] In our case it is the Boltzmann distribution.

is a straightforward task, as for a time series with N entries an estimator of $\sigma^2\left(\overline{O}\right)$ [see. Eq. (A.6)] is

$$\hat{\sigma}^2\left(\overline{O}\right) = \frac{1}{N(N-1)}\sum_{t=1}^{N}\left[O(t)-\overline{O}\right]^2, \tag{A.10}$$

which is an unbiased estimator, i.e., $\left\langle\hat{\sigma}^2\left(\overline{O}\right)\right\rangle = \sigma^2\left(\overline{O}\right)$, see e.g. Refs. [148, 190, 205]. For correlated data the situation is more involved, as according to Eq. (A.9) an estimation for the variance of the mean requires the estimate of the integrated autocorrelation time $\tau_{\mathrm{int},\,O}$, which in general is not a simple task and computationally expensive, see Appendix A.3. However, an estimate of the variance of $\overline{O}$ could be accomplished by employing the *binning method*, which is simple to implement and computational less demanding.

For the binning method we group the N entries of an initial time series $\{O(1), O(2), \ldots, O(N)\}$, in blocks of length $l = N/n$, where n is the number of blocks and for simplicity we assume that N is an integer multiple of n. Then at each block i we define the *block average* as

$$O^{\mathrm{b}}(i) = \frac{1}{l}\sum_{t=1}^{l} O[(i-1)l+t], \tag{A.11}$$

with $i = 1, 2, \ldots, n$. Which results in a new time series of smaller length n, $\left\{O^{\mathrm{b}}(1), O^{\mathrm{b}}(2), \ldots, O^{\mathrm{b}}(n)\right\}$. The mean $\overline{O}$ and its variance $\sigma^2\left(\overline{O}\right)$ will not change under this transformation. However, if the autocorrelation function of the initial series decays exponentially, see Eq. (A.2), it can be shown [206] that the variance of the individual measurements of the blocked time series $\sigma^2(O^{\mathrm{b}})$ is reduced, leading to a less correlated time series compared to the initial one. Additionally, as the length of the block increases correlations of the blocked time series should reduce, and for the limiting case of $l \to \infty$ the produced time series will be uncorrelated[2]. In that limit, we can use the estimator of Eq. (A.10) for uncorrelated data, to compute $\sigma^2\left(\overline{O}\right)$.

In the case of finite time series, one can utilise the blocking method by assuring that the length of the block is $l \gg \tau$ and $l \ll N$, where τ is the exponential of the integrated autocorrelation time, see Appendix A.1. This can be achieved by estimating the variance of the mean $\sigma^2\left(\overline{O}\right)$ using the estimator of Eq. (A.10) as a function of l. As the size of the blocks increases, $\hat{\sigma}^2\left(\overline{O}\right)$ approaches the asymptotic value $\sigma^2\left(\overline{O}\right)$ and eventually from a value l and above it reaches a plateau value where deviations from the asymptotic value are negligible compared to statistical fluctuations (an illustration of that can be found in Fig. 2 of Ref. [205]). In practice, as a rule of thumb, for a reliable estimation of statistical errors the length of the time series should be $N \gtrsim 10^4 \times \tau$, then the blocking method can be utilised by considering a number of blocks of the order of hundred, say $100 - 500$ blocks [205].

A.2.2 The Jackknife method

Let us introduce a time series of length N for an observable O, whose data are uncorrelated. This can be obtained directly from a MC process, or could be the result of the binning method described above (see Appendix A.2.1), where in the latter case N is the number of blocks

[2] Obviously, for the limiting case where blocks have infinite length we need an initial time series of infinite length ($N \to \infty$). Additionally, we need always to ensure that the number of blocks is relatively large.

used for the binning transformation. Since data are uncorrelated, estimates of $\langle O \rangle$ and $\sigma^2\left(\overline{O}\right)$ can be computed directly via Eqs. (A.5) and (A.10) respectively. For the case of quantities which are expressed as functions of the expectation value $F\left(\langle O \rangle\right)$, an estimate is provided by replacing the expectation value with the mean, i.e., $\hat{F}\left(\overline{O}\right) \equiv \hat{F}$. As for the variance of $\hat{F}$, $\sigma^2(\hat{F})$, the traditional approach is via error propagation formulas, which are based on Taylor expansions [207]. This is quite problematic as such expansions are usually of first order leading to truncation errors, and ignores cross-correlations between the observables[3]. Furthermore, error propagation assumes an analytic expression of the function F which is not always available, for example when finding the maximum of the specific heat as a function of temperature using histogram reweighting of the energy time series. In order to overcome such problems resampling methods have been utilised, which calculate variances in an automatic way, without the need of partial derivatives and keeping track of variances and covariances of the observables involved as in the error propagation method. Here we discuss one of such resampling schemes, namely the jackknife method; for that and other resampling schemes see Refs. [190, 208, 209].

Before discussing how the jackknife can be used to estimate the variance of quantities such as $F\left(\langle O \rangle\right)$, let us consider the *bias* of the estimator $\hat{F}$, i.e., how far on average the estimator is from the expectation value, $F\left(\langle O \rangle\right) - \langle \hat{F} \rangle$. For most commonly considered MC processes we can write that [190]

$$F\left(\langle O \rangle\right) = \langle \hat{F} \rangle + \frac{A_1}{N} + \frac{A_2}{N^2} + \dots, \tag{A.12}$$

meaning that the bias is of order $1/N$. If F depends linearly on $\langle O \rangle$, i.e., $F\left(\langle O \rangle\right) = \langle O \rangle$ it can be estimated from $\hat{F}\left(\overline{O}\right) = \overline{O}$ without bias. For non-linear functions F, however, bias is present (such as in the case of response functions, i.e., specific heat and magnetic susceptibility), and it reduces as the number of measurements N increases. We now remove one entry from the initial time series O, and denote the estimator of the expectation value $F\left(\langle O \rangle\right)$ as $\hat{F}\left(\overline{O'}\right) \equiv \hat{F}_{N-1}$. Note that $F\left(\langle O \rangle\right)$ does not change since it does not depend on the specific realization of the time series, whereas $\overline{O'}$ is a different mean value since we have excluded one measurement from the time series. Thus, we can rewrite Eq. (A.12) as

$$F\left(\langle O \rangle\right) = \langle \hat{F}_{N-1} \rangle + \frac{A_1}{N-1} + \frac{A_2}{(N-1)^2} + \dots, \tag{A.13}$$

where A_1, A_2 will not change, since the N and the $N-1$ entries are sampled from the same probability distribution [190]. Expressing now $F\left(\langle O \rangle\right)$ as

$$F\left(\langle O \rangle\right) = N\langle \hat{F} \rangle - (N-1)\langle \hat{F}_{N-1} \rangle, \tag{A.14}$$

the bias at first order eliminates. Thus, by constructing an estimator for the expectation value $\langle \hat{F}_{N-1} \rangle$, a reduced bias estimator for $F\left(\langle O \rangle\right)$ can be obtained. The jackknife method constructs such an estimator, by considering N time series of length $N-1$ each, where in each one of them a single entry, different each time, is omitted. Under this construction, the *jackknife block averages* are given as

[3] For simplicity we restrict F here to be a function of a single observable O, though in general it can depend on more than one, i.e., $F\left(\langle O_1 \rangle, \langle O_2 \rangle, \langle O_3 \rangle \dots\right)$. In the case of several observables if their respective time series have been generated from the same simulation, cross-correlation between them appear which enter as elements of the covariance matrix in the Taylor expansion [190, 207].

$$\overline{O}_{J,i} = \frac{1}{N-1} \sum_{\substack{t=1 \\ t \neq i}}^{N} O(t), \tag{A.15}$$

and the mean of the expectation value $\langle \hat{F}_{N-1} \rangle$ as

$$\hat{F}_{N-1} \equiv \hat{F}_J = \frac{1}{N} \sum_{i=1}^{N} F(\overline{O}_{J,i}). \tag{A.16}$$

According to Eq. (A.14), the jackknife reduced-bias estimator of $F\left(\langle O \rangle\right)$ can be written as

$$\hat{F}_{\mathrm{RB}} = N\hat{F} - (N-1)\hat{F}_J. \tag{A.17}$$

From Eqs. (A.12) and (A.13) it is easy to see that the the estimator $\hat{F}_{\mathrm{RB}}$ has a bias of leading order $1/N^2$ instead of $1/N$. Additionally, for the case where F depends linearly on $\langle O \rangle$, i.e. $F\left(\langle O \rangle\right) = \langle O \rangle$, it is easy to check that $\hat{F}_J = \hat{F}$, and consequently the estimator $\hat{F}_{\mathrm{RB}}$ has no bias.

In the jackknife scheme, $\sigma^2(\hat{F})$, i.e., the variance of the estimator $\hat{F}$, can be obtained via the following estimator [190, 208, 209]

$$\hat{\sigma}^2(\hat{F}) = \frac{N-1}{N} \sum_{i=1}^{N} \left[F(\overline{O}_{J,i}) - \hat{F}_J \right]^2. \tag{A.18}$$

This is similar to the estimator of the variance of the mean $\overline{O}$ for uncorrelated data in Eq. (A.10), with the difference that the $N-1$ factor appears in the denominator. If we were to interpret the different $F(\overline{O}_{J,i})$ estimates, as results from N performed simulations, then Eq. (A.10) could be utilised. Nonetheless, ignoring the fact that such estimates are highly correlated, since they differ by a single measurement, would result in an underestimation of the variance. Although, it has been shown [190, 208, 209] that such an underestimation of the variance can be quantified to a factor of $1/(N-1)^2$, from where we obtain the correct expression of the variance if we multiply the right-hand side of Eq. (A.10) with $(N-1)^2$.

As we stated in the beginning of this section, the jackknife method was performed in an uncorrelated time series, which could potentially be the result of the binning method applied to a time series of correlated data. This would require the additional effort to create an uncorrelated time series first and then perform the jackknife analysis. However, one can avoid the creation of the uncorrelated time series, and proceed with the jackknife analysis (almost) directly, see Ref. [205]. In that case the time series is divided into bins of length $l = N/n$, similarly defined as in Appendix A.2.1. Then, jackknife time series are constructed by excluding a single bin each time, resulting to n different time series of $N-l$ length each. Under this construction the jackknife block averages of Eq. (A.15) becomes

$$\overline{O}_{J,i} = \frac{1}{N-l} \sum_{\substack{t=1 \\ t \neq \{B_i\}}}^{N} O(t), \tag{A.19}$$

where $\{B_i\} = \{(i-1)l+1, \ldots, il\}$ is the i-th excluded bin. It is easy to check that the jackknife block averages of Eq. (A.19) applied to the correlated time series of length N are equal to those of Eq. (A.15), if one were to apply the binning transformation to the correlated time series, resulting in a new time series of length n. Correspondingly, the mean of the expectation value $\langle \hat{F}_{N-1} \rangle$ of Eq. (A.16) becomes

$$\hat{F}_{N-1} \equiv \hat{F}_J = \frac{1}{n} \sum_{i=1}^{n} F(\overline{O}_{J,i}). \tag{A.20}$$

and the estimator of the variance of $\hat{F}$ of Eq. (A.18) becomes

$$\hat{\sigma}^2(\hat{F}) = \frac{n-1}{n} \sum_{i=1}^{n} \left[F(\overline{O}_{J,i}) - \hat{F}_J \right]^2. \tag{A.21}$$

A.3 Numerical Estimation of Autocorrelation Times

An estimator of the autocorrelation function, see Eq. (A.1), of a time series of length N for an observable O is given by [206]

$$\hat{C}_O(t) = \frac{1}{N-t} \sum_{t'=1}^{N-t} \left[O(t') - \overline{O} \right] \left[O(t'+t) - \overline{O} \right], \tag{A.22}$$

where $\overline{O}$ is given by Eq. (A.5). The estimator in Eq. (A.22) is biased, and it can be shown [206, 210] that its bias, to leading order, is $-\sigma^2(O)\tau_{\text{int},\,O}/2N$. On the other hand, if $N \gg \tau_{\text{int},\,O}$, which is the necessary condition for a meaningful time series, this bias can be ignored. If we assume that the autocorrelation function has an exponential behaviour, then the exponential autocorrelation time $\tau_{\text{exp},\,O}$ can be estimated by performing non-linear fits of the form

$$\hat{C}_O(t) = a e^{-t/\tau_{\text{exp},\,O}}, \tag{A.23}$$

where a is a fitting parameter. For finite time series the behaviour can be reasonably described by the above exponential law only for a certain time range. As the time separation increases the variance of the estimator $\hat{C}_O(t)$ diverges rapidly, and the statistical noise becomes apparent up to the point that Eq. (A.23) is no longer valid.

Focusing now on the static properties of the system, the integrated autocorrelation time $\tau_{\text{int},\,O}$ is of more interest. An estimator of Eq. (A.8) can be given as

$$\hat{\tau}_{\text{int},\,O} = \frac{1}{2} + \sum_{t=1}^{N} \hat{\rho}_O(t), \tag{A.24}$$

where $\hat{\rho}_O(t)$ is the estimator of the normalized autocorrelation function, see Appendix A.1, which is given as

$$\hat{\rho}_O(t) = \frac{\hat{C}_O(t)}{\hat{C}_O(0)}. \tag{A.25}$$

The estimator in Eq. (A.25) behaves quite badly as the time separation increases, for the same reason as described above for $\hat{C}_O(t)$, resulting in a rather unreliable estimate for $\tau_{\text{int},\,O}$. As a compromise, Eq. (A.24) is estimated by introducing a cut-off $k < N$ in t, i.e.,

$$\hat{\tau}_{\text{int},\,O}(k) = \frac{1}{2} + \sum_{t=1}^{k} \hat{\rho}_O(t). \tag{A.26}$$

The introduced cut-off k will increase the systematic errors in the estimation of $\hat{\tau}_{\text{int},\,O}$, while the increase of k reduces it but increases the statistical error. Thus, as a compromise between systematic and statistical errors one proceeds by choosing the cut-off in a self-consistent manner, namely once $k \geq 6\,\hat{\tau}_{\text{int},\,O}(k)$ [148]. The variance of $\hat{\tau}_{\text{int},\,O}(k)$ can be approximately found, for $\tau_{\text{int},\,O} \ll k \ll N$, to be [200, 204, 211]

$$\sigma^2\left[\hat{\tau}_{\text{int},\,O}(k)\right] \approx \frac{2\,(2k+1)}{N}\tau^2_{\text{int},\,O}(k), \tag{A.27}$$

where "$\approx$" stands for "approximately equal to".

An alternative estimate of $\tau_{\text{int},\,O}$ can be obtained by using Eq. (A.9) as

$$\tau_{\text{int},\,O} = \frac{1}{2}\frac{\sigma^2(\overline{O})}{\sigma^2(O)/N}. \tag{A.28}$$

Then an estimator of $\tau_{\text{int},\,O}$, can be obtained from the estimators of $\sigma^2(\overline{O})$ and $\sigma^2(O)/N$ respectively. Such estimates can be found from the jackknife method for the case of correlated measurements, where we create n jackknife blocks of length $l = N - N/n$ each, where N is the length of the initial time series, see Appendix A.2.2. Then one proceeds by utilising the jackknife estimator of Eq. (A.21), which for the case of the variance of $\overline{O}$ is simply

$$\hat{\sigma}^2(\overline{O}) = \frac{n-1}{n}\sum_{i=1}^{n}\left[\overline{O}_{J,i} - \overline{O}_J\right]^2, \tag{A.29}$$

where $\overline{O}_{J,i}$ is given from Eq. (A.19) and $\overline{O}_J$ from Eq. (A.20) which becomes

$$\hat{F}_J = \overline{O}_J = \frac{1}{n}\sum_{i=1}^{n}\overline{O}_{J,i}. \tag{A.30}$$

The $\sigma^2(O)/N$ term could be understood as the variance of the mean $\sigma^2(\overline{O})$ for uncorrelated data, and an estimator can be provided by replacing n with N at Eqs. (A.29) and (A.30) above. The value of n should be chosen such that the jackknife blocks are statistically independent. To ensure this, one can plot $\hat{\sigma}^2(\overline{O})$ of Eq. (A.29), as a function of n and choose a value of n when a plateau is reached, cf. Appendix A.2.1. Finally, an estimate of the variance of $\hat{\tau}_{\text{int},\,O}$, could be given by repeating the jackknife procedure to second order, i.e., on each jackknife time series a second jackknife transformation is performed leading to $n-1$ new jackknife time series of length $N - 2l$ each, see Ref. [212] for the implementation details.

A.4 Histogram Reweighting

Performing a MC simulation at a specific temperature T_0, or inverse temperature β_0, we obtain information about thermal averages of observables explicitly at that temperature.

However, additional information for temperatures other than β_0 (in principle for any other temperature β) can be obtained implicitly by *reweighting* the data from temperature β_0[4]. This idea was developed by Ferrenberg and Swendsen [213, 214] (see also Refs. [57, 148]), which turned out to be a powerful tool, when combined with other MC schemes, in the study of phase transitions.

Let us re-express the partition function of the system at temperature β_0 as a sum over the different energies that the system possesses, instead of a sum over the different states of the system, i.e.,

$$Z(\beta_0) = \sum_{\{\sigma_i\}} e^{-\beta_0 \mathcal{H}(\{\sigma_i\})} = \sum_E \Omega(E) e^{-\beta_0 E}, \tag{A.31}$$

where E is the energy of the system, and $\Omega(E)$ is the number of states that have energy E. The term $\Omega(E)e^{-\beta_0 E}$ in Eq. (A.31) can be identified, apart from a normalization constant, as the energy histogram at temperature β_0, i.e., $P_{\beta_0}(E) \sim \Omega(E)e^{-\beta_0 E}$. For the energy histogram to be normalized $P_{\beta_0}(E)$ should be divided by $Z(\beta_0)$, but this is unimportant in what follows. Note that knowledge of $P_{\beta_0}(E)$ allows a direct evaluation of the observables. At a temperature β different from β_0 the energy histogram can be expressed as

$$P_\beta(E) \sim \Omega(E)e^{-\beta E} = \Omega(E)e^{-\beta_0 E}e^{-(\beta-\beta_0)E} \sim P_{\beta_0}(E)e^{-(\beta-\beta_0)E}. \tag{A.32}$$

Thus, from the energy histogram at β_0 we can estimate the energy histogram at β by *reweighting* the former histogram with a factor $\exp\left[-\left(\beta-\beta_0\right)E\right]$. For any observable O whose values solely depends on the configurational energy, such as internal energy or specific heat, the expectation value at a temperature β can be written as

$$\langle O \rangle (\beta) = \frac{\sum_E P_\beta(E)\, O(E)}{\sum_E P_\beta(E)} = \frac{\sum_E P_{\beta_0}(E)\, e^{-(\beta-\beta_0)E}\, O(E)}{\sum_E P_{\beta_0}(E)\, e^{-(\beta-\beta_0)E}}, \tag{A.33}$$

where the normalization constants cancel out.

For the case of observables O, whose values do not uniquely depend on the configurational energy, such as magnetization M, one proceeds by constructing expectation values at constant energy (microcanonical) $\langle\langle O \rangle\rangle$ which can then be identified as the $O(E)$ in Eq. (A.33). From the implantation perspective though, one has to decide beforehand which observables want to construct the respective histograms, e.g., which powers of k, l for $\left\langle\langle M^k \right\rangle\rangle$, or for mixed quantities as $\left\langle\langle E^l M^k \right\rangle\rangle$ one wants to consider .

An alternative, and somewhat simpler, method is to utilise the time series of the energy and the respective measurements of an observable O, (E_i, O_i). If we have performed simulations of length N at an inverse temperature β_0, the expectation value of any observable which depends on energy and magnetization at temperature β, $\langle O \rangle (\beta)$, is expressed as

$$\langle O \rangle (\beta) = \frac{\sum_{i=1}^{N} O_i\, e^{-(\beta-\beta_0)E_i}}{\sum_{i=1}^{N} e^{-(\beta-\beta_0)E_i}}. \tag{A.34}$$

Although, the reweighting method can be applied, in principle, for any temperature β, in practice meaningful results are restricted only to a finite temperature-range $|\beta - \beta_0|$. In

[4]Reweighting can be also employed to the other coupling parameters of the system, such as magnetic field, here though we consider only the temperature parameter for simplicity.

a MC process at an inverse temperature β_0, the vast majority of states are sampled only in the vicinity of the peak of the energy histogram $P_{\beta_0}(E)$. Thus, the tails of $P_{\beta_0}(E)$ are undersampled, which greatly influences the reweighted energy histogram at inverse temperature β $P_\beta(E)$. Thus, a sufficient overlap among the energy histograms is required in order to obtain reasonable estimates. This is why reweighting is mostly useful in the vicinity of the critical point, where the energy histograms are relatively broad, ensuring a sufficient overlap among different temperatures. As it is discussed in Ref. [148] a reliable reweighting range can be obtained from requiring

$$\frac{|T - T_0|}{T_0} \leq \frac{1}{\sqrt{VC(T_0)}}, \tag{A.35}$$

where T_0 and T are the input and reweighted temperatures respectively, V is the total number of sites, and $C(T_0)$ is the specific heat at temperature T_0. In the critical region the specific heat scales as $C \sim L^{\alpha/\nu}$, and assuming that hyperscaling holds, i.e., $\alpha = 2 - d\nu$, Eq. (A.35) can be asymptotically written as

$$\frac{|T - T_0|}{T_0} \leq L^{-1/\nu}, \tag{A.36}$$

where α, ν are the critical exponents of the specific heat and correlation length respectively, and d is the dimensionality of the system.

Reweighting for the multi-replica Ising model

Reweighting can also be also extended to the case of the multi-replica Ising model, see Chap. 5. Since replicas are at the same temperature and they are statistically independent, the partition function is identical to Eq. (A.31), with the energy E given by:

$$E = E^{(1)} + E^{(2)} + \cdots + E^{(k)}, \tag{A.37}$$

where $E^{(n)}$ is the energy of the n th replica and k the total number of replicas. Consequently, having the time series of energy for all replicas and the time series of an observable O, Eq. (A.34) transforms to

$$\langle O \rangle (\beta) = \frac{\sum_{i=1}^{N} O_i \, e^{-(\beta-\beta_0)\,[E_i^{(1)}+E_i^{(2)}+\ldots E_i^{(k)}]}}{\sum_{i=1}^{N} e^{-(\beta-\beta_0)\,[E_i^{(1)}+E_i^{(2)}+\ldots E_i^{(k)}]}}. \tag{A.38}$$

In Fig. A.1 the reweighting method for the case of the 2-replica Ising model is illustrated, for the wrapping probability in both directions of the soft constraint clusters. For a certain temperature range the reweighted estimates are in agreement with the estimates resulting from individual simulations. However, deviations are observed as the temperature increases.

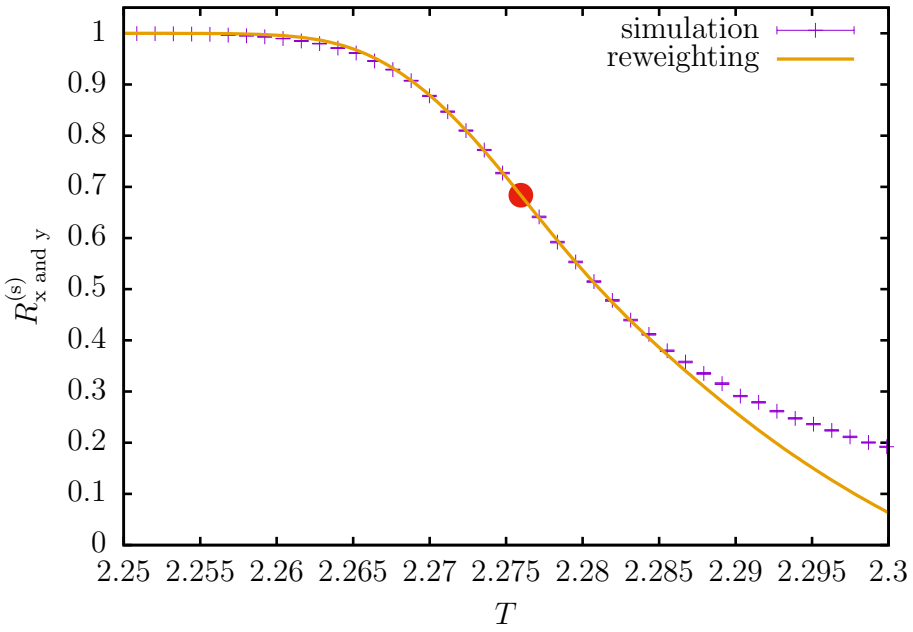

Figure A.1: Illustration example of the reweighting method for the wrapping probability in both directions for the soft constraint clusters of the 2-replica Ising model, for system of linear size $L = 256$. The red point corresponds to the temperature β_0, from where the reweighted estimates where extracted (orange line). The purple points correspond to individual simulations, and are plotted to show the extend of agreement with the reiweighted estimates.

Appendix B

Fit Results

Appendix B includes tables where the results of parameters obtained from the fitting routines are reported. Specifically, in Appendix B.1 the fitting results of the Ising (1-replica) ferromagnet are reported, see Chap. 4. Appendix B.2 includes the fitting results of the 2-replica Ising model, see Sec. 5.2. Finally, Appendix B.3 includes the fitting results of the 3-replica Ising model, see Sec. 5.3.

B.1 1-replica Ising model

Table B.1: Estimates of γ/ν, quality-of-fit parameter Q, and deviations from the exact value, $\gamma/\nu = 91/48 \approx 1.896$, in multiples of the estimated statistical errors $\Delta(\sigma)$, for the cluster sets of the average cluster size as introduced in Sec. 4.2.

	C			$C \setminus P_{\text{x and } \bar{\text{y}}}$			$C \setminus P_{\text{x and y}}$		
$L_{\min}$	γ/ν	Q	$\Delta(\sigma)$	γ/ν	Q	$\Delta(\sigma)$	γ/ν	Q	$\Delta(\sigma)$
16	1.89490(11)	0.001	8.28	1.89419(11)	0.001	15.03	1.7488(14)	0.000	101.59
32	1.89510(14)	0.010	5.36	1.89440(13)	0.008	10.76	1.7618(19)	0.000	71.51
64	1.89535(17)	0.044	2.83	1.89465(17)	0.042	7.11	1.770(2)	0.002	53.39
128	1.8957(2)	0.123	0.75	1.8950(2)	0.130	3.94	1.776(3)	0.021	36.14
256	1.8957(3)	0.078	0.52	1.8950(3)	0.079	2.78	1.788(5)	0.658	22.21
512	1.8964(4)	0.723	1.30	1.8958(4)	0.747	0.10	1.785(7)	0.575	15.78
600	1.8964(6)	0.613	1.03	1.8956(6)	0.668	0.46	1.791(9)	0.611	11.97
1000	1.8964(10)	0.568	0.60	1.8962(9)	0.623	0.35	1.779(15)	0.639	7.71
1200	1.8964(14)	0.300	0.40	1.8971(14)	0.628	0.86	1.76(2)	0.778	5.59
	$C \setminus P_{\text{x}}$			$C \setminus \max C$			$C \setminus P$		
$L_{\min}$	γ/ν	Q	$\Delta(\sigma)$	γ/ν	Q	$\Delta(\sigma)$	γ/ν	Q	$\Delta(\sigma)$
16	1.7413(16)	0.000	99.00	1.7469(11)	0.000	140.19	1.7321(11)	0.000	148.24
32	1.756(2)	0.000	70.11	1.7584(14)	0.000	97.21	1.7459(15)	0.000	102.89
64	1.764(2)	0.016	54.90	1.7663(18)	0.000	70.59	1.7540(18)	0.000	76.73
128	1.771(3)	0.307	37.30	1.774(2)	0.003	48.41	1.765(3)	0.008	52.35
256	1.779(5)	0.875	23.45	1.785(4)	0.868	30.87	1.774(4)	0.514	33.64
512	1.778(7)	0.794	16.59	1.783(5)	0.806	21.64	1.774(5)	0.374	23.01
600	1.783(9)	0.847	12.52	1.787(7)	0.860	16.57	1.781(7)	0.544	16.65
1000	1.774(15)	0.873	8.11	1.782(11)	0.754	9.87	1.787(12)	0.431	9.04
1200	1.77(2)	0.969	5.85	1.779(17)	0.484	6.76	1.793(17)	0.228	6.15

Table B.2: Estimates of β/ν, quality-of-fit parameter Q, and deviations from the exact value, $\beta/\nu = 5/96 \approx 0.052$, in multiples of the estimated statistical errors $\Delta(\sigma)$, for the cluster sets of the percolation strength as introduced in Sec. 4.3.

	max C			max P			max P_{x}		
$L_{\min}$	β/ν	Q	$\Delta(\sigma)$	β/ν	Q	$\Delta(\sigma)$	β/ν	Q	$\Delta(\sigma)$
16	0.05271(8)	0.005	7.94	0.05269(8)	0.008	7.65	0.05245(11)	0.230	3.30
32	0.05256(10)	0.030	4.94	0.05255(10)	0.036	4.76	0.05243(14)	0.166	2.56
64	0.05241(12)	0.081	2.66	0.05240(12)	0.092	2.55	0.05236(16)	0.136	1.68
128	0.05222(17)	0.141	0.81	0.05222(17)	0.136	0.83	0.0521(2)	0.216	0.06
256	0.0523(2)	0.109	1.14	0.0523(2)	0.103	1.13	0.0522(3)	0.156	0.43
512	0.0517(3)	0.744	1.06	0.0517(3)	0.718	1.07	0.0515(5)	0.597	1.32
600	0.0519(4)	0.670	0.44	0.0519(4)	0.653	0.42	0.0517(6)	0.494	0.70
1000	0.0514(7)	0.671	0.96	0.0514(7)	0.678	0.99	0.0507(9)	0.681	1.45
1200	0.0509(11)	0.586	1.17	0.0508(11)	0.600	1.19	0.0498(14)	0.955	1.61

	max $P_{\mathrm{x\ and\ y}}$			max $P_{\mathrm{x\ and\ }\overline{\mathrm{y}}}$					
$L_{\min}$	β/ν	Q	$\Delta(\sigma)$	β/ν	Q	$\Delta(\sigma)$	-	-	-
16	0.05224(14)	0.232	1.17	0.072(5)	0.432	4.38			
32	0.05227(17)	0.169	1.08	0.069(6)	0.402	2.87			
64	0.0522(2)	0.119	0.66	0.066(8)	0.347	1.78			
128	0.0520(3)	0.135	0.42	0.066(10)	0.251	1.43			
256	0.0523(4)	0.153	0.60	0.044(14)	0.730	0.56			
512	0.0514(6)	0.508	1.14	0.06(2)	0.763	0.35			
600	0.0517(7)	0.435	0.48	0.05(3)	0.676	0.07			
1000	0.0505(12)	0.569	1.30	0.08(5)	0.617	0.59			
1200	0.0490(19)	0.881	1.64	0.13(7)	0.651	1.04			

B.2 2-replica Ising model

Table B.3: Estimates of $\nu^{(s)}$, number of degrees of freedom (d.o.f.), χ^2 per degree of freedom $(\chi^2/\text{d.o.f.})$, quality-of-fit parameter Q, from the peaks of the derivatives with respect to temperature, of the wrapping probabilities R of the soft constraint clusters, for the 2-replica Ising model. Δ_σ denotes the deviation of the estimates from the exact value $\nu = 1$ of the 1-replica Ising model, in multiples of their estimated statistical errors.

$\left|\frac{dR^{(s)}_{x\text{ or }y}}{dT}\right|_{max}$

L_{min}	$\nu^{(s)}$	σ	Δ_σ	d.o.f.	χ^2/d.o.f.	Q
8	0.9003	0.0018	55.9507	21	57.9428	0.0000
10	0.9195	0.0020	39.5878	20	32.7718	0.0000
16	0.9393	0.0024	25.7471	19	15.1207	0.0000
20	0.9529	0.0027	17.4379	18	8.6417	0.0000
32	0.9667	0.0031	10.6291	17	3.6348	0.0000
40	0.9728	0.0035	7.7741	16	2.8241	0.0001
50	0.9773	0.0038	5.8963	15	2.3963	0.0018
64	0.9819	0.0043	4.2319	14	2.1318	0.0080
80	0.9881	0.0049	2.4593	13	1.6746	0.0590
100	0.9958	0.0055	0.7663	12	0.9391	0.5060
128	0.9987	0.0063	0.2030	11	0.9395	0.5006
160	1.0017	0.0072	0.2431	10	0.9585	0.4776
200	1.0076	0.0082	0.9262	9	0.8101	0.6068
256	1.0074	0.0096	0.7761	8	0.9113	0.5056
320	0.9978	0.0114	0.1954	7	0.7039	0.6688
400	1.0076	0.0145	0.5233	6	0.6174	0.7166
512	1.0244	0.0204	1.1934	5	0.4622	0.8046
640	1.0243	0.0223	1.0878	4	0.5777	0.6788
800	1.0417	0.0314	1.3253	3	0.5674	0.6364
1024	1.0183	0.0454	0.4032	2	0.6266	0.5344
1280	1.0430	0.0655	0.6571	1	0.9757	0.3233

$\left|\frac{dR^{(s)}_{x\text{ and }y}}{dT}\right|_{max}$

L_{min}	$\nu^{(s)}$	σ	Δ_σ	d.o.f.	χ^2/d.o.f.	Q
8	0.9716	0.0011	26.1497	21	16.8405	0.0000
10	0.9780	0.0012	18.1323	20	9.5453	0.0000
16	0.9848	0.0014	10.9866	19	4.0500	0.0000
20	0.9888	0.0015	7.2802	18	2.3077	0.0013
32	0.9924	0.0017	4.3410	17	1.1367	0.3102
40	0.9938	0.0019	3.2034	16	1.0491	0.3996
50	0.9951	0.0021	2.3506	15	0.9353	0.5233
64	0.9977	0.0024	0.9558	14	0.6206	0.8505
80	0.9982	0.0027	0.6584	13	0.6570	0.8066
100	0.9994	0.0031	0.2003	12	0.6568	0.7943
128	0.9985	0.0035	0.4288	11	0.6917	0.7479
160	0.9996	0.0040	0.0942	10	0.7225	0.7040
200	1.0035	0.0045	0.7900	9	0.3974	0.9370
256	1.0054	0.0053	1.0288	8	0.3893	0.9270
320	1.0047	0.0062	0.7573	7	0.4386	0.8785
400	1.0025	0.0074	0.3338	6	0.4619	0.8370
512	1.0008	0.0092	0.0887	5	0.5357	0.7494
640	1.0039	0.0116	0.3400	4	0.6194	0.6486
800	1.0130	0.0151	0.8627	3	0.5281	0.6630
1024	1.0066	0.0218	0.3016	2	0.7123	0.4905
1280	0.9831	0.0329	0.5153	1	0.5509	0.4579

$\left|\frac{dR^{(s)}_{x}}{dT}\right|_{max}$

L_{min}	$\nu^{(s)}$	σ	Δ_σ	d.o.f.	χ^2/d.o.f.	Q
8	0.9615	0.0018	20.9538	21	8.8272	0.0000
10	0.9690	0.0020	15.1860	20	5.1961	0.0000
16	0.9790	0.0024	8.7757	19	1.7209	0.0260
20	0.9828	0.0027	6.4395	18	1.2089	0.2428
32	0.9877	0.0030	4.0993	17	0.4530	0.9725
40	0.9884	0.0034	3.4525	16	0.4672	0.9630
50	0.9897	0.0037	2.7587	15	0.4593	0.9607
64	0.9888	0.0042	2.6772	14	0.4756	0.9471
80	0.9887	0.0048	2.3555	13	0.5121	0.9189
100	0.9886	0.0056	2.0419	12	0.5547	0.8795
128	0.9852	0.0062	2.3666	11	0.4729	0.9210
160	0.9891	0.0070	1.5726	10	0.3560	0.9650
200	0.9852	0.0079	1.8642	9	0.2829	0.9796
256	0.9868	0.0091	1.4494	8	0.2999	0.9663
320	0.9832	0.0101	1.6577	7	0.2495	0.9725
400	0.9875	0.0124	1.0086	6	0.2286	0.9676
512	0.9834	0.0144	1.1502	5	0.2128	0.9572
640	0.9873	0.0214	0.5917	4	0.2505	0.9095
800	0.9842	0.0245	0.6427	3	0.3116	0.8170
1024	0.9723	0.0451	0.6144	2	0.4164	0.6594
1280	0.9688	0.0685	0.4546	1	0.8282	0.3628

$\left|\frac{dR^{(s)}_{x\text{ and }\bar{y}}}{dT}\right|_{max}$

L_{min}	$\nu^{(s)}$	σ	Δ_σ	d.o.f.	χ^2/d.o.f.	Q
8	0.9840	0.0028	5.6639	21	2.2537	0.0008
10	0.9879	0.0031	3.8708	20	1.9036	0.0087
16	0.9943	0.0037	1.5546	19	1.3798	0.1243
20	0.9986	0.0041	0.3464	18	1.1520	0.2930
32	0.9997	0.0047	0.0692	17	1.2062	0.2492
40	1.0043	0.0052	0.8393	16	0.9686	0.4886
50	1.0063	0.0059	1.0590	15	1.0034	0.4477
64	1.0085	0.0066	1.2969	14	1.0294	0.4195
80	1.0035	0.0073	0.4848	13	0.9312	0.5190
100	1.0065	0.0083	0.7790	12	0.9630	0.4820
128	1.0101	0.0096	1.0557	11	0.9967	0.4463
160	1.0076	0.0109	0.6940	10	1.0753	0.3771
200	1.0111	0.0124	0.8957	9	1.1537	0.3203
256	1.0173	0.0150	1.1562	8	1.2294	0.2768
320	1.0179	0.0183	0.9784	7	1.4045	0.1983
400	1.0187	0.0201	0.9276	6	1.6373	0.1323
512	1.0113	0.0217	0.5205	5	1.8119	0.1067
640	0.9660	0.0305	1.1162	4	1.2644	0.2814
800	0.9681	0.0403	0.7915	3	1.6834	0.1682
1024	0.9171	0.0474	1.7472	2	0.7795	0.4586
1280	1.0164	0.1014	0.1621	1	0.0009	0.9767

Table B.4: Estimates of $\nu^{(\mathrm{h})}$, number of degrees of freedom (d.o.f.), χ^2 per degree of freedom $\left(\chi^2/\text{d.o.f.}\right)$, quality-of-fit parameter Q, from the peaks of the derivatives with respect to temperature, of the wrapping probabilities R of the hard constraint clusters, for the 2-replica Ising model. Δ_σ denotes the deviation of the estimates from the exact value $\nu = 1$ of the 1-replica Ising model, in multiples of their estimated statistical errors.

$\left|\frac{dR^{(\mathrm{h})}_{\mathrm{x\ or\ y}}}{dT}\right|_{\max}$

$L_{\min}$	$\nu^{(\mathrm{h})}$	σ	Δ_σ	d.o.f.	χ^2/d.o.f.	Q
8	0.9148	0.0008	101.7009	21	131.0008	0.0000
10	0.9301	0.0010	72.8297	20	66.3924	0.0000
16	0.9439	0.0011	51.0960	19	24.6452	0.0000
20	0.9518	0.0012	39.3014	18	11.9735	0.0000
32	0.9591	0.0014	29.2731	17	4.3528	0.0000
40	0.9630	0.0015	23.9251	16	2.2889	0.0024
50	0.9653	0.0017	20.1962	15	1.7667	0.0331
64	0.9678	0.0020	16.4426	14	1.2997	0.1980
80	0.9698	0.0022	13.8678	13	1.0510	0.3980
100	0.9712	0.0024	11.8558	12	0.9963	0.4492
128	0.9719	0.0028	10.1779	11	1.0592	0.3904
160	0.9730	0.0031	8.6113	10	1.1011	0.3567
200	0.9718	0.0036	7.9351	9	1.1649	0.3127
256	0.9700	0.0043	6.9277	8	1.2407	0.2703
320	0.9699	0.0051	5.9496	7	1.4176	0.1930
400	0.9726	0.0061	4.4714	6	1.5432	0.1595
512	0.9766	0.0078	3.0052	5	1.7033	0.1300
640	0.9705	0.0096	3.0849	4	1.8217	0.1215
800	0.9844	0.0129	1.2053	3	1.5024	0.2117
1024	1.0035	0.0188	0.1875	2	1.2089	0.2985
1280	1.0268	0.0287	0.9326	1	1.2325	0.2669

$\left|\frac{dR^{(\mathrm{h})}_{\mathrm{x\ and\ y}}}{dT}\right|_{\max}$

$L_{\min}$	$\nu^{(\mathrm{h})}$	σ	Δ_σ	d.o.f.	χ^2/d.o.f.	Q
8	0.9576	0.0008	55.9868	21	33.3510	0.0000
10	0.9632	0.0008	43.8880	20	20.9477	0.0000
16	0.9706	0.0010	30.6712	19	6.9630	0.0000
20	0.9737	0.0011	24.6858	18	4.4979	0.0000
32	0.9781	0.0012	17.9136	17	1.2782	0.1954
40	0.9798	0.0013	15.0890	16	0.7480	0.7461
50	0.9809	0.0014	13.2041	15	0.5107	0.9367
64	0.9819	0.0016	11.2074	14	0.4073	0.9734
80	0.9817	0.0018	10.0680	13	0.4333	0.9585
100	0.9816	0.0021	8.9718	12	0.4684	0.9340
128	0.9822	0.0023	7.8575	11	0.4697	0.9229
160	0.9836	0.0026	6.3711	10	0.3782	0.9566
200	0.9850	0.0030	5.0424	9	0.3268	0.9666
256	0.9866	0.0034	3.9356	8	0.2357	0.9843
320	0.9881	0.0041	2.8815	7	0.2142	0.9823
400	0.9880	0.0049	2.4389	6	0.2497	0.9596
512	0.9887	0.0064	1.7665	5	0.2921	0.9176
640	0.9868	0.0078	1.6881	4	0.3189	0.8655
800	0.9847	0.0104	1.4649	3	0.3948	0.7567
1024	0.9836	0.0152	1.0821	2	0.5863	0.5564
1280	0.9965	0.0240	0.1440	1	0.6576	0.4174

$\left|\frac{dR^{(\mathrm{h})}_{\mathrm{x}}}{dT}\right|_{\max}$

$L_{\min}$	$\nu^{(\mathrm{h})}$	σ	Δ_σ	d.o.f.	χ^2/d.o.f.	Q
8	0.9394	0.0009	67.6518	21	49.8816	0.0000
10	0.9492	0.0010	50.0611	20	26.3080	0.0000
16	0.9581	0.0011	36.7510	19	9.8627	0.0000
20	0.9618	0.0012	30.7316	18	6.8407	0.0000
32	0.9670	0.0014	23.4263	17	3.0629	0.0000
40	0.9695	0.0016	19.4680	16	2.3533	0.0017
50	0.9717	0.0017	16.5076	15	1.7658	0.0332
64	0.9736	0.0019	13.9541	14	1.4569	0.1181
80	0.9765	0.0021	11.1075	13	0.8390	0.6186
100	0.9772	0.0024	9.4439	12	0.8700	0.5774
128	0.9791	0.0028	7.5165	11	0.7802	0.6604
160	0.9785	0.0032	6.8005	10	0.8425	0.5874
200	0.9770	0.0037	6.2522	9	0.8638	0.5571
256	0.9742	0.0043	5.9881	8	0.7731	0.6266
320	0.9771	0.0050	4.5671	7	0.7000	0.6722
400	0.9779	0.0058	3.7977	6	0.8023	0.5679
512	0.9739	0.0070	3.7322	5	0.7452	0.5895
640	0.9724	0.0092	2.9879	4	0.9146	0.4542
800	0.9619	0.0127	3.0005	3	0.7203	0.5397
1024	0.9626	0.0186	2.0078	2	1.0791	0.3399
1280	0.9945	0.0321	0.1712	1	0.4877	0.4849

$\left|\frac{dR^{(\mathrm{h})}_{\mathrm{x\ and\ \overline{y}}}}{dT}\right|_{\max}$

$L_{\min}$	$\nu^{(\mathrm{h})}$	σ	Δ_σ	d.o.f.	χ^2/d.o.f.	Q
8	0.9943	0.0021	2.7298	21	0.8322	0.6819
10	0.9959	0.0023	1.7896	20	0.6936	0.8369
16	0.9980	0.0025	0.8123	19	0.5147	0.9582
20	0.9977	0.0027	0.8388	18	0.5402	0.9405
32	0.9980	0.0031	0.6539	17	0.5700	0.9161
40	0.9992	0.0034	0.2515	16	0.5568	0.9171
50	0.9979	0.0037	0.5819	15	0.5459	0.9160
64	0.9996	0.0042	0.0874	14	0.5328	0.9156
80	0.9998	0.0047	0.0351	13	0.5730	0.8776
100	0.9976	0.0052	0.4660	12	0.5343	0.8939
128	1.0002	0.0060	0.0407	11	0.5135	0.8958
160	0.9985	0.0067	0.2213	10	0.5291	0.8709
200	1.0001	0.0078	0.0147	9	0.5701	0.8227
256	1.0004	0.0089	0.0417	8	0.6410	0.7439
320	0.9950	0.0108	0.4657	7	0.6211	0.7390
400	1.0018	0.0128	0.1419	6	0.5523	0.7686
512	1.0002	0.0167	0.0140	5	0.6584	0.6551
640	1.0052	0.0203	0.2582	4	0.7750	0.5412
800	0.9962	0.0280	0.1342	3	0.9629	0.4091
1024	0.9764	0.0396	0.5952	2	1.2019	0.3006
1280	1.0568	0.0683	0.8315	1	0.0129	0.9095

Table B.5: Estimates of $T_c^{(s)}$, a [see Eq. (5.5)], number of degrees of freedom (d.o.f.), χ^2 per degree of freedom $\left(\chi^2/\text{d.o.f.}\right)$, quality-of-fit parameter Q, from straight-line fits using the crossing technique for the wrapping probabilities of the soft constraint clusters, for the 2-replica Ising model.

$R_{\text{x or y}}^{(s)}$								$R_{\text{x and y}}^{(s)}$							
$L_{\min}$	$T_c^{(s)}$	σ	a	σ	d.o.f.	χ^2/d.o.f.	Q	$L_{\min}$	$T_c^{(s)}$	σ	a	σ	d.o.f.	χ^2/d.o.f.	Q
8	2.269135	0.000033	-0.004	0.013	18	1.8320	0.0168	8	2.269196	0.000012	-0.003	0.005	18	0.7479	0.7635
10	2.269121	0.000034	0.005	0.014	17	1.7196	0.0324	10	2.269195	0.000013	-0.002	0.005	17	0.7794	0.7193
16	2.269116	0.000035	0.008	0.014	16	1.7866	0.0269	16	2.269196	0.000013	-0.003	0.005	16	0.8241	0.6591
20	2.269111	0.000036	0.011	0.015	15	1.8830	0.0201	20	2.269197	0.000013	-0.003	0.006	15	0.8713	0.5969
32	2.269110	0.000037	0.012	0.016	14	2.0153	0.0133	32	2.269198	0.000014	-0.004	0.006	14	0.9115	0.5454
40	2.269099	0.000038	0.019	0.017	13	2.0975	0.0114	40	2.269201	0.000014	-0.006	0.006	13	0.9111	0.5405
50	2.269091	0.000039	0.023	0.019	12	2.2232	0.0086	50	2.269204	0.000014	-0.008	0.007	12	0.9288	0.5165
64	2.269092	0.000041	0.023	0.020	11	2.4253	0.0051	64	2.269205	0.000015	-0.009	0.007	11	1.0105	0.4337
80	2.269093	0.000043	0.022	0.022	10	2.6665	0.0029	80	2.269203	0.000015	-0.008	0.008	10	1.0928	0.3631
100	2.269101	0.000045	0.017	0.024	9	2.9301	0.0018	100	2.269197	0.000017	-0.003	0.009	9	1.0841	0.3705
128	2.269111	0.000048	0.010	0.026	8	3.2499	0.0011	128	2.269187	0.000018	0.003	0.010	8	0.9415	0.4805
160	2.269140	0.000052	-0.010	0.029	7	3.3446	0.0014	160	2.269199	0.000019	-0.005	0.011	7	0.6593	0.7068
200	2.269076	0.000058	0.036	0.035	6	2.9962	0.0063	200	2.269202	0.000020	-0.007	0.012	6	0.7342	0.6220
256	2.269020	0.000065	0.078	0.041	5	2.7894	0.0159	256	2.269198	0.000022	-0.004	0.014	5	0.8372	0.5230
320	2.268947	0.000075	0.134	0.051	4	2.5807	0.0353	320	2.269177	0.000026	0.012	0.017	4	0.3602	0.8371
400	2.268976	0.000094	0.111	0.068	3	3.3550	0.0180	400	2.269164	0.000031	0.023	0.022	3	0.2974	0.8273
512	2.269128	0.000119	-0.016	0.091	2	2.8315	0.0589	512	2.269178	0.000038	0.011	0.029	2	0.2481	0.7803
640	2.269275	0.000183	-0.145	0.153	1	4.5512	0.0329	640	2.269151	0.000057	0.036	0.048	1	0.0971	0.7554

$R_{\text{x}}^{(s)}$								$R_{\text{x and }\overline{\text{y}}}^{(s)}$							
$L_{\min}$	$T_c^{(s)}$	σ	a	σ	d.o.f.	χ^2/d.o.f.	Q	$L_{\min}$	$T_c^{(s)}$	σ	a	σ	d.o.f.	χ^2/d.o.f.	Q
8	2.269188	0.000017	-0.002	0.007	18	1.5419	0.0659	8	2.269196	0.000021	-0.001	0.008	18	1.8857	0.0128
10	2.269183	0.000017	0.000	0.007	17	1.5341	0.0730	10	2.269210	0.000021	-0.009	0.008	17	1.2716	0.1999
16	2.269187	0.000018	-0.002	0.007	16	1.5678	0.0684	16	2.269209	0.000022	-0.008	0.008	16	1.3449	0.1594
20	2.269191	0.000018	-0.004	0.008	15	1.6223	0.0596	20	2.269207	0.000022	-0.007	0.009	15	1.4272	0.1243
32	2.269187	0.000019	-0.002	0.008	14	1.7061	0.0473	32	2.269214	0.000023	-0.011	0.009	14	1.3811	0.1525
40	2.269191	0.000019	-0.004	0.009	13	1.7948	0.0379	40	2.269218	0.000023	-0.014	0.010	13	1.4471	0.1291
50	2.269198	0.000020	-0.009	0.009	12	1.7727	0.0465	50	2.269217	0.000024	-0.013	0.010	12	1.5644	0.0941
64	2.269190	0.000021	-0.004	0.010	11	1.7849	0.0506	64	2.269227	0.000025	-0.019	0.011	11	1.4282	0.1522
80	2.269183	0.000022	0.000	0.011	10	1.8119	0.0530	80	2.269233	0.000026	-0.023	0.012	10	1.4906	0.1355
100	2.269179	0.000023	0.003	0.012	9	1.9773	0.0376	100	2.269226	0.000028	-0.019	0.014	9	1.6061	0.1070
128	2.269174	0.000025	0.006	0.014	8	2.1971	0.0246	128	2.269208	0.000030	-0.007	0.016	8	1.5257	0.1422
160	2.269194	0.000027	-0.007	0.015	7	1.9006	0.0650	160	2.269211	0.000032	-0.008	0.017	7	1.7370	0.0954
200	2.269181	0.000029	0.002	0.017	6	2.0102	0.0606	200	2.269231	0.000034	-0.023	0.019	6	1.4810	0.1801
256	2.269164	0.000032	0.014	0.020	5	2.1444	0.0572	256	2.269243	0.000038	-0.031	0.023	5	1.6822	0.1350
320	2.269122	0.000038	0.046	0.025	4	1.4548	0.2131	320	2.269247	0.000043	-0.035	0.028	4	2.0890	0.0794
400	2.269158	0.000045	0.018	0.032	3	1.2453	0.2914	400	2.269171	0.000053	0.027	0.038	3	0.8914	0.4446
512	2.269206	0.000056	-0.022	0.042	2	0.7983	0.4501	512	2.269142	0.000070	0.052	0.054	2	1.1247	0.3247
640	2.269245	0.000077	-0.056	0.063	1	1.0719	0.3005	640	2.269043	0.000100	0.142	0.085	1	0.3466	0.5561

Table B.6: Estimates of $T_c^{(h)}$, a [see Eq. (5.5)], number of degrees of freedom (d.o.f.), χ^2 per degree of freedom $\left(\chi^2/\text{d.o.f.}\right)$, quality-of-fit parameter Q, from straight-line fits using the crossing technique for the wrapping probabilities of the hard constraint clusters, for the 2-replica Ising model.

$R_{\text{x or y}}^{(h)}$								$R_{\text{x and y}}^{(h)}$							
$L_{\min}$	$T_c^{(h)}$	σ	a	σ	d.o.f.	χ^2/d.o.f.	Q	$L_{\min}$	$T_c^{(h)}$	σ	a	σ	d.o.f.	χ^2/d.o.f.	Q
8	2.269243	0.000017	-0.073	0.007	18	2.6913	0.0001	8	2.269216	0.000010	-0.043	0.004	18	1.2222	0.2320
10	2.269235	0.000017	-0.069	0.007	17	2.5096	0.0005	10	2.269213	0.000010	-0.041	0.004	17	1.1637	0.2855
16	2.269222	0.000017	-0.060	0.007	16	1.8857	0.0171	16	2.269212	0.000011	-0.041	0.004	16	1.2199	0.2427
20	2.269218	0.000018	-0.058	0.008	15	1.9202	0.0171	20	2.269211	0.000011	-0.040	0.005	15	1.2821	0.2035
32	2.269214	0.000018	-0.056	0.008	14	2.0027	0.0141	32	2.269208	0.000011	-0.038	0.005	14	1.3137	0.1895
40	2.269209	0.000019	-0.052	0.008	13	2.0519	0.0138	40	2.269209	0.000012	-0.039	0.005	13	1.4043	0.1480
50	2.269205	0.000020	-0.050	0.009	12	2.1823	0.0101	50	2.269209	0.000012	-0.039	0.006	12	1.5213	0.1081
64	2.269204	0.000020	-0.049	0.010	11	2.3771	0.0062	64	2.269209	0.000012	-0.039	0.006	11	1.6566	0.0766
80	2.269202	0.000021	-0.048	0.010	10	2.6018	0.0037	80	2.269207	0.000013	-0.037	0.006	10	1.7796	0.0585
100	2.269202	0.000022	-0.048	0.011	9	2.8908	0.0020	100	2.269205	0.000014	-0.036	0.007	9	1.9667	0.0388
128	2.269204	0.000023	-0.050	0.012	8	3.2410	0.0011	128	2.269198	0.000015	-0.031	0.008	8	1.9754	0.0453
160	2.269225	0.000025	-0.064	0.014	7	2.9196	0.0047	160	2.269208	0.000016	-0.038	0.009	7	1.8171	0.0792
200	2.269223	0.000027	-0.062	0.015	6	3.3951	0.0024	200	2.269208	0.000017	-0.039	0.010	6	2.1189	0.0478
256	2.269203	0.000029	-0.048	0.018	5	3.5555	0.0032	256	2.269195	0.000019	-0.029	0.011	5	1.9322	0.0854
320	2.269144	0.000034	-0.002	0.023	4	1.8286	0.1202	320	2.269173	0.000022	-0.012	0.014	4	1.3541	0.2472
400	2.269094	0.000043	0.038	0.030	3	1.0996	0.3478	400	2.269153	0.000026	0.004	0.019	3	1.2438	0.2920
512	2.269082	0.000054	0.049	0.042	2	1.5794	0.2061	512	2.269186	0.000032	-0.023	0.025	2	0.3964	0.6727
640	2.269056	0.000079	0.072	0.067	1	2.9577	0.0855	640	2.269157	0.000048	0.002	0.040	1	0.1554	0.6934

$R_{\text{x}}^{(h)}$								$R_{\text{x and }\overline{\text{y}}}^{(h)}$							
$L_{\min}$	$T_c^{(h)}$	σ	a	σ	d.o.f.	χ^2/d.o.f.	Q	$L_{\min}$	$T_c^{(h)}$	σ	a	σ	d.o.f.	χ^2/d.o.f.	Q
8	2.269221	0.000013	-0.049	0.005	18	1.9318	0.0101	8	2.269210	0.000020	-0.035	0.007	18	1.4877	0.0832
10	2.269216	0.000013	-0.046	0.005	17	1.7779	0.0248	10	2.269219	0.000020	-0.040	0.007	17	1.2803	0.1939
16	2.269216	0.000013	-0.046	0.005	16	1.8890	0.0169	16	2.269217	0.000020	-0.039	0.008	16	1.3467	0.1584
20	2.269216	0.000013	-0.046	0.006	15	2.0145	0.0112	20	2.269215	0.000021	-0.038	0.008	15	1.4189	0.1280
32	2.269209	0.000014	-0.042	0.006	14	1.9135	0.0205	32	2.269218	0.000021	-0.039	0.009	14	1.4890	0.1056
40	2.269209	0.000014	-0.042	0.006	13	2.0606	0.0133	40	2.269222	0.000022	-0.042	0.009	13	1.5502	0.0915
50	2.269212	0.000015	-0.043	0.007	12	2.1965	0.0095	50	2.269220	0.000023	-0.040	0.010	12	1.6639	0.0677
64	2.269202	0.000016	-0.037	0.007	11	1.9649	0.0275	64	2.269232	0.000023	-0.048	0.010	11	1.3214	0.2048
80	2.269197	0.000016	-0.034	0.008	10	2.0278	0.0267	80	2.269236	0.000024	-0.050	0.011	10	1.4166	0.1656
100	2.269197	0.000017	-0.034	0.009	9	2.2510	0.0164	100	2.269232	0.000026	-0.048	0.013	9	1.5577	0.1216
128	2.269201	0.000018	-0.037	0.010	8	2.4960	0.0105	128	2.269200	0.000029	-0.027	0.015	8	0.8199	0.5849
160	2.269218	0.000020	-0.048	0.011	7	2.0639	0.0438	160	2.269199	0.000030	-0.026	0.017	7	0.9351	0.4776
200	2.269211	0.000021	-0.043	0.012	6	2.2963	0.0322	200	2.269213	0.000033	-0.036	0.018	6	0.8460	0.5341
256	2.269188	0.000024	-0.027	0.015	5	1.7920	0.1107	256	2.269207	0.000037	-0.031	0.022	5	0.9901	0.4219
320	2.269152	0.000027	0.000	0.018	4	0.6061	0.6582	320	2.269205	0.000041	-0.030	0.027	4	1.2359	0.2932
400	2.269148	0.000033	0.004	0.023	3	0.7884	0.5002	400	2.269153	0.000051	0.012	0.036	3	0.6040	0.6123
512	2.269183	0.000041	-0.025	0.030	2	0.1402	0.8692	512	2.269186	0.000064	-0.016	0.048	2	0.5409	0.5823
640	2.269177	0.000058	-0.020	0.048	1	0.2589	0.6109	640	2.269116	0.000093	0.048	0.078	1	0.0004	0.9840

Table B.7: Estimates of $(\beta/\nu)^{(s)}$, number of degrees of freedom (d.o.f.), χ^2 per degree of freedom $\left(\chi^2/\text{d.o.f.}\right)$, quality-of-fit parameter Q, for the cluster sets of the percolation strength of the soft constraint clusters, for the 2-replica Ising model.

max $C^{(s)}$						max $P^{(s)}_{x \text{ or } y}$					
L_{min}	$(\beta/\nu)^{(s)}$	σ	d.o.f.	χ^2/d.o.f.	Q	L_{min}	$(\beta/\nu)^{(s)}$	σ	d.o.f.	χ^2/d.o.f.	Q
8	0.09559	0.00007	21	4.2770	0.0000	8	0.09567	0.00007	21	3.6964	0.0000
10	0.09544	0.00007	20	2.7264	0.0000	10	0.09551	0.00008	20	2.2767	0.0009
16	0.09531	0.00007	19	1.5251	0.0664	16	0.09535	0.00009	19	1.1198	0.3217
20	0.09523	0.00008	18	1.2876	0.1839	20	0.09529	0.00009	18	1.0379	0.4117
32	0.09510	0.00009	17	0.5889	0.9032	32	0.09516	0.00010	17	0.5184	0.9460
40	0.09506	0.00010	16	0.5613	0.9142	40	0.09513	0.00011	16	0.5174	0.9402
50	0.09502	0.00011	15	0.5334	0.9237	50	0.09506	0.00012	15	0.4489	0.9646
64	0.09505	0.00012	14	0.5414	0.9101	64	0.09506	0.00014	14	0.4809	0.9445
80	0.09500	0.00013	13	0.5168	0.9161	80	0.09503	0.00015	13	0.4964	0.9281
100	0.09497	0.00015	12	0.5314	0.8959	100	0.09498	0.00017	12	0.4976	0.9175
128	0.09497	0.00016	11	0.5782	0.8483	128	0.09500	0.00019	11	0.5341	0.8816
160	0.09498	0.00018	10	0.6353	0.7847	160	0.09497	0.00021	10	0.5765	0.8346
200	0.09482	0.00021	9	0.4527	0.9065	200	0.09480	0.00025	9	0.4441	0.9116
256	0.09481	0.00024	8	0.5072	0.8519	256	0.09479	0.00028	8	0.4977	0.8588
320	0.09475	0.00028	7	0.5562	0.7920	320	0.09472	0.00032	7	0.5463	0.7998
400	0.09464	0.00032	6	0.5659	0.7578	400	0.09460	0.00038	6	0.5743	0.7512
512	0.09451	0.00040	5	0.6250	0.6807	512	0.09436	0.00047	5	0.5344	0.7504
640	0.09447	0.00049	4	0.7751	0.5412	640	0.09412	0.00058	4	0.5441	0.7033
800	0.09418	0.00066	3	0.8952	0.4427	800	0.09395	0.00078	3	0.6916	0.5570
1024	0.09427	0.00093	2	1.3347	0.2632	1024	0.09408	0.00109	2	1.0242	0.3591
1280	0.09436	0.00146	1	2.6620	0.1028	1280	0.09418	0.00170	1	2.0425	0.1530

max $P^{(s)}_{x \text{ and } y}$						max $P^{(s)}_{x}$					
L_{min}	$(\beta/\nu)^{(s)}$	σ	d.o.f.	χ^2/d.o.f.	Q	L_{min}	$(\beta/\nu)^{(s)}$	σ	d.o.f.	χ^2/d.o.f.	Q
8	0.09598	0.00016	21	1.1801	0.2567	8	0.09575	0.00012	21	1.3104	0.1544
10	0.09582	0.00017	20	0.9134	0.5697	10	0.09560	0.00013	20	0.8897	0.6010
16	0.09572	0.00018	19	0.8525	0.6441	16	0.09547	0.00014	19	0.6441	0.8752
20	0.09574	0.00020	18	0.8963	0.5832	20	0.09545	0.00015	18	0.6712	0.8430
32	0.09560	0.00022	17	0.8029	0.6918	32	0.09531	0.00017	17	0.4634	0.9691
40	0.09565	0.00024	16	0.8363	0.6448	40	0.09527	0.00018	16	0.4798	0.9579
50	0.09562	0.00026	15	0.8861	0.5798	50	0.09526	0.00020	15	0.5081	0.9380
64	0.09576	0.00029	14	0.8603	0.6028	64	0.09531	0.00023	14	0.5209	0.9228
80	0.09569	0.00032	13	0.9047	0.5473	80	0.09521	0.00025	13	0.4858	0.9339
100	0.09574	0.00035	12	0.9713	0.4737	100	0.09519	0.00027	12	0.5219	0.9022
128	0.09570	0.00039	11	1.0530	0.3958	128	0.09513	0.00030	11	0.5499	0.8701
160	0.09568	0.00045	10	1.1576	0.3144	160	0.09517	0.00034	10	0.5987	0.8164
200	0.09511	0.00052	9	0.7666	0.6476	200	0.09487	0.00039	9	0.3883	0.9414
256	0.09510	0.00059	8	0.8620	0.5479	256	0.09482	0.00045	8	0.4311	0.9031
320	0.09496	0.00068	7	0.9595	0.4590	320	0.09478	0.00051	7	0.4892	0.8431
400	0.09448	0.00081	6	0.9334	0.4694	400	0.09451	0.00062	6	0.4633	0.8359
512	0.09400	0.00099	5	0.9742	0.4318	512	0.09454	0.00077	5	0.5552	0.7345
640	0.09383	0.00121	4	1.2021	0.3075	640	0.09417	0.00097	4	0.5957	0.6657
800	0.09350	0.00166	3	1.5742	0.1933	800	0.09354	0.00128	3	0.6093	0.6089
1024	0.09414	0.00233	2	2.2847	0.1018	1024	0.09411	0.00179	2	0.8099	0.4449
1280	0.09615	0.00360	1	4.0297	0.0447	1280	0.09397	0.00293	1	1.6159	0.2037

max $P^{(s)}_{x \text{ and } \overline{y}}$					
L_{min}	$(\beta/\nu)^{(s)}$	σ	d.o.f.	χ^2/d.o.f.	Q
8	0.08976	0.00179	21	1.3125	0.1530
10	0.08990	0.00192	20	1.3760	0.1212
16	0.08891	0.00210	19	1.3783	0.1251
20	0.08777	0.00230	18	1.3698	0.1347
32	0.08779	0.00251	17	1.4504	0.1027
40	0.08575	0.00274	16	1.3271	0.1697
50	0.08602	0.00293	15	1.4112	0.1316
64	0.08450	0.00318	14	1.4011	0.1427
80	0.08380	0.00354	13	1.4933	0.1109
100	0.08187	0.00399	12	1.5270	0.1062
128	0.08176	0.00446	11	1.6656	0.0744
160	0.08336	0.00499	10	1.7811	0.0582
200	0.08861	0.00569	9	1.5663	0.1189
256	0.08764	0.00668	8	1.7523	0.0813
320	0.09044	0.00783	7	1.9353	0.0599
400	0.09467	0.00928	6	2.1374	0.0459
512	0.10701	0.01138	5	1.8636	0.0970
640	0.10320	0.01393	4	2.2732	0.0588
800	0.09447	0.01871	3	2.8683	0.0350
1024	0.09387	0.02530	2	4.3018	0.0135
1280	0.03775	0.03940	1	5.1516	0.0232

Table B.8: Estimates of $(\beta/\nu)^{(\mathrm{h})}$, number of degrees of freedom (d.o.f.), χ^2 per degree of freedom $\left(\chi^2/\mathrm{d.o.f.}\right)$, quality-of-fit parameter Q, for the cluster sets of the percolation strength of the hard constraint clusters, for the 2-replica Ising model.

$\max C^{(\mathrm{h})}$						$\max P^{(\mathrm{h})}_{\mathrm{x\ or\ y}}$					
$L_{\min}$	$(\beta/\nu)^{(\mathrm{h})}$	σ	d.o.f.	χ^2/d.o.f.	Q	$L_{\min}$	$(\beta/\nu)^{(\mathrm{h})}$	σ	d.o.f.	χ^2/d.o.f.	Q
8	0.11452	0.00008	21	3.3023	0.0000	8	0.11614	0.00010	21	1.3262	0.1444
10	0.11462	0.00009	20	2.9359	0.0000	10	0.11619	0.00011	20	1.3182	0.1541
16	0.11475	0.00009	19	2.4601	0.0004	16	0.11630	0.00012	19	1.1513	0.2906
20	0.11490	0.00010	18	1.8246	0.0174	20	0.11646	0.00013	18	0.6613	0.8522
32	0.11499	0.00011	17	1.7118	0.0336	32	0.11651	0.00015	17	0.6687	0.8368
40	0.11510	0.00012	16	1.4982	0.0901	40	0.11660	0.00016	16	0.5793	0.9020
50	0.11522	0.00014	15	1.3426	0.1667	50	0.11667	0.00018	15	0.5697	0.9001
64	0.11546	0.00015	14	0.6321	0.8406	64	0.11682	0.00020	14	0.4233	0.9683
80	0.11552	0.00017	13	0.6030	0.8539	80	0.11690	0.00022	13	0.3983	0.9711
100	0.11560	0.00019	12	0.5786	0.8613	100	0.11692	0.00025	12	0.4273	0.9536
128	0.11573	0.00021	11	0.4535	0.9317	128	0.11704	0.00027	11	0.3593	0.9713
160	0.11582	0.00023	10	0.4164	0.9397	160	0.11707	0.00031	10	0.3910	0.9513
200	0.11582	0.00027	9	0.4626	0.9004	200	0.11708	0.00037	9	0.4342	0.9174
256	0.11592	0.00031	8	0.4645	0.8818	256	0.11714	0.00042	8	0.4806	0.8708
320	0.11600	0.00036	7	0.5062	0.8306	320	0.11714	0.00049	7	0.5492	0.7975
400	0.11594	0.00042	6	0.5793	0.7472	400	0.11713	0.00057	6	0.6408	0.6977
512	0.11585	0.00052	5	0.6769	0.6409	512	0.11690	0.00070	5	0.7060	0.6188
640	0.11590	0.00064	4	0.8417	0.4984	640	0.11690	0.00088	4	0.8825	0.4733
800	0.11559	0.00087	3	1.0309	0.3775	800	0.11646	0.00119	3	1.0780	0.3569
1024	0.11561	0.00122	2	1.5461	0.2131	1024	0.11620	0.00168	2	1.5936	0.2032
1280	0.11547	0.00193	1	3.0829	0.0791	1280	0.11599	0.00262	1	3.1756	0.0747

$\max P^{(\mathrm{h})}_{\mathrm{x\ and\ y}}$						$\max P^{(\mathrm{h})}_{\mathrm{x}}$					
$L_{\min}$	$(\beta/\nu)^{(\mathrm{h})}$	σ	d.o.f.	χ^2/d.o.f.	Q	$L_{\min}$	$(\beta/\nu)^{(\mathrm{h})}$	σ	d.o.f.	χ^2/d.o.f.	Q
8	0.12026	0.00019	21	0.7179	0.8191	8	0.11804	0.00015	21	0.7345	0.8011
10	0.12024	0.00021	20	0.7507	0.7756	10	0.11808	0.00017	20	0.7524	0.7737
16	0.12031	0.00023	19	0.7647	0.7521	16	0.11817	0.00018	19	0.7112	0.8113
20	0.12046	0.00025	18	0.6600	0.8534	20	0.11832	0.00020	18	0.5479	0.9363
32	0.12044	0.00027	17	0.6969	0.8093	32	0.11830	0.00022	17	0.5780	0.9108
40	0.12052	0.00030	16	0.7130	0.7836	40	0.11835	0.00023	16	0.5924	0.8924
50	0.12059	0.00033	15	0.7442	0.7410	50	0.11846	0.00026	15	0.5733	0.8975
64	0.12095	0.00037	14	0.4805	0.9447	64	0.11874	0.00030	14	0.3333	0.9899
80	0.12094	0.00040	13	0.5173	0.9158	80	0.11871	0.00032	13	0.3562	0.9825
100	0.12097	0.00045	12	0.5584	0.8767	100	0.11869	0.00035	12	0.3840	0.9698
128	0.12092	0.00050	11	0.6036	0.8275	128	0.11871	0.00039	11	0.4174	0.9493
160	0.12105	0.00057	10	0.6419	0.7789	160	0.11873	0.00046	10	0.4587	0.9170
200	0.12055	0.00067	9	0.4688	0.8964	200	0.11856	0.00053	9	0.4646	0.8991
256	0.12066	0.00077	8	0.5167	0.8449	256	0.11859	0.00061	8	0.5215	0.8412
320	0.12064	0.00090	7	0.5901	0.7646	320	0.11855	0.00071	7	0.5945	0.7610
400	0.12064	0.00107	6	0.6884	0.6590	400	0.11853	0.00084	6	0.6931	0.6552
512	0.11994	0.00130	5	0.6495	0.6619	512	0.11836	0.00105	5	0.8172	0.5371
640	0.11969	0.00159	4	0.7931	0.5294	640	0.11826	0.00130	4	1.0175	0.3966
800	0.11875	0.00212	3	0.9096	0.4354	800	0.11694	0.00173	3	0.9078	0.4363
1024	0.12047	0.00305	2	1.0578	0.3472	1024	0.11860	0.00240	2	0.8589	0.4236
1280	0.12122	0.00491	1	2.0771	0.1495	1280	0.11918	0.00397	1	1.6841	0.1944

$\max P^{(\mathrm{h})}_{\mathrm{x\ and\ \overline{y}}}$					
$L_{\min}$	$(\beta/\nu)^{(\mathrm{h})}$	σ	d.o.f.	χ^2/d.o.f.	Q
8	0.07362	0.00165	21	0.9916	0.4697
10	0.07514	0.00177	20	0.7624	0.7621
16	0.07611	0.00191	19	0.7083	0.8143
20	0.07629	0.00206	18	0.7445	0.7672
32	0.07674	0.00225	17	0.7740	0.7256
40	0.07669	0.00246	16	0.8222	0.6614
50	0.07748	0.00265	15	0.8348	0.6391
64	0.07647	0.00291	14	0.8435	0.6217
80	0.07645	0.00321	13	0.9083	0.5434
100	0.07569	0.00362	12	0.9668	0.4782
128	0.07774	0.00407	11	0.9461	0.4941
160	0.07659	0.00449	10	1.0032	0.4377
200	0.08177	0.00502	9	0.5214	0.8603
256	0.08045	0.00583	8	0.5622	0.8097
320	0.08048	0.00681	7	0.6425	0.7210
400	0.08038	0.00814	6	0.7495	0.6098
512	0.08939	0.00969	5	0.3097	0.9074
640	0.09243	0.01210	4	0.3432	0.8489
800	-0.08274	0.01681	3	0.2283	0.8767
1024	0.08392	0.02360	2	0.3399	0.7118
1280	0.07849	0.03468	1	0.6342	0.4258

Table B.9: Estimates of $(\gamma/\nu)^{(s)}$, number of degrees of freedom (d.o.f.), χ^2 per degree of freedom $\left(\chi^2/\text{d.o.f.}\right)$, quality-of-fit parameter Q, for the cluster sets of the average cluster size of the soft constraint clusters, for the 2-replica Ising model.

$C^{(s)}$

L_{min}	$(\gamma/\nu)^{(s)}$	σ	d.o.f.	χ^2/d.o.f.	Q
8	1.809513	0.000087	21	4.56308	0.00000
10	1.809689	0.000093	20	3.36933	0.00000
16	1.809859	0.000099	19	2.27779	0.00119
20	1.809977	0.000107	18	1.91364	0.01109
32	1.810199	0.000118	17	0.83035	0.65888
40	1.810257	0.000127	16	0.78912	0.69989
50	1.810354	0.000141	15	0.67823	0.80869
64	1.810300	0.000158	14	0.68458	0.79192
80	1.810363	0.000171	13	0.66681	0.79749
100	1.810464	0.000192	12	0.61268	0.83349
128	1.810470	0.000211	11	0.66791	0.77032
160	1.810471	0.000237	10	0.73470	0.69233
200	1.810672	0.000273	9	0.57059	0.82236
256	1.810668	0.000310	8	0.64185	0.74308
320	1.810797	0.000357	7	0.65814	0.70780
400	1.810961	0.000418	6	0.67337	0.67123
512	1.811193	0.000515	5	0.68959	0.63128
640	1.811376	0.000633	4	0.79992	0.52498
800	1.811826	0.000849	3	0.85586	0.46320
1024	1.811575	0.001184	2	1.23756	0.29009
1280	1.812003	0.001879	1	2.38908	0.12219

$C^{(s)} \setminus P^{(s)}_{\text{x and } \overline{\text{y}}}$

L_{min}	$(\gamma/\nu)^{(s)}$	σ	d.o.f.	χ^2/d.o.f.	Q
8	1.806586	0.000091	21	6.89517	0.00000
10	1.806788	0.000097	20	5.49746	0.00000
16	1.807028	0.000104	19	3.60654	0.00000
20	1.807197	0.000112	18	2.90055	0.00003
32	1.807485	0.000124	17	1.35701	0.14701
40	1.807573	0.000134	16	1.24337	0.22504
50	1.807709	0.000149	15	1.05187	0.39696
64	1.807679	0.000168	14	1.11553	0.33729
80	1.807762	0.000182	13	1.09076	0.36130
100	1.807916	0.000206	12	0.97618	0.46890
128	1.807941	0.000227	11	1.05848	0.39104
160	1.807950	0.000256	10	1.16370	0.31008
200	1.808238	0.000296	9	0.88174	0.54064
256	1.808233	0.000338	8	0.99187	0.43985
320	1.808437	0.000391	7	0.97972	0.44381
400	1.808690	0.000460	6	0.96293	0.44856
512	1.809055	0.000561	5	0.89512	0.48316
640	1.809274	0.000690	4	1.04442	0.38249
800	1.809707	0.000937	3	1.23714	0.29436
1024	1.809418	0.001306	2	1.80549	0.16439
1280	1.809459	0.002037	1	3.61031	0.05742

$C^{(s)} \setminus \max C^{(s)}$

L_{min}	$(\gamma/\nu)^{(s)}$	σ	d.o.f.	χ^2/d.o.f.	Q
8	1.665801	0.000483	21	112.24581	0.00000
10	1.670738	0.000523	20	87.66406	0.00000
16	1.676902	0.000576	19	58.42708	0.00000
20	1.682494	0.000639	18	38.88794	0.00000
32	1.687317	0.000703	17	25.07027	0.00000
40	1.690725	0.000769	16	19.20373	0.00000
50	1.694464	0.000853	15	13.60883	0.00000
64	1.698297	0.000956	14	8.97066	0.00000
80	1.700828	0.001055	13	7.19612	0.00000
100	1.703893	0.001177	12	4.92046	0.00000
128	1.707309	0.001345	11	2.85717	0.00094
160	1.709929	0.001512	10	1.70623	0.07300
200	1.711401	0.001742	9	1.57367	0.11664
256	1.713297	0.002001	8	1.30737	0.23428
320	1.715931	0.002348	7	0.83646	0.55676
400	1.716985	0.002750	6	0.88555	0.50430
512	1.719262	0.003394	5	0.80049	0.54906
640	1.721682	0.004153	4	0.74503	0.56116
800	1.722753	0.005636	3	0.96708	0.40710
1024	1.723473	0.008085	2	1.44290	0.23624
1280	1.732534	0.012848	1	2.06250	0.15096

$C^{(s)} \setminus P^{(s)}_{\text{x or y}}$

L_{min}	$(\gamma/\nu)^{(s)}$	σ	d.o.f.	χ^2/d.o.f.	Q
8	1.659965	0.000604	21	73.25593	0.00000
10	1.664319	0.000651	20	61.01093	0.00000
16	1.671293	0.000730	19	40.68242	0.00000
20	1.677430	0.000812	18	26.47943	0.00000
32	1.683154	0.000902	17	15.47274	0.00000
40	1.685792	0.000969	16	12.97854	0.00000
50	1.688838	0.001051	15	10.11248	0.00000
64	1.692906	0.001193	14	7.13598	0.00000
80	1.696715	0.001338	13	4.63310	0.00000
100	1.699313	0.001496	12	3.76750	0.00001
128	1.702759	0.001667	11	2.10556	0.01677
160	1.705713	0.001879	10	1.15636	0.31532
200	1.708056	0.002222	9	0.85181	0.56809
256	1.710198	0.002501	8	0.52209	0.84084
320	1.712202	0.002905	7	0.33457	0.93852
400	1.713422	0.003551	6	0.33081	0.92108
512	1.713786	0.004370	5	0.39288	0.85405
640	1.713360	0.005479	4	0.48694	0.74537
800	1.714998	0.007370	3	0.61241	0.60687
1024	1.717481	0.010531	2	0.86414	0.42141
1280	1.721781	0.016278	1	1.60828	0.20473

$C^{(s)} \setminus P^{(s)}_{\text{x and y}}$

L_{min}	$(\gamma/\nu)^{(s)}$	σ	d.o.f.	χ^2/d.o.f.	Q
8	1.687890	0.000588	21	50.84706	0.00000
10	1.691924	0.000645	20	41.84282	0.00000
16	1.698120	0.000730	19	26.85278	0.00000
20	1.703801	0.000826	18	16.29187	0.00000
32	1.707498	0.000905	17	11.38825	0.00000
40	1.710956	0.001000	16	7.97503	0.00000
50	1.713873	0.001107	15	5.98582	0.00000
64	1.717189	0.001231	14	3.69927	0.00000
80	1.719231	0.001354	13	2.97629	0.00022
100	1.722010	0.001514	12	1.82118	0.03919
128	1.724173	0.001731	11	1.38291	0.17300
160	1.726399	0.001963	10	0.94355	0.49133
200	1.726125	0.002265	9	1.04187	0.40325
256	1.728055	0.002600	8	0.88645	0.52678
320	1.729426	0.002996	7	0.89192	0.51163
400	1.728761	0.003643	6	1.02341	0.40764
512	1.728151	0.004481	5	1.21717	0.29795
640	1.728616	0.005469	4	1.51598	0.19442
800	1.729654	0.007488	3	2.00757	0.11051
1024	1.734054	0.010856	2	2.85466	0.05758
1280	1.747535	0.016877	1	4.62084	0.03159

$C^{(s)} \setminus P^{(s)}_{\text{x}}$

L_{min}	$(\gamma/\nu)^{(s)}$	σ	d.o.f.	χ^2/d.o.f.	Q
8	1.672312	0.000690	21	52.81165	0.00000
10	1.678316	0.000766	20	39.23729	0.00000
16	1.685037	0.000854	19	24.57939	0.00000
20	1.690142	0.000936	18	16.07468	0.00000
32	1.694648	0.001027	17	10.34203	0.00000
40	1.697673	0.001124	16	8.23978	0.00000
50	1.701234	0.001239	15	5.67292	0.00000
64	1.705202	0.001395	14	3.34484	0.00002
80	1.707637	0.001549	13	2.59955	0.00129
100	1.709678	0.001687	12	2.03769	0.01764
128	1.711888	0.001907	11	1.66022	0.07569
160	1.715298	0.002183	10	0.79549	0.63324
200	1.715966	0.002502	9	0.85077	0.56906
256	1.717949	0.002865	8	0.70466	0.68779
320	1.720439	0.003297	7	0.47273	0.85501
400	1.720922	0.004014	6	0.54410	0.77498
512	1.724297	0.005027	5	0.40427	0.84618
640	1.723668	0.006409	4	0.49907	0.73644
800	1.721117	0.008491	3	0.59553	0.61786
1024	1.727020	0.012126	2	0.66083	0.51642
1280	1.728886	0.019929	1	1.30774	0.25280

Table B.10: Estimates of $(\gamma/\nu)^{(\mathrm{h})}$, number of degrees of freedom (d.o.f.), χ^2 per degree of freedom $\left(\chi^2/\text{d.o.f.}\right)$, quality-of-fit parameter Q, for the cluster sets of the average cluster size of the hard constraint clusters, for the 2-replica Ising model.

$C^{(\mathrm{h})}$

$L_{\min}$	$(\gamma/\nu)^{(\mathrm{h})}$	σ	d.o.f.	χ^2/d.o.f.	Q
8	1.770965	0.000119	21	6.13409	0.00000
10	1.770689	0.000128	20	4.75150	0.00000
16	1.770417	0.000139	19	3.61742	0.00000
20	1.770155	0.000150	18	2.68125	0.00014
32	1.769958	0.000168	17	2.42980	0.00084
40	1.769764	0.000182	16	2.09578	0.00628
50	1.769550	0.000203	15	1.86606	0.02163
64	1.769129	0.000228	14	0.80836	0.66097
80	1.768998	0.000247	13	0.72269	0.74251
100	1.768863	0.000278	12	0.69275	0.76021
128	1.768660	0.000306	11	0.52482	0.88807
160	1.768488	0.000346	10	0.46179	0.91520
200	1.768442	0.000403	9	0.50751	0.87026
256	1.768221	0.000461	8	0.44973	0.89146
320	1.768151	0.000527	7	0.50314	0.83289
400	1.768183	0.000617	6	0.58533	0.74237
512	1.768352	0.000762	5	0.67389	0.64323
640	1.768438	0.000945	4	0.83648	0.50169
800	1.768988	0.001275	3	0.97713	0.40232
1024	1.768761	0.001807	2	1.44996	0.23458
1280	1.769525	0.002874	1	2.78290	0.09528

$C^{(\mathrm{h})} \setminus P^{(\mathrm{h})}_{\mathrm{x\ and\ \overline{y}}}$

$L_{\min}$	$(\gamma/\nu)^{(\mathrm{h})}$	σ	d.o.f.	χ^2/d.o.f.	Q
8	1.767109	0.000126	21	4.57046	0.00000
10	1.766833	0.000135	20	3.30221	0.00000
16	1.766598	0.000147	19	2.61195	0.00015
20	1.766370	0.000160	18	2.00965	0.00670
32	1.766218	0.000179	17	1.91950	0.01255
40	1.766047	0.000194	16	1.70671	0.03819
50	1.765862	0.000218	15	1.58843	0.06810
64	1.765435	0.000245	14	0.68357	0.79290
80	1.765319	0.000266	13	0.63840	0.82357
100	1.765214	0.000303	12	0.64738	0.80294
128	1.765034	0.000334	11	0.55641	0.86521
160	1.764855	0.000376	10	0.50568	0.88735
200	1.764926	0.000440	9	0.55094	0.83792
256	1.764705	0.000504	8	0.51893	0.84321
320	1.764659	0.000578	7	0.58928	0.76528
400	1.764741	0.000678	6	0.67837	0.66717
512	1.765107	0.000831	5	0.69868	0.62438
640	1.765320	0.001034	4	0.84318	0.49750
800	1.765820	0.001406	3	1.03278	0.37671
1024	1.765655	0.002021	2	1.54275	0.21379
1280	1.766768	0.003176	1	2.87899	0.08974

$C^{(\mathrm{h})} \setminus \max C^{(\mathrm{h})}$

$L_{\min}$	$(\gamma/\nu)^{(\mathrm{h})}$	σ	d.o.f.	χ^2/d.o.f.	Q
8	1.591108	0.000511	21	182.10057	0.00000
10	1.598295	0.000555	20	135.89038	0.00000
16	1.606323	0.000608	19	87.92373	0.00000
20	1.613705	0.000676	18	58.15690	0.00000
32	1.619892	0.000741	17	37.23581	0.00000
40	1.624991	0.000823	16	26.96965	0.00000
50	1.629703	0.000913	15	19.21269	0.00000
64	1.634387	0.001020	14	13.04721	0.00000
80	1.638007	0.001135	13	9.96984	0.00000
100	1.642168	0.001277	12	6.60563	0.00000
128	1.645839	0.001444	11	4.49728	0.00000
160	1.649351	0.001625	10	2.73303	0.00231
200	1.651359	0.001860	9	2.48847	0.00770
256	1.653624	0.002144	8	2.23556	0.02211
320	1.657852	0.002571	7	1.28799	0.25151
400	1.658642	0.003023	6	1.46153	0.18698
512	1.661892	0.003662	5	1.25937	0.27840
640	1.665459	0.004425	4	1.05842	0.37531
800	1.667140	0.006045	3	1.35571	0.25431
1024	1.670372	0.008458	2	1.88429	0.15194
1280	1.684913	0.013630	1	1.91779	0.16610

$C^{(\mathrm{h})} \setminus P^{(\mathrm{h})}_{\mathrm{x\ or\ y}}$

$L_{\min}$	$(\gamma/\nu)^{(\mathrm{h})}$	σ	d.o.f.	χ^2/d.o.f.	Q
8	1.617484	0.000678	21	88.41468	0.00000
10	1.623672	0.000736	20	69.73761	0.00000
16	1.632837	0.000826	19	41.78018	0.00000
20	1.640371	0.000920	18	24.80497	0.00000
32	1.646624	0.001020	17	14.41598	0.00000
40	1.650559	0.001119	16	10.78546	0.00000
50	1.653513	0.001210	15	8.74381	0.00000
64	1.657862	0.001378	14	6.25648	0.00000
80	1.661620	0.001531	13	4.30704	0.00000
100	1.664744	0.001719	12	3.33115	0.00007
128	1.667783	0.001899	11	2.34774	0.00689
160	1.671232	0.002165	10	1.48295	0.13840
200	1.673787	0.002542	9	1.23890	0.26556
256	1.676034	0.002953	8	1.11414	0.34968
320	1.678567	0.003456	7	0.98888	0.43703
400	1.681516	0.004097	6	0.85444	0.52768
512	1.683361	0.004913	5	0.93274	0.45828
640	1.685560	0.006238	4	1.08409	0.36240
800	1.684429	0.008495	3	1.43265	0.23104
1024	1.690380	0.011918	2	1.89558	0.15023
1280	1.692215	0.019119	1	3.77609	0.05199

$C^{(\mathrm{h})} \setminus P^{(\mathrm{h})}_{\mathrm{x\ and\ y}}$

$L_{\min}$	$(\gamma/\nu)^{(\mathrm{h})}$	σ	d.o.f.	χ^2/d.o.f.	Q
8	1.662465	0.000610	21	59.15485	0.00000
10	1.667275	0.000667	20	46.21631	0.00000
16	1.673828	0.000746	19	28.48176	0.00000
20	1.679222	0.000833	18	18.21956	0.00000
32	1.683856	0.000923	17	11.29818	0.00000
40	1.686728	0.001003	16	8.67517	0.00000
50	1.689592	0.001103	15	6.64914	0.00000
64	1.693736	0.001243	14	3.39266	0.00002
80	1.695887	0.001367	13	2.55763	0.00156
100	1.698161	0.001516	12	1.76828	0.04726
128	1.699633	0.001742	11	1.66083	0.07554
160	1.702437	0.001981	10	0.94511	0.48989
200	1.702026	0.002254	9	1.03386	0.40964
256	1.704147	0.002613	8	0.84029	0.56687
320	1.706004	0.003162	7	0.80513	0.58284
400	1.707430	0.003765	6	0.85819	0.52483
512	1.705995	0.004569	5	0.96843	0.43545
640	1.705413	0.005485	4	1.20133	0.30786
800	1.703463	0.007230	3	1.54465	0.20065
1024	1.717277	0.010884	2	0.87511	0.41682
1280	1.725465	0.017431	1	1.38852	0.23866

$C^{(\mathrm{h})} \setminus P^{(\mathrm{h})}_{\mathrm{x}}$

$L_{\min}$	$(\gamma/\nu)^{(\mathrm{h})}$	σ	d.o.f.	χ^2/d.o.f.	Q
8	1.642167	0.000721	21	62.78574	0.00000
10	1.649906	0.000806	20	42.83783	0.00000
16	1.657194	0.000890	19	25.45683	0.00000
20	1.662576	0.000975	18	16.65681	0.00000
32	1.667617	0.001076	17	10.42353	0.00000
40	1.670567	0.001169	16	8.47906	0.00000
50	1.674387	0.001295	15	5.89724	0.00000
64	1.679191	0.001469	14	2.89637	0.00021
80	1.681360	0.001609	13	2.27724	0.00537
100	1.683131	0.001749	12	1.91183	0.02822
128	1.685051	0.001999	11	1.72818	0.06091
160	1.688066	0.002327	10	1.26018	0.24680
200	1.688924	0.002642	9	1.34788	0.20603
256	1.690997	0.003047	8	1.28326	0.24685
320	1.692716	0.003585	7	1.34821	0.22275
400	1.694894	0.004272	6	1.42660	0.19990
512	1.697035	0.005365	5	1.62484	0.14952
640	1.697647	0.006672	4	2.02512	0.08797
800	1.690501	0.008788	3	2.17982	0.08812
1024	1.710058	0.012390	2	0.76310	0.46622
1280	1.722920	0.020914	1	0.94344	0.33140

Table B.11: Estimates of $(\gamma/\nu)^{(\mathrm{s})}$, $\omega^{(\mathrm{s})}$, number of degrees of freedom (d.o.f.), χ^2 per degree of freedom $\left(\chi^2/\text{d.o.f.}\right)$, quality-of-fit parameter Q, from the joint fits of the different cluster sets of the average cluster size of the soft constraint clusters, for the 2-replica Ising model.

$L_{\min}$	$(\gamma/\nu)^{(\mathrm{s})}$	σ	$\omega^{(\mathrm{s})}$	σ	d.o.f.	χ^2/d.o.f.	Q
8	1.811390	0.000371	0.359830	0.004932	124	1.138218	0.139235
10	1.811395	0.000471	0.359834	0.006307	118	1.055020	0.323360
16	1.811263	0.000517	0.355207	0.008225	112	1.005993	0.464423
20	1.811361	0.000570	0.342766	0.009803	106	0.882741	0.800453
32	1.810665	0.000679	0.333824	0.012648	100	0.754620	0.968087
40	1.810618	0.000737	0.329763	0.014456	94	0.776216	0.947034
50	1.810379	0.000906	0.320664	0.017689	88	0.759008	0.955187
64	1.811633	0.001267	0.305361	0.021440	82	0.664873	0.991655
80	1.811769	0.001542	0.299473	0.026023	76	0.678373	0.985782
100	1.811748	0.001974	0.287476	0.029534	70	0.697750	0.974460
128	1.812943	0.002753	0.264807	0.039112	64	0.652824	0.985793
160	1.815694	0.004755	0.227440	0.046825	58	0.557945	0.997441
200	1.814103	0.005005	0.250692	0.066069	52	0.540385	0.997269
256	1.818016	0.009095	0.231408	0.084336	46	0.540179	0.995425
320	1.822410	0.016902	0.182967	0.091874	40	0.558175	0.989254
400	1.822407	0.018788	0.202470	0.125647	34	0.629326	0.954388
512	1.823937	0.030203	0.185106	0.173036	28	0.713140	0.865631
640	1.826606	0.047056	0.188081	0.245855	22	0.870313	0.636241
800	1.815207	0.038453	0.256061	0.525071	16	1.153416	0.297953

Table B.12: Estimates of $(\gamma/\nu)^{(\mathrm{h})}$, $\omega^{(\mathrm{h})}$, number of degrees of freedom (d.o.f.), χ^2 per degree of freedom $\left(\chi^2/\mathrm{d.o.f.}\right)$, quality-of-fit parameter Q, from the joint fits of the different cluster sets of the average cluster size of the hard constraint clusters, for the 2-replica Ising model.

$L_{\min}$	$(\gamma/\nu)^{(\mathrm{h})}$	σ	$\omega^{(\mathrm{h})}$	σ	d.o.f.	χ^2/d.o.f.	Q
8	1.765286	0.000354	0.420846	0.004840	124	1.621569	0.000015
10	1.765241	0.000450	0.416482	0.006196	118	1.439385	0.001263
16	1.764923	0.000515	0.403877	0.007595	112	1.182591	0.090936
20	1.764917	0.000585	0.388444	0.009267	106	0.986672	0.520577
32	1.763818	0.000702	0.378186	0.012499	100	0.814381	0.912437
40	1.763670	0.000765	0.372318	0.014281	94	0.816499	0.902338
50	1.763132	0.000952	0.364162	0.017574	88	0.802815	0.912176
64	1.764243	0.001303	0.344508	0.022539	82	0.680493	0.988173
80	1.764284	0.001549	0.336953	0.026823	76	0.704124	0.976568
100	1.763859	0.001983	0.323147	0.031879	70	0.717411	0.964380
128	1.764818	0.002489	0.315016	0.041625	64	0.711214	0.961107
160	1.765909	0.003851	0.276662	0.051336	58	0.679679	0.970620
200	1.765423	0.004260	0.304791	0.069702	52	0.670405	0.967425
256	1.768600	0.006992	0.306598	0.093901	46	0.712551	0.928822
320	1.772304	0.011587	0.265977	0.115322	40	0.765549	0.857168
400	1.774685	0.014781	0.283488	0.146968	34	0.864560	0.692849
512	1.776114	0.021379	0.289084	0.206970	28	0.986415	0.484735
640	1.785511	0.046366	0.251442	0.258118	22	1.197071	0.237554
800	1.772523	0.017032	0.729094	0.614637	16	1.299761	0.186479

B.3 3-replica Ising model

Table B.13: Estimates of $\nu^{(\mathrm{s})}$, number of degrees of freedom (d.o.f.), χ^2 per degree of freedom $\left(\chi^2/\text{d.o.f.}\right)$, quality-of-fit parameter Q, from the peaks of the derivatives with respect to temperature, of the wrapping probabilities R of the soft constraint clusters, using logarithmic corrections [see Eq. (5.11)], for the 3-replica Ising model. Δ_σ denotes the deviation of the estimates from the exact value $\nu = 1$ of the 1-replica Ising model, in multiples of their estimated statistical errors.

$\left|\frac{dR^{(\mathrm{s})}_{\mathrm{x\ or\ y}}}{dT}\right|_{\max}$

$L_{\min}$	$\nu^{(\mathrm{s})}$	σ	Δ_σ	d.o.f.	χ^2/d.o.f.	Q
8	0.912	0.002	13.95	20	14.640	0.000
10	0.923	0.002	13.31	19	9.180	0.000
16	0.935	0.003	10.06	18	6.670	0.000
20	0.943	0.003	7.72	17	5.810	0.000
32	0.958	0.004	4.77	16	4.390	0.000
40	0.971	0.005	3.52	15	2.930	0.000
50	0.977	0.006	2.45	14	2.860	0.000
64	0.988	0.007	1.14	13	2.390	0.000
80	1.004	0.008	0.33	12	1.690	0.060
100	1.024	0.010	2.54	11	0.860	0.580
128	1.024	0.013	1.90	10	0.950	0.490
160	1.040	0.016	2.69	9	0.800	0.620
200	1.036	0.021	1.85	8	0.890	0.530
256	1.020	0.028	0.76	7	0.910	0.500
320	1.039	0.039	1.02	6	0.980	0.440
400	1.087	0.048	2.08	5	0.740	0.590
512	1.081	0.076	1.11	4	0.920	0.450
640	1.083	0.116	0.65	3	1.230	0.300
800	1.280	0.170	1.86	2	0.780	0.460
1024	0.853	1383538	0.00	1	0.220	0.640

$\left|\frac{dR^{(\mathrm{s})}_{\mathrm{x\ and\ y}}}{dT}\right|_{\max}$

$L_{\min}$	$\nu^{(\mathrm{s})}$	σ	Δ_σ	d.o.f.	χ^2/d.o.f.	Q
8	0.800	0.005	0.70	20	3875	0.000
10	0.797	0.006	0.57	19	4079	0.000
16	0.815	0.005	0.52	18	4302	0.000
20	0.869	0.004	0.47	17	4494	0.000
32	1.015	0.004	0.06	16	4512	0.000
40	1.208	0.005	0.71	15	4218	0.000
50	2.314	0.013	2.36	14	1731	0.000
64	1.023	0.009	1.93	13	1.687	0.056
80	1.031	0.011	2.14	12	1.705	0.059
100	1.018	0.014	0.95	11	1.642	0.080
128	1.010	0.018	0.40	10	1.747	0.065
160	0.976	0.026	0.77	9	1.385	0.188
200	0.986	0.033	0.34	8	1.530	0.141
256	1.025	0.038	0.56	7	1.397	0.201
320	1.056	0.048	0.96	6	1.477	0.181
400	1.066	0.064	0.78	5	1.761	0.117
512	1.228	0.087	2.90	4	0.824	0.510
640	1.285	0.130	2.22	3	0.982	0.400
800	1.305	0.211	1.19	2	1.466	0.231
1024	0.896	610401	0.00	1	1.635	0.201

$\left|\frac{dR^{(\mathrm{s})}_{\mathrm{x}}}{dT}\right|_{\max}$

$L_{\min}$	$\nu^{(\mathrm{s})}$	σ	Δ_σ	d.o.f.	χ^2/d.o.f.	Q
8	0.934	0.002	12.15	20	6.430	0.000
10	0.941	0.003	9.96	19	5.390	0.000
16	0.956	0.003	7.67	18	3.010	0.000
20	0.960	0.004	5.83	17	2.970	0.000
32	0.972	0.005	3.38	16	2.520	0.000
40	0.979	0.006	2.24	15	2.270	0.000
50	0.981	0.008	1.64	14	2.430	0.000
64	0.994	0.009	0.45	13	2.010	0.020
80	0.990	0.011	0.64	12	2.130	0.010
100	1.006	0.013	0.35	11	1.890	0.040
128	1.000	0.016	0.01	10	2.030	0.030
160	1.003	0.020	0.11	9	2.240	0.020
200	1.040	0.025	1.13	8	1.960	0.050
256	1.062	0.031	1.36	7	2.070	0.040
320	1.018	0.047	0.26	6	2.070	0.050
400	1.092	0.056	1.22	5	1.790	0.110
512	1.024	0.096	0.18	4	2.000	0.090
640	0.876	0.483	0.17	3	2.320	0.070
800	1.178	0.196	0.58	2	2.410	0.090
1024	0.855	330233	0.00	1	2.910	0.090

$\left|\frac{dR^{(\mathrm{s})}_{\mathrm{x\ and\ \overline{y}}}}{dT}\right|_{\max}$

$L_{\min}$	$\nu^{(\mathrm{s})}$	σ	Δ_σ	d.o.f.	χ^2/d.o.f.	Q
8	1.070	0.007	10.31	20	1.027	0.425
10	1.064	0.008	7.88	19	0.982	0.479
16	1.045	0.012	4.59	18	0.696	0.819
20	1.046	0.013	3.95	17	0.736	0.768
32	1.042	0.020	2.44	16	0.779	0.712
40	1.052	0.023	2.60	15	0.787	0.694
50	1.057	0.027	2.33	14	0.837	0.629
64	1.054	0.032	1.75	13	0.900	0.553
80	1.056	0.037	1.51	12	0.974	0.471
100	1.024	0.053	0.47	11	0.960	0.481
128	0.966	0.107	0.33	10	0.926	0.507
160	1.013	0.088	0.15	9	0.948	0.482
200	0.979	0.144	0.15	8	1.037	0.405
256	0.971	0.201	0.13	7	1.185	0.308
320	1.164	0.130	1.39	6	0.825	0.550
400	1.162	0.177	0.92	5	0.990	0.422
512	1.362	0.256	1.43	4	0.975	0.420
640	1.555	0.434	1.18	3	1.177	0.317
800	2.117	0.998	0.94	2	1.431	0.239
1024	0.993	694	0.00	1	2.329	0.127

Table B.14: Estimates of $\nu^{(\mathrm{h})}$, number of degrees of freedom (d.o.f.), χ^2 per degree of freedom $\left(\chi^2/\text{d.o.f.}\right)$, quality-of-fit parameter Q, from the peaks of the derivatives with respect to temperature, of the wrapping probabilities R of the soft constraint clusters, using logarithmic corrections [see Eq. (5.11)], for the 3-replica Ising model. Δ_σ denotes the deviation of the estimates from the exact value $\nu = 1$ of the 1-replica Ising model, in multiples of their estimated statistical errors.

$\left|\frac{dR^{(\mathrm{h})}_{\mathrm{x\ or\ y}}}{dT}\right|_{\max}$

$L_{\min}$	$\nu^{(\mathrm{h})}$	σ	Δ_σ	d.o.f.	χ^2/d.o.f.	Q
8	1.040	0.000	5.85	20	14.829	0.000
10	1.050	0.000	5.60	19	14.376	0.000
16	1.060	0.000	6.39	18	11.176	0.000
20	1.070	0.000	6.19	17	10.836	0.000
32	1.100	0.000	8.19	16	6.458	0.000
40	1.120	0.010	9.05	15	5.088	0.000
50	1.130	0.010	9.49	14	4.130	0.000
64	1.150	0.010	10.54	13	3.119	0.000
80	1.170	0.010	11.04	12	2.446	0.003
100	1.190	0.010	10.20	11	2.139	0.015
128	1.190	0.020	7.73	10	2.332	0.010
160	1.210	0.020	6.38	9	2.430	0.009
200	1.230	0.030	5.32	8	2.582	0.008
256	1.290	0.040	6.02	7	1.872	0.070
320	1.390	0.050	11.48	6	0.511	0.801
400	1.430	0.070	8.25	5	0.512	0.767
512	1.520	0.110	9.04	4	0.284	0.888
640	1.550	0.170	5.27	3	0.367	0.777
800	1.510	0.280	2.46	2	0.537	0.585
1024	2.040	0.700	4.51	1	0.109	0.742

$\left|\frac{dR^{(\mathrm{h})}_{\mathrm{x\ and\ y}}}{dT}\right|_{\max}$

$L_{\min}$	$\nu^{(\mathrm{h})}$	σ	Δ_σ	d.o.f.	χ^2/d.o.f.	Q
8	1.076	0.002	9.26	19	14.841	0.000
10	1.084	0.003	8.95	18	13.681	0.000
16	1.105	0.003	10.07	17	9.350	0.000
20	1.118	0.004	10.24	16	7.917	0.000
32	1.147	0.006	12.13	15	4.642	0.000
40	1.158	0.007	11.65	14	4.262	0.000
50	1.196	0.010	12.18	13	2.595	0.001
64	1.196	0.010	12.18	13	2.595	0.001
80	1.214	0.012	12.30	12	2.152	0.011
100	1.237	0.015	12.38	11	1.704	0.066
128	1.263	0.020	11.13	10	1.467	0.145
160	1.288	0.024	10.40	9	1.306	0.227
200	1.306	0.031	8.45	8	1.357	0.210
256	1.367	0.041	9.62	7	0.848	0.547
320	1.429	0.058	9.71	6	0.586	0.742
400	1.427	0.083	6.11	5	0.703	0.621
512	1.534	0.128	5.52	4	0.571	0.684
640	1.525	0.198	3.04	3	0.760	0.516
800	1.466	0.342	1.29	2	1.118	0.327
1024	1.245	0.885	0.19	1	2.139	0.144

$\left|\frac{dR^{(\mathrm{h})}_{\mathrm{x}}}{dT}\right|_{\max}$

$L_{\min}$	$\nu^{(\mathrm{h})}$	σ	Δ_σ	d.o.f.	χ^2/d.o.f.	Q
8	1.050	0.000	7.47	20	11.873	0.000
10	1.060	0.000	7.08	19	11.558	0.000
16	1.080	0.000	7.57	18	9.162	0.000
20	1.080	0.000	7.42	17	8.656	0.000
32	1.110	0.010	7.12	16	7.166	0.000
40	1.120	0.010	7.55	15	6.095	0.000
50	1.140	0.010	7.86	14	5.324	0.000
64	1.180	0.010	10.21	13	3.106	0.000
80	1.200	0.010	12.33	12	2.036	0.018
100	1.220	0.010	11.05	11	1.807	0.047
128	1.250	0.020	13.95	10	1.006	0.436
160	1.270	0.020	11.52	9	1.005	0.433
200	1.300	0.030	9.99	8	0.898	0.517
256	1.340	0.040	11.01	7	0.579	0.774
320	1.340	0.060	7.40	6	0.673	0.671
400	1.350	0.080	4.87	5	0.804	0.547
512	1.400	0.120	3.53	4	0.911	0.456
640	1.260	0.210	1.29	3	0.946	0.417
800	1.270	0.330	0.69	2	1.418	0.242
1024	1.140	0.970	0.09	1	2.806	0.094

$\left|\frac{dR^{(\mathrm{h})}_{\mathrm{x\ and\ \overline{y}}}}{dT}\right|_{\max}$

$L_{\min}$	$\nu^{(\mathrm{h})}$	σ	Δ_σ	d.o.f.	χ^2/d.o.f.	Q
8	1.031	0.007	2.96	20	2.206	0.001
10	1.030	0.008	2.43	19	2.320	0.001
16	1.035	0.011	2.09	18	2.420	0.001
20	1.048	0.013	2.32	17	2.424	0.001
32	1.031	0.018	1.09	16	2.441	0.001
40	1.052	0.020	1.64	15	2.376	0.002
50	1.029	0.026	0.71	14	2.340	0.003
64	1.030	0.032	0.59	13	2.519	0.002
80	1.058	0.036	1.01	12	2.575	0.002
100	1.088	0.041	1.31	11	2.670	0.002
128	1.063	0.054	0.70	10	2.864	0.001
160	1.151	0.061	1.49	9	2.710	0.004
200	1.203	0.075	1.59	8	2.897	0.003
256	1.224	0.103	1.20	7	3.299	0.002
320	1.269	0.136	1.01	6	3.809	0.001
400	1.308	0.187	0.77	5	4.554	0.000
512	0.935	786353	0.00	4	5.269	0.000
640	0.956	176628	0.00	3	6.450	0.000
800	1.552	0.664	0.38	2	4.685	0.009
1024	–	–	–	–	–	–

Table B.15: Estimates of $T_c^{(s)}$, ϵ [see Eq. (5.12)], number of degrees of freedom (d.o.f.), χ^2 per degree of freedom $\left(\chi^2/\text{d.o.f.}\right)$, quality-of-fit parameter Q, from non-linear fits of Eq. (5.12) using the crossing technique for the wrapping probabilities of the soft constraint clusters, for the 3-replica Ising model. Δ_σ denotes the deviation of the estimates from the exact critical temperature of the 1-replica Ising model, in multiples of their estimated statistical errors.

$R_{\text{x or y}}^{(s)}$

$L_{\min}$	$T_c^{(s)}$	σ	Δ_σ	ϵ	σ	d.o.f.	χ^2/d.o.f.	Q
8	2.269053	0.000022	5.99	1.013	0.020	17	0.807	0.687
10	2.269047	0.000023	6.08	1.020	0.022	16	0.813	0.673
16	2.269063	0.000025	4.80	0.999	0.025	15	0.666	0.821
20	2.269063	0.000027	4.61	0.999	0.028	14	0.713	0.763
32	2.269066	0.000029	4.09	0.995	0.033	13	0.763	0.700
40	2.269073	0.000032	3.53	0.984	0.037	12	0.791	0.661
50	2.269066	0.000033	3.62	0.996	0.041	11	0.826	0.614
64	2.269074	0.000037	2.99	0.982	0.049	10	0.881	0.550
80	2.269103	0.000045	1.84	0.932	0.058	9	0.650	0.755
100	2.269088	0.000047	2.06	0.959	0.068	8	0.670	0.719
128	2.269098	0.000058	1.51	0.940	0.089	7	0.750	0.630
160	2.269067	0.000060	1.97	1.004	0.114	6	0.746	0.612
200	2.269133	0.000097	0.55	0.870	0.153	5	0.530	0.754
256	2.269124	0.000116	0.53	0.887	0.204	4	0.659	0.621
320	2.269075	0.000121	0.92	1.002	0.288	3	0.782	0.503
400	2.269492	0.000836	0.37	0.460	0.482	2	0.101	0.904
512	2.269172	0.000529	0.03	0.809	0.990	1	0.047	0.829

$R_{\text{x and y}}^{(s)}$

$L_{\min}$	$T_c^{(s)}$	σ	Δ_σ	ϵ	σ	d.o.f.	χ^2/d.o.f.	Q
8	2.269083	0.000023	4.42	0.864	0.022	17	1.365	0.143
10	2.269081	0.000024	4.39	0.867	0.024	16	1.442	0.112
16	2.269083	0.000026	3.98	0.864	0.027	15	1.535	0.084
20	2.269064	0.000026	4.67	0.892	0.031	14	1.423	0.132
32	2.269095	0.000031	2.88	0.846	0.036	13	1.040	0.408
40	2.269099	0.000034	2.51	0.840	0.041	12	1.117	0.340
50	2.269115	0.000040	1.77	0.816	0.048	11	1.130	0.332
64	2.269106	0.000041	1.92	0.830	0.053	10	1.211	0.278
80	2.269156	0.000056	0.52	0.754	0.065	9	0.820	0.597
100	2.269164	0.000065	0.34	0.744	0.077	8	0.915	0.503
128	2.269173	0.000077	0.17	0.731	0.094	7	1.036	0.403
160	2.269149	0.000085	0.42	0.767	0.123	6	1.175	0.316
200	2.269226	0.000147	0.28	0.655	0.168	5	1.179	0.316
256	2.269069	0.000087	1.33	0.947	0.211	4	0.365	0.833
320	2.269092	0.000134	0.69	0.886	0.312	3	0.464	0.707
400	2.269207	0.000344	0.06	0.660	0.483	2	0.486	0.615
512	2.269036	0.000229	0.65	1.104	0.957	1	0.658	0.417

$R_{\text{x}}^{(s)}$

$L_{\min}$	$T_c^{(s)}$	σ	Δ_σ	ϵ	σ	d.o.f.	χ^2/d.o.f.	Q
8	2.269067	0.000024	4.90	0.905	0.024	17	0.677	0.829
10	2.269067	0.000025	4.69	0.905	0.025	16	0.719	0.777
16	2.269067	0.000027	4.35	0.905	0.029	15	0.767	0.716
20	2.269060	0.000028	4.43	0.915	0.032	14	0.787	0.685
32	2.269075	0.000032	3.40	0.893	0.038	13	0.758	0.706
40	2.269073	0.000035	3.23	0.895	0.043	12	0.820	0.630
50	2.269081	0.000039	2.68	0.882	0.050	11	0.870	0.569
64	2.269078	0.000041	2.59	0.888	0.056	10	0.953	0.482
80	2.269094	0.000048	1.89	0.860	0.067	9	0.988	0.447
100	2.269091	0.000054	1.75	0.865	0.079	8	1.110	0.352
128	2.269082	0.000059	1.75	0.882	0.097	7	1.253	0.269
160	2.269032	0.000057	2.69	1.001	0.130	6	1.149	0.331
200	2.269048	0.000076	1.81	0.960	0.175	5	1.350	0.240
256	2.268967	0.000056	3.90	1.252	0.227	4	0.722	0.577
320	2.268934	0.000058	4.35	1.444	0.349	3	0.804	0.492
400	2.269072	0.000240	0.47	0.839	0.580	2	0.294	0.745
512	2.268998	0.000258	0.73	1.108	1.192	1	0.514	0.473

$R_{\text{x and }\overline{\text{y}}}^{(s)}$

$L_{\min}$	$T_c^{(s)}$	σ	Δ_σ	ϵ	σ	d.o.f.	χ^2/d.o.f.	Q
8	2.269046	0.000069	2.01	0.837	0.071	17	1.475	0.093
10	2.269070	0.000080	1.45	0.805	0.081	16	1.510	0.086
16	2.268999	0.000067	2.81	0.913	0.088	15	1.238	0.234
20	2.268963	0.000062	3.60	0.983	0.097	14	1.211	0.259
32	2.269023	0.000091	1.79	0.868	0.129	13	1.185	0.283
40	2.269025	0.000099	1.61	0.864	0.148	12	1.283	0.220
50	2.269194	0.000204	0.04	0.630	0.183	11	0.946	0.495
64	2.269129	0.000179	0.32	0.707	0.205	10	0.997	0.443
80	2.269251	0.000303	0.22	0.571	0.246	9	1.017	0.423
100	2.269195	0.000281	0.03	0.628	0.282	8	1.132	0.338
128	7.004098	27328	0.00	0.000	0.402	7	0.311	0.949
160	34.609	1598623	0.00	0.000	0.496	6	0.349	0.911
200	6.285843	28713	0.00	0.000	0.590	5	0.394	0.853
256	2.270558	0.007394	0.19	0.183	0.731	4	0.448	0.774
320	27.819646	2296940	0.00	0.000	1.122	3	0.490	0.689
400	2.269355	0.001369	0.12	0.589	1.346	2	0.182	0.833
512	2.269107	0.000752	0.10	1.095	2.692	1	0.310	0.578

Table B.16: Estimates of $T_c^{(h)}$, ϵ [see Eq. (5.12)], number of degrees of freedom (d.o.f.), χ^2 per degree of freedom $\left(\chi^2/\text{d.o.f.}\right)$, quality-of-fit parameter Q, from non-linear fits of Eq. (5.12) using the crossing technique for the wrapping probabilities of the hard constraint clusters, for the 3-replica Ising model. Δ_σ denotes the deviation of the estimates from the exact critical temperature of the 1-replica Ising model, in multiples of their estimated statistical errors.

$R_{\text{x or y}}^{(h)}$

$L_{\min}$	$T_c^{(h)}$	σ	Δ_σ	ϵ	σ	d.o.f.	χ^2/d.o.f.	Q
8	2.268158	0.000018	56.8	1.046	0.015	17	1.440	0.107
10	2.268173	0.000020	50.2	1.026	0.018	16	1.255	0.217
16	2.268182	0.000022	45.9	1.015	0.021	15	1.244	0.229
20	2.268173	0.000023	44.8	1.027	0.023	14	1.230	0.245
32	2.268167	0.000024	41.8	1.035	0.027	13	1.302	0.203
40	2.268180	0.000027	37.6	1.016	0.031	12	1.241	0.247
50	2.268180	0.000029	34.8	1.016	0.036	11	1.354	0.188
64	2.268167	0.000030	33.7	1.038	0.041	10	1.382	0.181
80	2.268195	0.000038	26.1	0.987	0.053	9	1.264	0.251
100	2.268178	0.000041	24.5	1.020	0.066	8	1.339	0.218
128	2.268171	0.000046	22.2	1.034	0.081	7	1.518	0.156
160	2.268154	0.000049	21.0	1.074	0.100	6	1.703	0.116
200	2.268185	0.000068	14.7	0.999	0.133	5	1.917	0.088
256	2.268292	0.000139	6.4	0.794	0.196	4	1.937	0.101
320	2.268347	0.000234	3.59	0.713	0.291	3	2.546	0.054
400	30.04553	1053418	0.00	0.000	0.490	2	0.811	0.444
512	24.98703	1260741	0.00	0.000	0.889	1	1.574	0.210

$R_{\text{x and y}}^{(h)}$

$L_{\min}$	$T_c^{(h)}$	σ	Δ_σ	ϵ	σ	d.o.f.	χ^2/d.o.f.	Q
8	2.268165	0.000021	48.9	0.931	0.014	17	0.992	0.464
10	2.268166	0.000022	46.6	0.930	0.015	16	1.052	0.396
16	2.268163	0.000024	43.2	0.933	0.018	15	1.115	0.335
20	2.268150	0.000024	42.5	0.947	0.020	14	1.026	0.423
32	2.268171	0.000028	35.6	0.923	0.024	13	0.877	0.577
40	2.268160	0.000030	34.5	0.937	0.027	12	0.859	0.589
50	2.268168	0.000033	30.4	0.927	0.033	11	0.906	0.533
64	2.268177	0.000037	27.0	0.915	0.038	10	0.958	0.478
80	2.268187	0.000043	23.2	0.901	0.046	9	1.031	0.412
100	2.268168	0.000047	21.8	0.928	0.057	8	1.074	0.378
128	2.268155	0.000051	20.4	0.950	0.068	7	1.178	0.311
160	2.268111	0.000052	20.8	1.035	0.090	6	1.006	0.419
200	2.268057	0.000051	22.1	1.174	0.125	5	0.708	0.618
256	2.268076	0.000070	15.7	1.116	0.177	4	0.831	0.505
320	2.268134	0.000132	7.98	0.959	0.284	3	0.922	0.429
400	2.268023	0.000095	12.17	1.359	0.440	2	0.622	0.537
512	2.267954	0.000087	14.18	1.972	1.022	1	0.831	0.362

$R_{\text{x}}^{(h)}$

$L_{\min}$	$T_c^{(h)}$	σ	Δ_σ	ϵ	σ	d.o.f.	χ^2/d.o.f.	Q
8	2.268183	0.000021	48.7	0.963	0.014	17	0.504	0.953
10	2.268188	0.000022	46.0	0.958	0.016	16	0.489	0.954
16	2.268192	0.000024	42.0	0.954	0.018	15	0.513	0.935
20	2.268185	0.000025	40.7	0.962	0.020	14	0.495	0.938
32	2.268199	0.000029	34.2	0.946	0.026	13	0.442	0.955
40	2.268186	0.000030	33.2	0.962	0.029	12	0.374	0.973
50	2.268187	0.000034	29.5	0.961	0.036	11	0.408	0.954
64	2.268182	0.000037	27.5	0.968	0.042	10	0.437	0.929
80	2.268202	0.000043	22.7	0.938	0.051	9	0.354	0.956
100	2.268194	0.000049	20.4	0.951	0.063	8	0.383	0.930
128	2.268190	0.000053	18.6	0.957	0.075	7	0.434	0.881
160	2.268167	0.000059	17.3	1.002	0.098	6	0.420	0.866
200	2.268128	0.000062	17.0	1.096	0.137	5	0.309	0.908
256	2.268102	0.000069	15.6	1.174	0.194	4	0.308	0.873
320	2.268123	0.000106	10.0	1.101	0.303	3	0.378	0.769
400	2.268133	0.000157	6.72	1.069	0.472	2	0.564	0.569
512	2.268048	0.000147	7.72	1.501	0.994	1	0.903	0.342

$R_{\text{x and }\overline{\text{y}}}^{(h)}$

$L_{\min}$	$T_c^{(h)}$	σ	Δ_σ	ϵ	σ	d.o.f.	χ^2/d.o.f.	Q
8	2.267922	0.000079	16.0	0.836	0.044	17	1.214	0.243
10	2.267908	0.000082	15.5	0.847	0.050	16	1.278	0.201
16	2.267888	0.000086	15.0	0.864	0.058	15	1.343	0.167
20	2.267846	0.000086	15.6	0.903	0.066	14	1.357	0.165
32	2.267940	0.000118	10.6	0.817	0.082	13	1.224	0.254
40	2.267957	0.000135	9.09	0.802	0.097	12	1.320	0.199
50	2.268063	0.000189	5.94	0.715	0.117	11	1.262	0.239
64	2.268192	0.000275	3.61	0.629	0.142	10	1.247	0.255
80	2.268131	0.000280	3.77	0.668	0.169	9	1.365	0.198
100	2.268065	0.000275	4.07	0.720	0.200	8	1.507	0.149
128	2.267984	0.000267	4.50	0.798	0.249	7	1.685	0.108
160	2.267837	0.000203	6.64	1.004	0.310	6	1.796	0.096
200	2.267695	0.000140	10.6	1.367	0.421	5	1.962	0.081
256	26.89330	908959	0.00	0.000	0.683	4	0.950	0.434
320	41.34264	4099963	0.00	0.000	1.100	3	0.921	0.430
400	34.79650	3401478	0.00	0.000	1.449	2	1.001	0.368
512	24.30552	1971289	0.00	0.000	2.075	1	0.938	0.333

Bibliography

[1] M. E. Fisher, "The theory of equilibrium critical phenomena", Rep. Prog. Phys. **30**, 615–730 (1967) (pp. 1, 5, 8).

[2] H. E. Stanley, *Introduction to Phase Transitions and Critical Phenomena* (Oxford University Press, New York, 1971) (pp. 1, 5).

[3] M. E. Fisher, "The renormalization group in the theory of critical behavior", Rev. Mod. Phys. **46**, 597–616 (1974) (pp. 1, 5, 8, 9).

[4] R. J. Baxter, *Exactly Solved Models in Statistical Mechanics* (Academic Press, London, 1982) (pp. 1, 5).

[5] N. Goldenfeld, *Lectures on Phase Transitions and the Renormalization Group* (Addison-Wesley, 1992) (pp. 1, 5, 9, 11, 13).

[6] J. M. Yeomans, *Statistical Mechanics of Phase Transitions* (Oxford University Press, New York, 1992) (pp. 1, 5, 9, 11, 13).

[7] P. Christe and M. Henkel, *Introduction to Conformal Invariance and Its Applications to Critical Phenomena*, 16 (Springer, Berlin, 1993) (pp. 1, 5, 9, 12–14).

[8] J. Cardy, *Scaling and Renormalization in Statistical Physics* (Cambridge University Press, Cambridge, 1996) (pp. 1, 5, 8–10, 12–14).

[9] M. E. Fisher, "Renormalization group theory: Its basis and formulation in statistical physics", Rev. Mod. Phys. **70**, 653–681 (1998) (pp. 1, 5, 8, 9).

[10] M. Kardar, *Statistical Physics of Fields* (Cambridge University Press, Cambridge, 2007) (pp. 1, 5).

[11] L. P. Kadanoff, "Scaling laws for Ising models near T_c", Physics Physique Fizika **2**, Publisher: APS, 263 (1966) (pp. 1, 9).

[12] K. G. Wilson, "Renormalization Group and Critical Phenomena. I. Renormalization Group and the Kadanoff Scaling Picture", Phys. Rev. B **4**, 3174–3183 (1971) (pp. 1, 9).

[13] K. G. Wilson, "Renormalization Group and Critical Phenomena. II. Phase-Space Cell Analysis of Critical Behavior", Phys. Rev. B **4**, 3184–3205 (1971) (pp. 1, 9).

[14] K. G. Wilson and J. Kogut, "The renormalization group and the ϵ expansion", Phys. Rep. C **12**, 75–199 (1974) (pp. 1, 9).

[15] C. Domb and M. S. Green, eds., *Series expansions for lattice models*, Vol. 3, Phase transitions and critical phenomena 1974 (Academic Press, London, 1974) (p. 1).

[16] J. Oitmaa, C. Hamer, and W. Zheng, *Series Expansion Methods for Strongly Interacting Lattice Models* (Cambridge University Press, 2006) (p. 1).

[17] A. Hehn, N. van Well, and M. Troyer, "High-Temperature Series Expansion for Spin-1/2 Heisenberg Models", Comput. Phys. Commun. **212**, 180–188 (2017) (p. 1).

[18] D. Stauffer, "Scaling theory of percolation clusters", Phys. Rep. **54**, 1–74 (1979) (pp. 1, 17–20).

[19] D. Stauffer and A. Aharony, *Introduction to percolation theory*, Rev., 2nd ed (Taylor & Francis, London, 1994) (pp. 1, 17–19, 46, 50, 52, 75, 102, 119).

[20] G. R. Grimmett, *Percolation* (Springer, New York, 1989) (pp. 1, 17).

[21] G. R. Grimmett, "The work of Hugo Duminil-Copin", arXiv:2207.02022 [math.PR] (2022) (p. 1).

[22] P. W. Kasteleyn and C. M. Fortuin, "Phase transitions in lattice systems with random local properties", J. Phys. Soc. Japan **26**, 11–14 (1969) (pp. 1, 20, 21).

[23] C. M. Fortuin and P. W. Kasteleyn, "On the random-cluster model: I. Introduction and relation to other models", Physica **57**, 536–564 (1972) (pp. 1, 20, 21).

[24] C. M. Fortuin, "On the random-cluster model: II. The percolation model", Physica **58**, 393–418 (1972) (pp. 1, 20, 21).

[25] C. M. Fortuin, "On the random-cluster model: III. The simple random-cluster model", Physica **59**, 545–570 (1972) (pp. 1, 20, 21).

[26] A. Coniglio and A. Fierro, "Correlated percolation", in *Encyclopedia of complexity and systems science*, edited by R. A. Meyers (Springer, New York, NY, 2009), pp. 1596–1615 (pp. 2, 20, 24, 53).

[27] R. H. Swendsen and J.-S. Wang, "Nonuniversal Critical Dynamics in Monte Carlo Simulations", Phys. Rev. Lett. **58**, 86–88 (1987) (pp. 2, 35, 37, 43, 57).

[28] U. Wolff, "Collective Monte Carlo Updating for Spin Systems", Phys. Rev. Lett. **62**, 361–364 (1989) (pp. 2, 35, 37).

[29] A. Coniglio, "Percolation problems and phase transitions", J. Phys. A: Math. Gen. **8**, 1773 (1975) (pp. 2, 20, 48).

[30] A. Coniglio, C. R. Nappi, F. Peruggi, and L. Russo, "Percolation and phase transitions in the Ising model", Commun. Math. Phys. **51**, 315–323 (1976) (pp. 2, 20, 48).

[31] A. Coniglio, C. R. Nappi, F. Peruggi, and L. Russo, "Percolation points and critical point in the Ising model", J. Phys. A: Math. Gen. **10**, 205–218 (1977) (pp. 2, 20, 48).

[32] W. Janke and A. M. Schakel, "Geometrical vs. Fortuin-Kasteleyn clusters in the two-dimensional q-state Potts model", Nucl. Phys. B **700**, 385–406 (2004) (pp. 2, 23–25).

[33] W. Janke and A. M. J. Schakel, "Fractal structure of spin clusters and domain walls in the two-dimensional Ising model", Phys. Rev. E **71**, 036703 (2005) (pp. 2, 23–25, 49).

[34] M. P. M. den Nijs, "A relation between the temperature exponents of the eight-vertex and q-state Potts model", J. Phys. A: Math. Gen. **12**, 1857–1868 (1979) (pp. 2, 23).

[35] B. Nienhuis, "Analytical calculation of two leading exponents of the dilute Potts model", J. Phys. A: Math. Gen. **15**, 199–213 (1982) (pp. 2, 23).

[36] M. den Nijs, "Extended scaling relations for the magnetic critical exponents of the Potts model", Phys. Rev. B **27**, 1674–1679 (1983) (pp. 2, 23).

[37] H. Saleur and B. Duplantier, "Exact Determination of the Percolation Hull Exponent in Two Dimensions", Phys. Rev. Lett. **58**, 2325–2328 (1987) (pp. 2, 23, 24).

[38] B. Nienhuis, "Two-dimensional critical phenomena and the Coulomb Gas", in *Phase Transitions and Critical Phenomena*, Vol. 11, edited by C. Domb and J. L. Lebowitz (Academic Press, London, 1987), p. 1 (pp. 2, 23).

[39] J. L. Cardy, "Conformal invariance", in *Phase Transitions and Critical Phenomena*, Vol. 11, edited by C. Domb and J. L. Lebowitz (Academic Press, London, 1987), p. 55 (pp. 2, 23, 24).

[40] J. Machta, C. M. Newman, and D. L. Stein, "The Percolation Signature of the Spin Glass Transition", J. Stat. Phys. **130**, 113–128 (2008) (pp. 2, 40, 53, 122).

[41] H. Fajen, A. K. Hartmann, and A. P. Young, "Percolation of Fortuin-Kasteleyn clusters for the random-bond Ising model", Phys. Rev. E **102**, 012131 (2020) (pp. 2, 40, 53).

[42] K. Binder and A. P. Young, "Spin glasses: Experimental facts, theoretical concepts, and open questions", Rev. Mod. Phys. **58**, 801–976 (1986) (pp. 2, 25, 30).

[43] M. Mezard, G. Parisi, and M. A. Virasoro, *Spin glass theory and beyond*, v. 9 (World Scientific, Singapore, 1987), 461 pp. (pp. 2, 25).

[44] K. H. Fischer and J. Hertz, *Spin glasses* (Cambridge University Press, Cambridge, 1991), 408 pp. (pp. 2, 25, 30).

[45] A. P. Young, ed., *Spin Glasses and Random Fields* (World Scientific, Singapore, 1998), 454 pp. (pp. 2, 25, 30).

[46] C. M. Newman and D. L. Stein, "Ordering and broken symmetry in short-ranged spin glasses", J. Phys. Condens. Matter **15**, R1319–R1364 (2003) (pp. 2, 25, 28).

[47] N. Kawashima and H. Rieger, "Recent Progress in Spin Glasses", in *Frustrated Spin Systems* (World Scientific, Singapore, Jan. 2005), pp. 491–596 (pp. 2, 25, 28–30, 110, 122).

[48] J. Houdayer, "A Cluster Monte Carlo Algorithm for 2-Dimensional Spin Glasses", Eur. Phys. J. B **22**, 479–484 (2001) (pp. 2, 40, 53, 120).

[49] C. M. Newman and D. L. Stein, "Short-range spin glasses: results and speculations", in *Spin glasses*, Vol. 100, edited by E. Bolthausen and A. Bovier, Lecture Notes in Mathematics (Springer, Berlin, 2007), pp. 159–175 (pp. 2, 53).

[50] L. Chayes, J. Machta, and O. Redner, "Graphical Representations for Ising Systems in External Fields", J. Stat. Phys. **93**, 17–32 (1998) (pp. 2, 53).

[51] O. Redner, J. Machta, and L. F. Chayes, "Graphical representations and cluster algorithms for critical points with fields", Phys. Rev. E **58**, 2749–2752 (1998) (pp. 2, 53).

[52] N. Metropolis, A. W. Rosenbluth, M. N. Rosenbluth, A. H. Teller, and E. Teller, "Equation of State Calculations by Fast Computing Machines", J. Chem. Phys. **21**, 1087–1092 (1953) (pp. 2, 33).

[53] L. Münster and M. Weigel, unpublished (pp. 2, 122).

[54] S.-K. Ma, *Statistical mechanics* (World Scientific, Philadelphia, 1985), 548 pp. (p. 6).

[55] K. Huang, *Statistical Mechanics* (Wiley, New York, 1987), 493 pp. (pp. 6, 9).

[56] M. Le Bellac, F. Mortessagne, and G. G. Batrouni, *Equilibrium and Non-Equilibrium Statistical Thermodynamics* (Cambridge University Press, Cambridge, 2004) (pp. 6–9).

[57] M. E. J. Newman and G. T. Barkema, *Monte Carlo Methods in Statistical Physics* (Clarendon Press, Oxford, 1999) (pp. 7, 9, 32–35, 130).

[58] D. P. Landau and K. Binder, *A Guide to Monte Carlo Simulations in statistical Physics*, 2nd ed. (Cambridge University Press, Cambridge, 2005) (pp. 7, 32–34).

[59] K. Binder and D. W. Heermann, *Monte Carlo Simulation in Statistical Physics: An Intoduction*, 5th ed. (Springer, Berlin, 2010) (pp. 7, 9, 32).

[60] R. Toral and P. Colet, *Stochastic Numerical Methods: An Introduction for Students and Scientists* (Wiley, New York, 2014) (pp. 7, 32).

[61] R. B. Griffiths, "Dependence of Critical Indices on a Parameter", Phys. Rev. Lett. **24**, 1479–1482 (1970) (p. 9).

[62] L. P. Kadanoff, "Scaling and universality in statistical physics", Physica A **163**, 1–14 (1990) (p. 9).

[63] B. Widom, "Equation of State in the Neighborhood of the Critical Point", J. Chem. Phys. **43**, 3898–3905 (1965) (p. 9).

[64] A. Pelissetto and E. Vicari, "Critical phenomena and renormalization-group theory", Phys. Rep. **368**, 549–727 (2002) (pp. 9, 12, 16).

[65] R. H. Swendsen, "Monte Carlo renormalization-group studies of the $d = 2$ Ising model", Phys. Rev. B **20**, 2080–2087 (1979) (p. 10).

[66] B. Berche, T. Ellis, Y. Holovatch, and R. Kenna, "Phase transitions above the upper critical dimension", SciPost Phys. Lect. Notes, 60 (2022) (p. 14).

[67] M. E. Fisher, "Scaling, universality and renormalization group theory", in *Critical phenomena*, Vol. 186, edited by F. J. W. Hahne (Springer, Berlin, 1983), pp. 1–139 (p. 14).

[68] M. E. Fisher and M. N. Barber, "Scaling Theory for Finite-Size Effects in the Critical Region", Phys. Rev. Lett. **28**, 1516 (1972) (p. 14).

[69] M. N. Barber, "Finite-size scaling", in *Phase Transitions and Critical Phenomena*, Vol. 8, edited by C. Domb and J. L. Lebowitz (Academic Press, New York, 1983), p. 146 (p. 14).

[70] V. Privman, "Finite-Size Scaling Theory", in *Finite size scaling and numerical simulation of statistical systems*, edited by V. Privman (World Scientific, Singapore, 1990), p. 1 (p. 14).

[71] R. Kenna and B. Berche, "Scaling and Finite-Size Scaling above the Upper Critical Dimension", in *Order, Disorder and Criticality: Advanced Problems of Phase Transition Theory*, Vol. 4, edited by Y. Holovatch (World Scientific, Singapore, 2014), pp. 1–54 (pp. 14, 99).

[72] M. Suzuki, "Static and Dynamic Finite-Size Scaling Theory Based on the Renormalization Group Approach", Prog. Theor. Phys. **58**, 1142–1150 (1977) (p. 14).

[73] E. Brézin, "An investigation of finite size scaling", J. Phys. (Paris) **43**, 15–22 (1982) (p. 14).

[74] A. M. Ferrenberg and D. P. Landau, "Critical behavior of the three-dimensional Ising model: A high-resolution Monte Carlo study", Phys. Rev. B **44**, 5081–5091 (1991) (pp. 14–16, 46, 120).

[75] K. Binder and E. Luijten, "Monte Carlo tests of renormalization-group predictions for critical phenomena in Ising models", Phys. Rep. **344**, 179–253 (2001) (pp. 14, 15).

[76] K. Binder, "Finite Size Scaling Analysis of Ising Model Block Distribution Functions", Z. Phys. B **43**, 119–140 (1981) (pp. 15, 16).

[77] D. J. Amit and V. Martin-Mayyor, *Field Theory, The Renormalization Group, And Critical Phenomena: Graphs To Computers*, 3rd ed (World Scientific, 2005) (p. 16).

[78] H. G. Ballesteros, L. A. Fernández, V. Martín-Mayor, and A. M. Sudupe, "New universality class in three dimensions?: the antiferromagnetic RP^2 model", Phys. Lett. B **378**, 207–212 (1996) (p. 16).

[79] M. Hasenbusch, "A Monte Carlo study of leading order scaling corrections of ϕ^4 theory on a three-dimensional lattice", J. Phys. A: Math. Gen. **32**, 4851 (1999) (p. 16).

[80] M. Hasenbusch, "Finite size scaling study of lattice models in the three-dimensional Ising universality class", Phys. Rev. B **82**, 174433 (2010) (p. 16).

[81] A. M. Ferrenberg, J. Xu, and D. P. Landau, "Pushing the limits of Monte Carlo simulations for the three-dimensional Ising model", Phys. Rev. E **97**, 043301 (2018) (pp. 16, 119).

[82] F. Parisen Toldin, "Finite-size scaling at fixed renormalization-group invariant", Phys. Rev. E **105**, 034137 (2022) (p. 16).

[83] A. A. Saberi, "Recent advances in percolation theory and its applications", Phys. Rep. **578**, 1–32 (2015) (pp. 17, 18, 53).

[84] M. Aizenman, "On the number of incipient spanning clusters", Nucl. Phys. B **485**, 551–582 (1997) (p. 17).

[85] M. Caselle and A. Nada, " $\xi/\xi_{2\mathrm{nd}}$ ratio as a tool to refine effective Polyakov loop models", Phys. Rev. D **96**, 074503 (2017) (p. 18).

[86] M. E. Fisher, "The theory of condensation and the critical point", Physics **3**, 255 (1967) (p. 20).

[87] K. Binder, ""Clusters" in the Ising model, metastable states and essential singularity", Ann. Phys. (N. Y.) **98**, 390–417 (1976) (p. 20).

[88] M. F. Sykes and D. S. Gaunt, "A note on the mean size of clusters in the Ising model", J. Phys. A: Math. Gen. **9**, 2131 (1976) (p. 20).

[89] A. L. Stella and C. Vanderzande, "Scaling and Fractal Dimension of Ising Clusters at the $d = 2$ Critical Point", Phys. Rev. Lett. **62**, 1067–1070 (1989) (pp. 20, 23, 24, 48, 49, 52, 78, 119).

[90] H. Müller-Krumbhaar, "Percolation in a lattice system with particle interaction", Phys. Lett. A **50**, 27–28 (1974) (p. 20).

[91] A. Coniglio and W. Klein, "Clusters and Ising critical droplets: a renormalisation group approach", J. Phys. A: Math. Gen. **13**, 2775–2780 (1980) (p. 20).

[92] G. R. Grimmett, *The random-cluster model*, 333 (Springer, Dordrecht, 2006), 378 pp. (pp. 20–22).

[93] R. G. Edwards and A. D. Sokal, "Generalization of the Fortuin-Kasteleyn-Swendsen-Wang representation and Monte Carlo algorithm", Phys. Rev. D **38**, 2009–2012 (1988) (pp. 21, 22).

[94] O. Schramm, "Scaling limits of loop-erased random walks and uniform spanning trees", Israel J. Math **118**, 221–288 (2000) (p. 23).

[95] B. Duplantier, "Higher Conformal Multifractality", J. Stat. Phys. **110**, 691–738 (2003) (p. 23).

[96] J. Cardy, "SLE for theoretical physicists", Ann. Phys. (N. Y.) **318**, 81–118 (2005) (p. 23).

[97] M. Bauer and D. Bernard, "2D growth processes: SLE and Loewner chains", Phys. Rep. **432**, 115–221 (2006) (p. 23).

[98] H. C. Fogedby, "Stochastic Loewner Evolution", arXiv:0706.1177 [cond-mat.stat-mech] (2007) (p. 23).

[99] R. J. Baxter, "Potts model at the critical temperature", J. Phys. C **6**, L445–L448 (1973) (p. 23).

[100] B. Nienhuis, A. N. Berker, E. K. Riedel, and M. Schick, "First- and Second-Order Phase Transitions in Potts Models: Renormalization-Group Solution", Phys. Rev. Lett. **43**, 737–740 (1979) (p. 23).

[101] C. Vanderzande and A. L. Stella, "Bulk, surface and hull fractal dimension of critical Ising clusters in $d = 2$", J. Phys. A: Math. Gen. **22**, L445–L451 (1989) (p. 23).

[102] B. Duplantier and H. Saleur, "Exact Fractal Dimension of 2D Ising Clusters", Phys. Rev. Lett. **63**, 2536 (1989) (pp. 23, 24).

[103] C. Vanderzande, "Fractal dimensions of Potts clusters", J. Phys. A: Math. Gen. **25**, L75 (1992) (pp. 23, 24).

[104] A. Coniglio, "Fractal structure of Ising and Potts clusters: Exact results", Phys. Rev. Lett. **62**, 3054–3057 (1989) (p. 24).

[105] B. Duplantier, "Conformally Invariant Fractals and Potential Theory", Phys. Rev. Lett. **84**, 1363–1367 (2000) (p. 24).

[106] T. Grossman and A. Aharony, "Structure and perimeters of percolation clusters", J. Phys. A: Math. Gen. **19**, L745–L751 (1986) (p. 24).

[107] T. Grossman and A. Aharony, "Accessible external perimeters of percolation clusters", J. Phys. A: Math. Gen. **20**, L1193–L1201 (1987) (p. 24).

[108] H. E. Stanley, "Cluster shapes at the percolation threshold: and effective cluster dimensionality and its connection with critical-point exponents", J. Phys. A: Math. Gen. **10**, L211–L220 (1977) (p. 24).

[109] Y. Deng, H. W. J. Blöte, and B. Nienhuis, "Geometric properties of two-dimensional critical and tricritical Potts models", Phys. Rev. E **69**, 026123 (2004) (pp. 25, 99).

[110] Y. Deng, H. W. J. Blöte, and B. Nienhuis, "Backbone exponents of the two-dimensional q-state Potts model: A Monte Carlo investigation", Phys. Rev. E **69**, 026114 (2004) (p. 25).

[111] D. L. Stein and C. M. Newman, *Spin glasses and complexity* (Princeton University Press, Princeton, 2013) (p. 25).

[112] H. Nishimori, *Statistical Physics of Spin Glasses and Information Processing: An Introduction* (Oxford University Press, Oxford, 2001), 256 pp. (pp. 25, 27, 28).

[113] V. Cannella and J. A. Mydosh, "Magnetic Ordering in Gold-Iron Alloys", Phys. Rev. B **6**, 4220–4237 (1972) (p. 25).

[114] S. F. Edwards and P. W. Anderson, "Theory of spin glasses", J. Phys. F: Met. Phys. **5**, 965 (1975) (p. 26).

[115] G. Toulouse, "Theory of frustration effects in spin-glasses: I", Comm. Phys. **2**, 115–119 (1977) (p. 27).

[116] D. Sherrington and S. Kirkpatrick, "Solvable Model of a Spin-Glass", Phys. Rev. Lett. **35**, 1792 (1975) (pp. 27, 110).

[117] M. Mézard, G. Parisi, and M. A. Virasoro, "SK Model: The Replica Solution without Replicas.", EPL **1**, 77–82 (1986) (p. 27).

[118] D. J. Thouless, P. W. Anderson, and R. G. Palmer, "Solution of 'Solvable model of a spin glass' ", Phil. Mag. **35**, 593–601 (1977) (p. 28).

[119] J. R. de Almeida and D. J. Thouless, "Stability of the Sherrington-Kirkpatrick solution of a spin glass model", J. Phys. A: Math. Gen. **11**, 983 (1978) (p. 28).

[120] A. J. Bray and M. A. Moore, "Replica-Symmetry Breaking in Spin-Glass Theories", Phys. Rev. Lett. **41**, 1068–1072 (1978) (p. 28).

[121] G. Parisi, "Infinite Number of Order Parameters for Spin-Glasses", Phys. Rev. Lett. **43**, 1754 (1979) (p. 28).

[122] G. Parisi, "The order parameter for spin glasses: A function on the interval 0-1 ", J. Phys. A: Math. Gen. **13**, 1101 (1980) (p. 28).

[123] G. Parisi, "A sequence of approximated solutions to the S-K model for spin glasses", J. Phys. A: Math. Gen. **13**, L115 (1980) (p. 28).

[124] G. Parisi, "Order Parameter for Spin-Glasses", Phys. Rev. Lett. **50**, 1946–1948 (1983) (pp. 28, 109).

[125] M. Mézard, G. Parisi, N. Sourlas, G. Toulouse, and M. Virasoro, "Replica symmetry breaking and the nature of the spin glass phase", J. Phys. (Paris) **45**, 843–854 (1984) (pp. 28, 29).

[126] L. A. Pastur and M. V. Shcherbina, "Absence of self-averaging of the order parameter in the Sherrington-Kirkpatrick model", J. Stat. Phys. **62**, 1–19 (1991) (p. 28).

[127] A. Aharony and A. B. Harris, "Absence of Self-Averaging and Universal Fluctuations in Random Systems near Critical Points", Phys. Rev. Lett. **77**, 3700–3703 (1996) (p. 28).

[128] C. M. Newman and D. L. Stein, "Non-Mean-Field Behavior of Realistic Spin Glasses", Phys. Rev. Lett. **76**, 515–518 (1996) (p. 28).

[129] M. Mézard, G. Parisi, N. Sourlas, G. Toulouse, and M. Virasoro, "Nature of the Spin-Glass Phase", Phys. Rev. Lett. **52**, 1156–1159 (1984) (p. 29).

[130] R. Rammal, G. Toulouse, and M. A. Virasoro, "Ultrametricity for physicists", Rev. Mod. Phys. **58**, 765–788 (1986) (p. 29).

[131] N. D. Mackenzie and A. P. Young, "Lack of Ergodicity in the Infinite-Range Ising Spin-Glass", Phys. Rev. Lett. **49**, 301–304 (1982) (p. 29).

[132] D. L. Stein and C. M. Newman, "Broken ergodicity and the geometry of rugged landscapes", Phys. Rev. E **51**, 5228–5238 (1995) (p. 29).

[133] W. L. McMillan, "Scaling theory of Ising spin glasses", J. Phys. C: Solid State Phys. **17**, 3179–3187 (1984) (p. 29).

[134] D. S. Fisher and D. A. Huse, "Ordered Phase of Short-Range Ising Spin-Glasses", Phys. Rev. Lett. **56**, 1601–1604 (1986) (p. 29).

[135] A. J. Bray and M. A. Moore, "Scaling theory of the ordered phase of spin glasses", in Heidelberg Colloquium on Glassy Dynamics, edited by J. L. van Hemmen and I. Morgenstern (1986), pp. 121–153 (p. 29).

[136] A. J. Bray and M. A. Moore, "Chaotic Nature of the Spin-Glass Phase", Phys. Rev. Lett. **58**, 57–60 (1987) (p. 29).

[137] D. A. Huse and D. S. Fisher, "Pure states in spin glasses", J. Phys. A: Math. Gen. **20**, L997–L1003 (1987) (p. 29).

[138] D. S. Fisher and D. A. Huse, "Absence of many states in realistic spin glasses", J. Phys. A: Math. Gen. **20**, L1005–L1010 (1987) (p. 29).

[139] D. S. Fisher and D. A. Huse, "Nonequilibrium dynamics of spin glasses", Phys. Rev. B **38**, 373–385 (1988) (p. 29).

[140] D. S. Fisher and D. A. Huse, "Equilibrium behavior of the spin-glass ordered phase", Phys. Rev. B **38**, 386–411 (1988) (p. 29).

[141] F. Krzakala and O. C. Martin, "Spin and Link Overlaps in Three-Dimensional Spin Glasses", Phys. Rev. Lett. **85**, 3013–3016 (2000) (p. 30).

[142] M. Palassini and A. P. Young, "Nature of the Spin Glass State", Phys. Rev. Lett. **85**, 3017–3020 (2000) (p. 30).

[143] C. M. Newman and D. L. Stein, "Simplicity of state and overlap structure in finite-volume realistic spin glasses", Phys. Rev. E **57**, 1356–1366 (1998) (p. 30).

[144] C. M. Newman and D. L. Stein, "Finite-Dimensional Spin Glasses: States, Excitations, and Interfaces", Ann. Henri Poincaré **4**, 497–503 (2003) (p. 30).

[145] C. W. Gardiner, *Handbook of Stochastic Methods for Physics, Chemistry, and the Natural Sciences*, 2nd ed. (Springer, Berlin, 1985) (pp. 32, 33).

[146] B. A. Berg, *Markov Chain Monte Carlo Simulations And Their Statistical Analysis: With Web-based Fortran Code* (World Scientific, Singapore, 2004) (p. 32).

[147] O. Narayan and A. P. Young, "Convergence of Monte Carlo simulations to equilibrium", Phys. Rev. E **64**, 021104 (2001) (p. 33).

[148] W. Janke, "Monte Carlo Methods in Classical Statistical Physics", in *Computational Many-Particle Physics*, Vol. 739, edited by H. Fehske, R. Schneider, and A. Weiße, Series Title: Lecture Notes in Physics (Springer, Berlin, 2008), pp. 79–140 (pp. 34, 63, 125, 129–131).

[149] R. J. Glauber, "Time-Dependent Statistics of the Ising Model", J. Math. Phys. **4**, 294–307 (1963) (p. 34).

[150] M. P. Nightingale and H. W. J. Blöte, "Dynamic Exponent of the Two-Dimensional Ising Model and Monte Carlo Computation of the Subdominant Eigenvalue of the Stochastic Matrix", Phys. Rev. Lett. **76**, 4548–4551 (1996) (p. 34).

[151] M. P. Nightingale and H. W. J. Blöte, "Monte Carlo computation of correlation times of independent relaxation modes at criticality", Phys. Rev. B **62**, 1089–1101 (2000) (p. 34).

[152] P. Calabrese and A. Gambassi, "Ageing properties of critical systems", J. Phys. A: Math. Gen. **38**, R133–R193 (2005) (p. 34).

[153] U. Wolff, "Comparison between cluster Monte Carlo algorithms in the Ising model", Phys. Lett. B **228**, 379–382 (1989) (pp. 35, 37).

[154] U. Wolff, "Collective Monte Carlo updating in a high precision study of the $x - y$ model", Nucl. Phys. B **322**, 759–774 (1989) (p. 37).

[155] M. Hasenbusch, "Improved estimators for a cluster updating of $O(n)$ spin models", Nucl. Phys. B **333**, 581–592 (1990) (p. 37).

[156] U. Wolff, "Asymptotic freedom and mass generation in the $O(3)$ nonlinear σ-model", Nucl. Phys. B **334**, 581–610 (1990) (p. 37).

[157] K. Hukushima and K. Nemoto, "Exchange Monte Carlo Method and Application to Spin Glass Simulations", J. Phys. Soc. Jpn. **65**, 1604–1608 (1996) (pp. 37, 38).

[158] C. Predescu, M. Predescu, and C. V. Ciobanu, "The incomplete beta function law for parallel tempering sampling of classical canonical systems", J. Chem. Phys. **120**, 4119–4128 (2004) (pp. 38, 111).

[159] H. G. Katzgraber, S. Trebst, D. A. Huse, and M. Troyer, "Feedback-optimized parallel tempering Monte Carlo", J. Stat. Mech. **2006**, P03018–P03018 (2006) (pp. 38, 39, 111, 112).

[160] I. Rozada, M. Aramon, J. Machta, and H. G. Katzgraber, "Effects of setting the temperatures in the parallel tempering Monte Carlo algorithm", Phys. Rev. E **100**, 043311 (2019) (pp. 38, 111).

[161] E. Bittner, A. Nußbaumer, and W. Janke, "Make Life Simple: Unleash the Full Power of the Parallel Tempering Algorithm", Phys. Rev. Lett. **101**, 130603 (2008) (pp. 39, 112).

[162] R. Kumar, J. Gross, W. Janke, and M. Weigel, "Massively parallel simulations for disordered systems", Eur. Phys. J. B **93**, 79 (2020) (pp. 39, 40).

[163] D. A. Kessler and M. Bretz, "Unbridled growth of spin-glass clusters", Phys. Rev. B **41**, 4778–4780 (1990) (p. 40).

[164] L. de Arcangelis, A. Coniglio, and F. Peruggi, "Percolation Transition in Spin Glasses", EPL **14**, 515–519 (1991) (p. 40).

[165] F. Niedermayer, "General Cluster Updating Method for Monte Carlo Simulations", Phys. Rev. Lett. **61**, 2026–2029 (1988) (p. 40).

[166] S. Liang, "Application of Cluster Algorithms to Spin Glasses", Phys. Rev. Lett. **69**, 2145–2148 (1992) (p. 40).

[167] T. Jörg, "Cluster Monte Carlo Algorithms for Diluted Spin Glasses", Prog. Theor. Phys. Suppl. **157**, 349–352 (2005) (p. 40).

[168] T. Jörg, "Critical behavior of the three-dimensional bond-diluted Ising spin glass: Finite-size scaling functions and universality", Phys. Rev. B **73**, 224431 (2006) (p. 40).

[169] Z. Zhu, A. J. Ochoa, and H. G. Katzgraber, "Efficient Cluster Algorithm for Spin Glasses in Any Space Dimension", Phys. Rev. Lett. **115**, 077201 (2015) (p. 40).

[170] R. H. Swendsen and J.-S. Wang, "Replica Monte Carlo Simulation of Spin-Glasses", Phys. Rev. Lett. **57**, 2607–2609 (1986) (p. 40).

[171] J. Machta, Y. S. Choi, A. Lucke, T. Schweizer, and L. M. Chayes, "Invaded cluster algorithm for Potts models", Phys. Rev. E **54**, 1332–1345 (1996) (pp. 44, 57).

[172] H. Yang, "Alternative criterion for two-dimensional wrapping percolation", Phys. Rev. E **85**, Publisher: APS, 042106 (2012) (pp. 44, 57).

[173] M. E. J. Newman and R. M. Ziff, "Fast Monte Carlo algorithm for site or bond percolation", Phys. Rev. E **64**, 016706 (2001) (pp. 44, 45, 57, 63, 80).

[174] R. M. Ziff, "Spanning probability in $2D$ percolation", Phys. Rev. Lett. **69**, 2670–2673 (1992) (p. 45).

[175] R. M. Ziff and M. E. J. Newman, "Convergence of threshold estimates for two-dimensional percolation", Phys. Rev. E **66**, 016129 (2002) (p. 45).

[176] P. H. L. Martins and J. A. Plascak, "Percolation on two- and three-dimensional lattices", Phys. Rev. E **67**, 046119 (2003) (pp. 45, 57, 63).

[177] J. Wang, Z. Zhou, W. Zhang, T. M. Garoni, and Y. Deng, "Bond and site percolation in three dimensions", Phys. Rev. E **87**, 052107 (2013) (p. 45).

[178] A. A. Saberi and H. Dashti-Naserabadi, "Three-dimensional Ising model, percolation theory and conformal invariance", EPL **92**, 67005 (2010) (p. 45).

[179] P. Hou, S. Fang, J. Wang, H. Hu, and Y. Deng, "Geometric properties of the Fortuin-Kasteleyn representation of the Ising model", Phys. Rev. E **99**, 042150 (2019) (p. 45).

[180] W. Xu, Y. Sun, J.-P. Lv, and Y. Deng, "High-precision Monte Carlo study of several models in the three-dimensional $U(1)$ universality class", Phys. Rev. B **100**, 064525 (2019) (p. 45).

[181] C.-J. Huang, L. Liu, Y. Jiang, and Y. Deng, "Worm-algorithm-type Simulation of the Quantum Transverse-Field Ising Model", Phys. Rev. B **102**, 094101 (2020) (p. 45).

[182] B.-Z. Wang, P. Hou, C.-J. Huang, and Y. Deng, "Percolation of the two-dimensional XY model in the flow representation", Phys. Rev. E **103**, 062131 (2021) (p. 45).

[183] W. Press, S. Teukolsky, W. Vetterling, and B. Flannery, *Numerical Recipes in Fortran 77 - The Art of Scientific Computing*, 2nd ed. (Cambridge University Press, Cambridge, 1999), 973 pp. (pp. 47, 48, 63, 67, 86, 89, 91).

[184] S. Fortunato, "Site percolation and phase transitions in two dimensions", Phys. Rev. B **66**, 054107 (2002) (p. 49).

[185] M. Akritidis, N. G. Fytas, and M. Weigel, "Corrections to scaling in geometrical clusters of the $2D$ Ising model", J. Phys.: Conf. Ser. **2207**, 012004 (2022) (p. 52).

[186] F. Y. Wu, "The Potts model", Rev. Mod. Phys. **54**, 235–268 (1982) (p. 53).

[187] G. Kamieniarz and H. W. J. Blote, "Universal ratio of magnetization moments in two-dimensional Ising models", J. Phys. A: Math. Gen. **26**, 201 (1993) (p. 63).

[188] J. Salas and A. D. Sokal, "Universal Amplitude Ratios in the Critical Two-Dimensional Ising Model on a Torus", J. Stat. Phys. **98**, 551–588 (2000) (p. 63).

[189] X. S. Chen and V. Dohm, "Nonuniversal finite-size scaling in anisotropic systems", Phys. Rev. E **70**, 056136 (2004) (p. 63).

[190] P. Young, "Everything you wanted to know about Data Analysis and Fitting but were afraid to ask", arXiv:1210.3781 [cond-mat, physics:physics] (2014) (pp. 63, 89, 125–127).

[191] A. K. Hartmann, *Big Practical Guide to Computer Simulations*, 2nd ed. (World Scientific, Singapore, 2015), 462 pp. (p. 73).

[192] A. P. Young, "Direct Determination of the Probability Distribution for the Spin-Glass Order Parameter", Phys. Rev. Lett. **51**, 1206–1209 (1983) (p. 109).

[193] H. G. Katzgraber, M. Palassini, and A. P. Young, "Monte Carlo Simulations of Spin Glasses at Low Temperatures", Phys. Rev. B **63**, 184422 (2001) (pp. 110, 111, 116, 122).

[194] A. J. Bray and M. A. Moore, "Some observations on the mean-field theory of spin glasses", J. Phys. C: Solid State Phys. **13**, 419–434 (1980) (p. 110).

[195] A. P. Young and H. G. Katzgraber, "Absence of an Almeida-Thouless Line in Three-Dimensional Spin Glasses", Phys. Rev. Lett. **93**, 207203 (2004) (p. 111).

[196] S. El-Showk, M. F. Paulos, D. Poland, S. Rychkov, D. Simmons-Duffin, and A. Vichi, "Solving the 3D Ising model with the conformal bootstrap", Phys. Rev. D **86**, 025022 (2012) (p. 119).

[197] S. El-Showk, M. F. Paulos, D. Poland, S. Rychkov, D. Simmons-Duffin, and A. Vichi, "Solving the 3d Ising Model with the Conformal Bootstrap II. c-Minimization and Precise Critical Exponents", J. Stat. Phys. **157**, 869–914 (2014) (p. 119).

[198] F. Kos, D. Poland, D. Simmons-Duffin, and A. Vichi, "Precision islands in the Ising and $O(N)$ models", J. High Energ. Phys. **2016**, 36 (2016) (p. 119).

[199] D. Poland, S. Rychkov, and A. Vichi, "The conformal bootstrap: Theory, numerical techniques, and applications", Rev. Mod. Phys. **91**, 015002 (2019) (p. 119).

[200] A. D. Sokal, "Monte Carlo Methods in Statistical Mechanics: Foundations and New Algorithms", in *Functional integration*, Vol. 361, edited by C. DeWitt-Morette, P. Cartier, and A. Folacci, Series Title: NATO ASI Series (Springer, Boston, 1997), pp. 131–192 (pp. 123, 129).

[201] W. Janke, "Statistical Analysis of Simulations: Data Correlations and Error Estimation", in Quantum Simulations of Complex Many-Body Systems: From Theory to Algorithms, Vol. 10, edited by J. Grotendorst, D. Marx, and A. Muramatsu, NIC series (2002), pp. 423–445 (p. 124).

[202] M. B. Priestley, *Spectral Analysis and Time Series* (Academic Press, London, 1981) (p. 124).

[203] A. D. Sokal and L. E. Thomas, "Exponential convergence to equilibrium for a class of random-walk models", J. Stat. Phys. **54**, 797–828 (1989) (p. 124).

[204] N. Madras and A. D. Sokal, "The pivot algorithm: A highly efficient Monte Carlo method for the self-avoiding walk", J. Stat. Phys. **50**, 109–186 (1988) (pp. 124, 129).

[205] M. Weigel and W. Janke, "Error estimation and reduction with cross correlations", Phys. Rev. E **81**, 066701 (2010) (pp. 125, 127).

[206] H. Flyvbjerg and H. G. Petersen, "Error estimates on averages of correlated data", J. Chem. Phys. **91**, 461–466 (1989) (pp. 125, 128).

[207] J. R. Taylor, *An introduction to error analysis: the study of uncertainties in physical measurements*, 2nd ed (University Science Books, California, 1997) (p. 126).

[208] B. Efron, *The Jackknife, the Bootstrap, and Other Resampling plans* (Society for Industrial and Applied Mathematics, Philadelphia, 1982) (pp. 126, 127).

[209] B. Efron and R. J. Tibshirani, *An Introduction to the Bootstrap* (Chapman and Hall/CRC, New York, 1993) (pp. 126, 127).

[210] T. W. Anderson, *The Statistical Analysis of Time Series* (Wiley, New York, 1994) (p. 128).

[211] U. Wolff, "Monte Carlo errors with less errors", Comput. Phys. Commun. **156**, 143–153 (2004) (p. 129).

[212] B. A. Berg, "Double jackknife bias-corrected estimators", Comput. Phys. Commun. **69**, 7–14 (1992) (p. 129).

[213] A. M. Ferrenberg and R. H. Swendsen, "New Monte Carlo Technique for Studying Phase Transitions", Phys. Rev. Lett. **61**, 2635–2638 (1988) (p. 130).

[214] A. M. Ferrenberg and R. H. Swendsen, "New Monte Carlo Technique for Studying Phase Transitions", Phys. Rev. Lett. **63**, 1658–1658(E) (1989) (p. 130).